Comparison of static and transient face stability.

Case-study: The Rijnlandroute.

By

C.J. Lantinga

to obtain the degree of Master of Science at the Delft University of Technology,
to be defended publicly on Monday March 19, 2018 at 14:00 AM.

Student number:	4382978	
Supervisor:	Dr. ir. W. Broere,	TU Delft
Thesis committee:	Prof. dr. C. Jommi,	TU Delft
	Prof. dr. M. Bakker,	TU Delft
	Ir. H. Mortier.	COMOL5/DIMCO

Preface

This M.Sc. thesis have been performed in combination with the international project combination COMOL5 as a last part to fulfil my degree of Geo-Engineering at the Delft University of Technology. This thesis would have never succeeded without the help of numerous people.

First, I would like to thank Ing. R. Lensen, and H. de Jong, for giving me the opportunity to do this thesis at the Rijnlandroute project. These ten months have been a wonderful experience. Second, I would like to thank my graduation committee; Dr. Ir. W. Broere, Prof. dr. Ir. C. Jommi, Prof. dr. Ir. M. Bakker and Ir. H. Mortier, for the time and effort they put into this thesis. The results in this thesis would not have been achieved without their knowledge and commitment. However, in specific, I would like to thank Ir. H. Mortier for all the opportunities and weekly meetings. Third, I would like to thank Ir. Alexandre Barbieri, Ir. A. Bäcker, Ir. B. van de Water for their timely help and suggestions. Fourth, I would like to thank all the members of the project team for providing me the required data and for their help and suggestions. Last, I am grateful to my family, friends, and my fiancé Chris for their endless love, support and encouragement.

C.J. Lantinga
Breda, March 2018

"Do. Or do not. There is no try."
Yoda in The Empire Strikes Back.

Abstract

At the face of the TBM, called bore front, a pressurised slurry is used as face support. The aim of a tunnel face stability assessment is to determine the upper and lower bound of the support pressure, and the required support pressure belonging to a pre-defined ground deformation limit. This research is focussed on the determination of the lower bound of the support medium, which is defined by the horizontal effective stress and pore water pressure acting at the tunnel face both during boring and a standstill. While the pore water pressure distribution along the tunnel is clear, the estimation of the horizontal effective stress distribution is difficult. At the moment many calculation models have been developed to calculate the latter, but none ever made it into a standard. Most of the available model are based on static equilibrium conditions, e.g. the TBM does not move and the advancement process of the TBM is neglected. During tunnelling a continuous process of slurry penetration and excavation takes place and therefore, the interaction between the support fluid, advancement of the TBM and the soil needs to be taken into account. In this thesis, the combined assessment of these two components is called transient face stability. This contradiction between the models and the situation in practice have led to a research question in which a comparison is made between the static and transient face stability assessment.

The first part of this thesis is based on a static face stability assessment and consists of a comparative study between the Ruse-Vermeer (2002), Jancsecz-Steiner model (1994) and DIN4126+4085-model (2007,2013). A theoretical background analysis has been performed for each model; by using a case study analysis, the effect of the models' differences on the minimum support pressures has been determined. According to these two analysis, the different implementations of soil arching components between the models determine for a large part the difference in the minimum support pressure limit. In the second part of this chapter, the theoretical analysis has shifted to a more 'practical' project analysis by including external aspects like project aspects, soil conditions and contract requirements. From the practical project analysis it resulted that at the entrance zones, the soil cover is limited and thus additional surcharge is required. The placement of this additional surcharge leads to consolidation in the subsoil, and in case of a slow dissipation of the excess pore water pressure, this consolidation process influences the support pressure limits. Within this research two models have been developed in order to incorporate a one-dimensional vertical consolidation analysis within a static face stability assessment.

The second part of this thesis is based on a 'transient' face stability assessment. At first, both processes have been examined separately by assuming that they are not interdependent. From the analysis regarding the infiltration process, it resulted that the yield strength of the support medium is a controllable parameter which has a strong influence on the penetration depth of the support medium. The placement of the excavation tools on the cutting wheel and advancement of the TBM have a high impact on the excavation depth of the cutting wheel per turn and the available timespan for the built-up of the pressure transfer mechanism. The combination of the two time-dependent effects can possibly lead to the build-up of excess pore pressures in front of the tunnel face, which results in an additional force acting on the tunnel face which has to be counteracted. In this research, the possibility to include the time dependent effect of slurry infiltration and excavation within a transient face stability assessment is investigated. By using the same case study analysis as for the static face stability assessment, the excess pore water pressure development at the face of the TBM is determined. It resulted that in certain cases these excess pore water pressures have such a high impact on the minimum support pressure limit that the neglection of these pressures can lead to large deformations and at the end even in a global collapse mechanism.

The last part of this research is based on the role of slurry TBM parameters on ground deformations. Due to overcutting and the tapered shape of the TBM, a joint (annulus) is present between the TBM and the soil formation. As a consequence of this hydraulic connection, the annulus is pressurized with bentonite slurry originating from the face. Due to the slurry pressure gradient and hydraulic connection with the annulus, not at each location, the exact geostatic stress can be reached and this leads to ground-deformations. By using the same case study analysis as for static face stability assessment, the influence of this hydraulic connection on the ground deformations is investigated. For each case, the exact geostatic stress distribution, the pressure distribution within the excavation chamber, and the deficient pressure required at the annulus are determined. It turned out that in order to counteract the discontinuous horizontal stress distribution over the tunnel face due to a heterogeneous soil profile, results in an not optimal pressure distribution within the excavation chamber. In contrast, this higher pressure distribution than required is advantageous for the amount of ground deformations that develop.

Contents

Symbols

a:	relaxation length/the time required in order to reach half of the maximum penetration distance
AR:	advance rate of the TBM
A_s:	total penetrated area within the wedge
A_t:	total penetrated area of the support medium
c:	cohesion
$\tilde{c}$:	hydraulic resistance aquitard to vertical flow
C:	height of the soil overburden
c_b:	bentonite concentration of the support medium
c_v:	coefficient of consolidation
d_{10}:	10% fraction of the particle size distribution; characteristic grain size diameter
D:	diameter of the tunnel
$D^{(r)}$:	reduced wall length diameter *(DIN-model)*
E:	resulting horizontal wedge force *(Jancsecz-Steiner model)*
e:	penetration distance support medium
e_t:	penetration distance for a given time t
erf:	the complementary error function
e_{max}:	maximum penetration distance support medium
f:	pressure gradient over the pressure transfer mechanism
f_{so}:	stagnation gradient over the pressure transfer mechanism
G:	self-weight soil volume
G_s:	top load from soil prism at top wedge *(Jancsecz-Steiner model)*
G_w:	self-weight wedge *(Jancsecz-Steiner model)*
GLR:	Ground Loss Ratio
H:	height of the aquifer
H_{dr}:	drainage length
h_f:	height of the support medium
h_W:	height of the water column
i:	hydraulic gradient
f:	pressure gradient suspension saturated zone
f_{s0}:	stagnation gradient suspension saturated zone
k:	permeability of the aquifer
K/K_y:	coefficient of horizontal effective stress
K_{A3D}:	three dimensional earth pressure coefficient *(Jancsecz-Steiner model)*
K_a:	active earth pressure coefficient
K_{ac}:	active earth pressure coefficient for cohesion term $(2\sqrt{K_a})$*(DIN-model)*
$K_{0:}$	lateral earth pressure coefficient
l_{cut}:	cutting depth of the cutter tools
l_e:	percentage of the final penetration depth
n:	porosity of the soil
$p_{min:d}$:	design value of the minimum support pressure
$p_{max:r}$:	characteristic value of the maximum support pressure
$p_{max:d}$:	design value of the maximum support pressure
N:	shear force along slanted failure plane wedge *(Jancsecz-Steiner model)*
N_γ:	soil weight stability number *(Ruse-Vermeer model)*
N_c:	cohesion stability number *(Ruse-Vermeer model)*
N_q:	surface load stability number *(Ruse-Vermeer model)*
p_o:	equilibrium pore water pressure
P_s:	uplift force of the wedge *(Jancsecz-Steiner model)*
P_{wheel}:	penetration depth of cutting wheel per revolution

P_{tool}: actual penetration depth of a single cutting tool per passing through a particular point
q: discharge per unit area of the aquifer normal to the direction of flow
q_o: additional surcharge at surface
Q: discharge of the aquifer
R: shear force along slanted failure plane wedge *(Jancsecz-Steiner model)*
RPM: revolutions per minute of the cutting wheel
r: tunnel radius
S: pressure support medium *(Jancsecz-Steiner model)*
S_{eff}: effectiveness support pressure
S_h: horizontal displacement at a given location
$S_{h,max}$: maximum horizontal displacement
S_s: specific storage aquifer
S_v: vertical settlement at a given location
$S_{v,max}$: maximum vertical settlement at the location of tunnel axis
T: shear force T acting on triangular plane wedge *(Jancsecz-Steiner model)*
t_{cut}: time needed for a full turn of the cutter wheel
t_f: mean infiltration time
t_t: timespan between subsequent passing of the cutting tools
T_v: dimensionless time-factor
U: degree of consolidation
U_{avg}: average degree of consolidation
$u_{con}(t_i)$: value of the excess pore pressure with time t_i after start of the consolidation process
u_e: excess pore pressure distribution
V_s: volume of the settlement trough (per unit length of tunnel)
W: pore water pressure *(Jancsecz-Steiner model)*
y: horizontal distance between the observed location and the tunnel axis
z: depth below ground surface
z_{dr}: depth below/height above drainage layer
z^*: depth below tunnel crown

α: wall slope angle
α_r: relation between the grain size and the effective radius of a flow channel
β: ground slope angle (DIN-model)
γ: unit weight of soil
γ',γ'': effective unit weight of soil
γ_f: unit weight suspension
γ_h: safety factor for horizontal effective stress
$\gamma_{G;stb}$: partial safety factor for a permanent driving load
γ_s: unit weight of the individual grains
γ_{sat}: saturated unit weight of the soil
γ_{u1}: safety factor for pore water pressure
γ_w: unit weight of water
γ_φ: partial safety factor for the friction angle
δ_a: slip angle
Δp_{fc}: pressure drop over pressure transfer mechanism
Δp_p: excess pore pressure distribution due to boring
Δs: excess pressure over pressure transfer mechanism
η: viscosity of the suspension
η_F: safety factor accounting for deviations in the suspension yield point
θ: inclination angle of the sliding surface with the horizontal
λ: leakage length of the aquifer
μ_i: shape coefficients *(DIN-model)*
$\sigma'^{(r)}_h$: reduced horizontal effective stress acting at the tunnel face *(DIN-model)*

$\sigma'_{con}(t_i)$:	value of the vertical effective stress with time t_i after start of the consolidation process
$\sigma'_{v,a}$:	reduced vertical effective stress due to vertical soil arching
τ:	shear stress of the support medium
τ_F:	yield stress support medium
φ:	friction angle/head aquifer
φ_o:	constant head

1 Introduction

1.1 General introduction

Tunnel construction projects in the western part of the Netherlands are typically built in soft, heterogeneous ground conditions with low stiffness and high groundwater tables. The tunnelling technique is the 'slurry shield' method, which uses a tunnel-boring machine (TBM). The TBM consists of a steel cylinder with a cutting wheel at the front. The function of this steel shield is to provide radial support and to prevent inflow of groundwater during construction until the preliminary or final tunnel lining is built. At the face of the TBM, called bore front, a pressurised slurry is used as face support (Figure 1). In order to ensure stable working conditions, the support pressure applied lies between two limits that correspond to certain failure mechanisms, e.g., ultimate limit states. A support pressure below the lower limit results in a deformation of the soil towards the face, causing a large settlement at ground surface. A support pressure above the upper limit results in an upward deformation of the soil or in a blow out, with the subsequent loss of the support medium. Various models are available to calculate the face support pressure limits; they consist of empirical, analytical and numerical models used to calculate the necessary properties of the support medium to prevent collapse (Broere, 1998).

The other major concern that needs to be addressed during tunnelling is the serviceability limit state, which focuses on keeping ground deformations below a pre-determined limit that defines the support pressure based on the required ground deformation limit. Regardless of the tunnelling method used, the ground will be loaded or unloaded and deformation will inevitably take place (Möller, 2006). In the case of urban environments, even limited soil deformation may damage buildings.

The motivation for this research originates from the Rijnlandroute project constructed by COMOL5[1], in which aspects related to tunnel face stability require more in-depth research. Part of this project involves the construction of a new road N434 between the A4 (junction Hofvliet) and the A44 (junction Ommedijk); it will mostly be constructed as a tunnel (2.4 km) and a deepened road (1.3 km)(Figure 2). The tunnel will be executed as a bored tunnel consisting of two parallel tubes with a diameter of 10.59 metres. The ground profile consists of varying soft-top layers underlying the Pleistocene sand layer (Annex 1). Due to the timespan of this thesis with regard to the timespan of the project, the only detailed information available concerns the eastern entrance zone. The scope of this thesis, therefore, focusses mainly on this zone and the aspects involved in it.

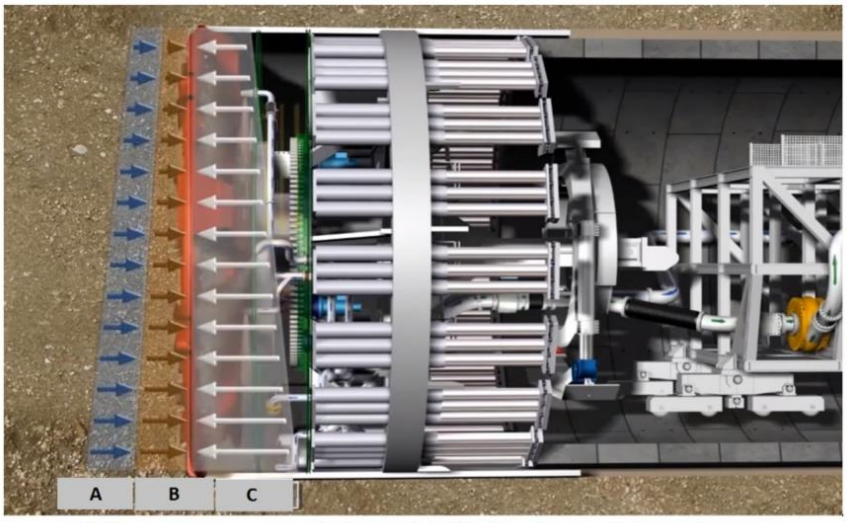

Figure 1. The principle of bore front stability (lower bound) is counter the horizontal effective stress and pore water pressure acting at the tunnel face (Herrenknecht, 2015).

[1] COMOL5 is an international contractor combination of the TBI companies Mobilis B.V. and Croonwolter & Dros B.V., VINCI Construction Grand Projets S.A.S. and DEME Infra Marine Contractors B.V.

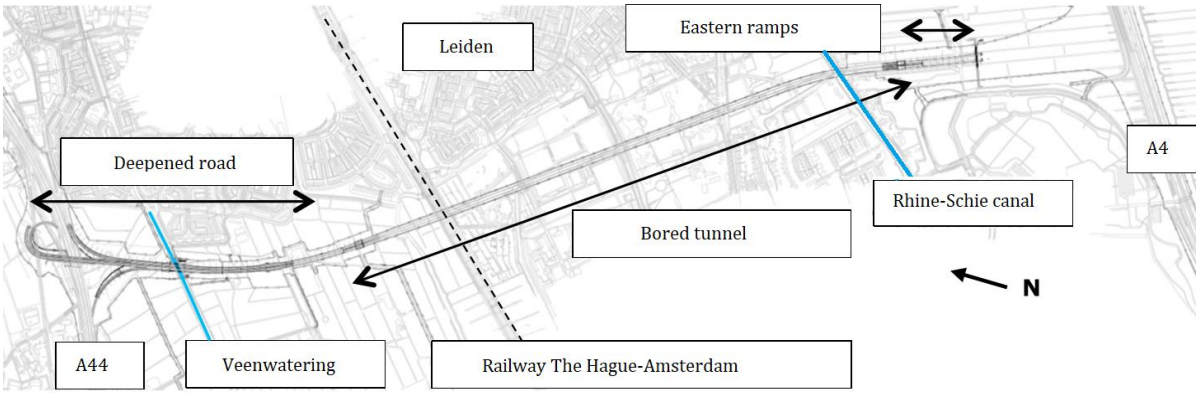

Figure 2. Overview of the subproject N434 which is part of the Rijnlandroute project (COMOL5, 2017).

The first and most important aspect that requires attention in this thesis are the dimension of the required stability embankments. At both entrance zones, a small soil cover is present, so an additional surcharge (stability embankment) is required to counterbalance the support pressure. In addition, these embankments are also required to prevent buoyancy of the tunnel. The dimensions of these required stability embankments have led to certain difficulties due to the presence of cables and ducts, boundaries provincial integration plan (PIP) and contract requirements. Therefore, these embankments must have the smallest possible dimensions. During the tender phase of the Rijnlandroute project, a face stability assessment was performed using three different models[2] in order to determine the minimum support pressure limit. The dimensions of these stability embankments required for these three models are displayed in Figure 3 and this figure reveals that the Ruse-Vermeer method is the most optimal design solution, due to the smallest dimensions of the balance embankments. For the Ruse-Vermeer model, there are no references available from projects in the Netherlands with equal soil conditions. An in-depth study is therefore required in order to determine the applicability of the Ruse-Vermeer method to the Dutch soil. Due to the numerical set-up of the Ruse-Vermeer model, the applicability of this method to the Dutch soil is difficult to determine and therefore a more general comparison is made between the three models.

The second aspect that requires more in-depth research is the possibility to extent (static) face stability assessment by taking time-dependent effects into account e.g. transient face stability assessment. These time-dependent effects are the slurry infiltration and excavation process of the TBM. The three models[2] used in the Rijnlandroute project disregard these aspects and assume a static face stability assessment. For both time-dependent effects, an separate parameter analysis is required in order to determine the influence of these aspects on the minimum support pressure. Research by Broere (1998) and Broere & van Tol (2000, 2001) determined that the combination of these two time-dependent processes leads to the build-up of excess pore pressures in front of the TBM. The inclusion of these excess pore water pressures in a face stability analysis can significantly increase the required support pressure.

The third aspect is based on the effect of (slurry) TBM parameters on ground deformations. In order to obtain zero surface deformations, the support pressure must match the exact geostatic stress conditions. Due to overcutting (excavated diameter is larger than the shield diameter) and the tapered shape of the TBM, a joint, called annulus, is present between the TBM and the soil formation. In addition, it is assumed that the shield is 'positioned' concentrically within the excavated diameter so that the shield is hydraulically connected to the tunnel face. This means that the annulus is pressurized with bentonite slurry originating from the face (Bezuijen and Talmon, 2008) (Mooney et al, 2016). Research by (Mooney et al, 2016) determined that it is not possible to match the exact geostatic stress at each required location due to the support pressure gradient and the hydraulic connection between the face and annulus. For a face stability assessment, the effect of the pressure distributions corresponding to the support pressure limits by taking the flow around the TBM into account needs to be reviewed.

[2] Jancsecz & Steiner (1994), DIN4126+DIN4085 (2007,2013) and the Ruse-Vermeer method (2002).

The last aspect which requires more in-depth research is based on the implementation of face stability assessment within the Rijnlandroute project. Therefore, each analysis/research within this thesis consists of a theoretical and practical component. The practical component considers external aspects like soil conditions, project aspects and contract requirements which influence the face stability assessment. When these project aspects are defined, it is analysed in which way these effects can be incorporated within a face-stability assessment.

1.2 Aims of this research

This research aims to determine the applicability of the Ruse-Vermeer method to Dutch soil. The validation process contains a comparative study with two other models that have been successfully applied in reference projects in the Netherlands. For a more comprehensive result, this main project objective has shifted to a more general comparison between the three static face stability models. A theoretical background analysis has been performed for each model; by using a case study analysis, the effect of the models' differences on the minimum support pressures has been determined. Thereafter, this theoretical analysis has shifted to a more 'practical' project analysis by including external aspects like project aspects, soil conditions and contract requirements. The research has been designed in such a way that the results of this comparison are suitable for validating the Ruse-Vermeer method in the project-specific underground.

The other aim involves the inclusion of the time-dependent excavation and slurry infiltration process in a transient face stability analysis. Both time-dependent effects have therefore first been reviewed separately and the combination determined thereafter. The model derived by Broere (1998) is used for the transient face stability analysis. By using the same case-study analysis as for the static face stability assessment a comparison can be made between transient and static face stability.

The last aim of this research is based on the inclusion of flow around the TBM within a face stability analysis. The effect of this flow on the pressure distribution for the support pressure limits is investigated.

The above leads to the following research question:

What is the difference between static and transient face stability? Case study: The Rijnlandroute.

This research question has been subdivided into the following sub-questions:

1. What is the minimum support pressure required based on a static face stability assessment for the eastern entrance zone (chainage 3900-4300).
    a) What are the differences between the three original face support models, and what is the effect of the differences between these models on the value of the minimum support pressure?
    b) Is it possible to improve the three face stability models by using aspects of other models?[3]
    c) How can the effect of slurry infiltration be modelled in the case of static face stability?
    d) How do the support medium properties influence static face stability?
2. What is the minimum required support pressure for the eastern entrance zone (M3970-M4240), based on a transient face stability assessment?
    a) How can the time-dependent infiltration process be modelled?
    b) How can the time-dependent behaviour of the advance rate be modelled?
    c) How can the build-up of excess pore pressures be modelled?
    d) In what way do the support medium properties influence transient face stability?
    e) What is the effect of the additional overburden on the minimum required support pressure?
3. What is the influence of slurry TBM parameters on ground deformation?

[3] This includes also other models than Jancsecz & Steiner-, DIN4126+DIN4085- and the Ruse-Vermeer method.

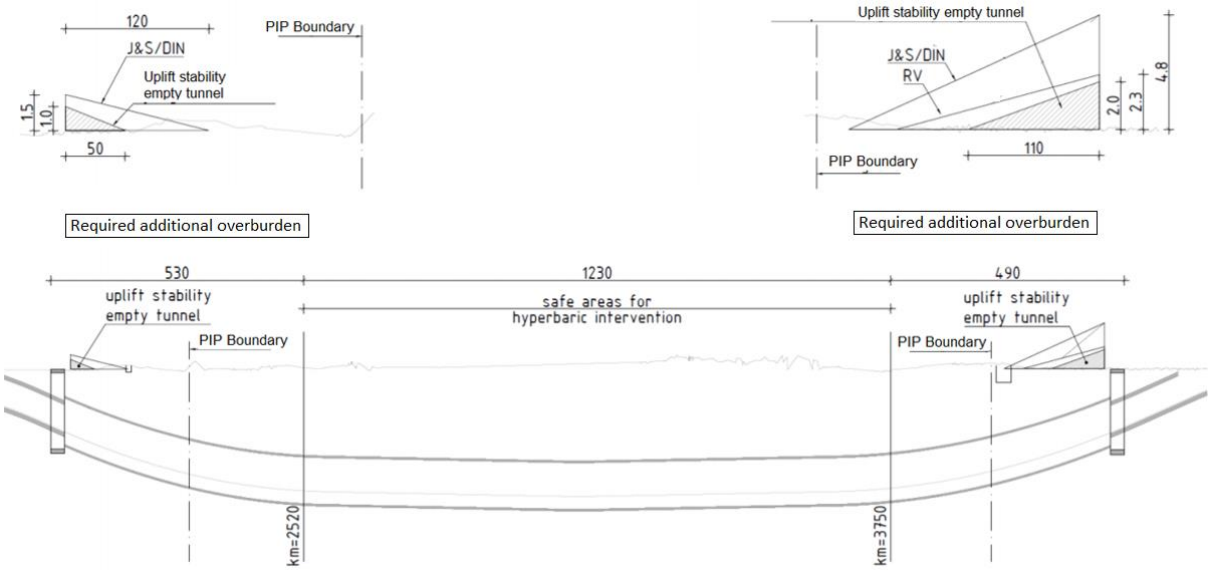

Figure 3. The additional overburden required for the bore front's stability and resistance against buoyancy during construction (COMOL5,2017).

Static face stability assessment (minimum support pressure limit): A static face stability assessment is based on static equilibrium conditions, e.g. the TBM does not move and the advancement process of the TBM is neglected. The minimum support pressure limit is determined by the horizontal effective stress and equilibrium pore water pressure acting at the tunnel face. Excess pore pressures due to consolidation are also assumed to be 'static' due to the large consolidation timespan compared to the timespan of TBM passing at that location.

Transient face stability assessment (minimum support pressure limit): In this thesis, transient face stability assessment is assumed to be an extension of static face stability by taking the time-dependent infiltration process and advancement of the TBM into account. In addition, the combination of these two effects can lead to the build-up of excess pore pressures in front of the tunnel face.

Demarcation:

1. A thorough background analysis, focussed on the following four models: Jancsecz & Steiner (JS), DIN4126+DIN4085 (DIN), Ruse-Vermeer method (RV) and Broere.
2. Only the project-specific parameters have been used.
3. The bentonite/grout flow around the TBM has not been modelled, but its influence on the static face stability is discussed.
4. The interaction of the excess pore water pressures due to the placement of additional surcharge and the excess pore water pressures due to the simultaneous process of boring and slurry infiltration is not investigated.

1.3 Outline of this thesis

Chapter 2 describes the static face stability assessment, considering both the support pressure limits and the support pressure properties. As these three aspects are related to a certain failure mechanism, the static face stability assessment has been divided into three failure classes. For each failure class, the corresponding calculation model is discussed. In addition, the practical component of each failure mechanism is discussed by using the case study project: The Rijnlandroute. The second part of this chapter focusses on the behaviour of the support medium (process). Within this part, the functions of the support medium, the rheological characteristics, slurry infiltrations process and the two pressure transfer models are discussed. In addition, the calculation method for slurry infiltration in case of static

face stability is discussed. The main findings of this chapter are summarized in the summary at the end of the chapter.

In Chapter 3, a thorough background analysis for the three different global stability models is conducted. Based on the outcomes of this analysis, eight case studies have been set up. Six different test series have been analysed in order to determine the effect of model differences on the support pressure. Thereafter, this theoretical analysis is extended by taking project-specific circumstances into account. One of these extensions is the process of consolidation and a calculation method is developed in order to integrate this process within a static face stability analysis. The main findings of this chapter are summarized at the end of each sub research.

Chapter 4 describes the transient face stability assessment. In the first part of the chapter, the time-dependent infiltration process and TBM's advance rate are reviewed. The interaction between these components which leads to the build-up of excess pore pressures in front of the tunnel face is investigated by using the model derived by Broere (1998). In the second part, a sensitivity and case-study analysis is performed based on a transient face stability assessment. The main findings of this chapter are summarized at the end of the chapter.

Chapter 5 describes the relation between the TBM parameters and ground deformations. In the first part, the volume loss components which induce settlements are described. The second part chapter focusses on the bentonite flow around the TBM and how this affects face support pressure distribution.

The final chapter gives a short overview of the main conclusions and a number of recommendations concerning face stability analysis. For a more detailed summary of the main findings, readers are referred to the summaries at the end of each chapter.

2 Static face stability: Assessment

2.1 Introduction

In case of an insufficient stand-up time of the soil, like cohesionless sand below groundwater level, frontal support is necessary. The value of this support pressure is based on the consideration of both the ultimate limit state and the serviceability limit state (Figure 4). The ultimate limit state focusses on the stability of the tunnel face and determines the face support pressure required to avoid a tunnel collapse; it does not take the development of ground deformations into account. In contrast, the serviceability limit state determines the support pressure for a pre-defined deformation limit (DAUB, 2016).

In fluid shields, the support pressure at the face is provided by a fluid, e.g. bentonite slurry, which is kept at a desired pressure to maintain equilibrium at the face. The ultimate limit state defines both an upper limit and a lower limit. In case of a support pressure below the lower bound, the soil and groundwater flow into the TBM and a large part or the entire face collapses (global collapse). In case of a support pressure above the upper limit, the soil is pushed away from the face, which subsequently leads to the loss of the support medium. Another important aspect to consider is the stability of a group of grains or a single grain at the tunnel face, which can introduce local(micro) collapse. The latter does not result in a support pressure limit but influences the support medium properties by imposing a yield-strength requirement. In summary, this leads to the following three failure classes which needs to be considered (Figure 4) (Broere, 1998):

1. loss support medium: determines the maximum support pressure;
2. external or global stability models: determine the minimum support pressure;
3. internal or micro stability models: determine the properties of the support medium.

This research is primarily based on the determination of the minimum required support pressure (class 2 models). Consequently, the three models which are thoroughly reviewed in this thesis are Jancsecz & Steiner (JS), DIN4126+DIN4085 (DIN) and the Ruse-Vermeer method (RV) method. Since the other two failure classes are (in)directly influenced by the minimum support pressure all three classes are discussed to a greater extent in the next paragraphs. Each analysis consists of a theoretical component and a practical component. This practical component discusses the practical implementation of each aspect within the case-study project The Rijnlandroute.

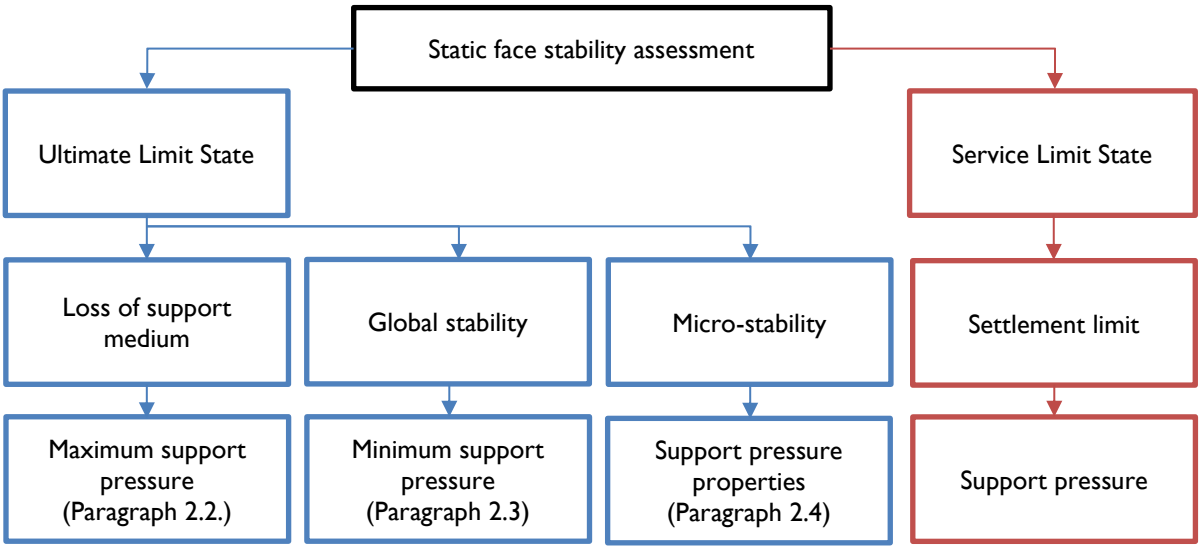

Figure 4. Overview of the static face stability assessment, which is based on a consideration of both the ultimate limit state as the serviceability limit state.

2.2 Class 1: Maximum support pressure

The face stability assessment for models in class 1 distinguishes different mechanisms that can occur due to a loss of the support medium originated by high support pressure, e.g., piping, soil fracturing, and (frictionless) blowout. The model, which yields the lowest maximum support pressure, is decisive. As this thesis mainly focusses on the minimum support pressure, only the lower bound of the maximum support pressure has been determined. Using Broere (1998) the results reveal that the lowest maximum support pressure is obtained in the case of a frictionless blowout. A blowout occurs when the support pressure at the tunnel face (or tail void) is too high and the soil overburden is pushed upward. At this moment, the support pressure escapes while the support pressure decreases. As the support pressure drops below the minimum support pressure limit, a global collapse of the tunnel face occurs.

In case of a frictionless blow-out, the friction of the soil-body with its surroundings is neglected. This is a valid assumption if the lifted soil body comprises a large volume e.g. the slurry penetrates to a large depth. Normally, the slurry will infiltrate to a certain distance in front of the tunnel face and therefore the friction of the lifted soil-body with its surroundings cannot be neglected. In order to take this friction into account, this blowout failure mechanism is schematised as the upward deformation of a soil column with height *C*, which leads to shear stresses acting at the sides (Figure 5)(Broere,1998). These stresses counteract the upward movement, resulting in an additional force downwards. This means that a blow-out mechanism including friction leads to a higher maximum support pressure limit than for the case without friction.

The characteristic maximum support pressure limit $p_{max:r}$ for a blow-out model is derived from vertical equilibrium of the failure mechanism shown in Figure 5. The resisting stress at the bottom of the soil column $p_{max:r}$ is the sum of the self-weight G of the soil column and the friction forces τ along the vertical sides of the soil column (Equation 2.1). The design value of the maximum support pressure $p_{max:d}$ is calculated by multiplying the characteristic maximum support pressure with a safety-factor $\gamma_{G:stb}$.

A point of attention within this analysis is the value of the lateral earth pressure coefficient K_y. This coefficient converts the vertical effective stress next to the soil column into a horizontal effective stress acting at the sides of the column. In the failure mechanism schematised in Figure 5, the horizontal stress acts perpendicular to the direction of movement and therefore the earth-pressure coefficient that needs to be used is unknown. Based on the schematisation of straight failure surfaces it is assumed that the soil surrounding the wedge has zero lateral strain and therefore it is assumed that a neutral earth pressure coefficient is valid.

$$p_{max:r} = C\ [\ \gamma + \frac{2c + C\,K_y\,\gamma' \tan\varphi}{D}]$$ **[Equation 2.1]**

$$p_{max:d} = \gamma_{G:stb}\ p_{max:r}$$ **[Equation 2.2]**

$\gamma_{G:stb}$:	partial safety factor for a permanent driving load (=0,9) (NEN-EN-1997-1)[4]	[-]
c:	cohesion	[-]
C:	height soil overburden	[m]
K_y:	coefficient of horizontal effective stress	[-]
D:	diameter tunnel	[m]
γ:	unit weight of the soil	[kN/m³]
γ':	effective unit weight of the soil	[kN/m³]

[4] In the Dutch guidelines, the calculation method for a frictionless blowout is not covered specifically; however, the assessment for hydraulic fracturing is used (NEN-EN-1997-1 paragraph 10.3).

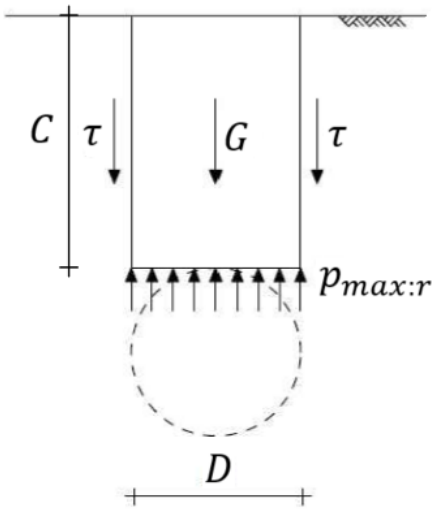

Figure 5. Blowout model, including friction along the sides (Broere, 1998).

2.2.1 Rijnlandroute case study

The theoretical analysis discussed in the previous paragraph has been implemented in the case study project in order to determine possible (external) influences that could affect the maximum support pressure limit. For the given case study project, the maximum support pressure for the eastern entrance zone (chainage 3900-4300) has been determined based on a blowout mechanism (including friction). Within this zone, a cross-section has been made every 20 m and the maximum support pressure has been calculated for each cross-section. This analysis reveals that the following (external) aspects directly influence the maximum support pressure distribution:

- the soil profile is heterogeneous for the entire eastern entrance zone;
- an additional surcharge (stability embankment) is required at chainage 4080-4210[5], and the construction of this embankment could induce consolidation in the subsoil;
- soil improvement is required for the upper soil layers at chainage 4150-4240.

In order to calculate the maximum support pressure for a heterogeneous soil profile, equation 2.2 has to be converted. The soil body has therefore been divided into *N* smaller horizontal layers, possibly of different thicknesses C_i, inside each of which the soil conditions are homogeneous. The maximum support pressure limit is equal to the sum of the total vertical stress of the soil overburden and the sum of the friction forces acting at the column sides (Equation 2.3).

$$p_{max:r} \leq \sigma_v + \sum_{i=1}^{n} C_i \left(\frac{2\, c_i + C_i K_{y:i}\, \sigma'_{v:i} \tan \varphi_i}{D_i} \right) \qquad \textbf{[Equation 2.3]}$$

The placement of an additional surcharge (stability embankments) on ground surface leads to consolidation in the subsoil. Due to the width of the embankment compared to the width of the tunnel face, this situation can be approximated by a one dimensional vertical consolidation analysis with zero lateral strain. During the consolidation process, the increase in vertical effective stress and decrease in excess pore pressure varies with time, e.g. it depends on the degree of consolidation. This means that the shear stresses in these consolidating soil layers are not constant and increase with time. In addition, the degree of consolidation at a given time also varies throughout the layer. Since in the maximum support pressure analysis only the weight of the soil is important and not the exact dissipation of the excess pore pressure within a soil layer, the average degree of consolidation is appropriate. The use of the average degree of consolidation leads to one degree of consolidation over the entire depth of the consolidating layer.

[5] Due to a lack of information, the embankment at chainage 4210-4240 is not taken into account.

The maximum support pressure at the time of boring $p_{max:r(t_{boring})}$ is calculated by the sum of the total vertical stress (time-independent) and the time-dependent friction forces along the vertical sides of the soil column (Equation 2.4). The total stress component consists of the initial total vertical stress acting at the tunnel crown σ'_{vi} increased with the load of the additional surcharge q_o. The time-dependent factor within the calculation of the friction forces is the vertical effective stress which increases with time during the consolidation process. The vertical effective stress at the time of boring $\sigma'_{v(t_{boring})}$ is calculated by the sum of the initial vertical effective stress σ'_{vi} and the increase in vertical effective stress $\sigma_{v(t)}$ for a given degree of consolidation.

$$p_{max:r} \leq (\sigma_{v:i} + q_o) + \sum_{i=1}^{n} C_i \frac{2c_i + C_i K_{y:i} (\sigma'_{v:i} + \sigma'_{v(t)}) \tan \varphi_i}{D}) \qquad \textbf{[Equation 2.4]}$$

At chainage 4150-4240, soil improvement of the upper soft layers is required for the placement of the additional surcharge. This means that at this zone, the subsoil is first subjected to a stress-release and thereafter to a stress-increase. The stress-release will lead to an overconsolidated soil (OCR[6] > 1,0). Due to a lack of information regarding this zone, the consolidation process cannot be considered. In order to estimate the maximum support pressure, it is assumed that the situation with soil improvement reflects the initial situation before the placement of the additional surcharge. Consequently, the maximum support pressure limit for this zone is calculated with equation 2.4.

The maximum support pressure for the eastern entrance zone is displayed in Figure 6. As described before, due to a lack of information regarding the embankment design at chainage 4210-4240, this zone is not taken into account. It can be seen that for the first part (chainage 4100- 4210) the maximum support pressure remains more or less equal. The reason for this is a combination of soil cover height, soil profile, soil improvement and stability embankment. From chainage 4100 to the channel at chainage 4010, the maximum support pressure increases due to a higher weight of the soil overburden. The soil weight of the overburden decreases at the location of the channel, which is revealed by a drop in the maximum support pressure.

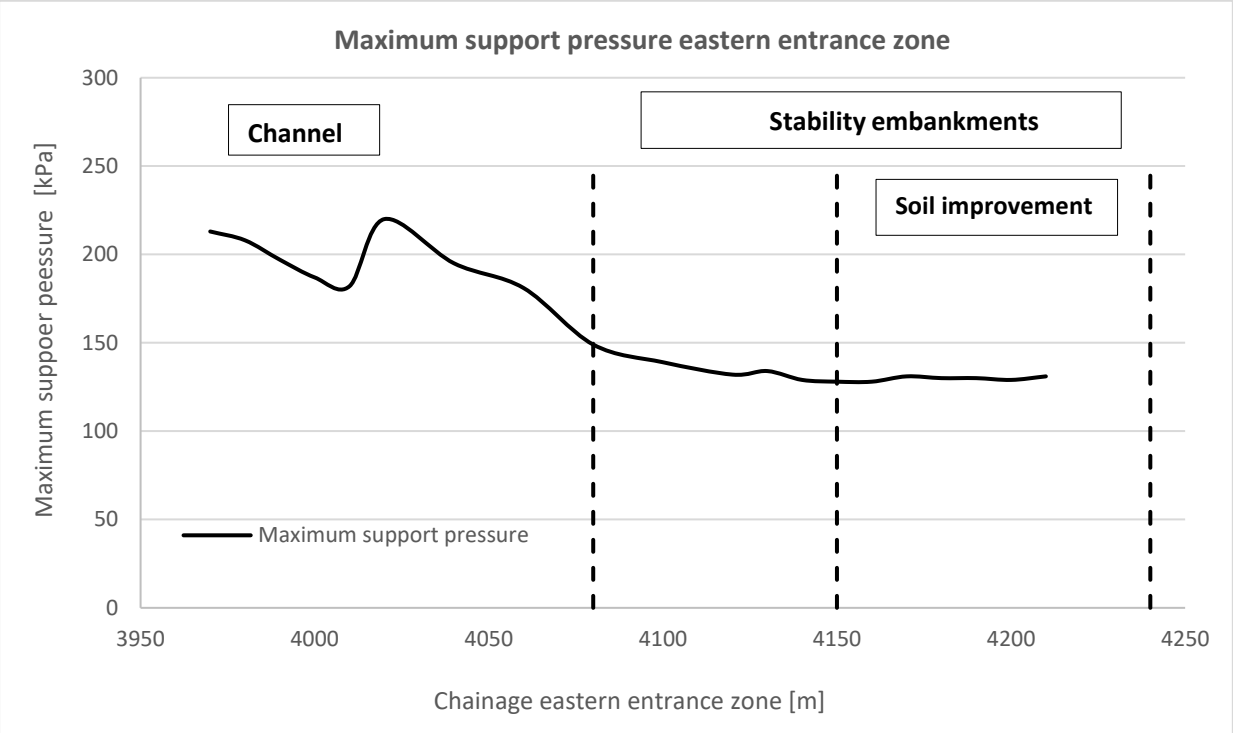

Figure 6. The maximum support pressure based on blowout mechanism including friction for chainage 3970-4230 (eastern entrance zone).

[6] OCR: Over-Consolidation Ratio.

2.3 Class 2: Minimum support pressure

Global stability models are based on a failure mode of a large part of the face or the entire face. This failure mode leads to global collapse (Figure 7). In the case of global collapse, the collapse propagates towards the surface, creating a chimney-shaped failure mechanism. The downward movement of this soil volume leads to friction on the sides and arching within the volume element. This type of active failure mechanism leads to excessive subsidence and possible damage to overlying structures. Extra attention needs to be paid when tunnelling under a river, a lake or the sea, as a direct channel is established between the tunnel and the water (Anagnostou and Kovári, 1994). The causes of a global collapse are a (sudden) decrease of effective support pressure at the tunnel face due to an extreme loss of bentonite concentration or an overly low support pressure. An extreme loss of bentonite concentration occurs in highly permeable soil layers which were unknown during the design or due to a failure mechanism like a blowout (described in the previous paragraph).

In order to prevent active failure, the required tunnel face support has to counter the horizontal effective stress and pore water pressures acting at the tunnel face. While the equilibrium pore water pressure distribution is clear, the estimation of the horizontal effective stress distribution is difficult. The reason for the latter is that the value for the earth pressure coefficient that needs to be used is unknown. If an active state is assumed by using an active earth pressure coefficient K_a, the soil deforms towards the TBM and this results in ground deformations. If a neutral state is assumed by using a neutral earth pressure coefficient K_0 ($> K_a$), the soil stays in place and no ground deformations are to be expected. In practice, it is beneficial for the process of the TBM to let the soil deform towards the face. The earth pressure coefficient will, therefore, fall between the active earth pressure coefficient K_a and the neutral earth pressure coefficient K_0. The minimum support pressure required is largely determined by the pore water pressure, as this has to be fully compensated by the support pressure in order to prevent a seepage flow towards the tunnel face (Anagnostou and Kovári, 1994).

Various empirical, analytical and numerical models are available to calculate the minimum support pressure, but the main problem is that no model has ever made this into a standard. Due to the project's specific requirements, the Jancsecz-Steiner and DIN4126+DIN4085 (analytical) models and the RV method (analytical based on numerical results) have been thoroughly examined. The first two analytical models are based on limit equilibrium, which assumes a failure mechanism in front of the tunnel face. The Jancsecz-Steiner model is based on a three-dimensional wedge model (Figure 8a) that consists of a sliding wedge loaded by a soil silo. The DIN model originates from the stability of diaphragm walls and therefore assumes a three-dimensional sliding wedge extending from the tunnel invert to ground surface (Figure 8b). In contrast, the RV model is a limit stress method that assumes a possible stress distribution at the tunnel face and from that determines the support pressure at collapse. The parameters in the RV analytical model (2002) can be considered as safety factors (called stability numbers) obtained by performing multiple numerical calculations.

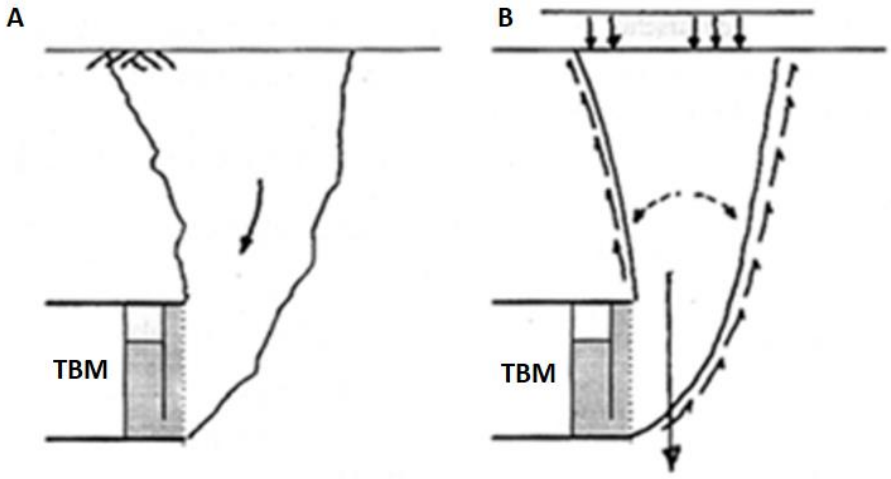

Figure 7. Schematisation of the global collapse mechanism: (a) the direction of soil movement and (b) the force mechanism (Arthe, 2016).

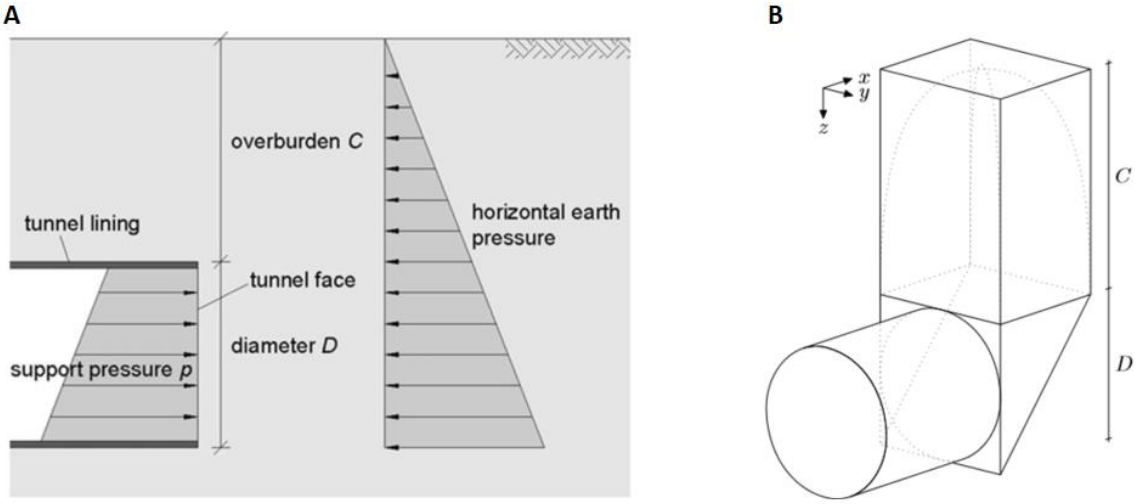

Figure 8. The failure mechanisms assumed by the analytical models. (a) 2D sliding wedge (DIN4126+DIN4085)(Idinger et al, 2010) (b) 3D wedge model (Jancsecz-Steiner model) (Broere,1998).

Regardless of the choice of model, all three face stability models can be written in the form of equation 2.5, which is a summation of the horizontal effective stress σ'_h multiplied by a safety factor γ_H and the pore water pressure u_1 multiplied by a safety factor γ_H . With this equation it is possible to determine the distribution of the minimum support pressure over the entire tunnel face. For all three models, the input values for the pore water pressure are the same[7], whereas the input values for the horizontal effective stress differs.

Although a higher face support pressure ($K_a > K_y < K_0$) than the minimum required face support contributes to a reduction of the settlements, this does not mean that a relatively high face support pressure is beneficial to the construction progress, as the use of a relatively high support pressure is detrimental to the excavation process. The optimal support pressure is therefore not the result of a combination of the two limit state approaches only, as operational and societal considerations (e.g. energy consumption) need to be considered (DAUB, 2016). *This topic falls outside the scope of this research and is therefore not further considered.*

$$p_{min:d} = \gamma_h \sigma'_h + \gamma_{u1} u_1 \qquad \textbf{[Equation 2.5]}$$

γ_{u1}:	safety factor for pore water pressure[8]	[-]
γ_h:	safety factor for horizontal effective stress[9]	[-]

2.3.1 Rijnlandroute case study

This research is primarily based on the determination of the minimum required support pressure (class 2 models) and the three models which are thoroughly reviewed in this thesis are Jancsecz & Steiner (JS), DIN4126+DIN4085 (DIN) and the Ruse-Vermeer method (RV) method. Therefore, the theoretical and practical component are discussed to a greater extent in the next chapter. A theoretical background analysis has been performed for each model; by using a case study analysis, the effect of the models' differences on the minimum support pressures has been determined. Thereafter, this theoretical analysis has shifted to a more 'practical' project analysis by including external aspects like project aspects, soil conditions, and contract requirements.

[7] The equation regarding the Ruse-Vermeer model is derived based on dry soil conditions, but within this thesis the pore water pressure distribution is incorporated in the same way as the two other models. This is discussed in more detail in the next chapter.

[8] The value of the safety factor for the for water pressure is equal to 1.05 (Jancsecz-Steiner and the DIN-model) and equal to unity for the DIN-model.

[9] The value of the safety factor for the lateral effective stress is equal to 1.5 (Jancsecz-Steiner and the DIN-model) and equal to unity for the DIN-model.

2.4 Class 3: Micro stability

Local stability models are based on micro stability, which is the stability of a single grain or a small group of grains at the tunnel face. This is mainly a problem in soils with no or low cohesion and a slurry- or air-supported tunnel face (Broere, 1998). The corresponding collapse mechanism is a local collapse mechanism (Figure 9) in which major soil movements are restricted to a zone close to the face of the TBM, which results in an obstruction of the cutting head's rotation. The downward movement of this soil volume leads to friction on the sides and arching within the volume element. In such situations, the soil has to be removed manually from the working area and therefore the excavation has to be disrupted (Anagnostou and Kovári, 1994). This results in a costly delay and, in the case of a slurry shield, the fluid pressure needs to be temporarily replaced by air pressure to remove the soil in the excavation chamber. The risks of instability in air pressure support are considerably large (Plantinga, 1998).

Micro-instability is prevented by the specific rheological properties of the support fluid.[10] The support slurry has a yield strength at standstill, and this yield point determines the ability of the slurry to 'set' in the ground. When a slurry penetrates the soil, the flow velocity decreases and the shear stresses become insufficient to allow it to flow further, and it sets. At stresses below this yield point, the slurry behaves like a solid. A minimal yield strength requirement must, therefore, be met. Micro-instability mainly occurs due to a combination of low yield stress and large grain sizes. CUR 231/DIN 4126 states that micro stability does not occur at d_{10}-values lower than 0.2 mm[11], cohesive layers or coarse layers with a thickness < 0.5 m.

Next, to micro-instability, the yield strength of the slurry also has a great impact on the minimum support pressure, because it affects the infiltration length of the support medium.

In the literature, various models are available in order to calculate the minimum yield strength requirement and within this thesis, the following models are compared:

- CUR 231 handbook diaphragm walls (2010) (Equation 2.6);
- The model derived by Broere (1998) (Equation 2.7);
- DIN 4126 Stability analysis of diaphragm walls (2013) (Equation 2.8).

From Equations 2.6-2.8, it is possible to observe that the setup of the models is the same, but the parameter of the effective unit weight varies. In addition, the DIN4126 method is the only method that uses safety factors to account for deviations in the yield point of the suspension. The effective unit weight of the soil, also called buoyant weight γ', is the weight of a saturated soil surrounded by support fluid per unit volume of the soil. In the case of the CUR231, the effective unit weight γ' is calculated by subtracting the unit weight of the support medium γ_f from the saturated unit weight γ_{sat} of the soil (Equation 2.6b). Following the DIN 4126 and Broere's model, the effective unit weight of a saturated soil sample is calculated by subtracting the unit weight of the support medium γ_f from an unit weight of the individual grains of the soil γ_s (Equation 2.7b&2.8b).

$$\tau_F \geq \frac{d_{10}\gamma'}{\frac{\tan\varphi'}{\gamma_\varphi}} \qquad \textbf{[Equation 2.6a]}$$

$$\gamma' = \gamma_{Sat} - \gamma_f \qquad \textbf{[Equation 2.6b]}$$

$$\tau_F \geq \frac{d_{10}\gamma''}{\frac{\tan\varphi'}{\gamma_\varphi}} \qquad \textbf{[Equation 2.7a]}$$

[10] In the next paragraph, the properties of the support medium are discussed to a greater extent.

[11] In soil profiles/layers with a d_{10} value lower than 0,2 mm, the support medium forms a membrane on the tunnel face. In the case of the membrane-like support medium, the so-called inner stability is always ensured, since the resulting filter cake prevents the soil grains from falling out of the wall and sinking in the suspension (Walz,1983).

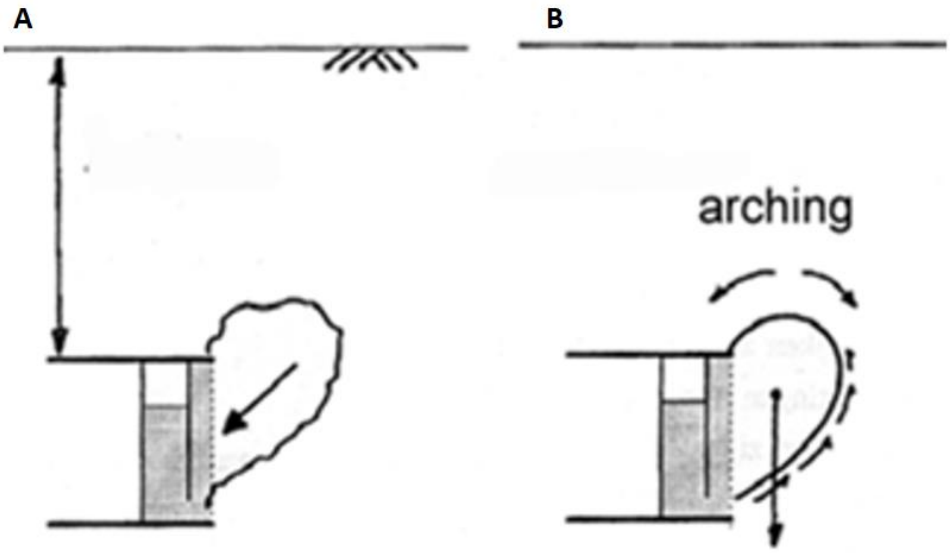

Figure 9. Schematisation of the local collapse mechanism. (a) the direction of soil movement and (b) the force mechanism (Arthe, 2016).

$$\gamma''_K = (1-n)(\gamma_s - \gamma_f) \qquad \textbf{[Equation 2.7b]}$$

$$\tau_F \geq \frac{d_{10}\gamma''}{2\eta_F \frac{\tan\varphi'}{\gamma_\varphi}} \qquad \textbf{[Equation 2.8a]}$$

$$\gamma''_K = (1-n)(\gamma_s - \gamma_f) \qquad \textbf{[Equation 2.8b]}$$

n:	soil porosity	[-]
d_{10}:	10% fraction of the particle size distribution	[m]
γ', γ'':	effective unit weight of soil	[kN/m³]
φ:	effective angle of internal friction	[°]
τ_F:	yield strength of the suspension	[Pa]
γ'':	effective unit weight of soil	[-]
η_F:	safety factor accounting for deviations in the suspension yield point of the suspension (= 0,6 DIN4126)	[-]
γ_φ:	partial safety factor for the friction coefficient of the drained soil in the limit state GEO [12,13]	[-]
γ_{sat}:	unit weight of saturated soil	[kN/m³]
γ_s:	unit weight of the individual grains (26.5 kPa)	[kN/m³]
γ_f:	unit weight of fresh slurry (10.5 kPa=standstill)	[kN/m³]

2.4.1 Rijnlandroute case study

In order to determine the model differences, the minimum required shear strength parameter was calculated for the given case-study using all three models. As micro-instability only occurs in soils with no or low cohesion and in soils with d_{10}-values higher than 0.2 mm, the only layer that is susceptible to micro-instability is the Pleistocene sand layer. The characteristic grain size diameter d_{10} for this layer was obtained by analysing a selection of 23 particle size distributions of the sand layer. From the sieve analysis, an average value of d_{10} (0.13 mm) and a maximum value of d_{10} (0.2 mm) was obtained. The unit weight of the soil particles γ_s equals 26.5 kN/m³ and the slurry equals 10.5 kN/m³ (standstill); an

[12] DIN 1054: 2010-12, Table A.2.2 γ_ϕ=1,15
[13] NEN-EN-1997-1 Table A.2 γ_ϕ=1,25

effective angle of internal friction of 30 degrees was used. Table 1 displays the minimum yield strength requirement for the three models. It can be seen that there is a small offset between the DIN model and the models of Broere/CUR231. The reason for this is that the DIN4126 model takes a safety factor for deviations in the yield point of the suspension into account. The result of this analysis indicates that this project's yield strength may not be lower than 3.20 Pa, which can be considered a lower bound solution. In order to determine the yield strength of the slurry, more about the behaviour of this support medium and its functions need to be known. This is discussed in the next paragraph.

2.5 Support medium

The properties of the support medium influence the minimum support pressure; therefore, an optimisation of these properties can lead to an optimal design. In the first part of this paragraph, the optimal parameters for each function of the support medium are discussed. As the scope of this thesis is based on the (minimum) support pressure; hence, the stabilisation function is the most critical. An important aspect of the stabilisation function is how the support pressure is transferred onto the soil skeleton. The second part of this paragraph focusses on the behaviour of the support medium (process). Within this part, the rheological characteristics, slurry infiltrations process and the two pressure transfer models are discussed. In addition, the calculation method for slurry infiltration in case of static face stability is discussed.

2.5.1 Functions of the support medium

Bentonite slurry fulfils several roles, and for each role, different parameters are important. The following functions can be observed: transport function, separation function, and stabilising function. These functions can be indicated within the support medium (bentonite slurry) circuit during TBM tunnelling. An example of a slurry treatment plant process as part of the complete bentonite slurry circuit is indicated in Figure 10.

2.5.1.1 Transport function

The mixture of natural soil with bentonite slurry is the excavated debris, and this mixture is pumped (hydraulic mucking) from the excavation chamber to a separation plant located on the surface, which enables the bentonite slurry to be recycled (Figure 10). A fundamental function of the bentonite slurry suspension is conveying the excavated debris by hydraulic means through a pipe system. For this function, it is beneficial to keep the plastic viscosity as low[14] as possible in order to decrease the pumping pressure and increase the flow rate. A high plastic viscosity leads to a sticky slurry, which is difficult to pump. One property of the support pressure is that above the yield point, the apparent viscosity decreases with increasing agitation. A turbulent flow regime is therefore created in the slurry pipes (Longchamp, 2005).

2.5.1.2 Separation function

At the slurry treatment plant, the excavated soil material is separated and removed from the bentonite suspension by a sequential series of processes (Figure 10) so that the clarified flushing medium can be recycled into the circuit. The separation of ultrafine particles is a vital capacity because otherwise, the bentonite suspension becomes denser and the transport medium thickens. The solids content of the slurry and the density of the solids in a given order of grain size have an impact on the excavation speed in mechanised tunnelling (Herrenknecht, 2009).

Table 1. Calculation results of the minimum yield strength required of the support medium for the three models.

Model	Minimum required yield-strength
[-]	[kPa]
DIN4126 (2013)	3.19
Model by Broere (2000)	4.16
CUR321 (2010)	4.11

[14] Note that in case of a too low plastic viscosity, the support medium is susceptible to segregation.

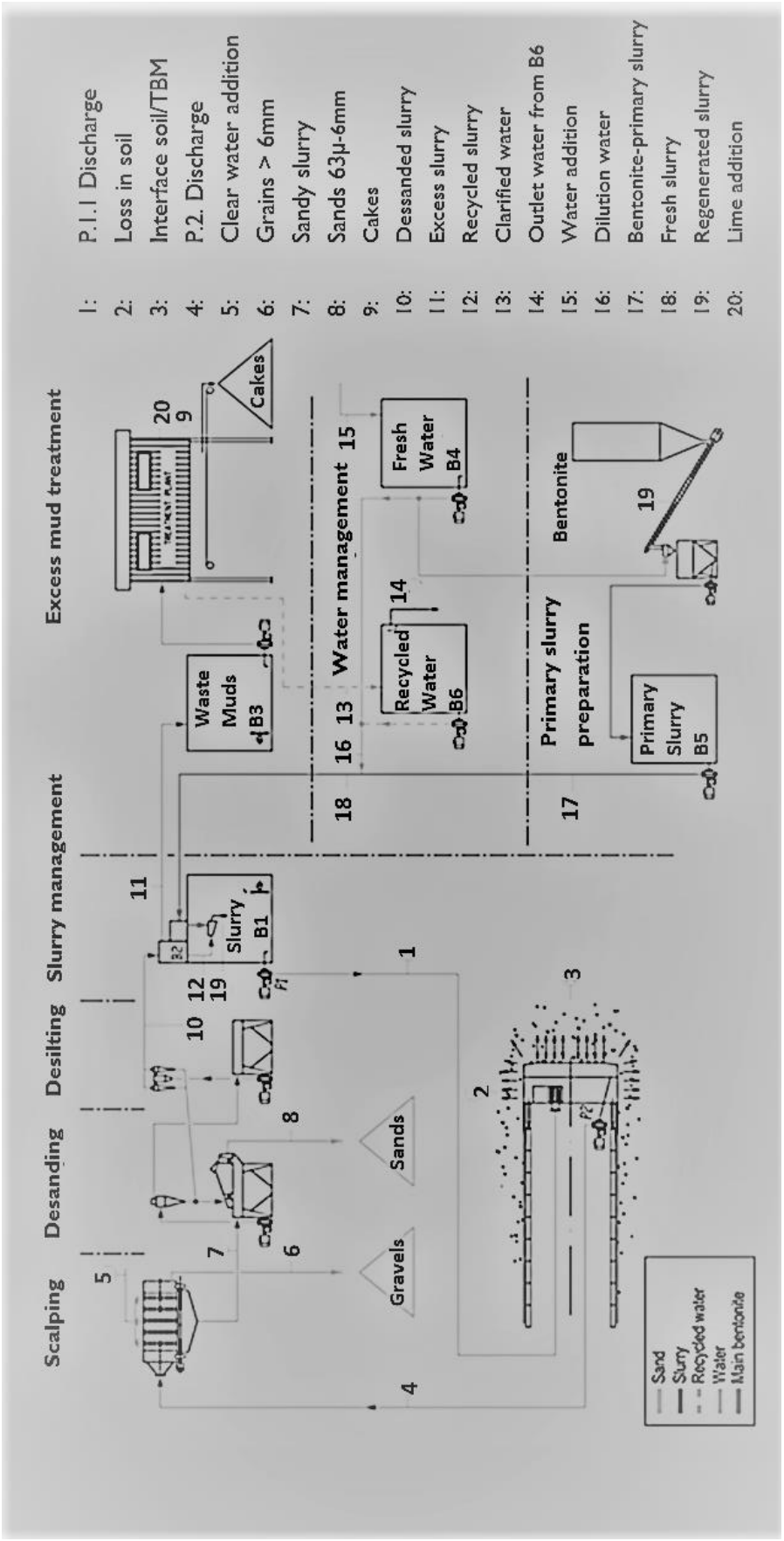

Figure 10. Example of a slurry treatment plant (STP). The different functions of the support medium are indicated (MS, 2017).

2.5.1.3 Stabilisation function

In slurry shields the support pressure at the face is provided by a fluid (generally a bentonite mix) that is kept at a desired pressure to keep equilibrium at the face. In a hydroshield, the excavation chamber is completely filled with bentonite slurry and in the working chamber the suspension level is usually adjusted to be slightly above the machine axis. In this way, the counter pressure is compensated inside the excavation chamber and is regulated by the compressed air reservoir in the working chamber (DAUB,2016) The most fundamental function of slurry shield tunnelling is the stabilisation of the tunnel face, which can be accomplished in the following ways:

- **Prevention of seepage flow towards the tunnel face:** The pressure distribution of the bentonite suspension must be higher than the (equilibrium) pore water pressure distribution acting at the tunnel face in order to prevent a seepage flow towards the tunnel face. The pressure distribution gradient of the support medium is higher due to the bentonite suspension having a slightly higher unit weight (≈10.5 kPa)[15] than the water pressure (≈10 kPa). The pressure distribution within the excavation chamber is linear (Figure 11). In case of a hydrostatic pore water pressure distribution this leads to a linearly increasing pressure difference between the support pressure and the equilibrium pore water pressure, also called excess pressure Δs.
- **Global stability:** Due to the pressure difference between the support pressure and the (equilibrium) pore water pressure, the bentonite suspension infiltrates the soil. In the case of fine-grained soil, this infiltration length is practically zero and a small impermeable layer develops, also called filter cake. In the case of coarse-grained soil layers, the slurry penetrates a certain distance into the soil, also called the penetration zone.
- **Filtration process:** Due to the filtration process of the slurry into the ground, the liquid and solid components are separated.
- **Stiffening of the slurry:** The flow velocity of the filtrating slurry decreases; consequently, it gradually stiffens and sets (thixotropic property). In this case, the shear stresses are not sufficient to further maintain the flow.
- **Micro stability mechanism:** the micro stability mechanism is prevented by the thixotropic property (the mixture becomes stiffer with decreasing velocity).

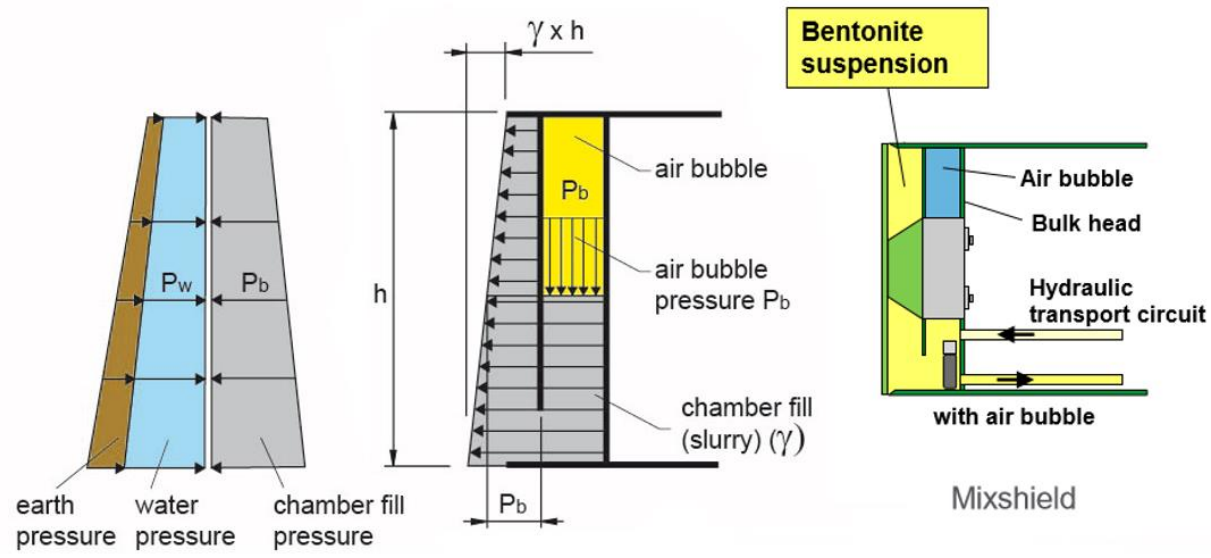

Figure 11. The stabilization(support) function of the bentonite slurry at the tunnel face (Herrenknecht, 2016)

[15] This is the unit weight of a bentonite suspension in case of a standstill. During TBM drive the bentonite suspension has an unit weight of 12 kN/m^3.

2.5.2 Characteristics bentonite suspension

The bentonite suspension used in slurry shield tunnelling consists of water and bentonite (3-10 %), to which polymers can be added. The molecular level of the bentonite suspension in contact with water forms a large-volume structure called a card-house structure. In its undisturbed state, the suspension sets to a hydrogel (gel). Intensive movement in the suspension through mechanical disturbances loosens the bonds between the card-house structure and the suspension changes to a flowing state (sol). This sol/gel conversion in bentonite suspensions is completely reversible (Praetorius and Schöβer, 2017).

2.5.2.1 Types of fluids

The primary concern of fluids are the rheological flow properties. Rheology is the science of flow and the deformation of matter (solid, liquid, gas) and is involved with the study of stress-strain-time relationships. Fluids can be divided into Newtonian or non-Newtonian fluids. Newtonian fluids have a constant relation (viscosity) between shear stress and shear rate (Equation 2.9). The higher the viscosity of a fluid, the less it moves. Newtonian fluids start at the origin, so these fluids immediately start to move when a force is applied to them. Water is an example of a Newtonian fluid. Non-Newtonian fluids do not present a constant viscosity; rather, it changes as shear rates are increased (apparent viscosity). These non-Newtonian fluids are further subdivided into the following fluid types (Figure 12):

1. Time-independent fluids: time plays a minor role in the stress-strain-time relationship.
    a) Bingham Plastic fluids: constant viscosity; a level of shear stress is required before the fluid is sheared.
    b) Pseudo-plastic fluids: shear stress-shear rate is described by a power-law model. In these models, the apparent viscosity decreases with an increasing shear rate.
    c) Dilatant: shear stress/shear rate is described by a power-law model. In these models, the apparent viscosity increases with an increasing shear rate.
2. Time-dependent fluids: In these models, the apparent viscosity depends on the shear rate and on for how long the shear is applied.
    a) Thixotropic: reversible, time-dependent reduction in viscosity in material subject to shear.
    b) Rheopectic: reversible, time-dependent increase in viscosity in material subject to shear.
3. Viscoelastic fluids: these fluids exhibit many characteristics of a solid.
4. Complex fluids: fluids that do not fit directly into one of the above (mathematical) models.

$$\eta = \frac{\tau}{D} \qquad \textbf{[Equation 2.9]}$$

η:	viscosity of the suspension	[N s/m^2]
τ:	shear stress of the suspension	[N/m^2]
D:	shear rate of the suspension	[s^{-1}]

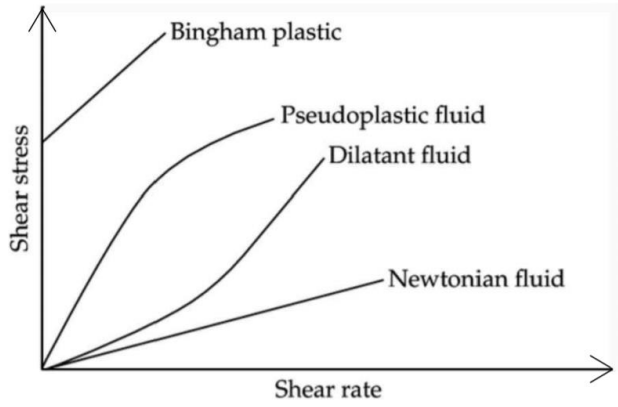

Figure 12. The relation between the shear stress and shear rate for Newtonian and non-Newtonian fluids.

2.5.2.2 Rheological model for bentonite suspension

The support medium used in slurry shield tunnelling exhibits a different rheology when at rest than when flowing; it can, therefore, be characterised as a complex fluid. Hence, the rheological model of the bentonite suspension is first described for the transport function and thereafter for the stabilising function (in rest conditions). For the transport function, complex fluids can be treated as simple Bingham plastic fluids with time-dependent thixotropic properties. The reason for this choice is that a finite amount of force is required before the flow is initiated. In other words, bentonite suspensions possess a yield point; the smallest shear stress, above which it behaves rheologically as a fluid. After reaching the yield-point, the viscosity reduces with increasing the shear rate and eventually become constant (Praetorius and Schößer, 2017).

The rheological model for the support function is based on the infiltration process of the support medium. This process is triggered by the pressure difference between the support pressure and the pore water pressure acting at the tunnel face. During infiltration, the flow velocity of the filtrating slurry decreases and it gradually stiffens (increase in viscosity) and sets. At this moment, the shear stresses are not sufficient to further maintain the flow. In terms of rheological behaviour, this infiltration process can be seen as the opposite of the separation function, but the same path is not followed backwards on the flow curve. These different paths result in hysteresis, as illustrated in Figure 13, which leads to two different yield stress values, i.e., static and dynamic yield stress.

2.5.3 Pressure transfer model

The flow of the bentonite slurry from the excavation chamber into the soil can be described by means of Darcy's law, as fluids flow from a location with a high pressure to a location with a low pressure. Due to the pressure difference Δs, the slurry infiltrates the soil. The filtration process of a colloidal slurry into a porous medium is divided into the following three stages, disregarding the advance rate of the TBM (Xanthakos, 1979):

1. penetration of the bentonite suspension into the soil (mud spurt phase);
2. clogging of the pores, first by large particles and later by finer particles from the slurry;
3. water leaving the slurry penetrates the soil mass (consolidation process).

In the filtration process described above, there are two limit cases for the infiltration distance. The lower limit of the infiltration distance occurs in fine-grained soil with a low permeability. In this case, the bentonite forms a thin impermeable filter cake on top of the face, also called membrane (Figure 14a). The upper limit of the infiltration distance occurs in coarse-grained soil with a high permeability or when the shear resistance of the slurry is low (Figure 14b). In this case, the slurry largely infiltrates the soil and the bentonite fails to form a filter cake. In practice, a situation occurs between these two limits which results in the formation of a filter cake and a certain infiltration length (Figure 14c).

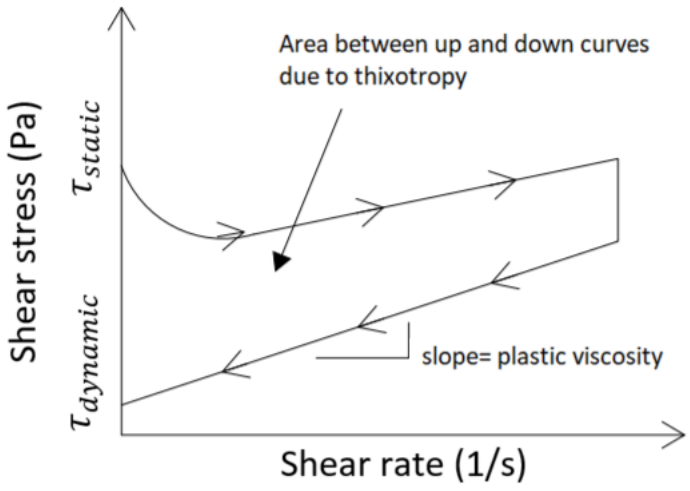

Figure 13. The effect of thixotropy on the relation between the shear stress and shear rate of the bentonite suspension.

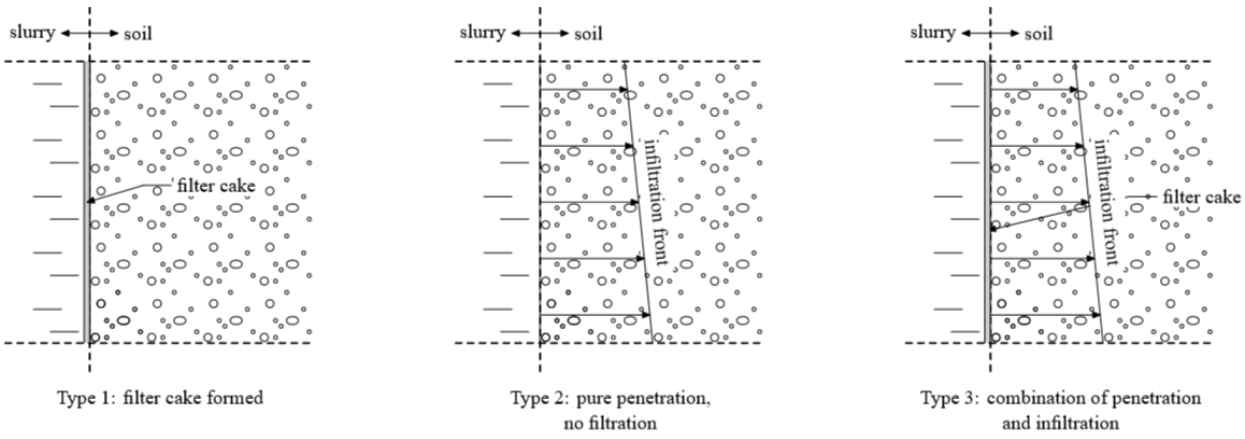

Figure 14. Three cases of slurry infiltration (1) formation of filter cake only; (2) pure penetration, no filtration; (3) combination of filtration and penetration (Broere after Müller-kirchenbauer,1977).

2.5.3.1 Pressure transfer mechanism

The two slurry infiltration limit cases lead to two different pressure transfer mechanisms that can occur at the tunnel face (Figure 15). In the case of a membrane model, the entire support force from the slurry is then transported onto the soil skeleton at the face. In case of a penetration zone, the support pressure is then transported by drag forces onto the soil skeleton over this infiltration length.

According to DIN 4126 (2007,2013), the development of a pressure transfer type depends on the value of the support pressure gradient, also called stagnation gradient. The pressure gradient *f* over the suspension-saturated zone is determined by the ratio of the excess pressure *Δs* to the penetration depth *e* of the slurry (Equation 2.10) and the pressure gradient for the maximum infiltration distance e_{max} is called the stagnation gradient (Equation 2.11). According to DIN 4126, a membrane model is valid when the stagnation gradient is higher than 200 kN/m³.

$$f = i = \frac{\Delta s}{e} \qquad \textbf{[Equation 2.10]}$$

$$f_{s0} = i = \frac{\Delta s}{e_{max}} = \frac{2\tau_f}{d_{10}} \qquad \textbf{[Equation 2.11]}$$

Walz (1967) has determined the maximum penetration depth by modelling a stretched capillary of diameter *d* filled with sand (Figure 16), connected at one side to a container filled with bentonite suspension and at the other side connected to a tank filled with water. Due to a pressure difference, the slurry penetrates the soil and stagnates after a certain penetration distance e_{max}. After the stagnation of the support medium, an equilibrium between the bentonite suspension and the water pressure is reached (Equation 2.12). This equilibrium can be rewritten in terms of the maximum penetration distance e_{max} (Equation 2.13) or the support pressure as a function of the penetration distance (Equation 2.14). In case of a maximum penetration distance, the pressure drop over the filtercake is equal to the excess pressure *Δs*.

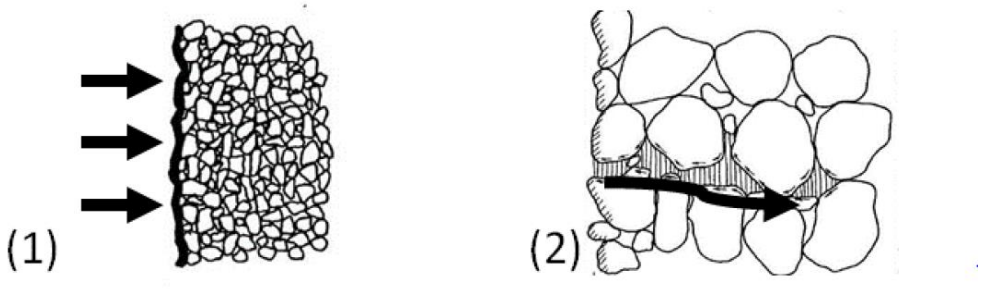

Figure 15. Pressure transfer mechanism in case of (1) membrane model and (2) penetration zone.

Compared to Walz (1967), the maximum penetration distance is written in terms of the characteristic grain size diameter d_{10} instead of the pore size, wherein the value 2 is the fitting parameter between d_{10} and the radius of the pores (Equation 2.15). Assuming that the slurry properties are optimised, the soil conditions are the critical factor for face stability.

$$\gamma_F \, h_F \, \pi \, \frac{d^2}{4} = \pi \, d \, l \, \tau_F + \gamma_w \, h_w \, \pi \, \frac{d^2}{4} \qquad \textbf{[Equation 2.12]}$$

$$l = e_{max} = \frac{(\gamma_F \, h_F - \gamma_w \, h_w) \, d}{4 \, \tau_F} = \frac{\Delta s \, d}{4 \, \tau_F} \qquad \textbf{[Equation 2.13]}$$

$$p_x = \gamma_F \, h_F - \frac{\tau_F \, 4}{d} \, x \qquad for \; x \leq l \qquad \textbf{[Equation 2.14]}$$

$$e_{max} = \frac{\Delta_p \, d_{10}}{2 \, \tau_F} \qquad \textbf{[Equation 2.15]}$$

γ_F:	unit weight bentonite suspension	[kN/m³]
h_F:	height of the bentonite suspension in the tank	[m]
γ_F:	unit weight water	[kN/m³]
h_F:	height of the water in the tank	[m]
l:	penetration distance	[m]
d:	diameter of the stretched capillary	[m]
p_x:	support pressure as a function of the penetration distance	[kN/m³]

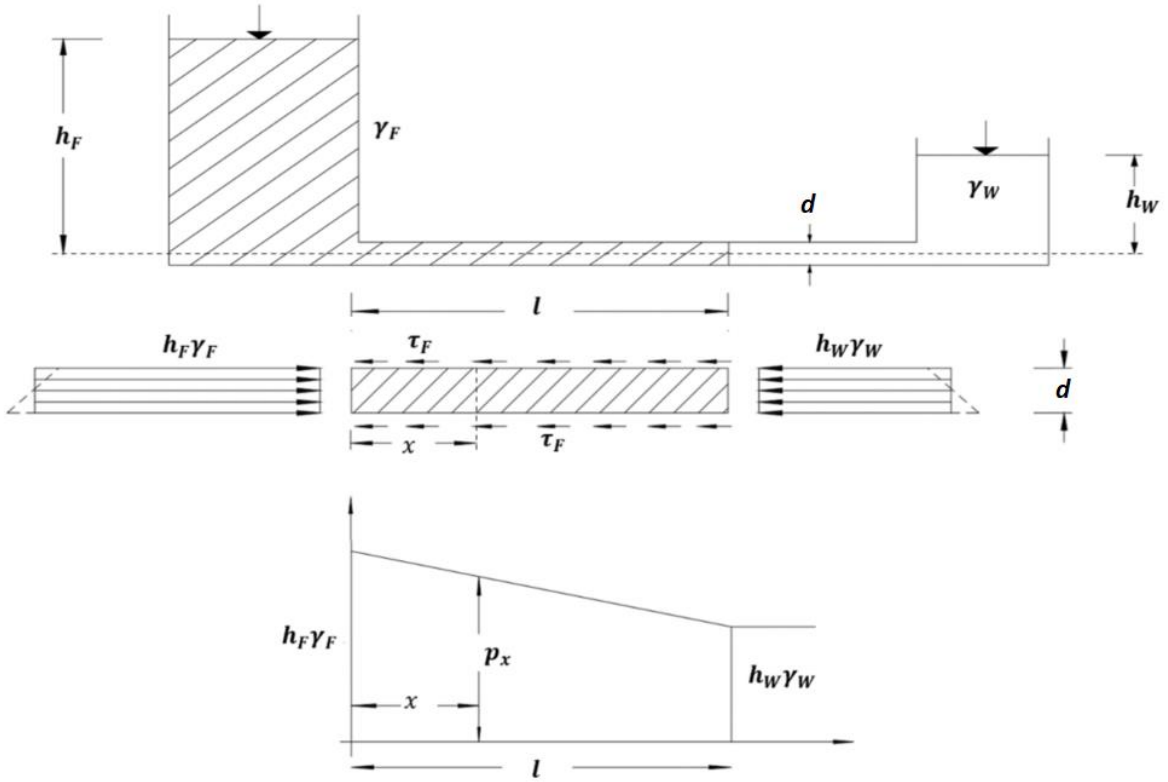

Figure 16. Determination of the maximum penetration distance by modelling a stretched capillary of diameter d filled with sand, connected at one side to a container filled with bentonite suspension and at the other side connected to a tank filled with water (Walz,1983)

2.5.4 Sensitivity parameters

The parameters that govern the maximum penetration depth are the excess pressure Δs, the characteristic grain size diameter d_{10} and the yield strength of the support medium, as detailed in Equation 2.13. The sensitivity of these parameters in the formation of the penetration zone is determined by assuming that the penetration zone develops fully e.g. the maximum penetration distance is reached. This is achieved in case of a standstill situation. Anagnostou and Kovári (1994, 1996) have performed a parametric study to determine the effect of varying these three parameters on the face stability. In this case study, a tunnel with a 10-metre diameter combined with an overburden of 10 metres of granular soil and a groundwater level 5 metres below ground level has been reviewed.

2.5.4.1 Characteristic grain size d_{10}

The safety factor as a function of the characteristic grain size diameter d_{10} is presented in Figure 17. The effect of the parameter d_{10} on the safety factor is determined by comparing curve A (excess pressure Δs = 20 kPa, bentonite concentration 4%) with the results from the corresponding membrane model (Δs = 20 kPa, bentonite concentration 4%). It can be seen that in soils with a d_{10} value lower than medium sand (0.6 mm), the deviation from the membrane model is negligible. This means that the slurry acts as though the face were sealed, regardless of whether a filter cake has been built up. A steep decrease in the safety factor occurs at d_{10} values in the range of coarse sand (0.60-2.00 mm).

2.5.4.2 Excess pressure Δs

The effect of a raise in the excess pressure Δs on the tunnel face stability is determined by comparing curve A (Δs = 20 kPa, bentonite concentration 4%) and B (Δs = 40 kPa, bentonite concentration 4%) as detailed in Figure 17. It can be seen that a raise in the excess pressure results in an increase of the safety factor for grain sizes smaller than 2 mm. This means that the range of characteristic grain size diameters that can be seen as a membrane model does not extend by a higher excess pressure. In the case of characteristic grain sizes bigger than approximately 2 mm, an increase in the fluid pressure results in further infiltration and fluid loss.

2.5.4.3 Effect of the bentonite concentration

The effect of the bentonite concentration on the face stability is determined by comparing curve A (Δs = 20 kPa, bentonite concentration 4%) and C (Δs = 20 kPa, bentonite concentration 7%) (Figure 17). It can be seen that a higher bentonite concentration extends the grain-size range of soils that can be supported by a bentonite slurry. The increase in bentonite has little effect on fine-grained soils; for these soils, a lower bentonite concentration is more effective because a high bentonite concentration results in a more difficult separation than a support pressure with a low bentonite concentration.

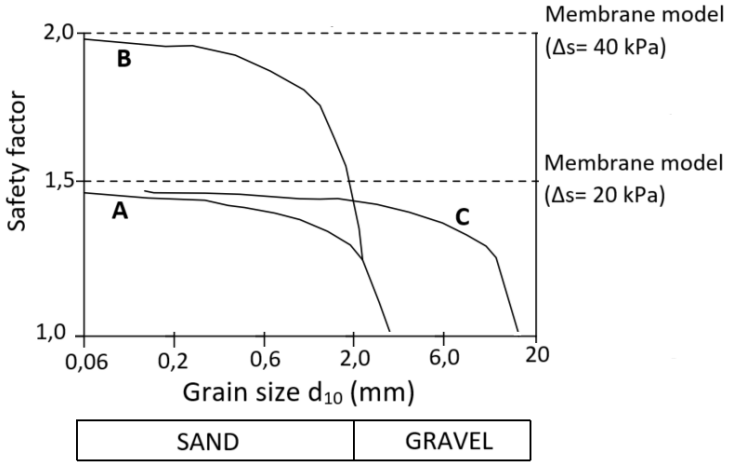

Figure 17. Safety factor as a function of characteristic grain size d_{10} (ϕ=37,5°)). Curve A: Δs= 20 kPa, 4% bentonite; Curve B; Δs= 40 kPa, 4% bentonite; Curve C Δs= 20 kPa, 7% bentonite (Anagnostou and Kovári 1994, 1996).

2.5.5 Slurry penetration: static situation

From a study by Xanthakos (1979), it resulted that the stabilizing force of the support medium depends essentially on the penetration distance of the support medium into the ground. In other words, the less the slurry penetrates, the greater the support force. Anagnostou and Kovári (1994, 1996) explained that this reduction is due to the amount of slurry which penetrates outside the assumed failure mechanism. The penetrated slurry exerts its thrust on a soil zone that is not involved in the failure mechanism. These stabilizing forces are thus withdrawn from the wedge and subsequently leads to a decrease of the support pressure. If due to the project-specific conditions a penetration zone model applies, the effect of the slurry penetration needs to be taken into account. An important aspect to note is that slurry infiltration is a time-dependent process and therefore this reduction effect is based on two limit cases, the membrane model (negligible penetration distance) and the penetration zone model (maximum penetration distance).

The only model of the three models reviewed which incorporates the effect of slurry infiltration is the DIN4085/4126 model. In contrast, the Jancsecz-Steiner and Ruse-Vermeer model assume that the entire support pressure is transferred onto the soil skeleton at the face. The background of the model described in the DIN4085 originates from the stability of diaphragm walls. This model takes the reduction due to slurry penetration outside the failure mechanism into account by a so-called effectiveness of the support medium. In case of no penetration outside the failure wedge, this effectivity is equal to 100%. This effectivity reduces with increasing amount of slurry penetration outside the failure mechanism. The effectiveness of the support pressure S_{eff} is obtained by the ratio of the penetrated area within the wedge A_s to the total penetrated zone A_t (Area **1-2-5-3-4-1**)(Equation 2.16)(Figure 18).

$$S_{eff} = \frac{A_s}{A_t} \qquad \textbf{[Equation 2.16a]}$$

$$A_s = Area\ zone\ 1-5-3-4-1 \qquad \textbf{[Equation 2.16b]}$$

$$A_t = Area\ zone\ 1-2-5-3-4-1 \qquad \textbf{[Equation 2.16c]}$$

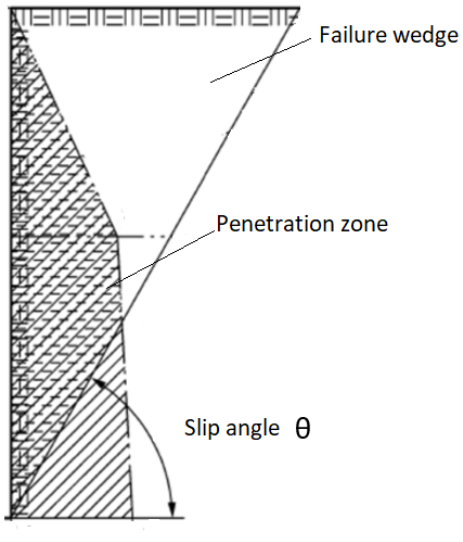

Figure 18. The method in order to determine the effectiveness of the support medium by the ratio of the amount of slurry penetration which falls inside and outside the zone of the failure mechanism.

2.6 Summary and conclusions

In this chapter the static face stability assessment is discussed. This assessment consists of three failure classes which determine the support pressure limits and support medium properties (yield strength requirement).

- **Maximum support pressure (upper limit support pressure):**
  - The maximum support pressure is a function of the weight of the soil cover above the TBM. In this thesis a blow-out model including friction is assumed to be equal to the lowest value for the upper-bound of the support pressure. In case of an insufficient soil overburden, additional surcharge is required in order to counteract the **minimum** support pressure and buoyancy of the tunnel. The placement of this additional surcharge results in an increase of the soil weight above the TBM. This means that the value of the maximum support pressure is influenced by the minimum support pressure. The placement of this additional surcharge leads to consolidation in the subsoil, and in case of a slow dissipation of the excess pore water pressure, this consolidation process influences the maximum support pressure limit. In case of a not completed consolidation process at the time the TBM passes that certain location, a more detailed analysis is required. Consequently, a 1D vertical consolidation analysis has been implemented within the calculation method. For this analysis, the average degree of consolidation is valid.
- **Support medium properties (yield strength requirement):**
  - The failure class regarding micro-stability imposes a yield-strength requirement to the support medium and this value has an effect on the (maximum) penetration distance of the support. For a given soil type, the penetration distance decreases with increasing yield-strength.
  - The yield-strength also influences the effectiveness of the support medium, as the smaller the penetration distance the less bentonite slurry (possibly) penetrates outside the failure wedge and therefore, the effectivity of the support medium increases.
- **Minimum support pressure (lower limit support medium):**
  - Regardless of the choice of model, all three face stability models can be written as a summation of the lateral effective earth pressure σ'_h multiplied by a safety factor γ_h and the pore water pressure u_1 multiplied by a safety factor γ_{u1}.
  - If an active state is assumed by using an active earth pressure coefficient K_a, the soil deforms towards the TBM and this results in ground deformations. If a neutral state is assumed by using a neutral earth pressure coefficient K_0 ($> K_a$), the soil stays in place and no ground deformations are to be expected. In practice, it is beneficial for the process of the TBM to let the soil deform towards the face. The earth pressure coefficient will, therefore, fall between the active earth pressure coefficient K_a and the neutral earth pressure coefficient K_0.
  - Although a higher face support pressure ($K_a > K_i < K_0$) than the minimum required face support contributes to a reduction of the settlements, this does not mean that a relatively high face support pressure is beneficial to the construction progress, as the use of a relatively high support pressure is detrimental to the excavation process.

3 Static face stability: Model analysis

3.1 Introduction

The previous chapter has discussed the static face stability assessment that needs to be performed for each project. This assessment is based on three types of failure mechanisms that can occur during slurry shield tunnelling: Local collapse (support medium properties), global collapse (minimum support pressure) and the loss of support medium (maximum support pressure). The failure mechanism regarding the maximum support pressure and support medium properties are not the main focus of this thesis, but they do have an effect on or are influenced by the minimum support pressure. The theoretical and practical components of the research on these two failure mechanisms have therefore been briefly described in the previous chapter. The results of this research serve as requirements/limitations for the minimum support pressure that is analysed in this chapter.

The model analysis contains a comparative study between the Ruse-Vermeer model (2002), the Jancsecz-Steiner model (1994) and the DIN4126/4085 (2007, 2013) model. The latter two have already been successfully applied in other Dutch reference projects. A theoretical background analysis has been performed for each model; by using a case study analysis, the effect of the models' differences on the minimum support pressures has been determined. This theoretical analysis is supported by experimental results from the literature. Thereafter, this theoretical analysis shifts to a more 'practical' project analysis by including external aspects such as project aspects, soil conditions, and contract requirements. The overview of this chapter is displayed in Figure 19.

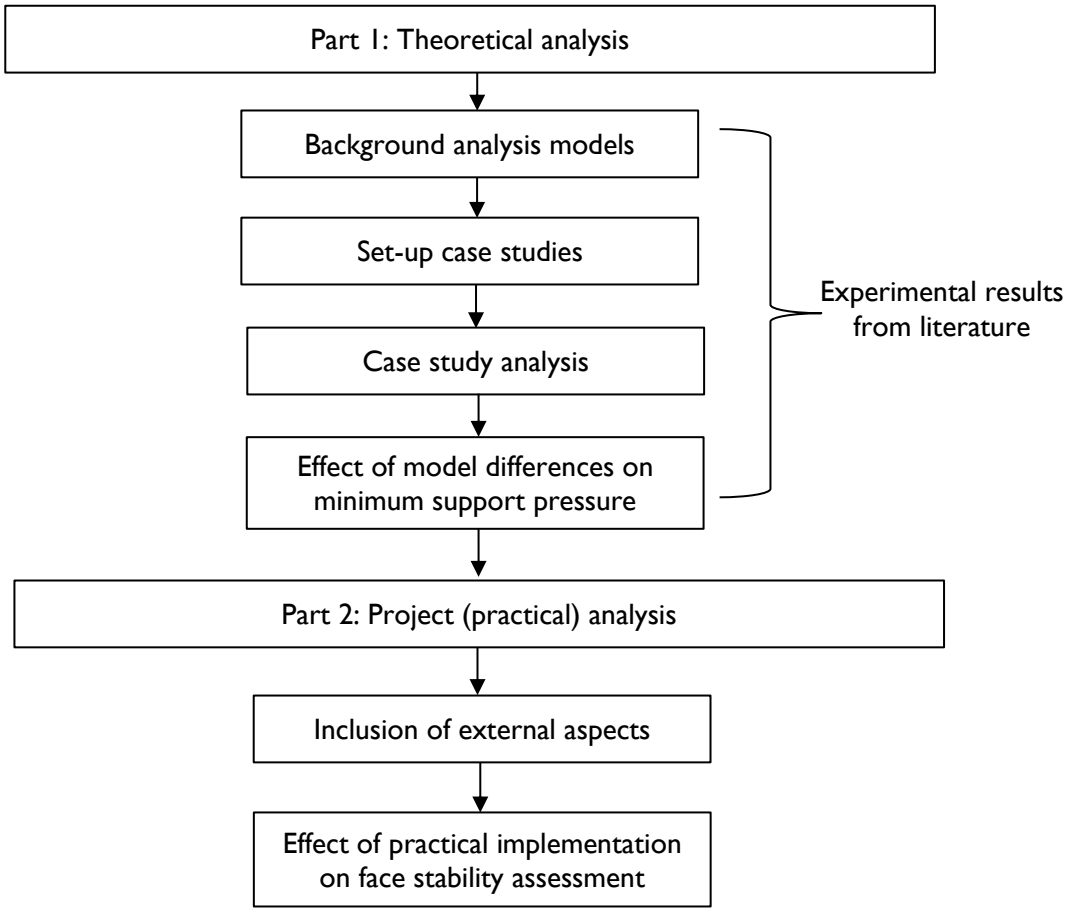

Figure 19. Chapter structure overview.

3.2 Theoretical background analysis

The tunnel face support required to prevent global collapse has to counter the horizontal effective stress and (equilibrium) pore water pressures acting at the tunnel face. Irrespective of the model choice, all three face stability models can be written in the form of Equation 2.4, which is a summation of the horizontal effective earth stress σ'_h multiplied by a safety factor γ_h and the pore water pressure u_l multiplied by a safety factor γ_{ul}. The input values for the pore water pressure are the same for all three models, whereas the input values for the horizontal effective stress component differ. The reason for the different input values of the horizontal effective stress is that all three models are based on different model assumptions. These model assumptions can be divided into the following aspects:

- model set-up assumptions
    - limit stress method (Ruse-Vermeer)
    - limit equilibrium method (DIN, Jancsecz-Steiner)
- assumption failure mechanism (DIN, Jancsecz-Steiner)
- applicable to certain soil conditions (frictional, cohesive, cohesive-frictional)
- implementation of soil arching (vertical, horizontal or a combination of both).

The differences between the two limit equilibrium models are mainly due to different implementations of the soil arching components within the models. The DIN model only takes horizontal soil arching into account, while the Jancsecz-Steiner model includes both horizontal and vertical soil arching. The next paragraphs therefore first discuss the general soil arching concept. The implementation of these soil arching components in each model is discussed in the background analysis for each model. As the Ruse-Vermeer method is a limit stress method, no predefined failure mechanism has been assumed and therefore the next paragraph is not applicable for this method.

3.2.1 Vertical soil arching

Vertical soil arching is based on the experimental and theoretical investigations on arching conducted by Terzaghi (1936,1943) in order to improve the understanding of arching phenomena in general and the stress distribution around tunnels in particular. Terzaghi's 'trapdoor test' experiment consisted of a box filled through a trapdoor with width 2a at its base (Figure 20). This box was tilted downwards, so that the trapdoor was loaded by the sand in the box. Due to this load, the trapdoor would open. The displacement during this downward soil movement was monitored. Figure 20 displays the real sliding surfaces (***uw*** and ***vz***), as observed in the experiments, and the yielding strip (***uv***). Vertical soil arching is the pressure transfer between a yielding soil mass and the adjoining stationary parts, where the relative movement of the soil is opposed by a shearing resistance within the contact zone of the yielding and stationary masses (Hsien-Jen Tien, 1990). This means that part of the soil load above the tunnel crown does not act as a load on it but is carried by the surrounding soil.

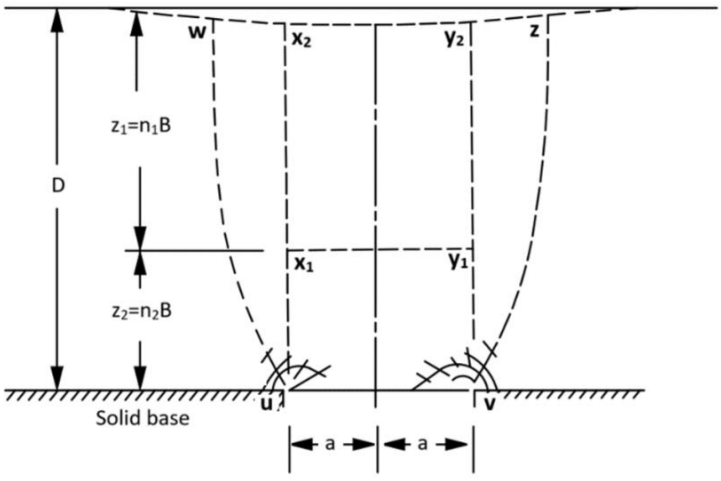

Figure 20. Trapdoor test result: Yielding in soil caused by downward movement of a long narrow section (Terzaghi,1943).

This failure mechanism in curved sliding surfaces is simplified by assuming vertical sliding surfaces (***ux*$_2$** and ***vy*$_2$**), as indicated in Figure 20. This means that the pressure on the yielding strip equals the weight of the sand located above the strip (***uv***) minus the shear resistance along the vertical sections. From the experimental investigations, Terzaghi (1936,1943) discovered that the shearing resistance is only active at the lower part (***ux*$_1$** and ***vy*$_1$**) of this vertical soil column, up to a height of 5*B* (n_1 = 5).
The soil prism is therefore divided in two parts:

- the upper part of the soil prism ***x*$_2$*x*$_1$*y*$_1$*y*$_2$**, which is treated as a surcharge q on the lower part;
- the lower part of the soil prism ***x1uvy*$_1$.**

The aforementioned arching theory can be applied to tunnel design, as the stress state in the soil above the top of a tunnel is similar to the stress state in the soil column above a yielding strip. As in the study by Terzaghi, the soil above the tunnel crown can be schematised as a rectangular soil column with a width 2a stretching from tunnel crown to ground surface (Figure 21). At the surface, a surface charge q_0 can additionally be present. Broere (1998) has derived the vertical effective stress acting at the yielding strip $\sigma'_{v,a}$ (tunnel crown) by the vertical equilibrium of a soil strip within this soil column (Equation 3.1). An important variable in Equation 3.1 is the relaxation length *a*. The value of relaxation length *a* depends on the manner in which soil arching has been taken into account. There are three possible ways to include the vertical soil arching component, and these can be roughly associated with the amount of deformation that occurs at the face (Broere, 1998):

1. No soil arching (Equation 3.2a). In the case of no vertical soil arching, it is possible to assume that no deformations occur that would trigger the vertical soil arching component. This, therefore, leads to an over prediction of the minimum support pressure.
2. Two-dimensional soil arching (Equation 3.2b). In the case of 2D soil arching, it is possible to assume that limited deformations occur that trigger the soil arching component. The model set-up assumes shear stresses on two sides of the soil prism.
3. Three-dimensional soil arching (Equation 3.2c). In the case of 3D soil arching, it is possible to assume that such large deformations take place that they resemble a total failure of the tunnel face. The model set-up assumes shear stresses on all four of the soil prisms.

$$\sigma'_{v,a} = \frac{a\,\gamma' - c'}{K_y \tan\varphi'}\left(1 - e^{-K_y \tan\varphi' \frac{z}{a}}\right) + q_0\, e^{-K_y \tan\varphi' \frac{z}{a}} \qquad \textbf{[Equation 3.1]}$$

$$a = \infty \qquad \textbf{[Equation 3.2a]}$$

$$a = R \qquad \textbf{[Equation 3.2b]}$$

$$a = R\,\frac{1}{1+\tan\theta} \qquad \textbf{[Equation 3.2c]}$$

Likewise, the maximum support pressure, i.e. the value of the lateral earth pressure coefficient K_y, is unknown. Various authors have suggested different coefficients, as indicated in Table 2. The lowest values equal the active earth pressure coefficient and the highest values assume a vertical effective stress equal to the horizontal effective stress. The background of these differences cannot be investigated due to the demarcation of this research to the four models. Based on the schematization of straight failure surfaces, as indicated in Figure 21, it has been assumed that the soil surrounding the wedge has zero lateral strain; it has therefore been assumed that a neutral earth pressure coefficient is valid.

Table 2. Lateral earth pressure coefficients within the soil silo above the TBM.

Authors	Lateral earth pressure coefficient K_y
Terzaghi and Jelinek (1954)	K_y = 1.0
Melix (1987) Anagnostou & Kovari (1994)	K_y =0.8
Jancsecz-Steiner (1994)	$K_y = K_{active}$
Kirsch & Kolymbas (2005), Janssen silo-theory (1895)	$K_y = K_{neutral}$

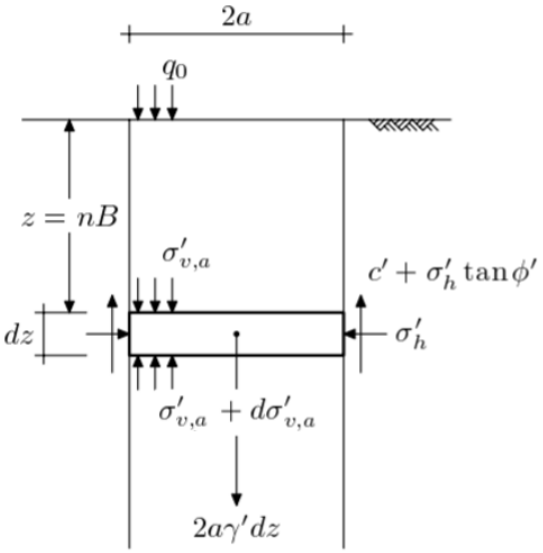

Figure 21. Forces acting on a strip of soil in an arching soil column (Broere, 1998).

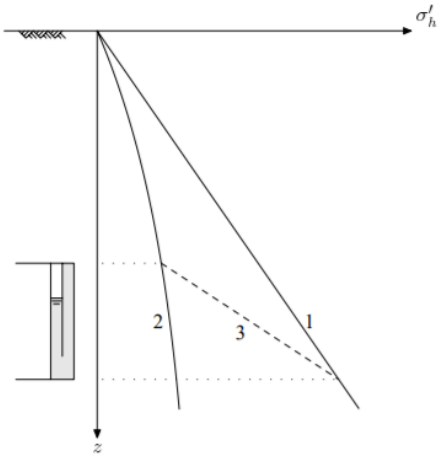

Figure 22. Possible horizontal stress distributions along tunnel face. (Broere, 1998).

3.2.2 Pressure distribution next to the wedge

In the case of (two- or three-dimensional) vertical soil arching, part of the soil load above the tunnel crown does not act as a load but is carried by the surrounding soil. This means that the pressure distribution next to the wedge is (possibly) influenced by the effect of vertical soil arching. Broere (1998) has suggested the following three possible implementations of vertical (effective) stress distribution next to a wedge (Figure 22):

1. Disregard the effect of vertical arching and assume an increasing vertical (effective) stress equal to the unit weight of the soil.
2. Continue the vertical arching stress distribution $\sigma'_{v,a}$ until the tunnel invert;
3. linear interpolation between the vertical (effective) stress, including arching at top of the wedge $\sigma'_{v,a}$, and the vertical (effective) stress without arching effects $\sigma'_{v,a}$ at bottom of the wedge.

Table 3. Lateral earth pressure coefficients acting on the vertical sides of the wedge.

Author	Lateral earth pressure coefficient K_y
Anagnostou & Kovari (1994)	K_y =0,.4
Jancsecz-Steiner (1994)	$K_y = (K_a+K_0)/2$
DIN 4126 (2013)	$K_y = K_{neutral}$

3.2.3 Horizontal soil arching

A two-dimensional face stability assessment assumes that the tunnel face wall extends to infinity, e.g. plane strain conditions. In case of a three-dimensional tunnel face stability assessment, this plane strain assumption is no longer valid, as the tunnel face has a certain length. In a three-dimensional approach, the influence of the spatial stress state of the soil therefore needs to be taken into account. These spatial stresses occur because the 'short wall' moves more than the surrounding soil, which results in friction forces along the sides of the failure mechanism. These shear stresses act in the opposite direction as the soil movement and therefore reduce the horizontal effective stress acting at the tunnel face. The determination of these shear stresses along the sides of the failure mechanism presents some difficulties due to certain unknown aspects, such as the distribution of the vertical (effective) stress next to the wedge and the choice of lateral earth pressure coefficient. Likewise, various authors have also suggested coefficients for the lateral earth pressure acting on the sides of the failure mechanism in vertical soil arching (Table 3).

3.2.4 DIN 4126/4085

The DIN model is based on the guidelines DIN 4085, 'Subsoil-Calculation of earth pressure' and DIN 4126, 'Stability analysis of diaphragm walls'. These guidelines are based on the stability of diaphragm walls for which the lateral earth pressure theory obtained by Coulomb (limit equilibrium) applies. With this theory, it is possible to determine the lateral stress on a retaining wall by assuming a failure wedge with straight slip surfaces that extends from wall toe to ground surface.

3.2.4.1 Two-dimensional approach: Homogeneous soil profile

The stability calculation for diaphragm walls is translated to tunnel face stability by 'replacing' the diaphragm wall by a TBM (Figure 8a). It should be noted that in this case, the failure wedge is still based on the presence of a diaphragm wall. Compared to a retaining wall, the tunnel face does not extend to ground surface but extends from tunnel invert to tunnel crown. The soil located between the tunnel crown and ground surface is seen as a surcharge. This 'reduced' wedge is incorporated in the calculation method by assuming an active state only at the location of the tunnel face and a neutral state for the remaining part. For tunnel face stability, it is assumed that an active state is obtained, as it is beneficial to the progress of the TBM to let the soil deform towards the face.

For a cohesionless homogeneous soil mass, the horizontal effective stress σ'_h acting at the tunnel face is determined by the product of the vertical effective stress with the active earth-pressure coefficient K_a. (Equation 3.3). In the case of a homogeneous cohesive (frictional) soil, the lateral earth pressure is reduced by the effect of cohesion (Equation 3.4). The background for this originates from the stability of diaphragm walls in the case of retention of a cohesive soil mass. For this situation, an active state involves a state of tension between the surface and a certain depth. The lateral stress acting on this zone of the 'wall' is neglected, which leads to a lower pressure acting on the tunnel face. This reduced effect due to cohesion is incorporated to the tunnel face stability assessment by an evenly distributed cohesion component over the complete tunnel face. In cases with a low overburden, this reduction effect can lead to very small -even negative- horizontal effective stresses at the top of the tunnel face. In order to counter possible weak points in the soil, a minimum value for the horizontal effective stress is used, which corresponds to a shear strength with $\varphi = 40°$ and $c = 0$ kPa.

The inclination of the sliding wedge with the horizontal is calculated using Equation 3.7. This component does not affect the horizontal effective stress distribution, but it does affect the effectiveness of the support medium (Paragraph 2.5).

$$\sigma'_h = \sigma'_v K_a \qquad \textbf{[Equation 3.3]}$$

$$\sigma'_h = \sigma'_v K_a - c K_{ac} \qquad \textbf{[Equation 3.4]}$$

$$K_a = \left[\frac{\cos(\varphi-\alpha)}{\cos\alpha\left(1+\sqrt{\frac{\sin(\varphi+\delta_a)\sin(\varphi-\beta)}{\cos(\alpha-\beta)\cos(\alpha+\delta_a)}}\right)}\right]^2 \qquad \textbf{[Equation 3.5]}$$

$$K_{ac} = \frac{2\cos(\alpha-\beta)\cdot\cos\varphi\cdot\cos(\alpha+\delta_a)}{[1+\sin(\varphi+\alpha+\delta_a-\beta)]\cos\alpha}$$ **[Equation 3.6]**

$$\theta = \varphi + \arctan\left(\frac{\cos(\varphi-\alpha)}{\sin(\varphi-\alpha)+\sqrt{\frac{\sin(\varphi+\delta_a)\cos(\alpha-\beta)}{\sin(\varphi-\beta)\cos(\alpha+\delta_a)}}}\right)$$ **[Equation 3.7]**

K_a:	active earth pressure coefficient	[-]
K_{ac}:	active earth pressure coefficient for cohesion term	[-]
α:	wall slope angle (Figure 23)	[°]
β:	ground slope angle (Figure 23)	[°]
δ_a:	slip angle (Figure 23)	[°]
θ:	inclination angle of the sliding surface with the horizontal	[°]

3.2.4.2 Two dimensional approach: simplification

The general equations for the earth pressure coefficients and sliding angle of the wedge can be simplified by assuming a horizontal ground surface (β=0), a vertical tunnel face (α=0) and a zero slip angle (δ_a=0)[16], which leads to Equations 3.8-3.10. From these equations, it can be observed that the only variable left is the internal friction angle. In Figure 24, earth pressure coefficients K_a and K_{ac} are plotted versus the angle of internal friction, illustrating that a decrease in the friction angle leads to higher earth pressure coefficient values. The earth pressure coefficient K_{ac} presents the same curve as K_a, as K_{ac} is equal to $2\sqrt{K_a}$.

$$K_a = \frac{1-\sin\varphi}{1+\sin\varphi} = \tan^2(45-\frac{\varphi}{2})$$ **[Equation 3.8]**

$$K_{ac} = \frac{2\cos\varphi}{1+\sin\varphi} = 2\sqrt{K_a}$$ **[Equation 3.9]**

$$\theta = 45^\circ + \frac{\varphi}{2}$$ **[Equation 3.10]**

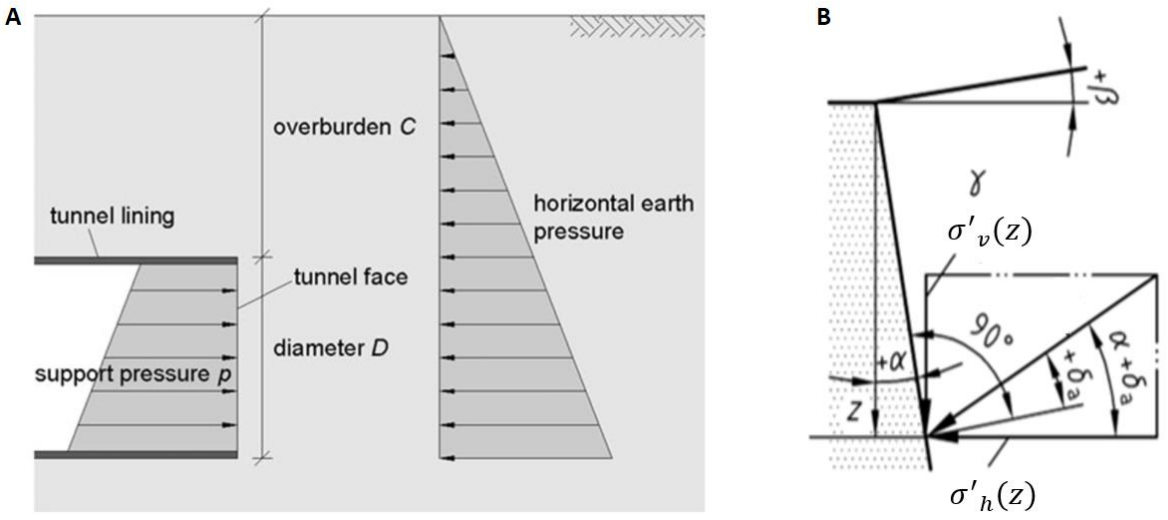

Figure 23. The two-dimensional sliding wedge model as assumed in the Din method (Idinger et al, 2010) with (a): force mechanism and (b) Sign rule for the angle used in determining the lateral stress. (Figure 4- DIN 4085:2007-10).

[16] In the DIN4126, a zero wall friction angle is assumed.

3.2.4.3 Two-dimensional approach: heterogeneous soil profile

The previous analysis, which was based on homogeneous soil profiles, can be extended by taking stratified soil profiles into account. The soil wedge (and surcharge) are therefore divided into *N* horizontal layers, with possible variable thickness d_i and constant soil properties. In this approach, the shearing stresses between the layers are disregarded so that the entire soil profile above each soil layer can be considered as a surcharge. Due to the constant soil properties for each layer, only the horizontal effective stress acting at the top and bottom of each soil layer has to be calculated (Equation 3.11)(Figure 25). This procedure leads to sharp transitions at the layer boundaries. The wedge angle with the horizontal is not constant for the complete wedge due to the varying friction angle over the tunnel face. The latter does not influence the determination of the horizontal effective stress acting at the tunnel face, but it is an important factor for the effectivity of the support pressure.

$$\sigma'_{h:i:b} = \sum \gamma'_i \, d_i \, K_{a:i} - c \, K_{ac:i} \qquad \textbf{[Equation 3.11a]}$$

$$\sigma'_{h:i:t} = \sum \gamma'_i \, d_i \, K_{a:i} - c \, K_{ac:i} \qquad \textbf{[Equation 3.11b]}$$

$\sigma'_{h:i:t}$:	horizontal effective soil stress acting at the top of layer i	[kPa]
$\sigma'_{h:i:b}$:	horizontal effective soil stress acting at the bottom of layer i	[kPa]
d_i:	thickness of layer i	[m]
$K_{a:i}, K_{ac:i}$	earth pressure coefficient of layer i	[-]

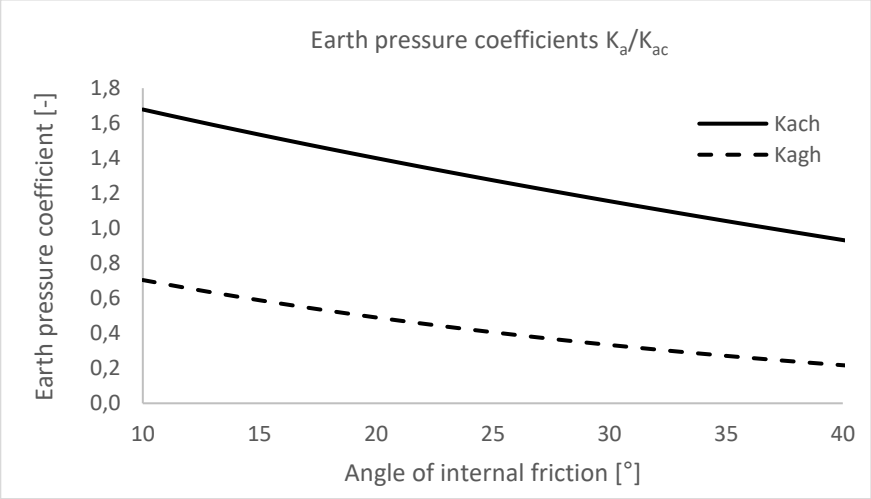

Figure 24. The active earth pressure coefficients for different internal friction angle values. Valid for soil profiles with $\alpha=\beta=\delta_a=0$.

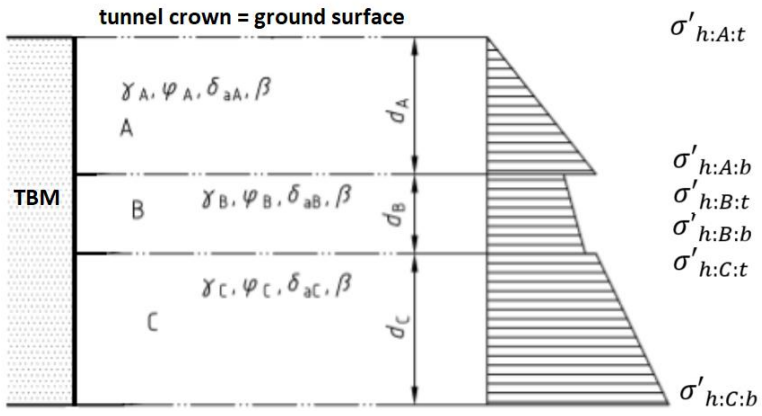

Figure 25. Model for determining the horizontal effective stresses acting at the tunnel face in the case of a stratified soil profile. For simplicity tunnel crown is equal to ground surface.

3.2.4.4 Three-dimensional approach: Horizontal soil arching

In order to incorporate the horizontal soil arching component, the DIN method assumes a three-dimensional failure body (Figure 26) suggested by Piatkowski& Kowalski (1965), in combination with shape-coefficients μ_i. These shape factors determine the horizontal effective stress, including horizontal soil arching, that is present at the tunnel face (Equation 3.12). The cohesion component assumes a shape factor μ=1 and therefore does not contribute to horizontal soil arching. The graphical representation of Equation 3.12 is presented in Figure 27, which illustrates that horizontal soil arching depends on the angle of internal friction φ and the ratio between the depth *z* and length *l* of the tunnel face. This thesis has assumed that the length of the tunnel face is equal to the diameter *D* of the tunnel.

Another way to express the reduced horizontal stress that acts on the tunnel face is the 'wall length' reduction method. The spatial stress distribution is taken into account by the introduction of a 'wall length' that is smaller than the actual 'wall length', thus reducing the lateral earth pressure per unit area of the 'wall' (Equation 3.13).[17] The failure mechanism corresponding to the latter is displayed in Figure 8.

$$\sigma'_h{}^{(r)} = [\sigma'_v K_a]\mu_a - [cK_{ac}]\mu_{ac} \quad \textbf{[Equation 3.12a]}$$

$$\mu_a = 1 - \frac{2}{\pi} \arctan\left(\frac{\varphi - z}{2\,D}\right) \quad \textbf{[Equation 3.12b]}$$

$$\mu_c = 1 \quad \textbf{[Equation 3.12c]}$$

$$\sigma'_h{}^{(r)} = \frac{\sigma'_v\, K_a\, D^{(r)}}{D} - [c\, K_{ac}] \quad \textbf{[Equation 3.13a]}$$

$$D^{(r)} = D\,\left(1 - \frac{2}{\pi} \arctan\left(\frac{\varphi - z}{2\,D}\right)\right) \quad \textbf{[Equation 3.13b]}$$

z:	depth below ground surface	[m]
D:	diameter of the tunnel	[m]
$\sigma'^{(r)}_h$:	reduced horizontal effective stress acting on the tunnel face	[kPa]
$D^{(r)}$:	reduced wall length/diameter	[m]

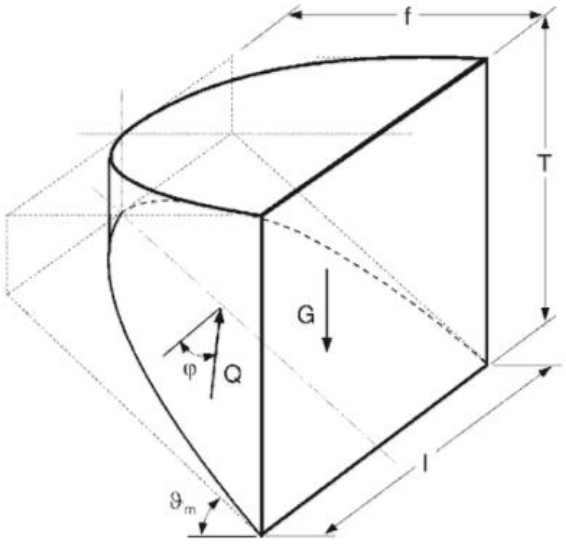

Figure 26. Three-dimensional failure body suggested by Piaskowski & Kowalewski (1965). This thesis has assumed that the length of the tunnel face is equal to the diameter of the tunnel.

[17] Note that the wall length reduction is based on $\alpha=\beta=\delta_a=0$. Following Corrigendum DIN 4085:2007-10 the cohesion component is not subjected to a wall length reduction.

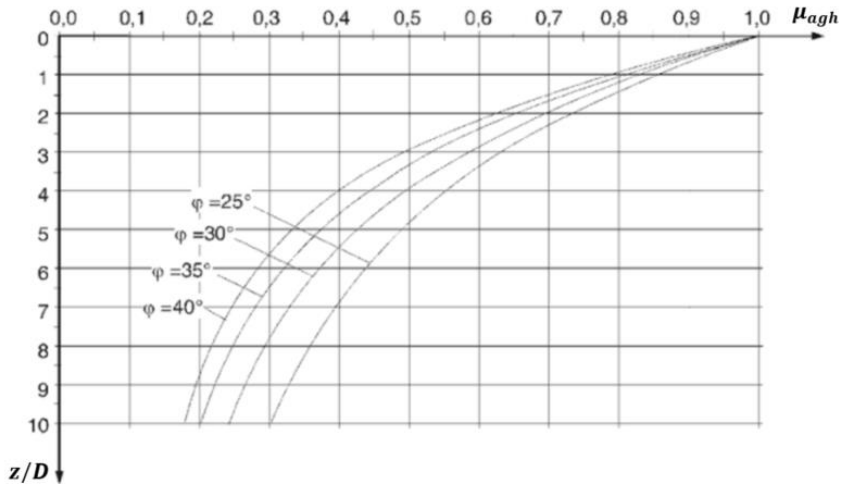

Figure 27. Wall length reduction/shape coefficients as a function of the friction angle and z/D ratio.

In order to compare between the models, it is important to determine how the horizontal effective stress reduction due to horizontal soil arching is calculated. Vertical soil arching is not taken into account in the DIN model; therefore, it is can be assumed that the vertical (effective) stress distribution next to the wedge is equal to the stress distribution in front of the tunnel face. The horizontal effective stress reduction is equal to the shear stresses acting on both sides of the failure mechanism. The reduction in horizontal effective stress can be obtained by using (1-μ_i) instead of μ_i in Equation 3.12a, which leads to

$$\sigma'_h = \sigma'_v K_a \frac{(1-\mu_i)}{2} = \frac{\sigma'_v K_a \left(\frac{2}{\pi}\arctan\left(\frac{\varphi-z}{2\cdot D}\right)\right)}{2} \qquad \textbf{[Equation 3.14]}$$

Equation 3.14 reveals that the value of the shear stress acting on one side the failure body is calculated by using an earth pressure coefficient $K_a(1-\mu_i)$ that is lower than the active earth pressure coefficient K_a. This active earth pressure coefficient $K_a(1-\mu_i)$ is a function of the internal friction angle φ and the depth/length ratio (z/D). The earth pressure coefficient is therefore plotted as a function of the friction angle for various ratios of z/D (Figure 28). Figure 28 illustrates that the earth pressure coefficient decreases with an increasing friction angle (φ >15°) and a decreasing z/D ratio. In addition, from this friction angle on, the curves for the different z/D ratio's follow the shape of the active earth pressure coefficient. In case of high z/D ratio's (> 8.5), the active earth pressure coefficient is approached.

An important aspect to note is that the horizontal soil arching component is based on the stability analysis of the diaphragm walls. As described, the failure wedge of a diaphragm wall extends from wall toe to ground surface with no ground cover on top, while in the case of a tunnel face stability assessment, it is assumed that an active state is only valid at the location of the tunnel face. This means that horizontal soil arching only occurs at the location of the tunnel face. Due to this, the depth z in Equations 3.12b/3.13b has to be modified for the depth z below the tunnel crown (z*) (Equation 3.15). As the width L of the failure wedge is constant and equal to the diameter D, this means that the z/D ratio is equal to zero at the tunnel crown and at tunnel invert equal to unity[18]. From the z/D ratio (=1,0) displayed in Figure 28, it results that this leads to a small reduction in the horizontal effective stress acting at the tunnel face. In the case study analysis, the effect of this modification on the minimum support pressure has been determined.

$$\mu_a = 1 - \frac{2}{\pi}\arctan\left(\frac{\varphi-z^*}{2\cdot D}\right) \qquad \textbf{[Equation 3.15a]}$$

$$D^{(r)} = D\left(1 - \frac{2}{\pi}\arctan\left(\frac{\varphi-z^*}{2\cdot D}\right)\right) \qquad \textbf{[Equation 3.15b]}$$

[18] This is based on a failure body with straight slip surfaces and not the failure body shown in figure 28.

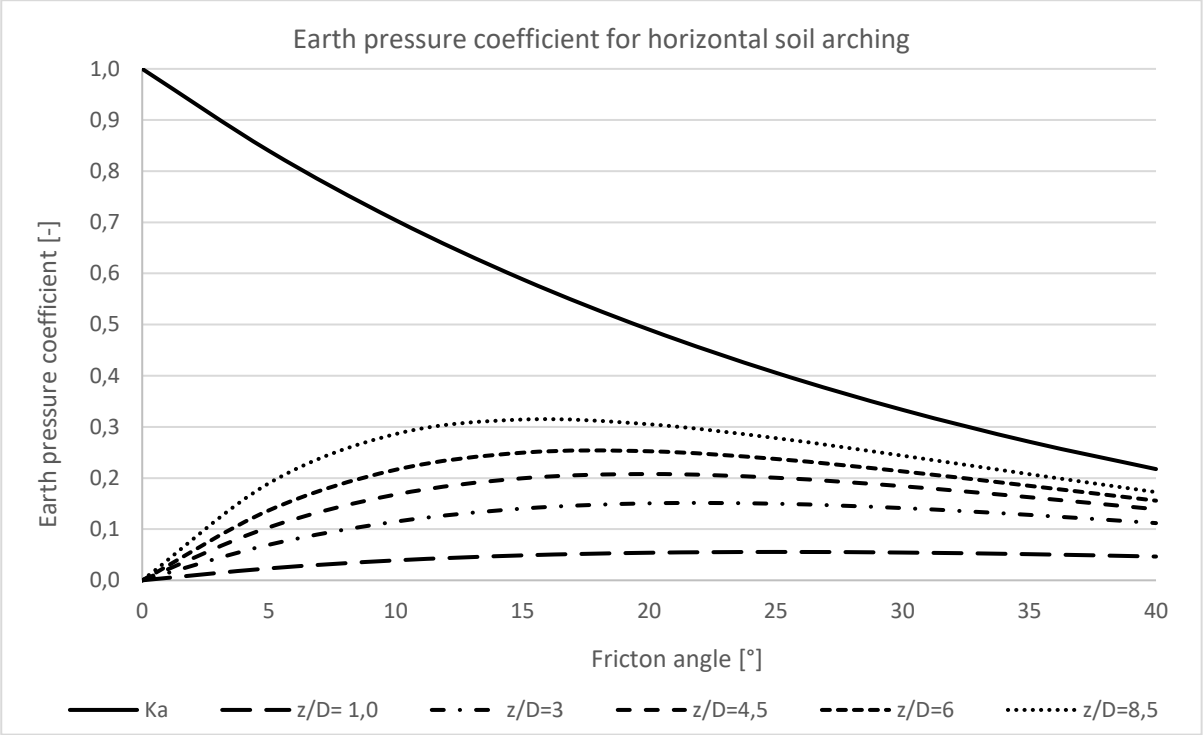

Figure 28. The earth pressure coefficient used to determine the reduction in horizontal stress due to the counteracting shear stresses, as a function of the friction angle and z/D ratio.

3.2.4.5 Two/Three-dimensional approach: Pressure transfer mechanism

The pressure transfer mechanism adopted by the DIN model depends on the penetration distance e of the slurry, which is a function of the characteristic grain size d_{10}, excess pressure Δs and yield strength of the slurry. In the case of a negligible penetration distance, it is assumed that the support pressure is transferred to the soil skeleton by a membrane. For cases with a higher penetration distance, a penetration zone applies and the effect of slurry infiltration should be taken into account. The approach adopted by the DIN model in order to take the effect of slurry penetration for a homogeneous soil profile into account is described in Paragraph 2.5. In this case, the wedge angle with the horizontal is the same for the entire tunnel face and therefore the amount of slurry that penetrates outside the failure wedge zone is easily determined. In the case of a heterogeneous soil profile, this is more complicated, as the wedge angle with the horizontal varies per layer. The way to cope with this topic is described in Paragraph 3.4.8 (test series 6).

3.2.4.6 Two/Three-dimensional approach: Effect of an additional surcharge q_o on ground surface

At the eastern entrance zone, where a small soil cover is present, an additional surcharge is required to counteract the buoyancy of the tunnel and the minimum face support pressure. The second part of this chapter, which focusses on the practical implementation, discusses the effect of this additional surcharge on the subsoil. For this practical component, it is necessary to know how an additional load on the ground surface translates to a horizontal effective stress acting on the tunnel face. Following DIN 4085/4126, a surface load q is translated to the tunnel face by multiplying the load q_o by an earth pressure coefficient K_{ap} (Equation 3.16). By assuming $\alpha = \beta = 0$, this earth pressure coefficient K_{ap} is equal to the active earth pressure coefficient (Equation 3.17).

$$\sigma'_{h:q} = q_o K_{ap} \qquad \textbf{[Equation 3.16]}$$

$$K_{ap} = \frac{\cos\alpha \cos\beta}{\cos(\alpha-\beta)} K_a = K_a \qquad \textbf{[Equation 3.17]}$$

3.2.4.7 Two/Three-dimensional approach: Vertical soil arching

The effect of vertical soil arching has not been incorporated into the original DIN model, as above the diaphragm wall no soil cover is present where soil arching could develop. This method is translated to tunnel face stability assessment by maintaining the failure wedge which extends from tunnel invert to tunnel crown, but with the assumption that an active state is only valid at the location at tunnel face. Due to this hypothesis, it can be assumed that the soil profile above the TBM stays within place and acts as a surcharge. This means that when this model has translated to tunnel face stability, it is possible to implement the effect of vertical soil arching. Note that this schematisation of the failure wedge supports the modification of the horizontal soil arching component discussed in the previous paragraph.

3.2.4.8 Summary

Based on the theoretical analysis, the following conclusions can be reached:

- In the two-dimensional plane strain approach, the tunnel face can be translated into a sliding wedge extending from tunnel invert to ground surface. An active state is only assumed at the location of the TBM.
- In the case of a homogeneous soil profile, the horizontal effective stress acting at the tunnel face is determined by the multiplication of the vertical effective stress with the active earth pressure coefficient. In the case of cohesive soil, the horizontal effective stress that acts on the tunnel face is reduced by the effect of cohesion.
- In the three-dimensional approach, the plane strain assumptions are no longer valid. This approach takes the effect of the spatial stress distribution into account. This result in shear stresses acting on the sides of the failure model, which reduces the horizontal effective stress acting on the tunnel face. This reduced horizontal effective stress is calculated by using shape coefficients which are a function of the friction angle and depth/length z/D ratio.
- Both in the 2D and the 3D models, a stratified soil profile can be taken into account by neglecting the shearing stresses between the different soil layers. The soil profile can, therefore, be divided into N different layers, possibly with variable thickness, in which the soil properties are constant.
- In the case of a stratified soil profile, the wedge angle ϑ with the horizontal is not constant, due to the different friction angle for each layer. This wedge angle is not an important parameter for the calculation of the horizontal effective stress acting on the tunnel face, but it is an important parameter for the effectiveness of the support pressure (paragraph 2.5).
- In both the 2D and 3D models, the effect of vertical soil arching has not been incorporated into the original DIN model. The reason for this is that the original model assumes a failure wedge that extends from tunnel invert to ground surface, so no soil cover is present above this failure wedge where vertical soil arching could develop. Due to the assumption of a neutral state in the soil profile above the TBM, no lateral strain occurs and thus the soil volume stays within place. Therefore, it can be assumed that the soil profile above the TBM acts as a surcharge and vertical soil arching can be implemented within this zone. This implementation is further discussed in test series 5.
- The load from the additional surcharge q_o is transferred to the tunnel face by multiplying the increase in vertical effective stress by an active earth pressure coefficient. Note that for this part, drained behaviour is assumed. The effect of consolidation is discussed in paragraph 3.5.
- The DIN model takes the effect of slurry penetration/infiltration into account (paragraph 2.5).

Based on the results of the theoretical analysis, the effect of the following modifications/extensions of the original DIN model have been investigated using case studies:

- What happens to the minimum support pressure when working with the assumption that, in the case of a 3-dimensional approach (Equation 3.15), the depth z extends from tunnel crown (**Test series 4**)?
- What happens to the minimum support pressure if two-/three- dimensional soil arching is taken into account (**Test series 5**)?

3.2.5 Ruse-Vermeer model

3.2.5.1 Three-dimensional approach: Homogeneous soil conditions

The Ruse-Vermeer model is based on a single equation (Equation 3.18), consisting of stability numbers to calculate the horizontal effective stress acting on the tunnel face. The stability numbers are obtained by executing many three-dimensional finite element method (FEM) calculations on dry homogeneous sand. In this FEM mesh, the following boundary conditions have been applied: the ground surface is free to displace, the side surfaces of the mesh have roller supports and the base of the mesh is fixed. The initial stress distribution is geostatic, based on a neutral earth pressure coefficient. The minimum support pressure is determined by a step-wise reduction of the support pressure, e.g. a limit load analysis.

The Ruse-Vermeer model assumes that for friction angles φ >20°, the soil weight of the overburden may be neglected. This is also demonstrated in Equation 3.18, where the vertical effective is calculated by multiplying the effective unit weight of the soil with the diameter of the tunnel. This set up leads to a constant horizontal effective stress acting on the tunnel face.

Compared to the other two models, the Ruse-Vermeer model is based on dry soil conditions, e.g. the equilibrium pore water pressure is zero. Despite neglecting the weight of the soil overburden, the hydrostatic pore water pressure distribution is taken into account in the calculation of the minimum support pressure in combination with a safety factor γ_{u1} equal to unity (Equation 3.19).

In this model, the safety factor regarding the horizontal effective stress is incorporated within the calculation of σ'_h; it is therefore possible to assume that γ_h is also equal to unity. In the subsequent paragraphs, the derivation of the three stability numbers N_γ, N_c and N_q is discussed. It should be noted that the determination of the stability numbers is based on homogeneous dry/drained soil conditions and is only valid for friction angles φ > 20° in combination with an overburden height *C* greater than or equal to the diameter of the tunnel (*C*/*D* >1).

$$\sigma'_h = q_o\, N_q \;+\; \gamma'_{sat:H}\; D\, N_\gamma - \left(\frac{1}{\gamma_{\varphi' c'}}\right) c'\, N_c \qquad \textbf{[Equation 3.18]}$$

$$p_{min:d} = \gamma_h\; \sigma'_h + \gamma_{u1}\, u_1 = \sigma'_h + u_1 \qquad \textbf{[Equation 3.19]}$$

Soil weight stability number N_γ

One of the most important assumption in the Ruse Vermeer model is that for friction angles larger than 20° and *C*/*D* >1, the stress arch carries the ground cover regardless of the magnitude of its thickness. This in based on a study by Vermeer and Ruse (2001) that considers non-cohesive dry ground and no surface load, where the groundcover has been varied systematically to assess its influence on the failure pressure.

The effect of soil arching for a tunnel (*C*/*D* = 5) in non-cohesive dry soil with a varying friction angle is illustrated in Figure 29. In the case of soil with a friction angle equal to zero (Figure 29a), the principal stresses rotate around the tunnel face and they all have the same size, which indicates a high support pressure. In the second case (Figure 29b), the friction angle is increased to 20°; it can be seen that the principal stresses around the tunnel face decrease. The arching effect is extremely clear in the last case. The analysis resulted in that the supporting pressure is nearly equal to zero and a strong stress arch is observed directly between the top and the bottom of the tunnel.

This arching effect for varying friction angles is also demonstrated by the corresponding failure patterns in Figure 29d-f, which illustrates that with an increasing friction angle, the failure zone decreases to a relatively small zone at the front of the tunnel face (Ruse and Vermeer, 2002). Due to the effect of soil arching, the soil weight stability number is only dependent on the friction angle and not on the groundcover (Equation 3.20).

$$N_\gamma = \frac{1}{9 \cdot \tan \varphi_d} - 0{,}05 \qquad \phi' > 20\,° \text{ and } \mathrm{C/D} > 1 \qquad \textbf{[Equation 3.20]}$$

Cohesion stability number *Nc*

Unlike the other stability numbers, the cohesion stability number N_c has been derived theoretically (Equation 3.21).

$$N_c = \cot \varphi_d \qquad \textbf{[Equation 3.21]}$$

Surface load stability number *Nq*

The influence of an additional surcharge q_o on the surface is determined by performing a series of 24 finite element analyses with different uniformly distributed surface loads $\mathbf{q_o}$. The analyses revealed that, due to the effect of soil arching, all surface loads can be carried for friction angles larger than φ = 25°, regardless of the groundcover. For friction angles lower than 25°, the stability term N_q (Equation 3.22) is equal to zero when the groundcover is twice the tunnel diameter. For other cases, the surcharge stability number is equal to $Nq \approx 0.01$.

$$N_q = 0 \;\; for\, \varphi > 25° \;\; \& \;\; \varphi < \; 25° \, with \, \frac{C}{D} \geq 2 \qquad \textbf{[Equation 3.22a]}$$

$$N_q = 0.01 \;\; for \;\; \varphi < \; 25° \, with \, \frac{C}{D} < 2 \qquad \textbf{[Equation 3.22b]}$$

3.2.5.2 Three-dimensional approach: Effect of an additional surcharge q_o on surface

The effect of an additional surcharge q_o on the surface in the tunnel face stability calculation highly depends on the friction angle of the soil. In the case of a friction angle of around φ = 20-25°, only 1% of the additional load on the ground surface affects the horizontal effective stress acting on the tunnel face. For friction angles larger than φ = 25°, the complete load on the ground surface is carried by vertical soil arching. As this method is based on drained soil behaviour, the influence of consolidation cannot be incorporated.

3.2.5.3 Three-dimensional approach: Pressure transfer mechanism

The Ruse-Vermeer model is based on a limit load analysis and the minimum support pressure is determined by using a load reduction method, e.g. the support pressure is reduced until the collapse of the tunnel face. This method assumes that the support pressure is transferred to the soil skeleton by a membrane.

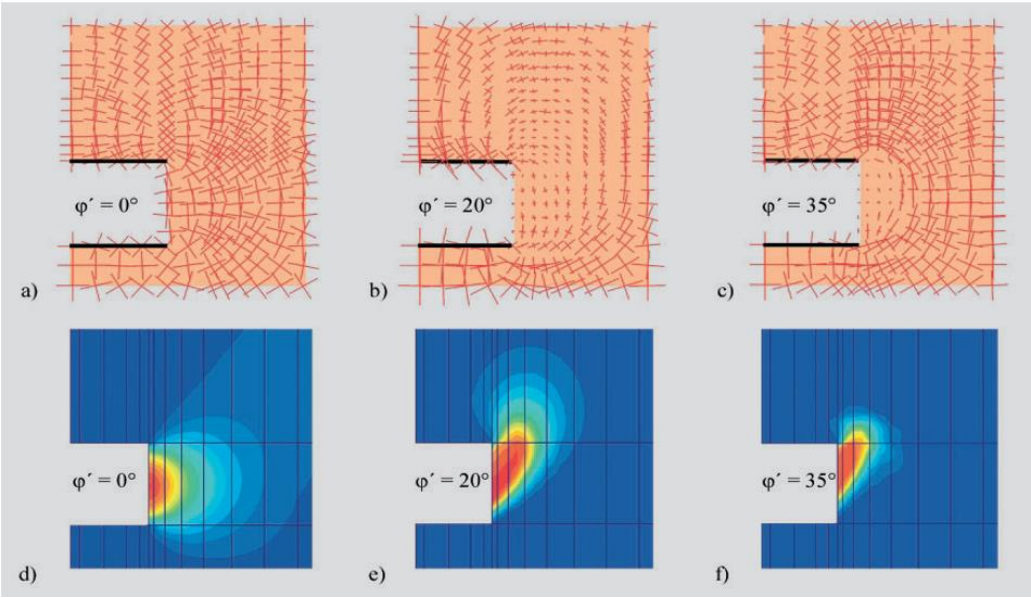

Figure 29. Principal stresses (a - c) and incremental displacements (d - f) at failure. Close-up around the face for a tunnel with H/D = 5. (Increasing displacements at failure are shown in graded shades from blue to red) (Ruse and Vermeer, 2002).

3.2.5.4 Three-dimensional approach: Heterogeneous soil conditions

This model cannot be directly transformed to a heterogeneous layered soil profile like the DIN model, as the development of soil arching is highly influenced by the friction angle of the soil above and in front of the TBM. In the case of a layered soil profile, the stability numbers are calculated based on the soil type located at the tunnel face, while a different soil type is possibly present at the top of the TBM. In addition, the stability numbers are obtained from homogeneous soil conditions. The most erroneous interpretation occurs when soil layers with a high friction angle (φ >20°) are present at the tunnel face, while above the TBM soil layers with a low friction angle (φ <20°) are present. By simply using the equations, it is possible to assume that soil arching occurs and this results in an overly low support pressure. This means that, in the case of heterogeneous soil profiles, wrong assumptions can be made and therefore this method must be used with great caution.

Another important aspect to take into account is that, in the case of homogeneous soil, this model assumes a constant support pressure over the complete tunnel face. This aspect leads to a transformation of the diameter D (Equation 3.20) to the depth of the soil layer boundaries below the tunnel crown.

The applicability of the Ruse-Vermeer method for soil profiles with friction angles lower than twenty degrees will be investigated by means of a case-study analysis. As this analysis relates to different parts of this model, this analysis is split into two parts. In the first part of this research, the minimum support pressure is calculated, for soil profiles with a friction angle φ>20, by taking the full weight of the overburden into account. In the second part, the minimum support pressure is recalculated by reducing the friction angle below twenty degrees.

3.2.5.5 Summary

- The Ruse-Vermeer model is based on a limit stress method. The is applicable for homogeneous (drained) soil profiles with a friction angle higher than φ = 20° and $C/D \geq 1$. This means that the soil weight of the ground cover is neglected within the calculation of the minimum support pressure.
- This model takes a constant vertical effective stress into account which is equal to the vertical effective stress at tunnel invert.
- The horizontal effective stress acting at the tunnel face is calculated by the multiplication of the constant vertical effective stress with the soil weight stability number. In the case of cohesive soil, the horizontal effective stress that acts on the tunnel face is reduced by the effect of cohesion. In addition, the minimum support pressure is increased by the effect of the additional surcharge q_o on ground surface. Note that the influence of the latter is negligible.
- The Ruse-Vermeer model takes both horizontal and vertical soil arching into account. Due to the numerical background of this calculation method, these aspects cannot be analysed further.
- In heterogeneous soil profiles, this method can lead to wrong interpretations and must be used with great caution.
- The Ruse-Vermeer model does not take the effect of slurry penetration/infiltration into account, as this method is a limit stress method and therefore no failure mechanism is assumed.

Based on the results of the theoretical analysis, the effect of the following modifications/extensions of the original Ruse-Vermeer model have been investigated using case studies:

- What happens with the minimum support pressure in the case of soil profiles with ϕ > 20° if vertical soil arching is neglected and the full weight of the overburden is considered **(Test series 2)**?
- What happens with the minimum support pressure in the case of soil profiles with ϕ < 20° if vertical soil arching is neglected and the full weight of the overburden is considered **(Test series 3)**?

3.2.6 Jancsecz & Steiner

3.2.6.1 Three dimensional approach: Homogeneous soil conditions

The Jancsecz and Steiner model (Figure 8), also called wedge model, consists of a sliding wedge in front of the tunnel face that is loaded by a rectangular prism stretching up to surface level. The circular borefront is approximated by a squared borefront, with sides equal to the diameter of the tunnel. The bottom surface of the soil prism is equal to the top surface of the wedge and the height of the soil prism is equal to the height of the overburden. The following forces act on the wedge (Figure 30):[19]

- self-weight of the wedge G_w;
- top load from soil prism G_s at interface CBEF;
- shear force R and normal forces N along the slanted failure plane ADEF;
- shear force T acting on triangular sliding planes ABE and DCF;
- slurry support pressure S; and
- the pore water pressure W (which is disregarded in this analysis).

The resulting horizontal wedge force E (horizontal effective force) for a given wedge angle ϑ is determined by an equilibrium analysis of the failure wedge (Equation 3.23). The full derivation is presented in Annex 2. The critical sliding angle $\boldsymbol{\theta}_{crt}$ is the angle that corresponds to the maximum value of the horizontal wedge force E. The Jancsecz-Steiner wedge model includes both vertical and horizontal soil arching.

$$E = -\frac{\zeta_-(G_S+G_W)+(K+2T)}{\zeta_+} \qquad \textbf{[Equation 3.23a]}$$

$$\zeta_- = \tan\varphi\cos\theta - \sin\theta \qquad \textbf{[Equation 3.23b]}$$

$$\zeta_+ = \tan\varphi\sin\theta + \cos\theta \qquad \textbf{[Equation 3.23c]}$$

3.2.6.2 Three-dimensional approach: Vertical soil arching

The inclusion of vertical soil arching within the Jancsecz-Steiner model results in a reduction of the top load G_s acting at the top of the wedge. This reduced soil load is calculated using Equations 3.1 and 3.2. Jancsecz-Steiner (1994) requires that vertical soil arching can only be included in cases in which the height of the overburden is twice the diameter of the tunnel (C/D >2); however, Anagnostou & Kovári (1994) have suggested always using vertical soil arching despite the height of the overburden.

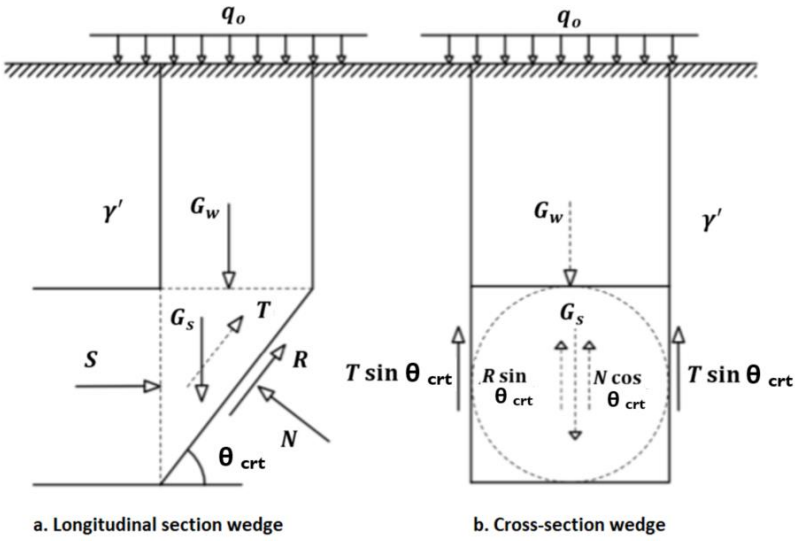

Figure 30. The static force mechanism of the wedge model used by Jancsecz and Steiner.

[19] The equations are presented in Annex 2.

Vertical soil arching can be implemented by means of two-dimensional or three-dimensional analysis. In a two-dimensional analysis, it is assumed that the counteracting shear stresses act on two sides of the soil prism and in a three-dimensional analysis, these friction forces act on all four sides of the soil prism. In their wedge model, Jancsecz and Steiner (1994) have assumed that the shear stresses act on all four silo boundaries; therefore, a three-dimensional vertical soil arching analysis is valid. The shear stresses are calculated by using an active earth pressure coefficient, as detailed in Table 2.

3.2.6.3 Three-dimensional approach: Horizontal soil arching component

The Jancsecz-Steiner model includes the effect of horizontal soil arching by taking the influence of the spatial stress state of the soil into account. These spatial stresses occur because the wedge moves more than the surrounding soil, which results in friction forces along the sides of the wedge. These forces reduce the horizontal effective stresses acting on the tunnel face.

The soil is idealised as a rigid-plastic material, following the Mohr-Coulomb condition, with cohesion c and angle of internal friction φ. The shear force T acting on the wedge sides can therefore be separated into a cohesion and friction component. The cohesion force is calculated by multiplying the cohesion with the area of the failure surface. Compared to the cohesion component, the determination of the friction component faces some difficulties due to certain unknown aspects such as the distribution of the vertical effective stress next to the wedge and the choice of lateral earth pressure coefficient. In this model, it is assumed that the vertical effective stress distribution next to the wedge does not include any arching effects. The lateral earth pressure coefficient used to calculate the horizontal effective stress is equal to the average of the neutral and active earth pressure coefficient (Table 3). The friction force is calculated by multiplying the shear stress with the area of the failure surface. The combination of these two force components leads to the shear forces acting on the triangular planes of the wedge (Equation 3.24).

$$T = \frac{D^2 \cot\theta}{2}\left(c + K_y\,\overline{\sigma'_v}\tan\varphi\right) \qquad \textbf{[Equation 3.24]}$$

3.2.6.4 Three-dimensional approach: Three-dimensional earth pressure coefficients

The wedge model illustrated in Figure 30 is a time-consuming analytical method for determining the separate forces and subsequently finding the wedge angle with the horizontal for which the wedge force E is maximal. In addition, in case of a heterogeneous soil profile, the required time will be even more increased. This method can therefore be simplified by using a three-dimensional earth pressure coefficient.[20] This coefficient is derived from an equilibrium analysis of the lower part of the wedge failure mechanism for a given critical wedge angle. The horizontal effective stress acting on the tunnel face is determined by multiplying the vertical effective stress distribution in front of the tunnel face with this coefficient (Equation 3.25-3.29).

By considering this three-dimensional earth pressure coefficient KA_{3D} further, it can be noted that this factor depends on the angle β , the friction angle φ, the earth pressure coefficient K_y, and the geometry parameter *C*/*D*. The effect of each of these parameters on the coefficient KA_{3D} is determined by performing a sensitivity analysis whose results are presented in Figure 31. From this analysis, it is possible to observe that the *C*/*D* ratio influences the α-factor and the K_{A3D} coefficient. It should be noted that the K_{A3D} coefficient is independent of the *C*/*D* ratio for ratios greater than unity. It can therefore be concluded that the geometry factors have a negligible influence on the resulting wedge force. The angle of internal friction influences both the angle β and earth pressure coefficient K_y (for friction angles φ > 15°). The graph in the upper left corner demonstrates that the three-dimensional earth pressure coefficient KA_{3D} is only affected by the friction angle (*C*/*D* >1).

$$\sigma'_h = \sigma'_v\,K_{a3D} \qquad \textbf{[Equation 3.25]}$$

[20] In this thesis we call this method the K_{A3D} model.

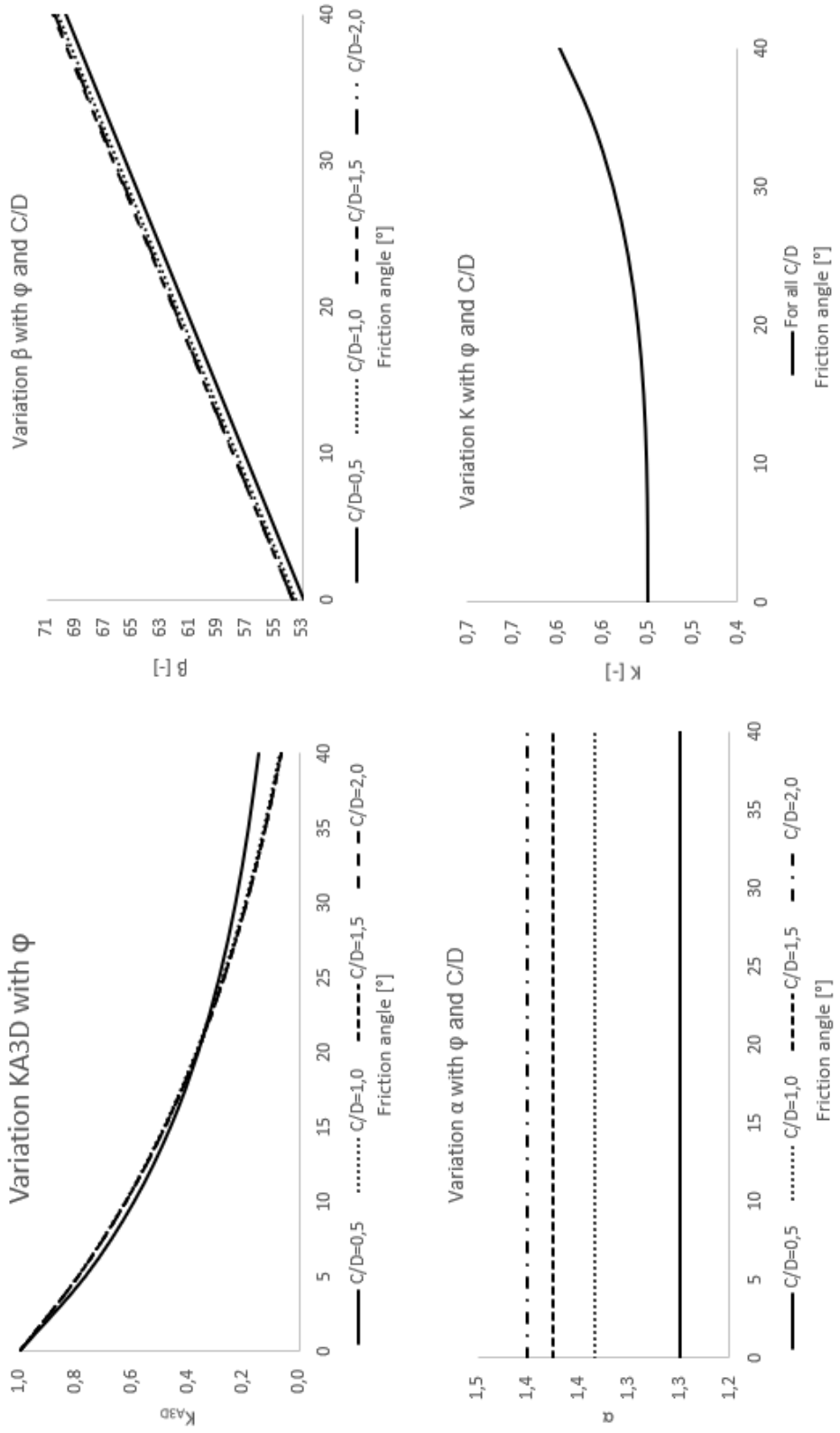

Figure 31. Sensitivity analysis parameter: Earth pressure coefficient K_{A3D}.

An important aspect to note is that this three-dimensional earth pressure coefficient has been determined from an equilibrium analysis of the lower part of the wedge. This means that only the horizontal soil arching component has been taken into account. This model can be extended by incorporating vertical soil arching through a reduced value of the vertical effective stress. It should be noted that this leads to a reduction of the horizontal soil arching component, as the earth pressure coefficient K_{A3D} is multiplied by a reduced value of the vertical effective stress. In the combination of both soil arching components, each separate component cannot reach its full potential, as only the vertical effective stress distribution in front of the tunnel face is used, while the horizontal soil arching is based on the vertical effective stress distribution next to the wedge.

$$K_{a3D} = \frac{\sin\beta\cos\beta - cos^2\beta\tan\varphi - \frac{Ka}{1,5}\cos\beta\tan\varphi}{\cos\beta\sin\beta + \tan\varphi\, sin^2\beta} \quad \textbf{[Equation 3.26]}$$

$$K_y = \frac{1-\sin\varphi + tan^2\left(45-\frac{\varphi}{2}\right)}{2} \quad \textbf{[Equation 3.27]}$$

$$\alpha = \frac{1+3\ C/D}{1+2\ c/D} \quad \textbf{[Equation 3.28]}$$

$$\beta = -0,6\left(\frac{C}{D}\right)^2 + \frac{2C}{D} + 0,42\varphi + 52,1 \quad \textbf{[Equation 3.29]}$$

3.2.6.5 Three-dimensional approach: Pressure transfer mechanism

The Jancsecz-Steiner model assumes that the support pressure mechanism is transferred to the soil skeleton by an infinitely small membrane. This is a valid assumption in the case of fine-grained soils, but for coarser soils the effect of slurry infiltration should be analysed.

3.2.6.6 Three-dimensional approach: Heterogeneous soil conditions

Due to the simplicity of the K_{A3D} model, it is possible to transform this model to include heterogeneous soil conditions. As in the DIN model, the soil wedge and surcharge are divided into *N* horizontal layers with a possible variable thickness d_i and constant soil properties. In this approach, the shear stresses between the layers are disregarded and therefore the entire soil profile above each soil layer can be considered a surcharge. For each soil layer, the vertical effective stress at the top and bottom is calculated and multiplied by the three-dimensional earth pressure coefficient K_{A3D} (Equation 3.25-3.29).

3.2.6.7 Three-dimensional approach: Effect of an additional surcharge q_o on ground surface

At the eastern entrance zone, where a small soil cover is present, an additional surcharge is required to counteract the buoyancy of the tunnel and face support pressure. The second part of this chapter, which focusses on the practical implementation, discusses the effect of this additional surcharge on the subsoil. For this practical component, it is necessary to know how an additional load on the ground surface translates to a horizontal effective stress acting on the tunnel face. Following the Jancsecz-Steiner model, a load on the ground surface has been multiplied by the same earth pressure coefficient K_{A3D}, so the full load of the additional surcharge contributes to the horizontal effective stress at the tunnel face.

3.2.6.8 Summary

The Jancsecz-Steiner model consists of two different approaches in order to calculate the minimum support pressure acting at the tunnel face. The first approach, also called wedge model, assumes a three dimensional failure wedge in front of the tunnel face. The minimum support pressure is calculated with equation 3.23, in which the forces are calculated based on the critical wedge angle. It can be concluded that this is an iterative and time-consuming method. The second approach is based on a three dimensional earth pressure coefficient, also called K_{A3D} model, which is derived based on a equilibrium analysis of the three dimensional failure wedge. The minimum support pressure is calculated by the multiplication of this three dimensional earth pressure component with the vertical effective stress in front of the tunnel face. In contrast to the first approach, this method requires less time.

Based on the theoretical analysis, the following conclusions can be drawn:

- **Both models:** The soil profile can be translated into a sliding wedge extending from tunnel invert to tunnel crown. The vertical (effective) stress resulting from the overburden acts as a surcharge.
- **Both models:** The implementation of vertical soil arching leads to a lower vertical (effective) stress acting at tunnel crown.
- **Both models:** The load from the additional surcharge q_o is fully transferred to the tunnel face.
- **Both models:** The effect of slurry infiltration is not taken into account, as the model assumes a negligible penetration distance (filter cake).
- **Wedge model:** The implementation of vertical soil arching leads to a reduction of the force G_s.
- **Wedge model:** The method assumes a vertical (effective) stress next to wedge without the effects of arching. This means that not the same pressure distribution is used for both soil arching components.
- **Wedge model:** Horizontal soil arching is implemented within the model by shear forces T which act on the triangular sides of the failure wedge.
- **KA3D model:** This 3D earth pressure coefficient depends only on the friction angle. With an increasing friction angle, the coefficient K_{A3D} decreases.
- **KA3D model:** Only the effect of horizontal soil arching is included in the three-dimensional earth pressure coefficient. Vertical soil profile is taken into account by a reduced vertical (effective) stress distribution in front of the tunnel face. This method only takes the vertical (effective) stress distribution in front of the tunnel face into account. This means that a reduction in this pressure distribution due to vertical soil arching also affects the horizontal soil arching component.
- **KA3D model:** a stratified soil profile can be taken into account by neglecting the shearing stresses between the different soil layers. The soil profile can therefore be divided into N different layers, possibly with variable thickness, in which the soil properties are constant.

Based on the results of the theoretical analysis, the effect of the following modifications/extensions of the original Jancsecz-Steiner model are investigated using case studies:

- What is the reduction in the support pressure effectiveness when slurry infiltration is taken into account **(Series 6)**?

3.2.7 Model coefficient K_m

The previous paragraph detailed the theoretical analysis into the background of the DIN model, the Ruse-Vermeer model and the Jancsecz-Steiner model. The latter model can be further subdivided into the wedge model and K_{A3D} model. The case study analysis is largely based on the K_{A3D} model; hence, the K_{A3D} model is meant when the Jancsecz-Steiner model is mentioned. The minimum support pressure required at the tunnel face for all three models is calculated using Equation 2.5. In the case of a soil with zero cohesion, the horizontal effective stress acting on the tunnel face can be further subdivided in the multiplication of the vertical effective stress with an 'model coefficient' K_m (Equation 3.30). This model coefficient K_m determines likewise the earth pressure coefficient the ratio of the horizontal and vertical effective stress.

The value of this model coefficient per model is obtained by equating the cohesion term to zero within the equation regarding the horizontal effective stress acting at the tunnel face. For the DIN-model equation 3.13a is used and it results that the model coefficient is equal to the multiplication of the active earth pressure coefficient with the wall length reduction component (Equation 3.30b). For the Ruse-Vermeer model equation 3.18 and this leads to a model coefficient equal to the stability number N_γ (Equation 3.30c). For the Jancsecz-Steiner model equation 3.25 is used and it immediately follows that the model coefficient is equal to $K_{A3D.}$

$$p_{min:d} = \gamma_h \, \sigma'_h + \gamma_{u1} \, u_1 = \gamma_h \, (\sigma'_v \, K) + \gamma_{u1} \, u_1 \qquad \textbf{[Equation 3.30a]}$$

$$\sigma'_h{}^{(r)} = \frac{\sigma'_v\ K_a\ D^{(r)}}{D} - [c\ K_{ac}] = \sigma'_v\ K_a\ \frac{D^{(r)}}{D} \rightarrow \boldsymbol{K = K_a\ \frac{D^{(r)}}{D}}$$ **[Equation 3.30b]**

$$\sigma'_h = q\ N_q + \gamma'_{sat:H}\ D\ N_\gamma - \left(\frac{1}{\gamma_{\varphi' c'}}\right) c' N_c = \gamma'_{sat:H}\ D\ N_\gamma \rightarrow \boldsymbol{K = N_\gamma}$$ **[Equation 3.30c]**

$$\sigma'_h = \sigma'_v\ K_{a3D} \rightarrow \boldsymbol{K = K_{A3D}}$$ **[Equation 3.30d]**

The model coefficient for each model[21] for **c=0** as a function of the friction angle and *C/D* ratio (>1) are presented in Figure 32. This graph indicates that the value of the model coefficient in the case of the DIN model depends on both the *C/D* ratio and the friction angle. The model coefficients of the other two models are only a function of the friction angle.

In Figure 32, the active and neutral earth pressure coefficients are also plotted. In case of the Jancsecz-Steiner model, the model coefficient K_m lies between the active and neutral earth pressure coefficient between (12°> φ <17°) and thereafter the model coefficient drops below the active earth pressure coefficient. In case of the Ruse-Vermeer model, the model coefficient K_m is lower than the active earth pressure coefficients for friction angles larger than 17 degrees. The model coefficient for the DIN model for friction angles higher than 20° is situated between the active and neutral earth pressure coefficient.

By using the model coefficients indicated within Figure 32, the difference in minimum support pressure between the models becomes clear. It can be seen that the Ruse-Vermeer model will results in the lowest minimum support pressure and the DIN-model in the highest support pressure. In addition, the difference between the Jancsecz-Steiner model and the DIN-model depends on the *C/D* ratio.

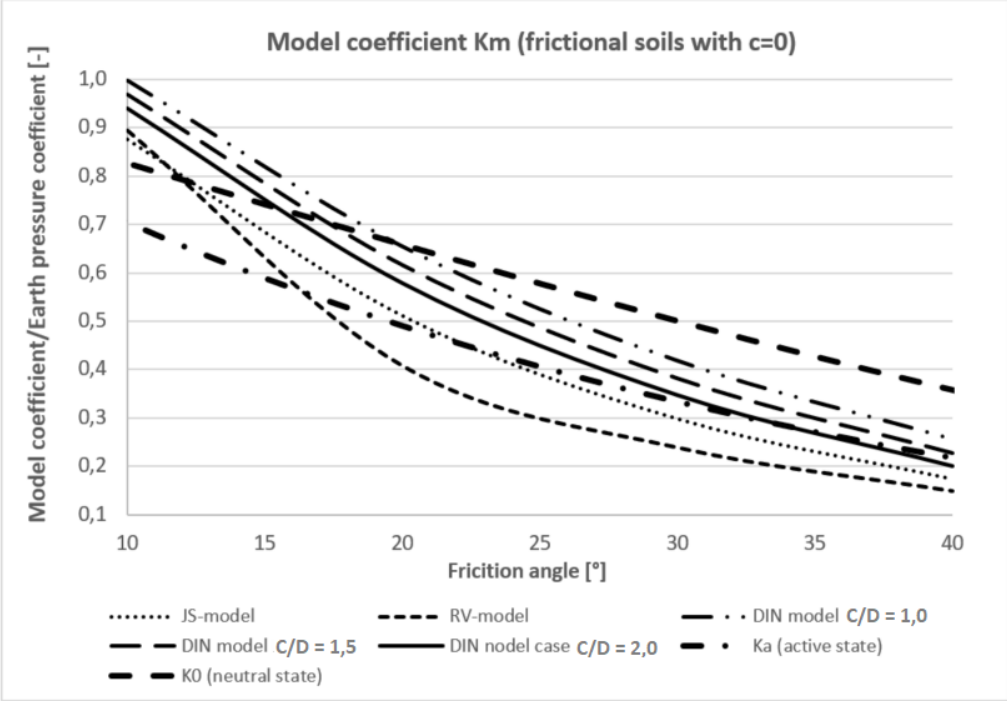

Figure 32. The model coefficient K_m as a function of the friction angle and C/D ratio in case of zero cohesion.

[21] As the Ruse-Vermeer model incorporates the safety factor in the determination of the earth pressure coefficients, this has also be done for the other models.

3.3 Experimental results from the literature

3.3.1 Possible combinations horizontal and vertical soil arching

The previous paragraphs have determined that one of the main differences between the limit equilibrium models is the implementation of horizontal soil arching and/or vertical soil arching. In paragraph 3.2, the general concept of these arching implementations is discussed. For both horizontal and vertical soil arching, the determination of the counteracting shear stresses has led to difficulties, as different authors assume different values for the lateral earth pressure coefficient K_y (Table 2 &Table 3). The lowest values equal the active earth pressure coefficient and the highest values assume a vertical effective stress equal to the horizontal effective stress. The background of these differences cannot be investigated due to the demarcation of this research to the four models.

It is possible to conclude that the combination of these two arching components leads to many different combinations. Therefore, it is beneficial to identify some basic cases to make a structural and clearer comparison between the models. In this thesis, the possible combinations suggested by Broere (1998) have been used as the minimum support pressure for these combinations are also calculated and compared with experimental results. In these combinations only one implementation of the vertical soil arching component is taken into account. Based on the schematization of straight failure surfaces, as indicated in Figure 21, it has been assumed that the soil surrounding the wedge has zero lateral strain; it has therefore been assumed that a neutral earth pressure coefficient is valid. For the horizontal soil-arching component, implementation of both a neutral and an active earth coefficient has been considered, as different shapes of the failure mechanism have been assumed, e.g. curved or straight slip surfaces, leading to 14 possible combinations of horizontal and vertical soil arching (Table 4). Following Broere (1998), a linear interpolation between the vertical stress, including arching at top of the wedge $\sigma'_{v,a}$ (curve 3 displayed in Figure 22) and the vertical stress without arching effects σ'_v at the bottom of the wedge, is not considered likely and the amount of possible combinations has therefore been reduced to 10 possibilities.

In order to illustrate the effect of these different combinations on the minimum support pressure, experimental results of centrifuge tests performed by Bezuijen (1997) and Chambon (1994) have been used. The minimum support pressure was calculated for each centrifuge test set up for the 10 possible combinations of vertical and horizontal soil arching (Table 5). The calculation model used for this analysis is the wedge model derived by Broere (1998), which, in the case of homogeneous soil, is quite similar to the Jancsecz-Steiner wedge model. In this analysis, it is not possible to determine which combination best yields the measured minimum support pressure, as the theoretical background of this model is not discussed within this thesis.

Table 5 reveals the following effects of the different arching implementations on the minimum support pressure:

- $a_{,m} \rightarrow b_{n,m} \rightarrow c_{n,m}$**:** If the dimension of vertical soil arching is increased, e.g. the number of sides including the counteracting shear stresses increases, this leads to a higher reduction of the vertical stress acting on the tunnel crown. A decrease in the vertical (effective) stress results in a decrease of the minimum support pressure.
- $a_{1,m} \rightarrow a_{2,m}$**:** If the stress distribution next to the wedge changes from a linear stress distribution to a distribution including arching effects, this leads to a lower vertical (effective) stress distribution next to the wedge. In addition, this reduction in vertical (effective) stress will result in a lower horizontal soil-arching component. As the horizontal soil-arching component is reduced, the lower the minimum support pressure is counteracted, leading to a higher minimum support pressure.
- $a_{n,0} \rightarrow a_{n,a}$**:** If the horizontal soil-arching component is calculated using an active earth pressure coefficient instead of a neutral earth pressure coefficient, the counteracting shear stresses acting on the wedge sides decrease and the minimum support pressure increases. The reason for this is that the value of the active earth pressure coefficient is lower than a neutral earth pressure.

Table 4. Different combinations of vertical and horizontal soil arching (Broere,1998).

Format	Vertical soil arching: K_0- conditions	Horizontal soil arching: σ_v next to the wedge	Horizontal soil arching: lateral earth pressure coefficient
$a_{,0}$	none	linear without arching	neutral
$a_{,a}$	none	linear without arching	active
$b_{1,0}$	2D	linear without arching	neutral
$b_{1,a}$	2D	linear without arching	active
$b_{2,0}$	2D	including arching effects	neutral
$b_{2,a}$	2D	including arching effects	active
$c_{1,0}$	3D	linear without arching	neutral
$c_{1,a}$	3D	linear without arching	active
$c_{2,0}$	3D	including arching effects	neutral
$c_{2,a}$	3D	including arching effects	active

[a]Format: $a_{n.m}$
a = arching model (a= none, b=2D, c=3D)
n = stress on wedge sides (1=linear (curve 1- Figure 22), 2 = incl arching (curve 3- Figure 22))
m= K_y value used (0=K_0 , a=K_a)

Table 5. Comparison of centrifuge test results with models with different arching implementations (Broere,1998).

Test[b]	Meas. [kPa]	Ratio calculated minimum support pressure with measured [a] [kPa]										Best result
Test	S'	$a_{,0}$	$a_{,a}$	$b_{1,0}$	$b_{1,a}$	$b_{2,0}$	$b_{2,a}$	$c_{1,0}$	$c_{1,a}$	$c_{2,0}$	$c_{2,a}$	
CS0.5/5	3,6	3,65	4,45	3,26	4,2	3,76	4,42	2,54	3,7	3,73	4,31	$C_{1,0}$
CS0.5/5	3,3	4	4,88	3,58	4,61	4,12	4,85	2,79	4,06	4,09	4,73	$C_{1,0}$
CS1/5	3,5	5,52	6,85	4,08	5,81	5,14	6,33	1,97	4,19	4,48	5,52	$C_{1,0}$
CS1/5	3	6,41	7,95	4,73	6,74	5,97	7,35	2,28	4,87	5,2	6,41	$C_{1,0}$
CS1/5	3,3	5,79	7,18	4,27	6,09	5,39	6,64	2,06	4,39	4,7	5,79	$C_{1,0}$
CS1/10	7,4	5,13	6,35	3,77	5,4	4,78	5,89	1,83	3,89	4,15	5,13	$C_{1,0}$
CS2/5	4	7,64	9,6	3,52	6,48	5,78	7,67	0	2,88	4,12	5,53	$C_{1,0}$, $C_{1,a}$
CS2/10	8	7,66	9,63	3,53	6,48	5,79	7,68	0	2,88	4,12	5,54	$C_{1,0}$, $C_{1,a}$
CS4/10	8,2	13,2	16,8	1,81	6,91	6,82	10,1	0	0,12	4,09	5,81	$b_{1,0}$
CS4/13	13,4	10,9	13,8	1,4	5,58	5,53	8,17	0	0,02	3,31	4,7	$b_{1,0}$
BS0.8/10	6,6	1,76	3,24	1,76	2,91	2,16	2,67	0,98	2,41	1,96	2,41	$C_{1,0}$
BC0.8/10	17	1,3	1,5	1,04	1,29	1,22	1,39	0,67	0,99	1,09	1,25	$b_{1,0}$
BC0.6/10	11	1,69	1,69	1,45	1,51	1,65	1,87	1,07	1,16	1,55	1,75	$C_{1,0}$

[a]Format: $a_{n.m}$
a=arching model (a= none, b=2D, c=3D)
n= stress on wedge sides (1=linear, 2=incl arching,3= linear interpolation)
m= K value used (0=K_0, a=K_a)

[b]Format: ATn/m:
A= Author (B=Bezuijen C=Chambon)
T= Type of Test (S=Sand, C=Clay)
n=Overburden-Diameter Ratio
m=Diameter in m.

Table 6. Implementation of the model combination for the DIN model (2007,2013) and the Jancsecz-Steiner model (1994).

Model	Vertical soil arching		Horizontal soil arching	
	dimension	earth pressure coefficient	Stress distribution next to wedge	earth pressure coefficient
DIN408/4126	x	x	linear	$K < K_a$
JS Wedge model (1994)	x	x	linear	$K = 1/2 (K_a+K_o)$
JS Wedge model including vertical soil arching (1994)	3D	K_a	linear	$K = 1/2 (K_a+K_o)$
JS K_{a3D} model (1994)	x	x	linear	$K = 1/2 (K_a+K_o)$
JS K_{a3D} model including vertical soil arching (1994)	3D	K_a	combination*	$K = 1/2 (K_a+K_o)$

x: Does not take this component into account

*: This method only takes the vertical (effective) stress distribution in front of the tunnel face into account. Therefore, the assumed pressure distribution next to the wedge is equal to a vertical effective stress including arching at the top of the failure wedge and from this point increases following the unit weight of the soil.

3.3.2 Combination of the analysed models

The different arching implementations used in the two limit equilibrium models (DIN & Jancsecz-Steiner) analysed in this thesis are presented in Table 6. These specific combinations have been translated to the basic cases indicated in Table 4 in order to obtain a clearer and more structured comparison. The following observations have been made:

- **DIN model:** This model does not include the effect of vertical soil arching. It can therefore be concluded that this method falls in the $a_{n,m}$-classes. Due to the neglection of vertical soil arching, the vertical pressure distribution next to the wedge is linear ($a_{1,m}$-classes). As the DIN model uses a different and lower earth pressure coefficient than the active or neutral earth pressure coefficient, this DIN model is not exactly equal to one of the pre-defined combinations. The earth pressure coefficient used in the DIN model results in a higher minimum support pressure than the two other classes ($a_{1,a}$ and $a_{1,0}$) due to a lower value of the horizontal soil-arching component. Despite this, the combination is approximately equal to combination $a_{1,a}$.
- **Jancsecz-Steiner wedge and K_{A3D}-model without vertical soil arching:** Both models neglect the effect of vertical soil arching and therefore fall into the $a_{n,m}$-classes. Due to the neglection of vertical soil arching, the vertical pressure distribution next to the wedge is linear ($a_{1,m}$-classes). The earth pressure coefficient used in order to calculate the shear stresses acting on the wedge sides is equal to the average of the active and neutral earth pressure coefficient. This model is therefore equal to the average of model combinations $a_{1,0}$ and $a_{1,a}$.
- **K_{A3D}-model wedge model with vertical soil arching:** This model includes three-dimensional vertical soil arching and therefore is a $c_{n,m}$-class type model. The assumed pressure distribution next to the wedge is equal to a vertical effective stress including arching at the top of the failure wedge $\sigma'_{v,a}$; from this point, it increases following the unit weight of the soil. It can therefore be assumed that the pressure distribution next to wedge is equal to the average of $c_{1.m}$ and $c_{2.m}$. The earth pressure coefficient used is the average of the active and neutral earth pressure coefficient, so this model is equal to the average of ($c_{1,a}$ and $c_{1,0}$) and ($c_{2,a}$ and $c_{2,0}$).
- **Jancsecz-Steiner wedge model with vertical soil arching:** This model includes three-dimensional vertical soil arching and therefore is a $c_{n,m}$-class type model. The model assumes a linear pressure distribution next to the wedge and therefore falls in the $c_{1,m}$-classes. The earth pressure coefficient used is the average of the active and neutral earth pressure coefficient, so this model is equal to the average of $c_{1,a}$ and $c_{1,0}$.

3.4 Case-study analysis

3.4.1 Similarities and differences between the models

Based on the theoretical background analysis, the similarities and differences between the models have been obtained. The following are the similarities:

- The division of the minimum support pressure into a horizontal effective stress component and a (equilibrium) pore water pressure component (Equation 2.5).
- The horizontal effective stress acting on the tunnel face in case of a zero cohesion is determined by multiplying the vertical effective stress with an model coefficient K_m.
- In all three models horizontal soil arching is taken into account.
- In the case of a heterogeneous soil profile, the soil profile in front of the TBM is divided into N soil layers, possibly with variable thickness d_i, with constant soil properties. At the layer boundaries, the minimum support pressure is calculated by using the properties of the layer above the boundary and the layer below this boundary. This leads to sharp transitions in the minimum support pressure at the layer boundaries.

The following differences have been obtained from the theoretical background analysis:

- Unlike the DIN model, the Jancsecz-Steiner and Ruse-Vermeer models take the effect of vertical soil arching into account.
- For the two limit equilibrium models, the value for the earth pressure coefficients K_y is different when calculating the horizontal and vertical soil-arching component. In addition, these values also differ between the models.
- The Ruse-Vermeer model is only valid for soils with a friction angle higher than 20°.
- The Ruse-Vermeer and DIN models take the effect of cohesion into account.
- The model coefficients in order to determine the horizontal effective stress acting at the tunnel face are a function of the friction angle only (Ruse-Vermeer/Jancsecz-Steiner model).
- The earth pressure coefficients in order to determine the horizontal effective stress acting at the tunnel face are a function of both the friction angle and the *C*/*D* ratio (DIN-model).

3.4.2 Set-up case studies

In order to determine the effect of these models' differences on the minimum support pressure, eight case studies have been set up (Figure 33) and six test series have been performed. These case studies have been designed in such a way as to investigate the effect of heterogeneous soil conditions in front of and above the TBM. In addition, a change in the height of the soil cover has also been investigated. The project-specific soil parameters utilised are presented in Table 7 and in all cases, the groundwater level is equal to the ground surface. In test series 1, the minimum support pressure has been calculated using the original models. In the subsequent test series, possible model modifications/extensions to improve the models have been investigated. In these test series, the model aspect indicated is modified/extended, while the other model parameters remain equal, based on the original model in test series 1. In this thesis, the following test series have been investigated:

- First part: original models
  - Calculation of the face support pressure for the eight case studies by using soil layers with friction angles φ >20° **(Series 1).**
- Second part: extensions/modifications to improve original models[22]
  - Ruse-Vermeer model without vertical soil arching – by taking the weight of the soil cover into account **(Series 2)**.
  - Ruse-Vermeer model for soil layers with friction angles φ < 20° **(Series 3).**
  - DIN model, changing the depth parameter of horizontal soil arching **(Series 4).**
  - DIN model, taking vertical soil arching into account **(Series 5).**
  - Reduction of the effectiveness of the support pressure by taking slurry infiltration into account **(Series 6).**

[22] Only the relevant model is modified, while the remaining models remain the same as the original (test-series 1).

The main objective of this case study analysis is to obtain more insight into the different model aspects and their subsequent influence on the minimum support pressure. Some improvements/modifications have been suggested in order to obtain a smaller range in the minimum support pressure calculations following a static face stability analysis.

Table 7. Soil parameters used for case studies.

Description	$\gamma_{sat;H}$	$c'_{2\%;L}$	φ'_{H}
[-]	[kPa]	[kPa]	[°]
Clay, silty	16.8	4.5	23
Sand, medium	20	0	30.6
Peat	10.9	0	15

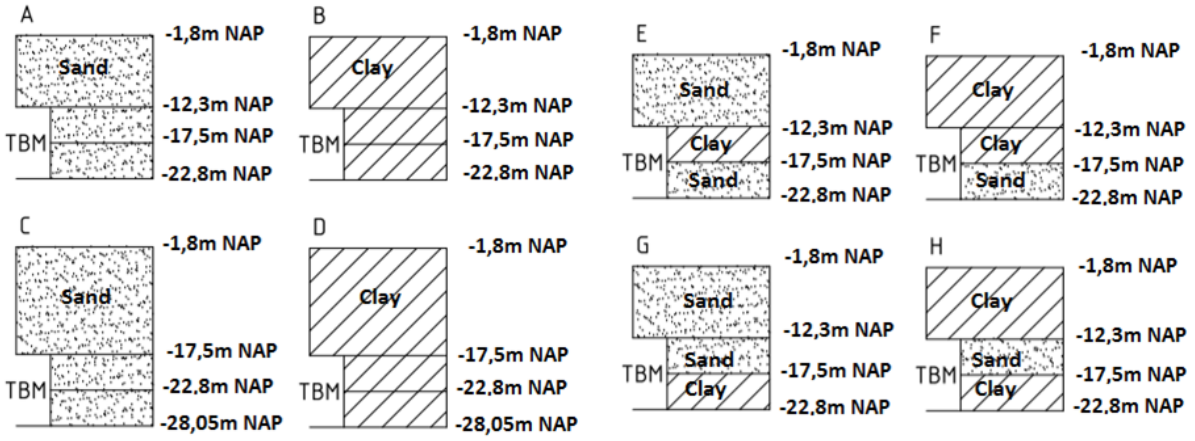

Figure 33. Case studies used to investigate the differences between the models.

3.4.3 Test series 1

In test series 1, the minimum support pressure is calculated based on the original models. The results are detailed in Annex 3.1. The results of test series 1 indicate that the minimum support pressure required is the lowest in the Ruse-Vermeer model and the highest in the DIN/JS models. In order to determine the influence of the model differences on the minimum support pressure, the following aspects have been investigated:

1. the effect of a change in the height of the soil cover (homogeneous soil profile), which leads to a change in the vertical (effective) stress distribution;
2. the effect of a change in the soil profile above the tunnel crown, which leads to a change in the vertical (effective) stress distribution;
3. the effect of a change in the soil profile in front of the TBM, which leads to a change in the vertical (effective) stress distribution (below the tunnel crown) and a change in the model parameters.

1. Increase in soil cover (homogeneous soil profile)

The effect of an increase in the soil cover has been investigated by comparing case A (C/D=1.0) with case C (C/D=1.5), as illustrated in Figure 34.[23] Both cases consist of a homogeneous sand profile and therefore constant soil properties. It can be seen that the minimum support pressure in the case of the Ruse-Vermeer model is equal for case A and C, despite the fact that the vertical (effective) stress acting on the tunnel crown has changed. A change in the height of the soil cover does not affect the Ruse-Vermeer model, as this model neglects the soil weight of the overburden. An important aspect to note is that this is only a valid assumption for soils with a friction angle larger than 20° and C/D>1. The Jancsecz-Steiner model (without vertical soil arching) and the DIN model are affected by a change in the height of the soil overburden due to a change in the vertical (effective) stress acting on the tunnel

[23] Or compare case B (C/D=1.0) with case D (C/D=1.5).

crown. Figure 34 reveals that an increase in the soil cover leads to a higher minimum support pressure. In contrast to the Jancsecz-Steiner model, the DIN model is also affected by the 'wall length' reduction component, which lowers the minimum support pressure. This reduction coefficient is a function of the depth z below the ground surface and therefore increases with an increasing height of the soil cover. The Jancsecz-Steiner model (including soil arching) is also affected by a change in the height of the soil overburden, but to a lesser extent than the previous two models. The reason for this is that in the case of an increase in the soil cover, the full weight does not act on the tunnel crown; rather, part of the load is transferred to the wedge sides. The vertical effective stress at tunnel crown and in front of the tunnel face is therefore lower than in the situation without vertical soil arching.

2. Change in the soil profile above the TBM (stratified soil profile)

The effect of a change in the soil type of the cover has been investigated by comparing case E (sand) with case F (clay), as illustrated in Figure 35[24] It can be seen that the Ruse-Vermeer model leads to the lowest minimum support pressure and the DIN/Jancsecz-Steiner models to the highest minimum support pressure. This paragraph only discusses the effect of a change in the soil cover and not the shape of the required minimum support pressure profiles below tunnel crown. As with the previous comparison, the Ruse-Vermeer model neglects the soil weight of the overburden and therefore changes in its soil type do not affect it. The DIN/Jancsecz-Steiner model (without vertical soil arching) are affected by a change in the soil type of the soil cover because this results in a change of the vertical (effective) stress distribution. In addition, the wall-length reduction component depends on the friction angle φ and is therefore affected by changes in the soil type of the soil overburden. The Jancsecz-Steiner model (including soil arching) is influenced by a change in the soil type of the overburden, due to a change in the vertical (effective) stress distribution. As discussed in the previous paragraph, due to the vertical soil-arching component, the model is influenced to a lesser extent than the Jancsecz-Steiner model without vertical soil arching.

3. Change of soil profile in front of the TBM (stratified soil profile)

The effect of a different soil profile in front of the tunnel face has been investigated by comparing case E with case G, as indicated in Figure 35[25] This change leads to both a different vertical (effective) stress distribution below the tunnel crown and a change in the model coefficients/parameters for the bottom and upper layers. In addition, as the total soil weight for the given case does not change when the soil profile in front of the TBM is turned around, the vertical (effective) stress at the tunnel invert remains equal. The subsequent paragraphs discuss the behaviour per model in the case of a change in the soil profile in front of the TBM.

a. Ruse-Vermeer model

Figure 35 reveals that the required minimum support pressure for each soil layer is constant. The reason for this is that this model assumes a vertical (effective) stress equal to the bottom of each soil layer to be valid for the complete soil layer. At the layer boundaries, sharp transitions occur. Figure 35 illustrates that the change from case E to case G only has a small impact on the required minimum support pressure distribution. This is justified by a combination of a change in the vertical (effective) stress distribution, a change in model coefficients/parameters and a reduction effect due to cohesion in the clay layer. The upper layer changes from a clay layer to a sand layer, thus increasing the vertical effective stress at the bottom of the upper layer. The model coefficient is simultaneously reduced due to the higher friction angle of the sand layer compared to the clay layer (Figure 32). In addition, the minimum support pressure in the upper layer is no longer reduced due to cohesion. Due to these factors, the minimum stress required increases in the upper layer. The bottom layer changes from a sand layer to a clay layer, but the vertical (effective) stress at the tunnel invert remains equal because the total soil weight has not changed. The model coefficient increases simultaneously due to the lower friction angle of the clay layer compared to the sand layer (Figure 32). Due to this layer's large cohesion component, the minimum support pressure is reduced. These factors result in a slight increase in the minimum stress required in the bottom layer.

[24] Alternatively, compare case G (sand) with case H (clay).
[25] Alternatively, comparing case F with case H.

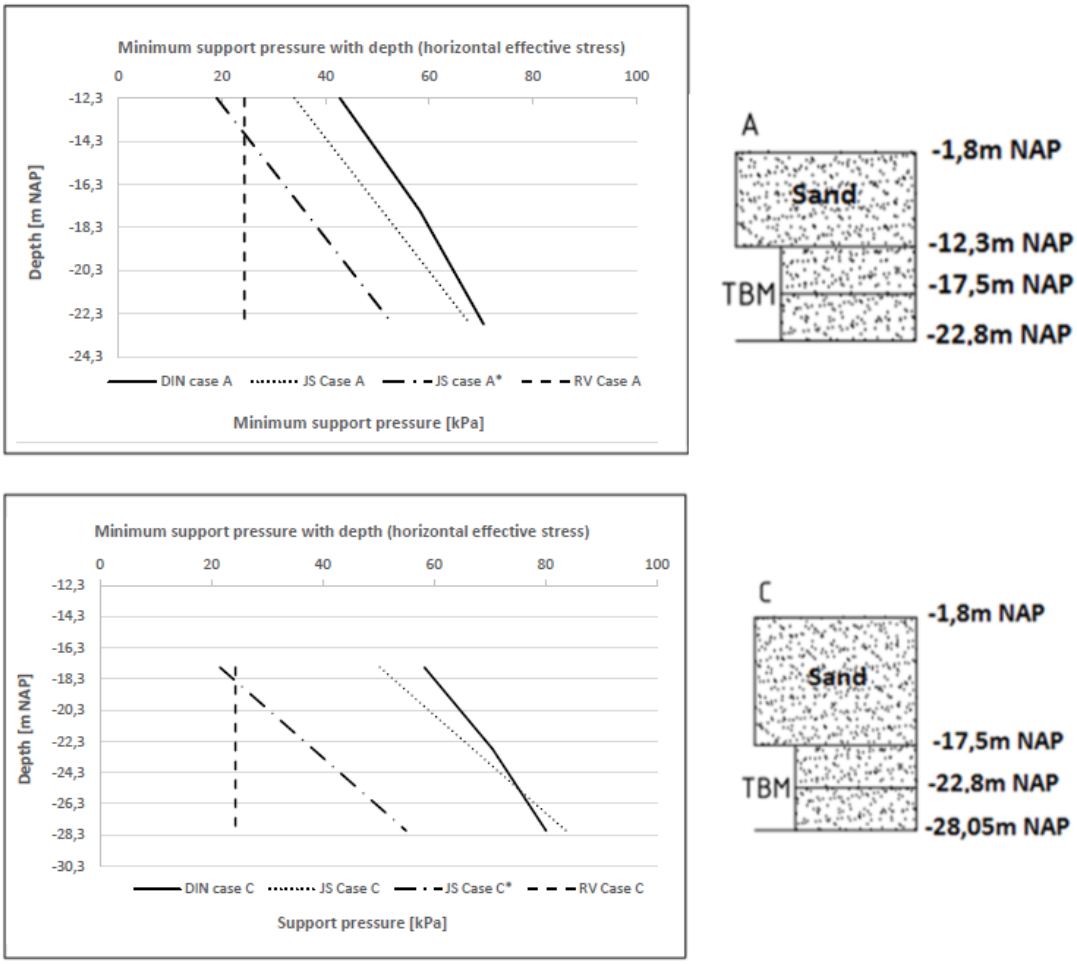

Figure 34. Test series 1: Comparison of case A and case C in order to determine the effect of a change in the soil cover.

b. Jancsecz-Steiner model (without vertical soil arching)

Compared to the Ruse-Vermeer model, the Jancsecz-Steiner model does not assume a constant vertical effective stress for each soil layer. The minimum support pressure required therefore increases linearly for each layer. In addition, sharp transitions are present at the layer boundaries. Figure 35 illustrates that the change from case E to case G leads to a lower minimum support pressure for the upper layer and a higher support pressure for the bottom layer. The upper layer changes from a clay layer to sand layer; this results in a higher unit weight of the upper layer, leading to a higher vertical effective stress distribution in the upper layer. The model coefficient is simultaneously reduced due to the higher friction angle of the sand layer compared to the clay layer (Figure 32). In the bottom layer, the sand layer changes to a clay layer with a lower unit weight. Despite this lower unit weight, the vertical (effective) stress within this layer is higher, due to the higher weight of the soil profile above. The model coefficient simultaneously increases due to the lower friction angle of the clay layer compared to the sand layer (Figure 32). Through the combination of this increase in vertical (effective) stress and the increase in the model coefficient, the shape of the graph is flipped over.

c. Jancsecz-Steiner model (including vertical soil arching)

The Jancsecz-Steiner model (including vertical soil arching) presents the same behaviour as the Jancsecz-Steiner model (without vertical soil arching). The change from case E to case G results in no changes in the height of the soil overburden or the soil type; therefore, the vertical (effective) stress at the tunnel crown remains equal. This means that the findings discussed in the previous paragraph are also valid for this case.

d. DIN-model

In the DIN model, a change from case E to case G leads to a lower minimum support pressure for the upper layer and a higher minimum support pressure for the bottom layer (Figure 35). The upper layer changes from a clay layer to a sand layer and therefore the steepness of the vertical (effective) stress distribution increases. Due to the higher friction angle of the sand layer, the model coefficient for the upper layer decreases and the 'wall-length' reduction coefficient increases. In addition, the cohesion reduction component is no longer applicable. The combination of these four effects, increased vertical effective stress, reduced model coefficient, increased wall-length reduction coefficient and a non-applicable cohesion reduction coefficient, result in a higher minimum support pressure for the upper soil layer. In the bottom layer, the opposite effect of these aspects occurs and results in a reduction of the minimum support pressure.

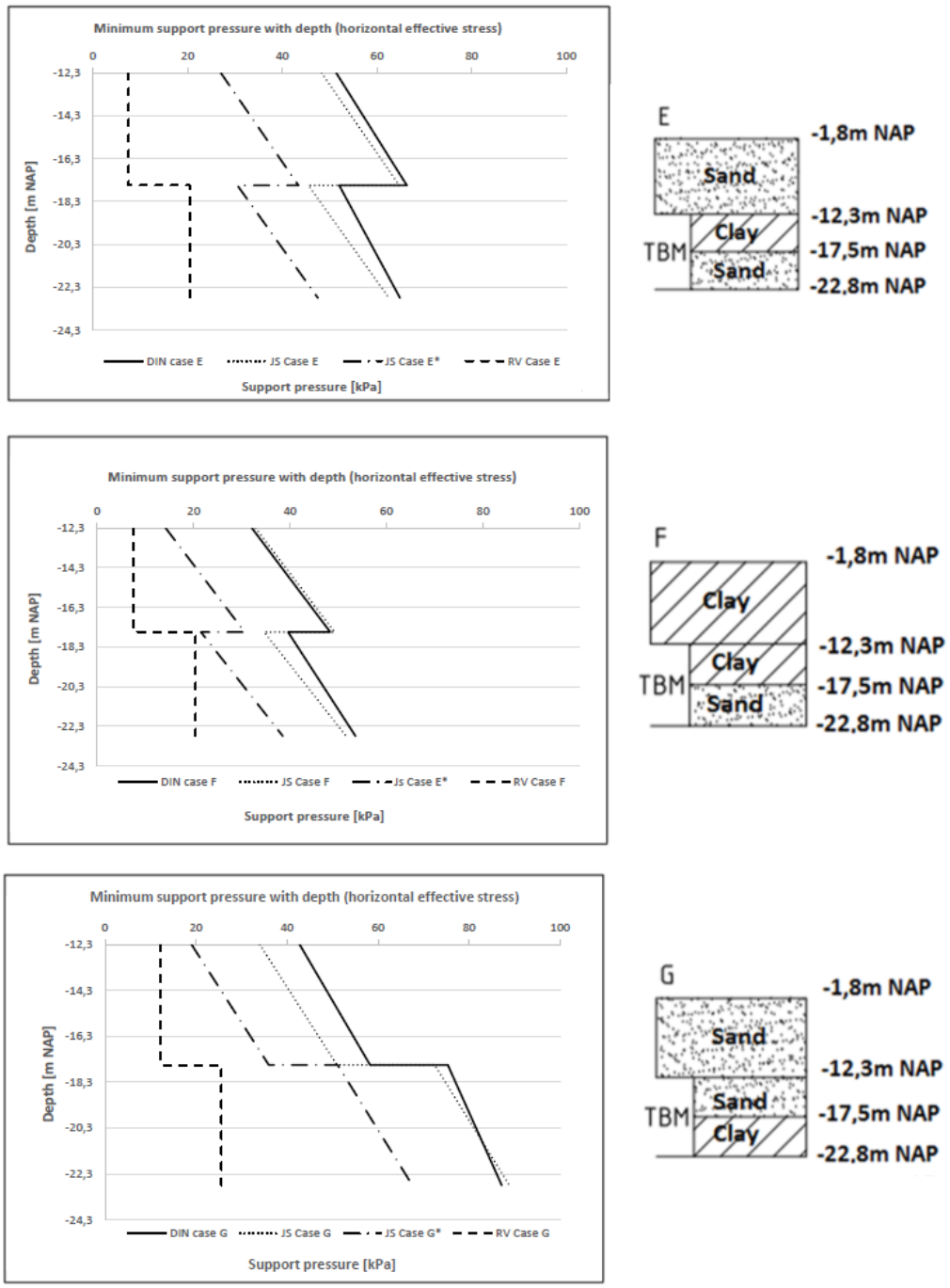

Figure 35. Test series 1: Comparison of case E with case F to display the effect of a change in the soil cover and comparison of case E and case G to show the effect of a change in the soil profile in front of the TBM.

3.4.4 Test series 2

Case studies A1-H1 (Annex 3.1) indicate that the Ruse-Vermeer model results, on average, in the lowest and the DIN/JS model in the highest minimum support pressure distribution. The main reason for this is that the Ruse-Vermeer model takes vertical soil arching into account by neglecting the complete soil weight of the overburden.[26] The Ruse-Vermeer model should be used with great caution in stratified soil profiles, because the setup of this model is based on homogeneous soil conditions. It is therefore possible that, based on the soil profile in front of the TBM, vertical soil arching is applicable, while this is not the case for the soil profile above the TBM. The behaviour of this model for friction angles lower than 20° has therefore been investigated. A first step in this research is to investigate the behaviour of this model without vertical soil arching, e.g. the full weight of the soil overburden is taken into account. For the given case studies, this can be done in the following two ways:

1. A constant vertical effective stress, by multiplying the unit weight of the soil by the height of the overburden.
2. An increasing vertical effective stress, by multiplying the effective unit weight of the soil by the depth starting from ground surface. This method is also applied in the other two models.

The second method has been used in this analysis because it is more suitable in the case of heterogeneous soil profiles and it complies with the other two models. For this test series, Equation 3.18 has been changed to Equation 3.31.

$$\sigma'_h = q\,N_q + \sigma'_v\,N_\gamma - \left(\frac{1}{\gamma_{\varphi' c'}}\right) c' N_c \qquad \textbf{[Equation 3.31]}$$

In this test series, the minimum support pressure has been calculated for case E-H. The DIN and JS models have been calculated based on the original models (case E1-H1). In order to demonstrate the effect of Equation 3.31, the Ruse-Vermeer model has been calculated based on the original model E1 (test series 1) and the modified model E2 (test series 2). All calculations of test series 2 are presented in Annex 3.2. Figure 36 displays the minimum support pressure distributions calculated for case E. It can be observed that when the soil weight of the overburden is taken into account, this leads to a higher minimum support pressure and to a smaller range between the minimum support pressure distributions. The reason for this is that the vertical effective stress acting on the tunnel crown increases while the soil profile in front of the TBM remains equal.

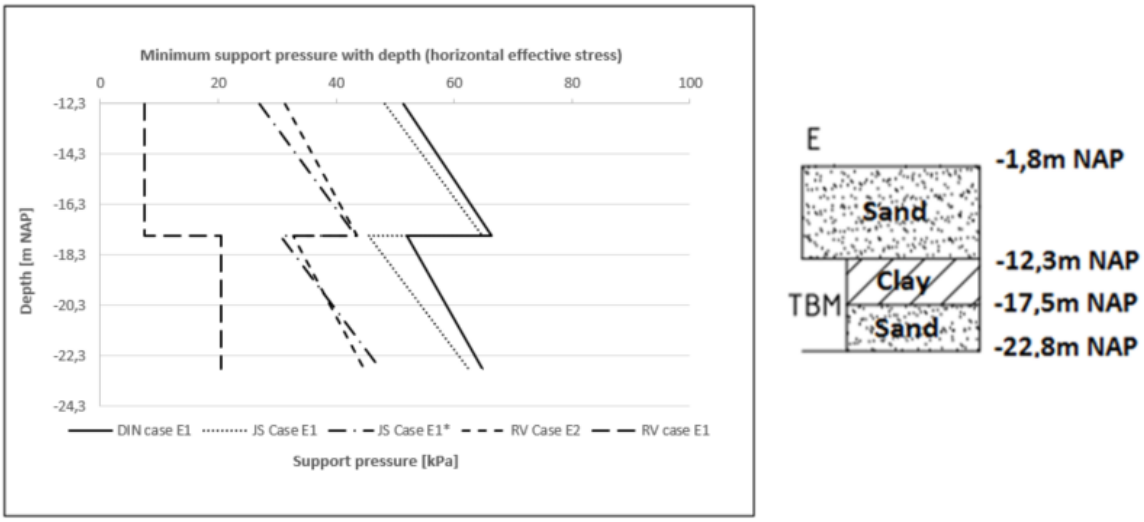

Figure 36. Comparison of case E-1 (test series 1) with case E-2 (test series 2), in order to determine the effect of neglecting the vertical soil-arching component on the minimum support pressure.

[26] This assumption is valid for homogeneous soil profiles (with C/D ≥1.0) with a friction angle ϕ>20 (Ruse-Vermeer, 2002).

3.4.5 Test series 3

Test series 3 is a continuation of test series 2, conducted in order to investigate the behaviour of the Ruse-Vermeer model for soils with friction angles lower than 20°, e.g. in which the full weight of the overburden is taken into account. In the previous test series, the vertical effective stress distribution has been adapted in order to include the soil weight of the overburden. The next step, which has been investigated in this test series, is the applicability of Equation 3.18 to soil layers with a friction angle below 20 degrees. An important aspect to note is that this research contradicts the model assumptions described in the theoretical background analysis (Paragraph 3.2.5). For this test series, the clay layer has been changed into a peat layer with a friction angle of 15 degrees with zero cohesion (Table 7)

This analysis has calculated the minimum support pressure for case E-H, including the peat layer. The DIN and the JS models[27] have been calculated based on the original models (case E1-H1) and the Ruse-Vermeer model has been calculated based on the original model (E3), with the assumption that Equation 3.20 is also valid for friction angles lower than 20°. All calculation results of this test series are presented in Annex 3.3. Figure 37 displays the results of the minimum support pressure calculation for case E, and it can be noted that the Ruse-Vermeer models remains offset with the other models. The reasons for this offset are, as in the previous test series, the difference in earth pressure coefficients, the reduction of the cohesion effect and the 'wall-length' reduction effect.

Annex 3.3 presents the minimum support pressure distribution for cases F and H. These two cases consist of a peat cover. Due to the low effective unit weight of peat, this results in very low horizontal effective stresses at the tunnel crown. At some locations, the minimum support pressure in order to counteract the effective earth pressure is close to zero. In the DIN model, such a situation is prevented by applying a lower boundary of the minimum support pressure (Paragraph 3.2.4). From the above, it is possible to conclude that the Ruse-Vermeer model is not applicable for soils with a friction angle below 20°. This is also the case for the JS* model that includes vertical soil arching.

3.4.6 Test series 4

The DIN model utilised for the face stability assessment originates from the stability analysis of the diaphragm walls. The corresponding failure mechanism therefore consists of a failure wedge that extends from wall toe to ground surface. The DIN model is translated to tunnel face stability by assuming an active state only at the location of the tunnel; therefore, the actual height of the failure wedge is equal to the diameter of the tunnel. This height reduction of the failure wedge results in smaller areas of the wedge sides in order to incorporate the horizontal soil-arching component. Due to this, the depth z below ground surface in Equations 3.12/3.13 has to be modified in the depth z below the tunnel crown (z^*) (Equation 3.15). Assuming that the width of the wedge is equal to the diameter of the tunnel, the C/D ratio is equal to zero at the tunnel crown and equal to unity at the tunnel invert. In this test series, the effect of this modification on the minimum support pressure has been determined.

For this test series analysis, the minimum support pressure distribution has been calculated for cases A-D. The JS and RV models have been calculated based on the original model assumptions (cases A1-D1). The DIN model has been calculated based on both the original model assumptions (A1-D1) and the modified model based on Equation 3.15 (A4-D4). Annex 3.4 presents the minimum support pressure distributions for cases A-D. Figure 38 illustrates the pressure distributions for cases A and C, both of which consist of a homogeneous sand profile. It can be noted that the change of the depth parameter within the 'wall-length' reduction component results in a higher minimum support pressure distribution over the tunnel face. Comparing case A (C/D=1.0) and case C (C/D=1.5), the increase in minimum support pressure is higher for case C. The reason for this is that the original DIN model (Equations 3.12/3.13) utilises the depth below the ground surface and the modified model uses the depth below the tunnel crown. As the latter is not a function of the height of the soil cover, the difference in the wall-length reduction component is therefore greater in case C, which consists of a larger soil cover.

[27] This minimum support pressure cannot be calculated for the JS* model that includes vertical soil arching.

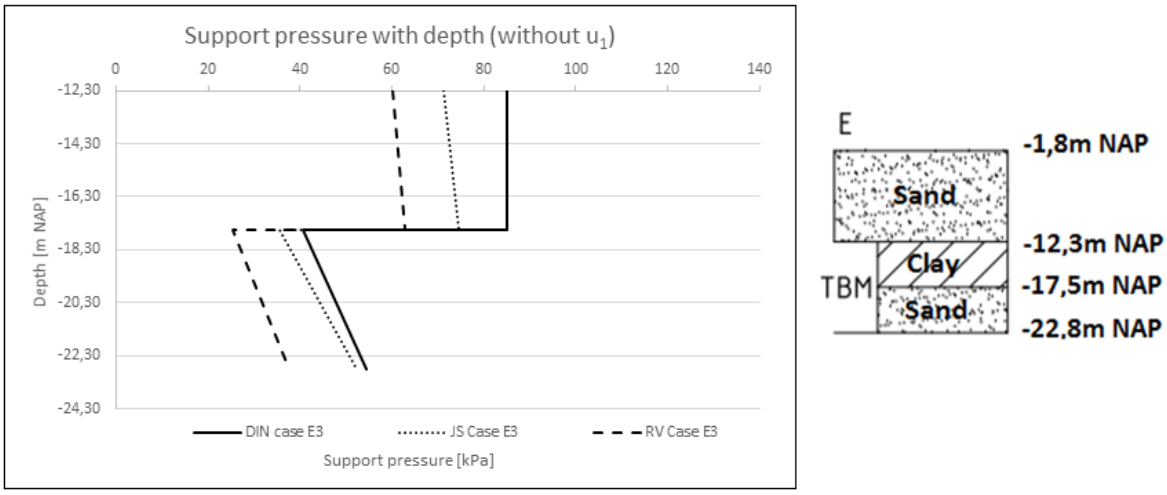

Figure 37. Comparison of case E-1 (test series 1) with case E-3 (test series 3), in order to determine the effect of a soil layer with a friction angle below 20 degrees on the minimum support pressure.

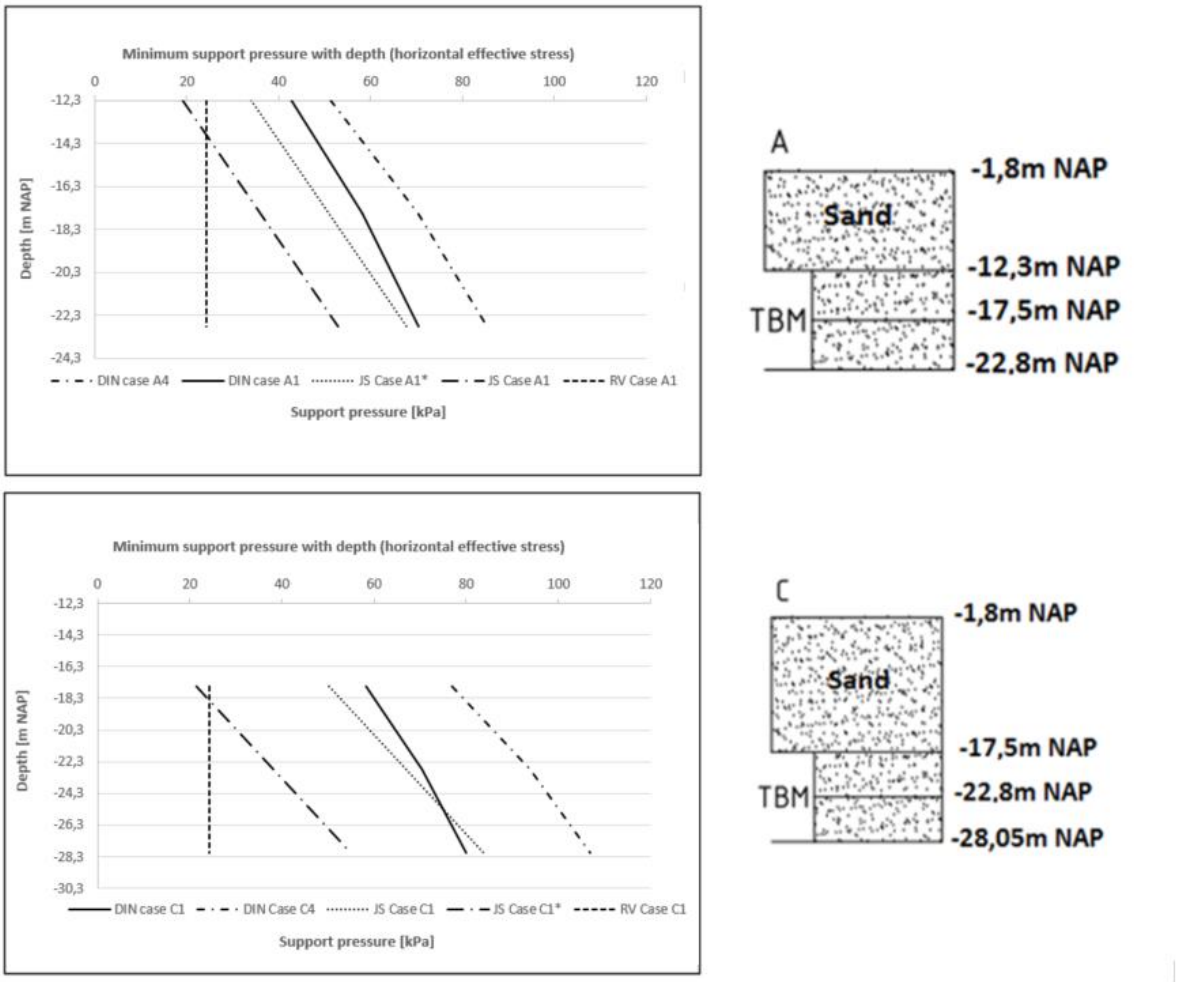

Figure 38 . The effect of modifying the wall-length reduction is demonstrated by comparing cases C-D (original model) with cases C4-D4 (modified model).

3.4.7 Test series 5

In test series 5, the possibility to include vertical soil arching within the DIN model has been investigated. The DIN model for tunnel face stability assumes a failure wedge that extends from the tunnel crown to the tunnel invert, while the soil overburden acts as a surcharge. Vertical soil arching can consequently be implemented in the DIN model using the same method described in the Jancsecz-Steiner model (K_{A3D} model). This is a valid assumption, as both models are limit equilibrium wedge models and both assume that the soil cover acts as a surcharge. The incorporation of vertical soil arching leads to a lower vertical effective stress acting on the tunnel crown compared to the situation where no vertical soil arching is taken into account. The reduced vertical effective stress for each separate layer in a layered soil profile has been determined by using the effective stress at the bottom of the previous layer as the continuity condition for the next layer and by integrating from top to bottom (Broere, 1998). For a layer *i* with top $z=t^i$ it has been found that:

$$\sigma'^{(i)}_{v,a} = \frac{a\,\gamma'^{(i)} - c'^{(i)}}{K_y{}^{(i)} \tan\varphi'^{(i)}} \left(1 - e^{-K_y{}^{(i)} \tan\varphi'^{(i)} \frac{z}{a}}\right) + \sigma'^{(i-1)}_{v,a}(t_i) e^{-K_y{}^{(i)} \tan\varphi'^{(i)} \frac{z}{a}} \quad \textbf{[Equation 3.32]}$$

$$for\ t^{(i)} \leq z \leq t^{(i+1)}$$

As described in Paragraph 3.2.2, there is some disagreement about which value to use for the lateral earth pressure coefficient. Based on the schematization of straight failure surfaces, as indicated in Figure 21, it has been assumed that the soil surrounding the wedge has zero lateral strain; it has therefore been assumed that a neutral earth pressure coefficient is valid.

The effect of vertical soil arching on the vertical effective stress acting on the tunnel crown has been investigated before implementing the vertical soil-arching component to the DIN model. Figure 39 displays the vertical effective stress distribution for both a homogeneous sand profile and clay profile. For both soil types, vertical soil arching leads to a decrease in the vertical effective stress with depth below the ground surface compared to the situation without soil arching. The reason for this is that the vertical effective stress increases with depth, leading to higher shear stresses acting on the sides of the soil prism[28]. The higher these shear stresses, the higher the reduction of the vertical effective stress acting on the tunnel crown.

For test series 5, the minimum support pressure has been calculated for cases A-D. The Jancsecz-Steiner and Ruse-Vermeer models have been calculated based on the original model assumptions (cases A1-D1). The DIN model has been calculated based on the original model (A1-D1) and the modified model, which includes vertical soil arching (A5-D5). For each case, the effect of no vertical soil arching (A5:(0)-D5(0)), 2D vertical soil arching (A5:(2D)-D5(2D)) and 3D vertical soil arching (A5:(3D)-D5(3D)) have been investigated.

As the analysis resulted in the fact that the minimum support pressure distribution strongly depends on the height of the soil cover a more in-depth analysis is required. Four extra cases have been added to determine the effect for a soil cover of *C/D* =2 and *C/D* =2.5: Two cases that consist of a homogeneous sand profile (cases I and J) and two extra cases that consist of a homogeneous clay profile (cases K and L). The results of the calculations for this test series are presented in Annex 3. Figure 40 illustrates the influence of vertical soil arching on the minimum support pressure distribution for a homogeneous sand profile with increasing height of the soil cover. The following observations have been made:

- **DIN-model without vertical soil arching**

The case without vertical soil arching is equal to the original model described in test-series 1. Therefore, the minimum support pressure distribution for the case without soil arching is not indicated within each graph. By using Figure 40, the effect of the wall-length reduction component[29] on the minimum support pressure distribution becomes more clear as cases with higher *C/D* ratios are also

[28] As described before, for the development of these shear stress it is assumed that the soil deforms towards the tunnel face.

[29] It should be noted that some doubts remain regarding this endless increasing wall-length reduction with depth (case study 4).

displayed. In the upper left corner (*C*/*D*=1,0) we see that the DIN-model results in the highest minimum support pressure. When the *C*/*D* ratio increases, the DIN-model will cross the Jancsecz-Steiner model and eventually be smaller than the Jancsecz-Steiner model (*C*/*D*=2,5).

- **DIN-model with 2D vertical soil arching**

By using Figure 40, it can be seen that the implementation of 2D vertical soil arching leads to a lower minimum support pressure distribution compared to the situation without vertical soil arching. In case A (*C*/*D*=1,0) the support pressure distribution is approximately equal to the Jancsecz-Steiner model (without soil arching). With an increasing *C*/*D* ratio, the vertical soil-arching component increases and the minimum support pressure distribution decreases. In case J (*C*/*D*=2,5) the DIN-model including 2D vertical soil arching is situated between the Ruse-Vermeer model and Jancsecz-Steiner model including vertical soil arching. In contrast to the other models, the Ruse-Vermeer model remains constant for each case indicated in Figure 40 due to the fact that it neglects the soil weight of the soil overburden.

- **DIN-model with 3D vertical soil arching**

Likewise 2D vertical soil arching, it can be seen that the implementation of 3D vertical soil arching leads to a lower minimum support pressure distribution compared to the situation without vertical soil arching. In the upper left corner (Case A with *C*/*D*=1.0), the DIN model lies between the Ruse-Vermeer model and the Jancsecz-Steiner model (including soil arching). With an increasing *C*/*D* ratio, the vertical soil-arching component increases and the support pressure distribution decreases. In case J (*C*/*D*=2,5) the DIN-model including 3D vertical soil arching approximates the Ruse-Vermeer model.

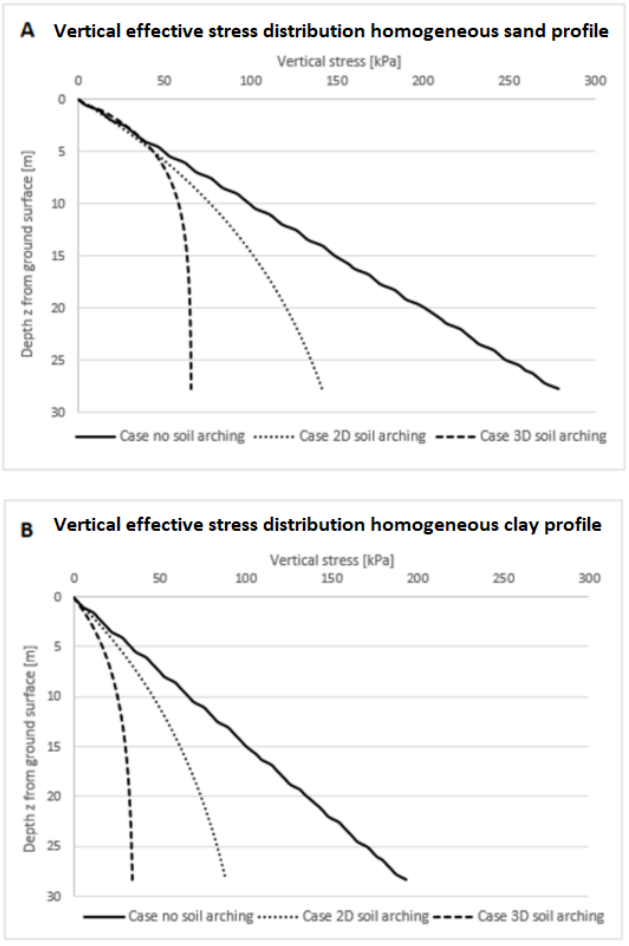

Figure 39. Vertical effective stress distribution, including soil-arching effects in (a) homogeneous sand profile and (b) homogeneous clay profile.

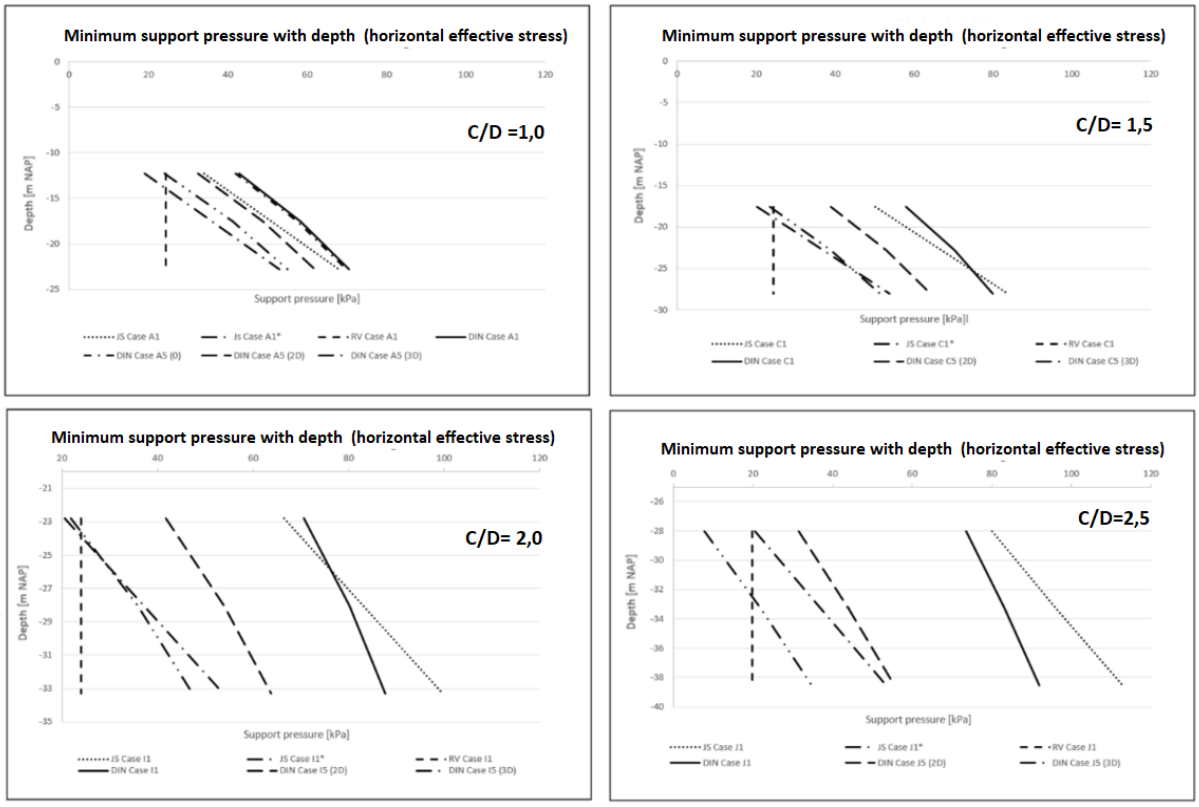

Figure 40. Influence of vertical soil arching on the minimum support pressure for a homogeneous sand profile, for case A (C/D=1.0), case C (C/D=1.5), case I (C/D=2.0) and case J (C/D=2.5).

3.4.8 Test series 6

The determination of the effectiveness of the support medium due to slurry infiltration in a static face stability assessment is incorporated in the DIN4085/4126 model. This process is described in Paragraph 2.5 and is based on two limit cases, the membrane model (negligible penetration distance) and the penetration zone model (maximum penetration distance). In this assessment, the governing parameters are the penetration distance and the distance (amount) of slurry penetration that falls outside the failure wedge. The amount of slurry penetration that falls outside the failure wedge does not contribute to the stability of the wedge; consequently, only the limit case concerning the maximum penetration distance affects the effectiveness of the support medium.

The maximum penetration distance is a function of the excess pressure Δs, yield strength slurry τ_F and the characteristic grain size diameter d_{10} of the soil (Equation 2.13). In the case of a homogeneous soil profile, the reduction is easily determined, as the slip angle of the failure wedge, d_{10} value and yield strength of the slurry are constant parameters. For this reason, the maximum penetration distance is only a function of the excess pressure distribution over the tunnel face. In the case of stratified soil profiles, however, these factors are not constant. The following paragraphs describe how to cope with these factors.

3.4.8.1 Excess pore pressure distribution

The support pressure needs to be higher than the pore water pressure in order to prevent a seepage flow towards the tunnel face. The TBM assumes a linear increasing pressure distribution within the excavation chamber (Figure 11). In case of a hydrostatic pore water pressure distribution, the excess pressure increases with depth due to the difference in unit weight of water pressure and bentonite slurry. In contrast, for a non-hydrostatic pore water pressure distribution the excess pressure distribution varies over the tunnel face. In this thesis, only a hydrostatic pore water pressure distribution has been assumed.

3.4.8.2 Variation wedge angle θ over tunnel face

The two limit equilibrium models (Jancsecz-Steiner and DIN) assume a wedge-shaped failure mechanism. The inclination of this failure wedge, also called wedge angle ϑ with the horizontal, depends on the friction angle of the soil. As the shape of the wedge is a function of the wedge angle and the wedge height, the shape of the wedge has been plotted for various friction angles (Figure 41). This figure displays that the width of the wedge increases for lower values of the wedge angle and vice versa. In the case of a homogeneous soil profile, the friction angle is constant and therefore the wedge angle is equal for the complete wedge. In the case of a stratified soil profile, the friction angle varies between the soil layers and therefore the wedge angle varies.

A method to incorporate a failure plane for a stratified soil profile is to regard each soil layer as a separate 'failure wedge'. At the bottom of each soil layer, the failure surface is inclined at a wedge angle ϑ that corresponds to the friction angle of the soil layer concerned. This way, a non-straight failure plane is obtained over the full height of the wedge. It should be noted that the failure surface obtained only acts as a kind of boundary when determining the effectiveness of the support medium and does not resemble the assumed shape of the failure wedge. In order for this method to be valid, the penetration distance for each soil layer must be independent of the soil properties of the other layers. This aspect is investigated by looking at the combination of the variation of permeability and the excess pressure distribution over the tunnel face.

3.4.8.3 Variation of permeability (d_{10} value) over the tunnel face

The maximum penetration depth of the bentonite slurry in a soil layer is determined by the combination of the 'permeability' d_{10} of the soil, excess pressure distribution and yield strength of the slurry. In this paragraph, the effect of a variation of the d_{10} value over the tunnel face in the shape of the penetration zone/filter cake is investigated. For this analysis, the unit weight of the bentonite suspension equal to the unit weight of water has been used in order to obtain a constant excess pressure distribution over the tunnel face. Due to this assumption, this problem can be modelled as the horizontal flow through a layered soil profile by assuming a three-layered soil profile (Figure 42) consisting of different hydraulic conductivities (k_1, k_2 and k_3), thicknesses (D_1, D_2 and D_3) and a constant hydraulic gradient (Equation 3.33), which applies to the flow of each layer. This problem can be calculated by means of Darcy's law, with the assumption that no vertical flow occurs. This is a valid assumption in the case of tunnelling, due to the short time span of a standstill phase between the boring phases and the higher permeability in the horizontal direction. In addition, during boring the available time span for the built-up of the filtercake/penetration zone is limited.

The discharge q_i per layer has been determined using Equation 3.34 and the total flow through the cross section is equal to the sum of the different layers (Equation 3.35). The latter equation indicates that the amount of discharge q_i for each layer is independent of the soil properties of the other layers.

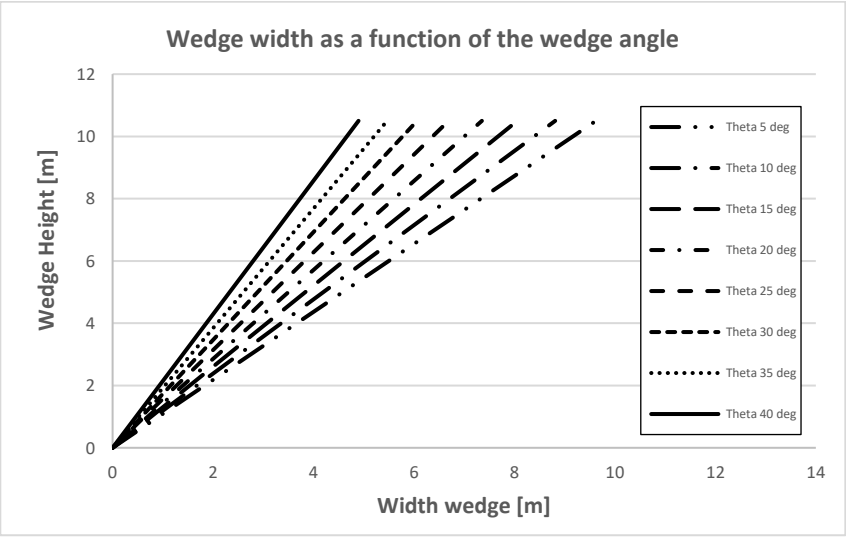

Figure 41. Wedge width for various wedge angles as a function of the wedge height.

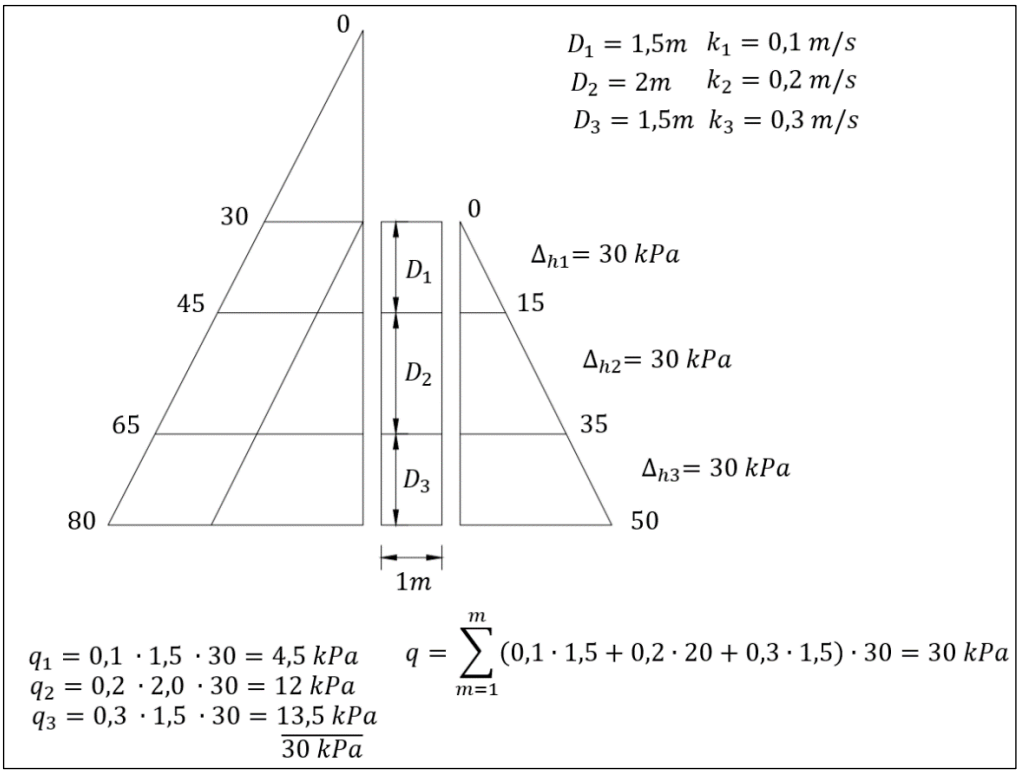

Figure 42. Horizontal flow through a layered soil profile with a constant hydraulic gradient.

$$i = \frac{(h_1 - h_2)}{L} = \frac{\Delta h}{L} \qquad \textbf{[Equation 3.33]}$$

$$q_i = k_i D_i i \qquad \textbf{[Equation 3.34]}$$

$$q = \sum_1^n (k_i D_i) i \qquad \textbf{[Equation 3.35]}$$

q:	discharge per unit area of the aquifer	[m/s]
k_i:	permeability layer i	[m/s]
i:	hydraulic gradient	[-]

3.4.8.4 Linear increasing excess pressure Δs over tunnel face

In the previous paragraph, the discharge q_i per layer was determined for a stratified soil profile with a constant excess pressure distribution. This model has been extended by including a linearly increasing hydraulic gradient (Figure 43). The unit weight of the support medium has therefore been increased to 10.5 kPa. It should be noted that the support medium has a higher unit weight during boring, but this analysis is based on the fact that the TBM does not move, which reflects a standstill situation/ring building phase.

Figure 43 displays two methods for calculating the flow through each layer for a situation with a linearly increasing excess pressure over the tunnel face. In the first calculation method, each layer is assumed a separate aquifer with a constant hydraulic gradient. The flow through each layer has been calculated with Equation 3.34 and the total flow through the soil profile with Equation 3.35. In the second calculation method, the pressure distribution of the support medium is divided into three zones in order to obtain a constant hydraulic gradient for the complete layered soil profile. For this second approach, the flow through each soil layer and the complete soil profile have been calculated for each zone. Due to the shape of a linearly increasing pressure distribution, zones 2 and 3 do not affect the complete profile (Figure 43). The same answer has been obtained from the results of both calculation methods.

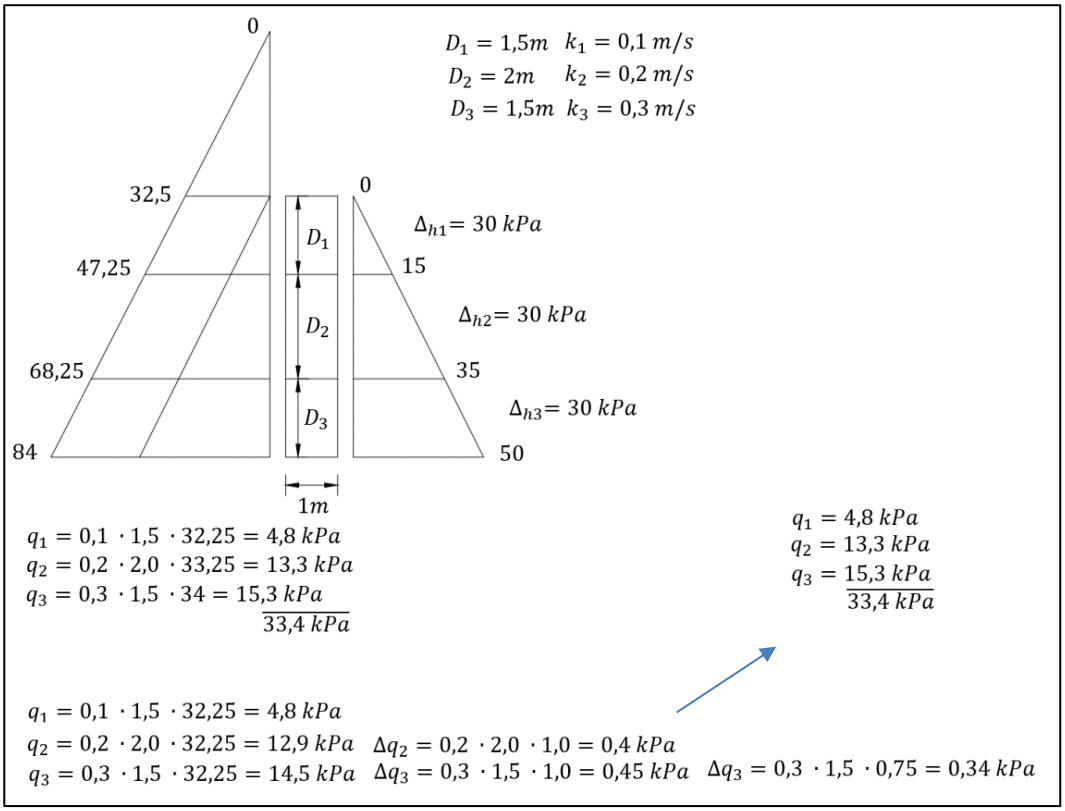

Figure 43. Horizontal flow through a layered soil profile with a linearly increasing hydraulic gradient.

3.4.8.5 Penetration distance and wedge geometry

The cases with a constant and a linearly increasing hydraulic gradient reveal that the flow through each layer does not depend on the (soil) properties of the other layers. The shape of the penetration zone/filter cake in a stratified soil profile can consequently be determined in a straightforward manner. In test series 6, the shape of the maximum penetration zone/filter cake for each case (except C-D) has been determined using Equation 2.13. The properties of the soil and support medium used in this analysis are indicated in Table 7. For the yield strength, the minimum required yield strength in terms of micro-stability (paragraph 2.4) has been used. Due to the use of the lower limit of the yield strength, the highest maximum penetration distance was reached. When a higher value of the yield strength is used, the maximum penetration distance is reduced.

For each case and model, by using the results of test series 1, the excess pressure has been determined by subtracting the hydrostatic pore water pressure from the design value of the minimum support pressure.[30] The calculation results are presented in Annex 3.6. It should be noted that in this analysis, the minimum required support pressure has not been translated to a linear pressure distribution in the excavation chamber of the TBM; this way, the relationship between the components of Equation 2.13 are explained.

Table 8. Properties of the soil and support medium used for this analysis.

Property	
yield-strength support medium	3.4 Pa
d_{10} value sand layer	0.2 mm
d_{10} value clay-layer	4.0 μm

[30] It should be noted that this value is equal to the earth pressure component of the minimum support pressure, e.g. the horizontal effective stress acting on the tunnel face.

Figure 44 displays the penetration distance and wedge shapes for cases A, B and E. The shape of the wedge in the case of a stratified soil profile has been determined by the method described in Paragraph 3.4.8.2. In this analysis, the behaviour of the Ruse-Vermeer model has not been considered, as this is a no limit equilibrium model. It can be seen that the Jancsecz-Steiner model (including vertical soil arching) leads to the lowest penetration distance and the DIN model to the highest penetration distance. In practice, a support pressure distribution higher than the minimum support pressure is used and hence a higher excess pressure is present, which results in an even higher penetration distance. As this topic falls outside the scope of this thesis, this will not be further considered.

Figure 44 displays the difference in penetration distances between the different soil profiles. For the two homogeneous soil profiles (case A and B), the difference in penetration distance is obvious. Due to the lower excess support pressure and lower d_{10} value, an almost negligible penetration distance, also called filter cake, develops within the clay layer. On the other hand, in the sand layer the support medium penetrates the soil to a certain distance and, due to the increase in excess pressure with depth, the penetration distance also increases with depth. In case A it can be observed that near the tunnel invert the highest penetration distances are obtained in combination with the smallest width of the failure wedge. It is therefore possible to conclude that the soil profile near the tunnel invert is the most crucial for determining the effectiveness of the support medium.

In the case of a stratified soil profile, the penetration distance for each soil layer is independent of the penetration distances reached in the other layers. This finding has been validated by the shape of the penetration zone for case E. The upper soil layer in front of the TBM consists of a clay layer in which a filter cake develops, as in case B. The bottom soil layer consists of a sand layer and, as in case A, a penetration zone develops. The shape of this penetration zone is determined by the excess pressure at the tunnel invert, so a large penetration distance is reached. In cases G and H, the soil profile in front of the TBM is switched compared to case E. From this analysis, it is possible to determine that a penetration zone develops in the upper part and a filter cake in the lower part. As the penetrated zone does not fall outside the failure wedge zone, this does not affect the effectiveness of the support medium. These findings indicate that the presence of a highly permeable layer near the tunnel invert has a high influence on the effectiveness of the support medium.

The reduction in effectiveness of the support medium for the three cases indicated in Figure 44 is determined by the ratio of the penetrated area within the wedge with the total penetrated zone (Equation 2.16). The results are displayed in Table 9 which reveals that in cases A and E almost the same effectivity is obtained despite the smaller size of the penetration zone in case E. This is because in case A the penetration zone for the upper layer falls inside the failure wedge. It can therefore be concluded that the effectivity of the support medium only depends on the amount of support medium that falls outside the failure wedge. The only two parameters that can be controlled in order to reduce the penetration distance are the excess pressure and the yield strength of the slurry. The effect of the yield strength of the support medium on the penetration distance is discussed in the next chapter, which describes the time-dependent infiltration process. A more precise analysis has been obtained by including a time component within this analysis, as the exact penetration distances can be obtained instead of using the two limit cases.

In contrast, during boring the effectivity of the support medium is not an important aspect to consider due to the short time span between subsequent passes of the cutting tools, despite the fact that the unit weight of the support medium is higher (12 kN/m^3), which leads to a higher excess pressure.

Table 9. Effectivity of the support pressure for cases A, B and E.

Case [-]	Effectivity support medium	
Case A	**DIN 4126/4085**	**Jancsecz-Steiner**
	83%	79%
Case B	**DIN 4126/4085**	**Jancsecz-Steiner**
	100%	100%
Case E	**DIN 4126/4085**	**Jancsecz-Steiner**
	74%	75%

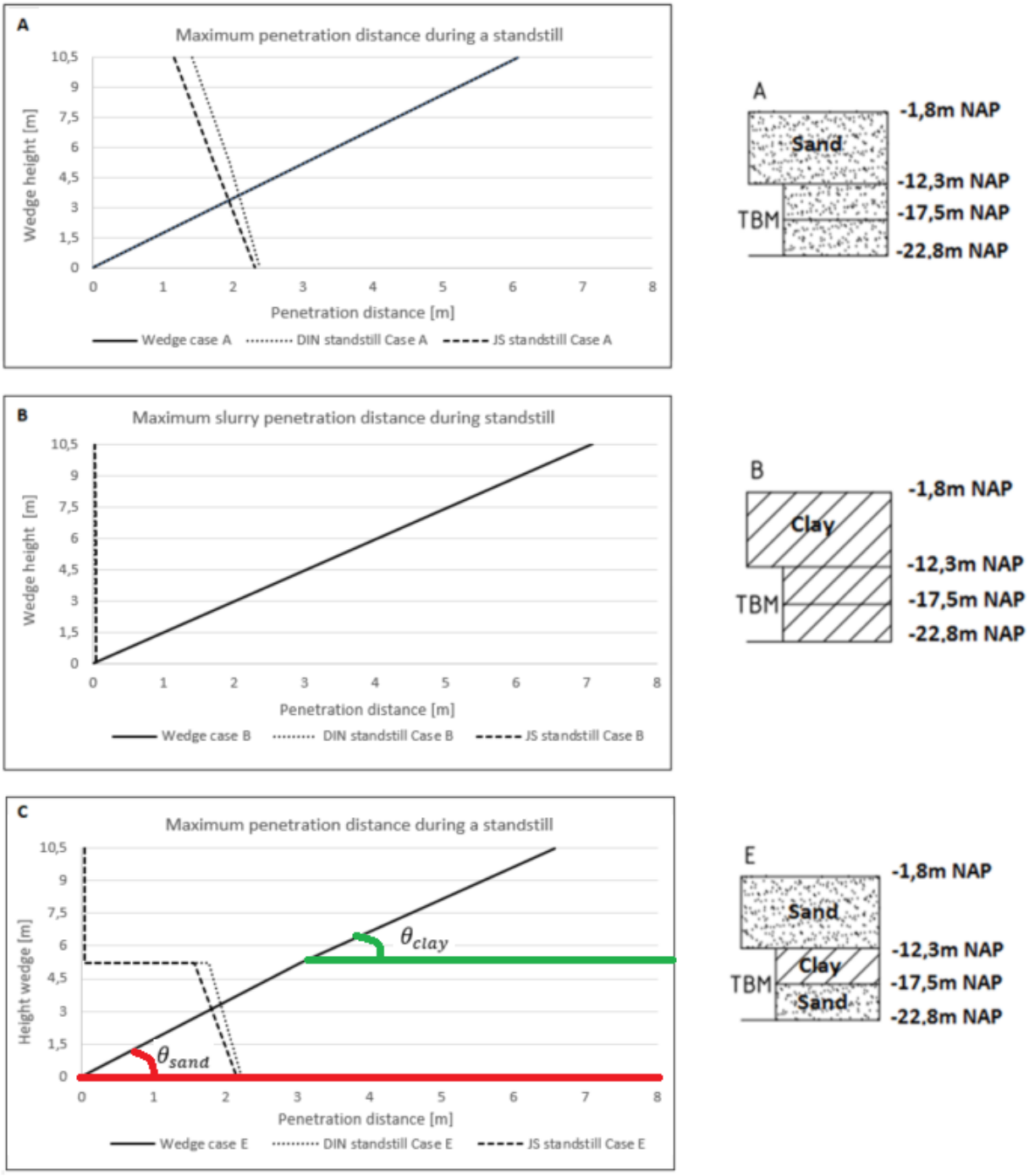

Figure 44. Penetration distance for (a) a homogeneous sand profile (case A), (b) a homogeneous clay profile (case B), and (c) a heterogeneous soil profile (case E).

3.5 (Practical) project analysis

The previous paragraphs describe a thorough background analysis used to determine the differences between the three static models. By using eight case studies, the effect of these differences on the minimum support pressure has been investigated. In addition, some modifications/extensions to the model have been suggested, and the effect of these on the support pressure have been determined. In this paragraph, a more (practical) project analysis is performed, based on the case-study project: The Rijnlandroute. In this analysis, the project design has been evaluated and typical (external) project aspects/objectives that may influence the (static) face stability assessment have been determined. As with the theoretical analysis, the background for each relevant aspect/objective has been reviewed first, and then how these items could be incorporated to the (static) face stability assessment has been investigated. When this is possible, a normative cross-section has been evaluated.

3.5.1 Project design: Eastern entrance zone

This thesis focusses on the Eastern entrance zone (chainage 3900-4300). The tunnel alignment presented in Annex I reveals that the bored tunnel trace lies mainly within the sand layers (4D, 4E and 6), with an overburden of alternating soft layers. The tunnel alignment is situated within the soft layers near the starting shaft. When a more detailed ground investigation was conducted and additional CPTs and boreholes were analysed, it resulted that a large 4C clay layer was present in the tunnel trace (approximately, chainage 4000-4100). From the design phase it resulted, that zone 4080-4240[31] requires additional surcharge in order to counteract for both buoyancy and the minimum support pressure. In addition, zone 4160-4240 requires soil improvement in order to construct these embankments.

The project design at the Eastern entrance zone has been highly influenced by two contract requirements, which are:

1. The Rijnlandroute should maintain the functionality of the waterways it crosses (Rhine-Schie canal).
2. Shipping on the Rhine-Schie canal should not be hindered by construction activities on the Rijnlandroute.

The forgoing leads to two 'problems' that need to be investigated in more detail. The first problem arises due to the contract requirements, which state that no additional ballast that could influence shipping activities is allowed in the canal. This zone therefore requires the lowest possible additional surcharge. The second problem is that the placement of an additional surcharge can induce consolidation in the soil layers above or in front of the tunnel face. These two problems are highly related. For the same soil conditions, a decrease in the minimum support pressure results in a decrease of the required additional surcharge and, consequently, the (one dimensional vertical) consolidation process leads to a smaller value of the excess pore pressures within the consolidating layer[32]. In the case of a partially complete consolidation process, during passing of the TBM, within the consolidating layer above or in front of the TBM, the non-dissipated excess pore pressures result in an additional pressure on the tunnel face, which has to be counteracted. Due to this remaining excess pore pressure, the minimum support pressure required increases. Hence, the increase in minimum support is counteracted by an increase in the amount of additional surcharge. Given these points, it is necessary to incorporate a (simple) consolidation analysis to the face stability assessment.

3.5.2 Minimum support pressure: Canal zone

In order to meet the project objectives a low as possible minimum support pressure is required within the canal zone. The theoretical background analysis has revealed that, in most cases, the Ruse-Vermeer model leads to the lowest minimum support pressure. Despite this, the model assumptions prevent the use of this method. The remaining part of this analysis consequently focusses on the two limit equilibrium models, the DIN4085/4126 model and the Jancsecz-Steiner (K_{A3D}) model.

[31] Due to confidentiality issues, the actual amount of additional surcharge within the canal zone is not discussed.
[32] The required additional surcharge in order to counteract the buoyancy of the tunnel is disregarded.

In contrast to the Jancsecz-Steiner model, some improvements/modifications of the DIN model have been suggested in the theoretical background analysis, namely:

- modification of the horizontal soil-arching component;
- inclusion of the vertical soil-arching component.

The following paragraphs explores the combined implementation of these two components on the minimum support pressure. The implementation of these two components has been investigated for the part without the additional surcharge (chainage 3900-4100) so that the effect of the consolidation process can be neglected. Each implementation has been compared with the minimum support pressure according to the Jancsecz-Steiner models.

3.5.2.1 Modification: Horizontal soil-arching component

Based on the results of the theoretical background analysis and test series 4, the modification of the horizontal soil-arching component in the DIN model is recommended. The depth *z* below the ground surface is translated to the depth *z* below the tunnel crown. The reason for this change is that horizontal soil arching only occurs at the tunnel face; consequently, the spatial state of the stress has only been incorporated in this location. For the Eastern entrance zone (chainage 3900- 4100), the minimum required support pressure has been calculated for the following situations:

- DIN model
    - depth *z* below ground surface
    - depth *z** below tunnel crown
- Jancsecz-Steiner K_{A3D} model without soil arching (JS-model)
- Jancsecz-Steiner K_{A3D} model including soil arching (JS*-model)

Figure 45 displays the minimum support pressure required at the tunnel axis for the Eastern entrance zone. It should be noted that a higher minimum support pressure is required in the case of the DIN model with the modified horizontal soil-arching component, as the wall-length reduction component decreases along with the horizontal soil-arching component. In addition, this difference increases with increasing soil cover. Figure 45 also displays the required minimum support pressure obtained by the Jancsecz-Steiner models. Likewise, in the case-study analysis, the original DIN model and the Jancsecz-Steiner model without vertical soil arching result in almost identical support pressure, as both these limit equilibrium models disregard the effect of vertical soil arching. If the Jancsecz-Steiner model includes vertical soil arching (JS*-model), then the minimum support pressure drops and an offset is present.

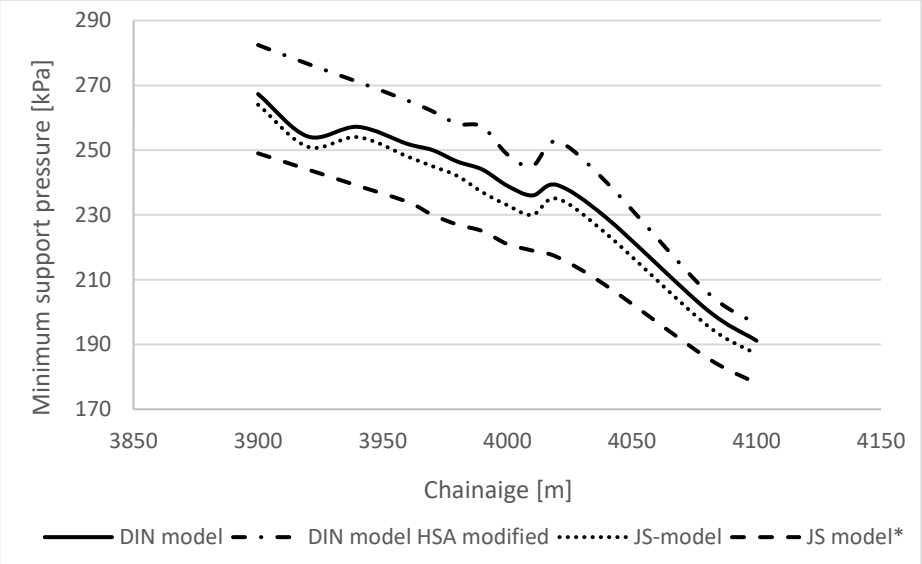

Figure 45. Minimum support pressure required at the tunnel axis for the eastern entrance zone. The Jancsecz-Steiner model indicated by a * take the modified horizontal soil arching approach (depth z below tunnel crown) into account.

3.5.2.2 Modification: Vertical soil-arching component

In the original DIN model, vertical soil arching has not been taken into account, so the full weight of the overburden acts as a surcharge. The theoretical background analysis and test series 5 have revealed that when vertical soil arching is considered, this leads to a reduction in the support pressure. In this analysis, the minimum support pressure at the tunnel axis has been calculated for both 2D and 3D soil arching.[33] The results are displayed in Figure 46. This figure illustrates that the reduction effect is the strongest in the case of 3D soil arching, as in this case friction along all the sides of the soil overburden has been taken into account. Other important aspects that can be obtained from Figure 46 are that, for the given soil profile within the Eastern entrance, the original DIN model that includes 3D vertical soil arching approaches the Jancsecz-Steiner model that includes vertical soil arching. One of the reasons for this is that the incorporation of vertical soil arching to the DIN model is based on the same method as that used for the Jancsecz-Steiner model. Both models take vertical soil arching into account through a reduction of the vertical effective stress acting on the tunnel crown. Therefore, the vertical effective stress from tunnel crown to tunnel invert decreases.

3.5.2.3 Combining horizontal and vertical soil-arching component

The previous two paragraphs and Figure 45-46 indicate that the modification of the horizontal soil-arching component results in a higher minimum support pressure, and the inclusion of the vertical soil-arching component leads to a lower minimum support pressure. In order to find the combined behaviour of these two model components, the minimum support pressure has been calculated including both components; the results are illustrated in Figure 47. This figure reveals that the offset between the DIN model including 2D/3D vertical soil arching[34] and the original DIN model has been reduced. The DIN model that includes 2D vertical soil arching is equal to the original DIN model, and around chainage 3900-4000 it becomes even higher than the original DIN model. The reason for this is that in the original DIN model, the horizontal arching effect in terms of wall length reduction is highly influenced by the thickness of the soil cover. For chainage 3900-4000, the soil overburden is so high that the original model results in a lower minimum support pressure than the model that includes both 2D vertical soil arching and a modification of the horizontal soil-arching component. The offset between the original DIN model and both Jancsecz-Steiner models remains constant, as those two models have not been changed. In summary, the reduction of vertical soil arching within the DIN model is lowered by including the modification of the horizontal soil-arching component.

3.5.3 Consolidation analysis of the additional surcharge

As described before, it is necessary to incorporate a (simple) consolidation analysis to the face stability assessment. In order to do so, first the background of the consolidation analysis has been investigated and thereafter a method is proposed for the implementation of this analysis within a face stability assessment. In the Rijnlandroute project, the additional surcharge has been be placed at chainage 4080-4240, and a cross-section has been made each 10/20 metres. Due to a lack of information about the soil improvement, only the zone without soil improvement has been analysed further (chainage 4080-4160). For each cross-section the following properties are determined:

- drainage paths;
- consolidation time;
- degree of consolidation.

In these calculations, it has been assumed that the additional surcharge had been placed two years prior to tunnel boring[35]. The calculations of the relevant cross-section[36] are presented in Annex 4, while a summary of the results is detailed in Table 10. The background of these calculations are discussed in detail for the normative cross-section.

---

[33] In this analysis, the horizontal soil arching component is based on the original DIN model. This means that for the wall length reduction, a depth z below the ground surface has been taken into account.

[34] This model incorporates both vertical soil arching and the modification of the horizontal soil arching component.

[35] This assumption is made based on the available project information.

[36] The relevant cross-sections are those in which consolidation occurs.

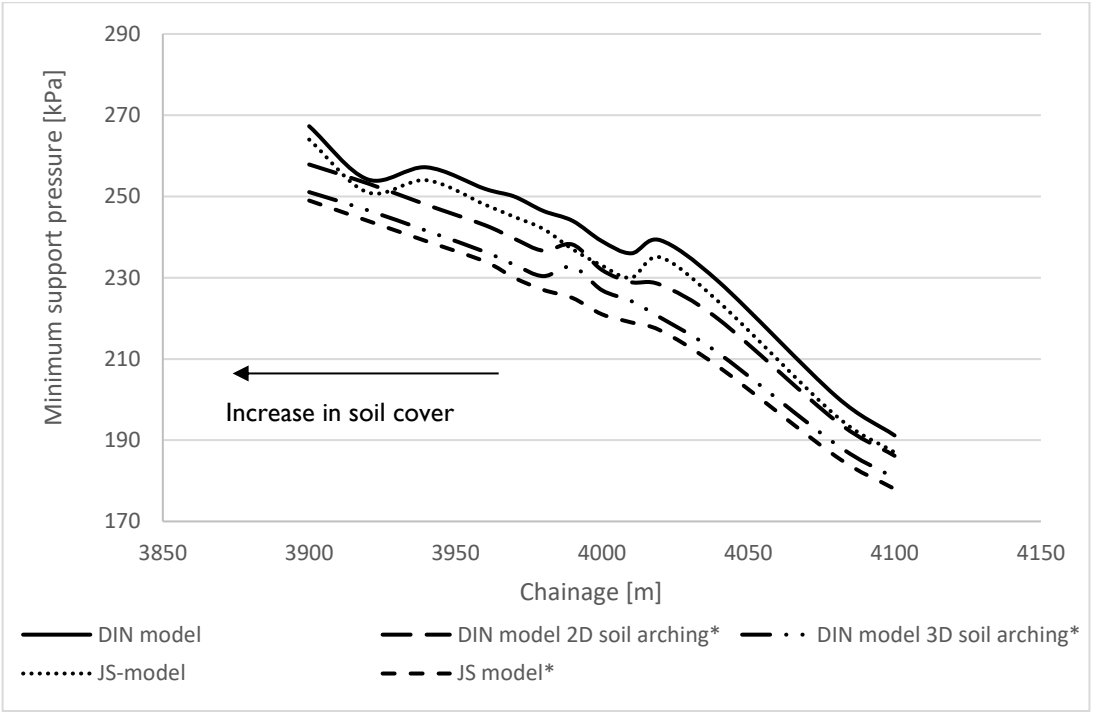

Figure 46. Minimum support pressure required at the tunnel axis for the eastern entrance zone. The DIN models indicated by a * take 2D/3D vertical soil arching into account in combination with the original horizontal soil arching approach (depth z below the ground surface).

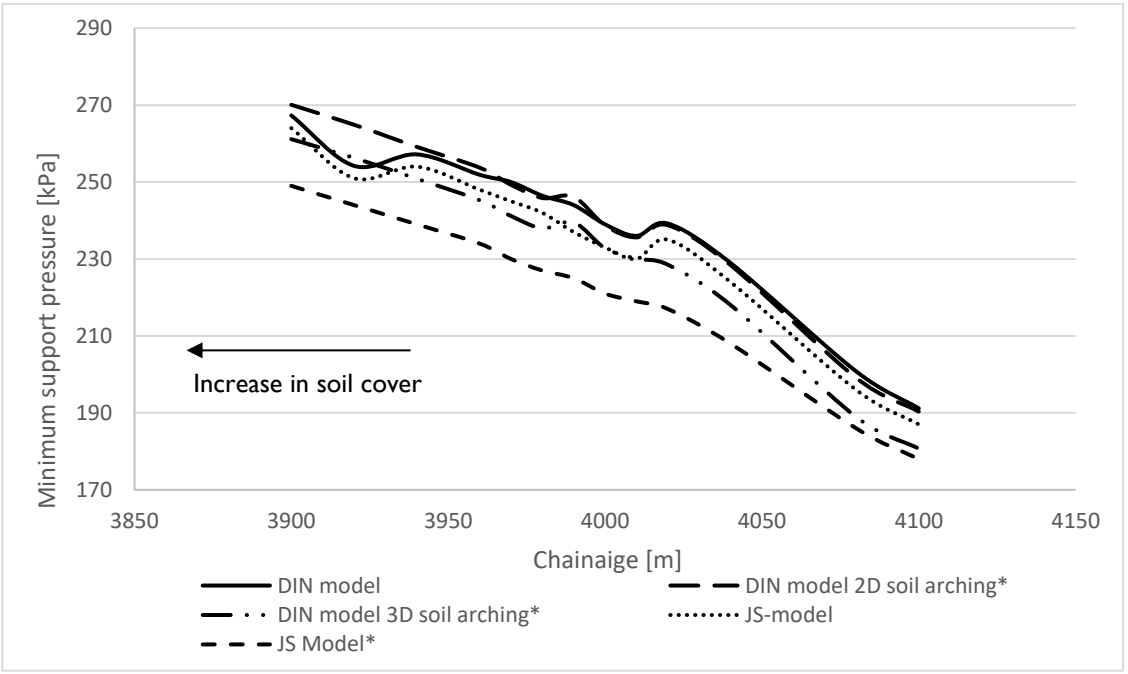

Figure 47. Minimum support pressure required at the tunnel axis for the eastern entrance zone. The DIN models indicated by a * take 2D/3D vertical soil arching into account in combination with the modified horizontal soil arching approach (depth z below tunnel crown).

3.5.3.1 One-dimensional vertical consolidation analysis

Both limit equilibrium models use the full weight of the additional surcharge as an increase in the total vertical stress, which is thereafter converted to a horizontal (effective) stress at the tunnel face by using the model's parameters. The placement of the additional surcharge q_o on the (soft) subsoil leads to a total stress increment of Δq_o. Due to the width of the embankment compared to the width of the tunnel face, this problem can be approximated by a 1D vertical consolidation analysis with zero lateral strain. In a first instance, this stress is fully carried by the excess pore water pressure u_e. By draining some of the pore water, the process continues until the excess pore water pressure set up by an increase in the total stress has completely dissipated (Figure 48). Simultaneously, the vertical effective stress increases from its initial value σ'_{vi} to σ'_{v1} ($=\sigma'_{vi} + \Delta q_o$). At each moment during the consolidation process, the sum of the vertical effective stress increase and the remaining excess pore water pressure is equal to the change in the total stress Δq_o.

In addition to the vertical stress change component due to consolidation, also the horizontal stress change component due to consolidation is relevant. The excess pore water pressure is uniform and therefore the lateral excess pore water pressure is equal to the vertical excess pore water pressure. This means that the lateral excess pore water pressure dissipates with time equal to the distribution u_e as displayed in Figure 48. In contrast, the increase in horizontal effective stress is not equal to the increase in vertical effective stress. The reason for this is that the horizontal effective stress is obtained by a multiplication of the vertical effective stress with a lateral earth pressure coefficient, which can either be equal to the active, neutral or passive earth pressure coefficient.

In case of tunnel face stability, the horizontal effective stress acting at the tunnel crown is derived in the same manner as in the soil. Both Jancsecz-Steiner models, determine the horizontal effective stress by a multiplication of the vertical effective stress with a coefficient $K_{A3D.}$ The value of this coefficient is a function of the friction angle and is approximately equal to the active earth pressure coefficient (Figure 32). In case of the DIN-model, the horizontal effective stress is determined by an active earth pressure coefficient and reduced by the effect of cohesion. In addition, in case of a three dimensional analysis, the minimum support pressure is reduced by introducing shape coefficients.

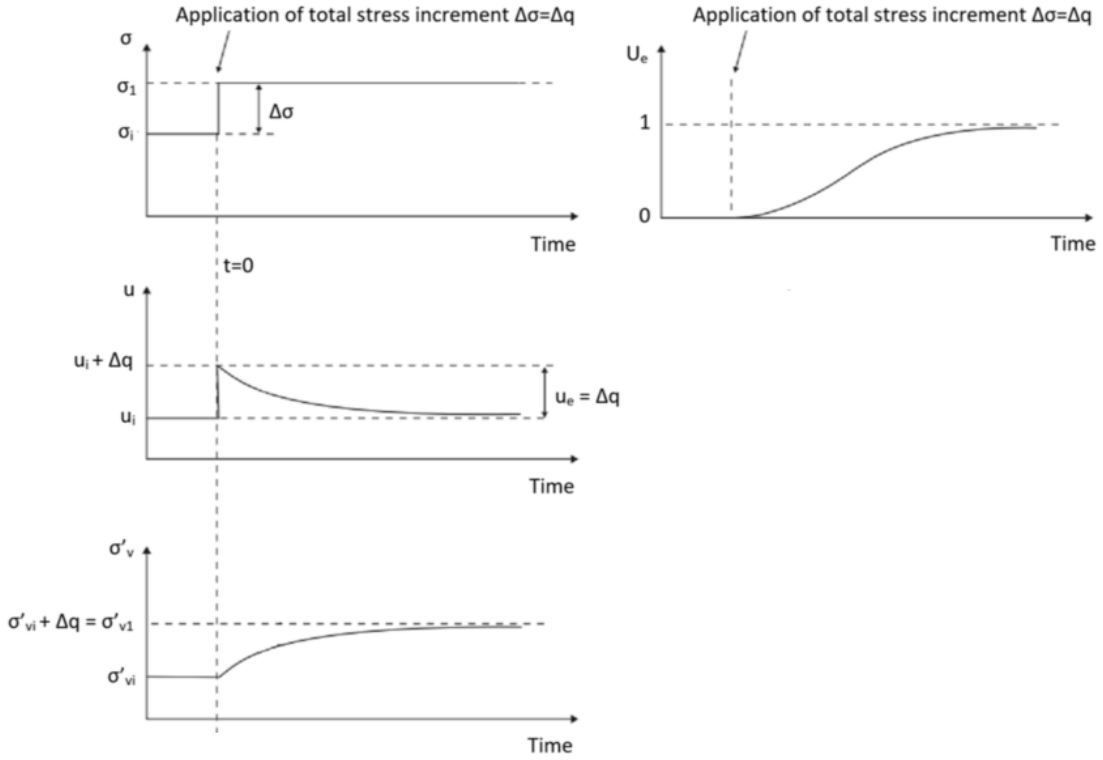

Figure 48. Consolidation analysis of a soil element under an increase in total vertical stress $\Delta\sigma=\Delta q_o$.

3.5.3.2 Normative cross-section

From the calculation results in Annex 4 and the summary in Table 10, a normative cross-section has been chosen, for which a more-in depth study have been performed. From the analysis, it is possible to conclude that chainage 4080 and 4100 are both normative. At these two locations, a large, not-fully-consolidated clay layer (4C) is present during boring in front of the TBM. This layer leads to an additional lateral stress, acting on the tunnel face, which has to be counteracted by the support pressure. In addition, a soft low-permeable layer with a long consolidation time is also present above the TBM. The consolidation process within this layer affects the vertical effective stress distribution with time in the soil overburden and therefore also the vertical soil arching calculation.

As in chainage 4080 the soil layers in the overburden can be analysed separately, this cross-section has been used as the normative cross-section. In cross-section 4080 (Figure 49), the peat layer (3) is completely situated in the soil overburden and the clay layer (4C) is situated both in the soil overburden and the soil profile in front of tunnel face; consequently, the placement of an additional surcharge leads to two different 'mechanisms' that need to be investigated. The first mechanism corresponds to the maximum support limit (paragraph 2.2) and the second mechanism corresponds to the minimum support pressure limit. The way in order to incorporate a consolidation analysis within the calculation of the two limits is described in the next paragraphs.

Table 10. Summary of the calculation results of the consolidation analysis detailed in Annex 4.

Chainage	Results consolidation analyse
4080	**Soil profile:** The soil cover consists of a thick peat layer (3) and a clay layer (4C). The latter is situated above and below the tunnel crown. **Consolidation time:** The two soil layers have a long drainage path that, in combination with a low consolidation coefficient, leads to a large consolidation time. **Degree of consolidation:** The degree of consolidation at the (closed) boundary of the peat layer equals 1% and 5% for the closed boundary of the clay layer. **Face stability problems:** At the time of boring, the degree of consolidation for the 4C clay layer is low, which leads to an additional lateral stress (excess pore pressure) that has to be counteracted. **Maximum support pressure:** The increase in vertical effective stress is almost nil; therefore, the maximum support pressure needs to be calculated with the initial vertical effective stress.
4100	**Soil profile:** The soil cover consists of a clay layer (2A), a peat layer (3) and a clay layer (4C). The latter is situated above and below the tunnel crown. **Consolidation time:** The soil layers have a long drainage path that, combined with a low equivalent consolidation coefficient, leads to a large consolidation time. **Degree of consolidation:** The degree of consolidation at the middle of the three soil layers equals 6%. **Face stability problems:** At the time of boring, the degree of consolidation for the 4C clay layer is low, which leads to an additional lateral stress (excess pore pressure) that has to be counteracted. **Maximum support pressure:** The maximum support pressure for the soil layers above the tunnel crown is calculated by taking the increase in vertical effective stress into account.
4120 **4140**	**Soil profile:** The soil cover consists of a clay layer (2A), a peat layer (3), a clay layer (4C), and a peat layer (3) is located at the tunnel face. **Consolidation time:** The soil layers have a long drainage path that, in combination with a low equivalent consolidation coefficient, leads to a large consolidation time (>2 years). **Degree of consolidation:** The degree of consolidation at the middle of the three soil layers together equals 30%. The degree of consolidation for the peat layer located at the tunnel face equals 50%. **Face stability problems:** The peat layer (3) is not fully consolidated, which leads to an additional lateral stress (excess pore pressure) during boring. **Maximum support pressure:** The maximum support pressure for the soil layers above the tunnel crown is calculated by taking the increase in vertical effective stress into account.

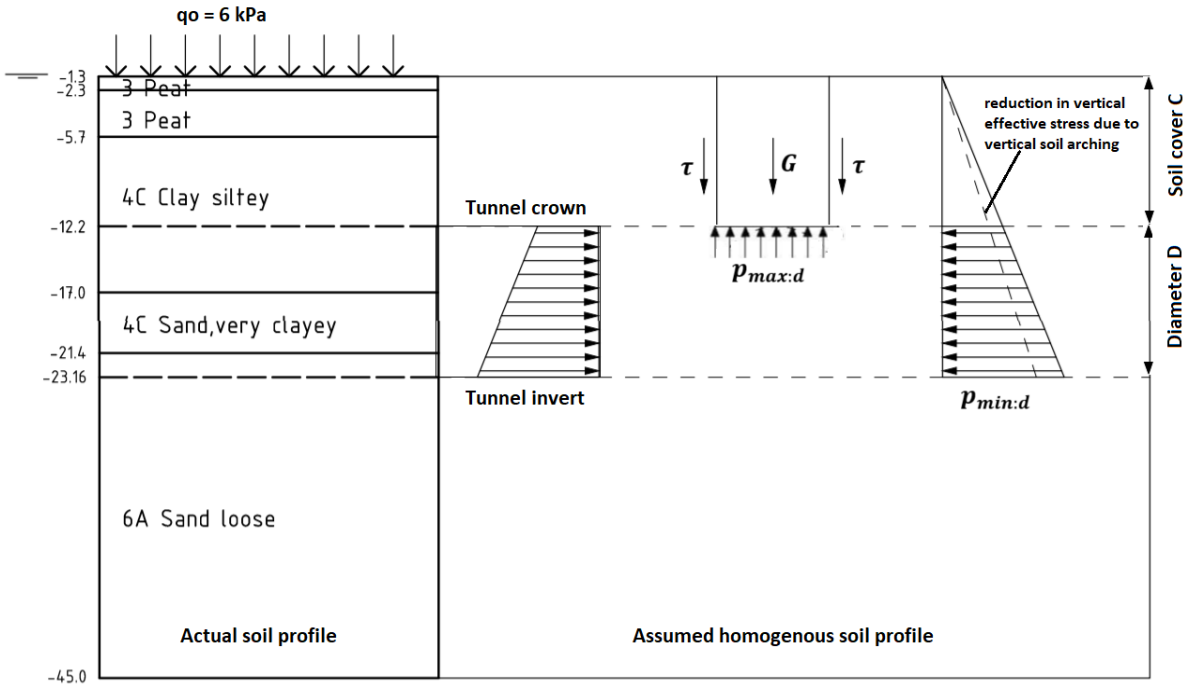

Figure 49. The normative cross-section at chainage 4080. The two mechanism which needs to be reviewed are indicated. For simplicity these mechanism are indicated within a homogeneous soil profile.

3.5.3.3 Consolidation process: Both layers

Both the 4C clay layer and the 3 peat layer in the normative cross-section are half-closed: In the top peat layer, the excess pore pressures can only dissipates to the top, and in the bottom clay layer, the excess pore pressures can only dissipates to the bottom of the layer (Figure 50a). From the calculations in Annex 4, it resulted that the consolidation time for the peat layer equals 7494 days and the consolidation time for the second layer equals 14779 days. In order to visualise the consolidation process, the degree of consolidation for a time step of 1500 days is calculated. In addition, the increase in vertical effective stress and decrease in excess pore pressure are calculated for each time step.

The distribution of the excess pore pressures within a soil layer as a function of time is represented by isochrones as displayed in Figure 50b. Because of the set-up of this graph, the distribution of the excess pore pressures within a soil layer for different drainage boundaries can be determined. In case of a soil-layer with two drainage boundaries, the drainage path is equal to half of the soil layer. The shape of the isochrones show that the degree of excess pore pressure dissipation at the upper part of the soil layer is equal to the bottom part of the soil layer. In case of a half closed soil layer, the excess pore pressures dissipates in only one direction. Therefore, the degree of excess pore pressure dissipation at a point as a function of time and depth for a half closed layer can be determined by the upper half or the bottom half of the graph.

For both soil layers, the increase in vertical effective stress and decrease in excess pore pressure with time at the boundary between the two layers is calculated (Figure 50a&b). The reason for this is that for both layers, this location has the longest drainage path and thus the consolidation process take the longest time. Figure 51 indicates the increase in vertical effective stress and decrease in excess pore pressure at the boundary of the two soil layers. It can be observed that at the layer boundary for a given time, neither the increase in vertical effective stress nor the decrease in excess pore pressure of the peat and clay-layer are equal. The reason for this behaviour is that the analysis assumes that these layers are not 'coupled', so a separate analysis is performed for each layer. This means that it is assumed that the boundary between the two layers is impermeable, and so no flow occurs over this boundary.

From the soil parameters it can be obtained that the peat layer has a vertical permeability of $4 \cdot 10^{-9}$ m/s and the clay layer has a vertical permeability of $5 \cdot 10^{-9}$ m/s. Despite the low values of the vertical permeability, the soil layers are not impermeable and so drainage will occur at the boundary of these two layers. The combined behaviour is modelled by using an equivalent consolidation coefficient for the two layers together. The combined soil profile is free to drain on both sides and therefore the drainage length changes to an equivalent drainage length H^{eq} (Figure 50a). The increase in vertical effective stress and decrease in excess pore pressures are calculated at the exact same location and the results has been added to Figure 51. As this location is not located in the middle of the soil profile, the ratio z_{dr}/H_{dr} is not equal to unity, but a z_{dr}/H_{dr} ratio = 3,4/7,35=0,46 applies. This figure illustrates that the curves obtained lie exactly between the curves of the separate analysis.

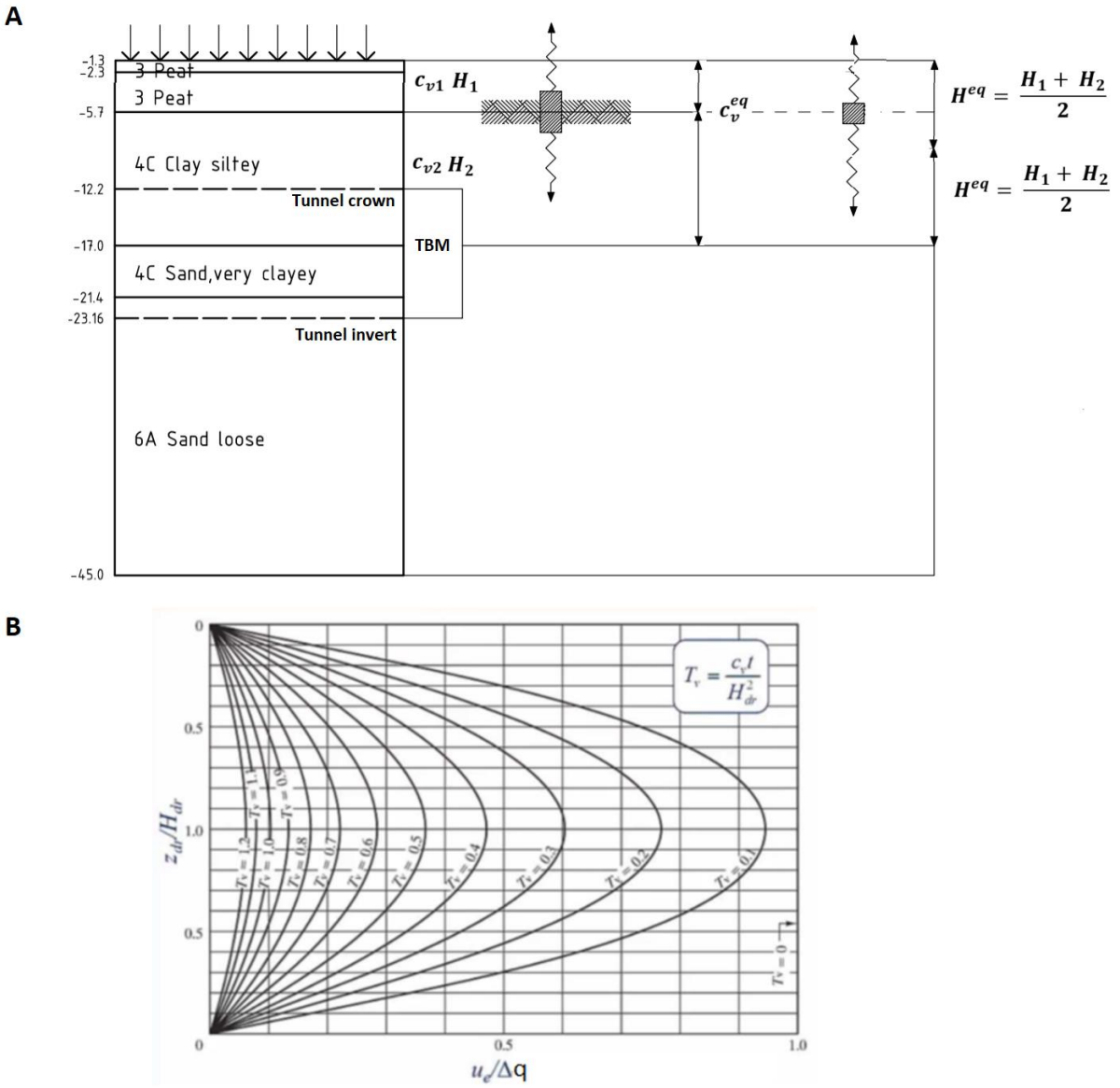

Figure 50. The consolidation process for the soft soil layers. In (a) both a coupled as uncoupled consolidation process for both soil layers is indicated and (b) the universal graph with isochrones is used to determine the degree of excess pore pressure dissipation at a point as a function of time and depth (Kitch,2015).

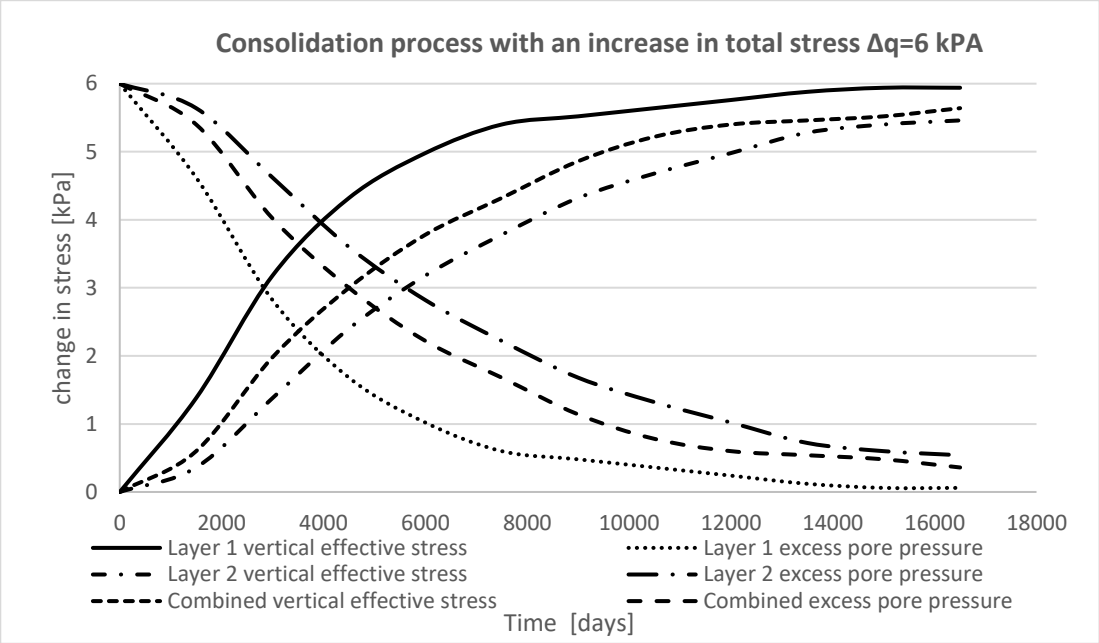

Figure 51. Consolidation process for the peat layer, the clay layer, and the two layers combined, due to the placement of an additional surcharge Δq_o.

3.5.3.4 Consolidation process: Soil layer located in soil overburden

A soil layer located in the soil overburden contributes to the maximum and minimum pressure limits of the support medium (Figure 49). The placement of an additional surcharge increases both the total stress as the effective stress distribution within the soil cover. The effect of the consolidation process for both support pressure limits is described in the following two paragraphs.

3.5.3.4.1 Influence consolidation process on the maximum support pressure limit

The maximum support pressure limit is a function of the weight of the soil cover that is present above tunnel crown. As described in paragraph 2.2, the maximum support pressure limit is based on a blow-out mechanism and this is schematised as the upward deformation of a soil column with height *C*. Due to the upward movement, shear stresses are generated at the sides of the soil column (Figure 49). The upper limit is calculated as the sum of the self-weight of the soil column (total stress) and the friction forces (effective stress). This means that the placement of an additional surcharges affects both components. In contrast to the total stress change, the increase in vertical effective stress is a function of time and thus the friction forces acting at the sides of the soil column increases with time.

In paragraph 2,2, an equation have been set-up for the maximum support pressure for both homogeneous and stratified soil profiles, including consolidation effects. As the total vertical stress remains constant during the consolidation process, this means that only for the friction forces a time-component has been integrated within the equation. For the calculation of the maximum support pressure at the time of boring $p_{max;r}(t_{boring})$ the increase in vertical effective stress is required. As the time span between the placement of the additional surcharge and the passing of the TBM is known, the exact increase in vertical effective stress can be determined by a consolidation analysis. The consolidation process for a soil layer located in the overburden can be simplified by using the average degree of consolidation. This is a valid assumption, as instead of the exact vertical effective stress distribution over the height of the soil layer as a function of time, the cumulative gain in effective stresses with time is required. Instead of using the isochrones from Figure 50, the average degree of consolidation $U_{average}$ has been calculated utilising Equation 3.36. Figure 52 displays the average increase in the vertical effective stress and the average decrease in the excess pore pressure with time for the complete peat layer. For this consolidating soil layer located in the soil overburden, only the change in vertical effective stress with time is important. The decrease in excess pore pressures can be neglected unless the dissipation of these excess pressures is confined. As this is not the case for the Eastern entrance zone, the lateral stresses have been neglected.

$$U_{average}[\%] = \sqrt{\frac{4T_v}{\pi}} x100 \qquad T_v \leq 0{,}217 \qquad \textbf{[Equation 3.36a]}$$

$$U_{average}[\%] = \left[1 - 10^{-\left(\frac{0{,}085+T_v}{0{,}933}\right)}\right] x100 \qquad T_v > 0{,}217 \qquad \textbf{[Equation 3.36b]}$$

3.5.3.4.2 Influence consolidation process on the minimum support pressure limit

The minimum support pressure limit is determined by using the vertical effective stress distribution in front of the tunnel face. This stress distribution is a function of the soil profile above the tunnel face. The placement of an additional surcharge leads to a total vertical stress increment over the complete soil profile, and depending on the soil properties of each layer, the increase in vertical effective stress is whether of or not instantaneously. The vertical (effective) stress distribution in front of the tunnel face is not affected by a consolidating layer above tunnel crown, in which the vertical effective stress increases with time.

In contrast, the incorporation of vertical soil arching within the soil overburden results in a reduction of the vertical (effective) stress acting on the tunnel crown and, subsequently, on the vertical (effective) stress distribution in front of the tunnel face (Figure 49). The reduced value of the vertical effective stress including arching at tunnel crown is calculated with Equation 3.1 (homogeneous soil) or Equation 3.31 (stratified soil). Despite the fact that the additional surcharge q_o and increase in vertical effective stress with time are known, these parameters cannot be implemented simply within the formulas, as these equations are based on drained conditions and thus the placement of an additional surcharge q_o on the surface leads to an instantaneous increase of the vertical effective stress within the soil layer. There is currently no method to determine the amount of vertical soil arching in a consolidating soil layer; however, this paragraph details a method that makes this possible. In order to determine a possible method for incorporating vertical soil arching, it has been assumed that the peat layer analysed resembles the complete soil overburden, e.g. a homogeneous soil overburden. For this soil layer, the increase in vertical effective stress with time, due to the placement of an additional surcharge of 6 kPa is indicated in Figure 52. Instead of setting the additional surcharge as equal to the 6 kPa, the additional surcharge has been increased by time till a value of 6 kPa. The increase in additional surcharge at each time step is equal to the increase in the vertical effective stress with time in the consolidating soil layer. In this way, the value of the partial additional surcharge leads to an instantaneous increase of the vertical effective stress within the soil layer equal to the increase in vertical effective stress resulting from the consolidation process. It should be noted that this method is only applicable because the complete layer lies within the soil overburden, like the peat layer, and is not part of the tunnel face, like the clay layer. The reason for this is that, in the latter case, the average consolidation cannot be used and a detailed consolidation analysis is required.

To 'validate' this method, the vertical effective stress acting on the bottom of the peat layer for the normative cross-section 4080 has been determined for the situation without vertical soil-arching, with 2D soil arching and with 3D soil-arching. In addition, these three situations have also been calculated for a case without consolidation e.g. the situation including the additional surcharge reflects the initial situation. The results of these six calculations are indicated in Figure 53.

This figure reveals that the curves of the three cases including the consolidation process have the same shape but are located at a different offset. The reason for this is that the same increase in the additional surcharge q has been used as an input for all three situations. By comparing the case including consolidation (increasing q_o) with the case without consolidation (constant q_o), it can be seen that the case including consolidation approaches the latter situation at the end of the consolidation process. This is logical, as near the end of the consolidation process the additional surcharge is fully transferred to the effective stresses and all excess pore pressures have been dissipated.

From Figure 53 it can be seen that the vertical effective stress acting at the bottom of the peat layer increases with time. In case of a conservative approach, equations 3.1 and 3.31 can be used by taking the full load of the additional surcharge into account. This is a valid assumption as an increase in the vertical effective stress acting at tunnel crown leads to a higher vertical effective stress distribution in front of the tunnel face. For the same soil profile, a higher vertical effective stress distribution leads to a higher value of the horizontal effective stress acting at tunnel face. For situations where a less conservative approach is required, a similar analysis as described above is valid.

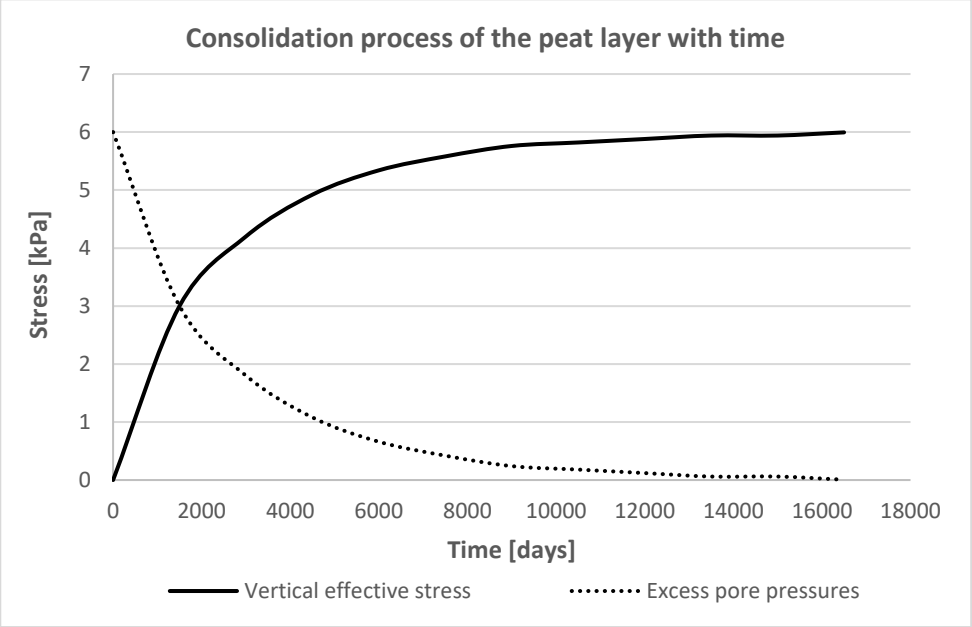

Figure 52. Average consolidation process with time for the peat layer located in the soil overburden.

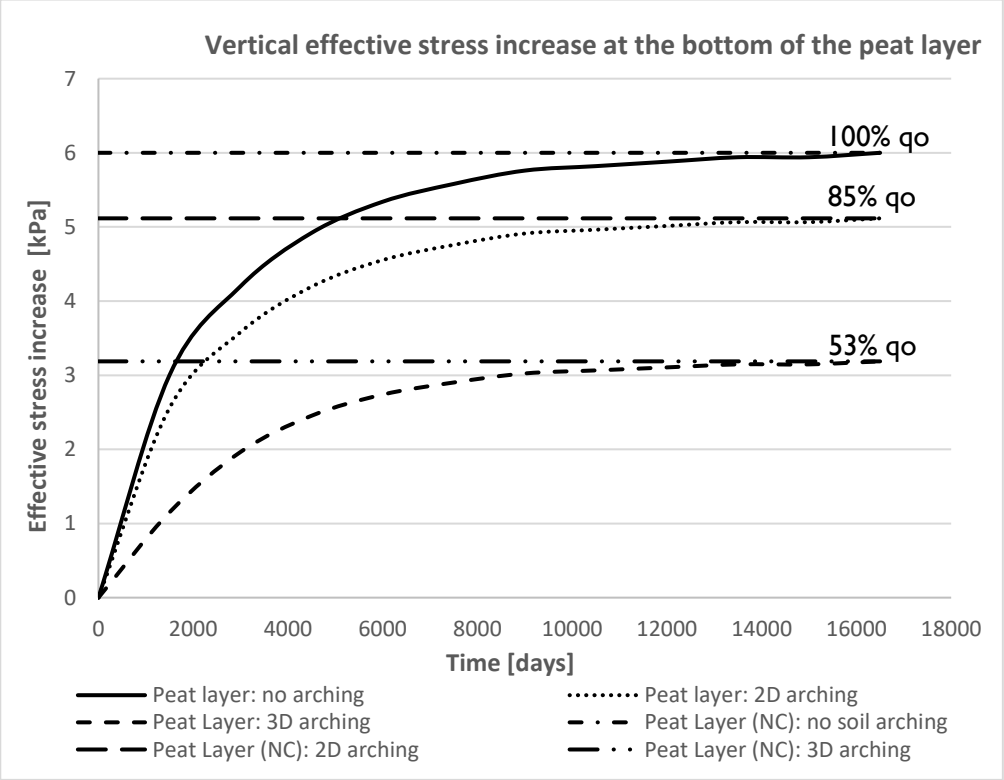

Figure 53. Vertical effective stress increase (including soil arching) at the bottom of the peat layer due to the placement of the additional surcharge.

3.5.3.5 Consolidation process: Soil layer located at the tunnel face

The soil profile located in front of the tunnel face contributes to the minimum support pressure limit. The placement of an additional surcharge increases the vertical (effective) stress, and thus the minimum support pressure (Figure 49). In the case of a consolidating layer situated in front of the TBM, the vertical effective stress increases and the excess pore water pressures reduces with time.

In contrast to a soil layer located at the soil overburden, the incorporation of the consolidation process for a soil layer located at tunnel face is different. In this situation, both the change in the vertical effective stress over the height of the soil layer and the dissipation of the excess pore pressures over the height of the soil layer with time are important. Therefore, in this case, the average degree of consolidation is not applicable, and thus the degree of consolidation needs to be determined. The degree of consolidation $U_{average}$ at a point in the soil layer as a function of depth and time is calculated using isochrone curves (Figure 50).

The soil profile in front of tunnel face consists of a 4C clay layer, a 4D sand layer and a 6A sand layer (Annex 4.1). The placement of an additional surcharge at the surface leads to an increase in the total vertical stress. For the 4D and 6A sand layer, this increase in total vertical stress is instantaneously transferred to the vertical effective stress. This is not the case for the 4C clay layer, as the increase in total stress is first carried by the pore water pressure (excess pore water pressure). This means that the change in the vertical effective stress and excess pore pressure for each soil layer differ between the layers within the soil profile in front of the TBM. This means that the set-up of the method to incorporate the consolidation process has to be designed in such a way that the change in both components per layer can differ.

The calculation method for the minimum support pressure in case of a stratified soil profile is used as a starting point (paragraph 3.2-3.4 and Annex 3.1). The minimum support pressure for a stratified soil profile is determined by dividing the failure mechanism into *N* horizontal layers, with a possible variable thickness d_i and constant soil properties. In this approach, the shearing stresses between the layers have been disregarded so that the entire soil profile above each soil layer can be considered as a surcharge.

For the calculation, the consolidation process over the height of the soil layer is important to determine. As described, the top boundary of the 4C clay layer is closed and the bottom boundary can be seen as a drainage layer. Due to the fact that the clay layer is partly situated in front of the TBM, instead of the top boundary, the location at the tunnel crown has been considered. These three locations can be translated to the isochrones (Figure 54) and it can be observed that at the bottom boundary of the clay layer, no excess pore pressure develops because at this location, the layer is able to drain. In addition, at the top closed-boundary of this clay layer the highest excess pore pressure develops, due to the longest drainage path at this location. Using these isochrones, the increase in the vertical effective stress and the decrease in the excess pore water pressure with time at the tunnel crown and bottom layer boundary have been calculated. The results are illustrated in Figure 55 and this figure confirms the observations of the isochrone analysis.

The change in the vertical effective stress and excess pore water pressure due to consolidation with time are taken into account by extending the minimum support pressure calculation for a stratified soil profile with two time-dependent components called $\sigma'_{consolidation}(\sigma'_{con})$ and $u_{consolidation}(u_{con})$. Using these additional two components, it is easy to differentiate between the increase in the vertical effective stress and decrease in excess pore water pressure for each soil layer. The minimum support pressure before the placement of the additional surcharge reflects the initial minimum support pressure. After the placement of the additional surcharge per soil layer, the change in both the vertical effective stress σ'_{con} and the excess pore pressure u_{con} have been taken into account by the additional components for each time step. In addition, in the case of a soil layer, where the placement of the additional surcharge leads to an instantaneously transfer to the vertical effective stress, these additional components have been set, as a constant, to $\sigma'_{con} = \Delta q_o$ and $u_{con} = 0$.

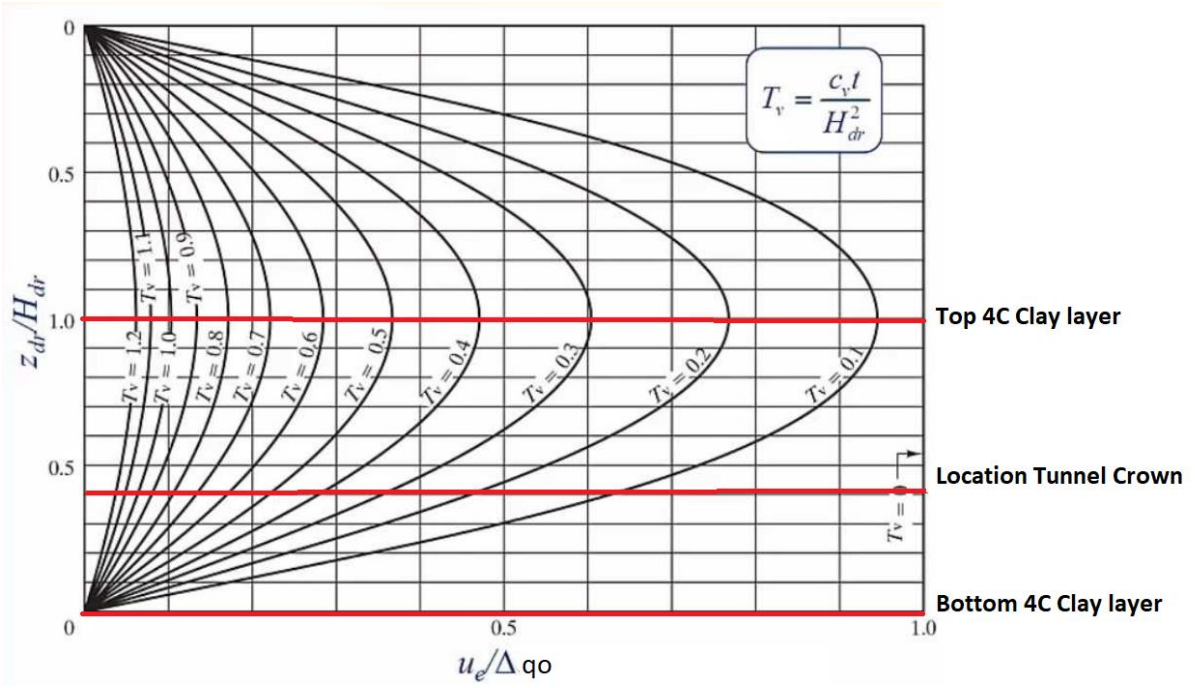

Figure 54. The locations at the isochrones (z_{dr}/H_{dr} *ratio*) which are used to calculate the increase in vertical effective stress and decrease in excess pore pressure with time for the clay layer located in front of the tunnel face.

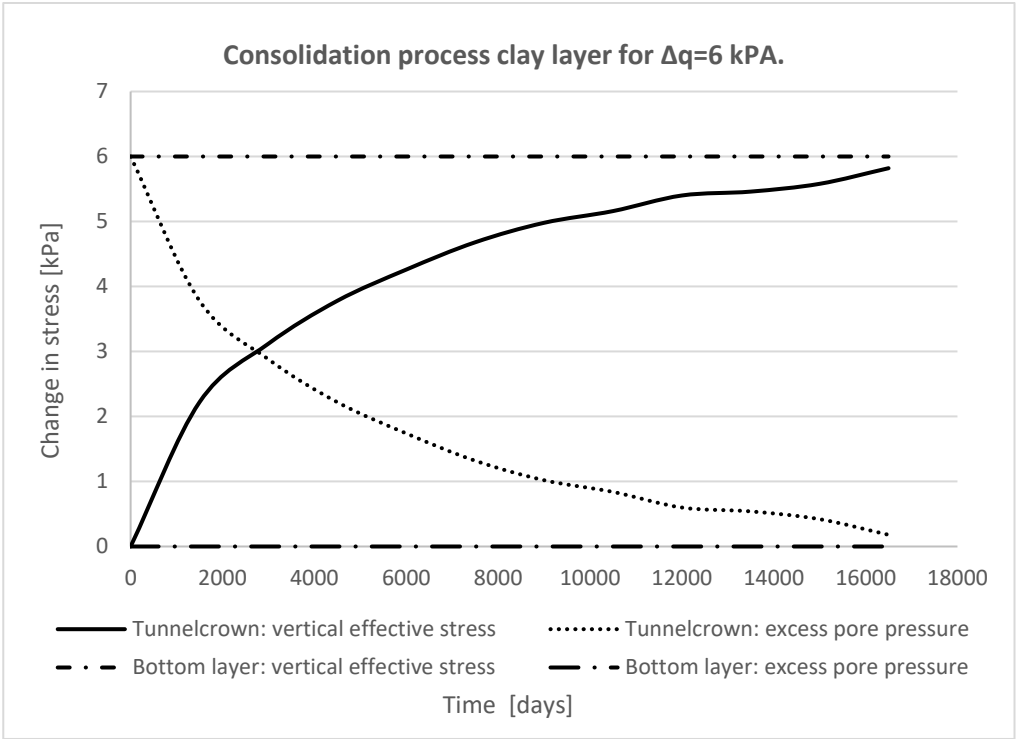

Figure 55. Consolidation process of the 4C clay layer at the location of the tunnel crown and the 4C bottom layer.

With the analysis described above, the consolidation process can be integrated within a minimum support pressure calculation. Due to the difference in model parameters, the incorporation of this process differs between the Jancsecz-Steiner models (Equation 3.37a) and the DIN-model (Equation 3.37b). For both models, the input values for the additional components σ'_{con} and u_{con} have been obtained through a separate analysis, based on the isochrones and the degree of consolidation $U_{average}$.

The minimum support pressure for the normative cross-section 4080 has been calculated using Equation 3.37 for a time step Δt of 1,500 days. In both sand layers (4D and 6A), the increase in total stress is instantaneously transferred to the vertical effective stress, therefore these additional components have been set, as a constant, to $\sigma'_{con} = \Delta q_o$ and $u_{con} = 0$. For the 4C clay layer, the consolidation process has to be taken into account, which means that at these locations the minimum support pressure is a function of both the vertical effective stress and the excess pore pressure with time.

The minimum support pressure with time has been calculated at both the tunnel crown and the bottom boundary of the 4C clay layer. As described, this bottom boundary is a drainage layer; therefore, no excess pore pressures are generated at this location, as indicated in Figure 55. This means that the change in the minimum support pressure by including consolidation is clarified by plotting the minimum support pressure at the tunnel crown as a function of time (Figure 56).

$$p_{min:d}(t_i) = \gamma_h \left((\sigma'_v + \sigma'_{con}(t_i))\, K_{A3D}\right) + \gamma_{u1} \left(u_1 + u_{con}(t_i)\right) \qquad \textbf{[Equation 3.37a]}$$

$$p_{min:d}(t_i) = \left[\gamma_h \left(\frac{(\sigma'_v + \sigma'_{con}(t_i))\, K_A\, D^r}{D}\right) - cK_{ac}\right] + \gamma_{u1}(u_1 + u_{con}(t_i)) \qquad \textbf{[Equation 3.37b]}$$

$\sigma'_{con}(t_i)$:	vertical effective stress increase with time t_i after start of the consolidation process (placement of the additional surcharge)	[kN/m³]
$u_{con}(t_i)$:	decrease in excess pore pressure with time t_i after start of the consolidation process (placement of the additional surcharge)	[kN/m³]

The minimum support pressure at the tunnel crown before the placement of an additional surcharge ($t_i < 0$) equals 124 kPa. Immediately after the placement of the additional surcharge ($t_i = 0$), the increase in the total vertical stress is carried by the excess pore water pressure ($u_{con} = \Delta q_o$). As this stress is uniform, this means that this results in a lateral stress equal to the value of the additional surcharge q_o. From this time step on ($t_i > 0$), these excess pore water pressures dissipates and hence the lateral excess pore water pressure decreases. In addition, the vertical effective stress increases simultaneously, and the horizontal effective stress increases consequently. An import aspect to note is that the value of these horizontal effective stress is not equal to the vertical effective stress.

The minimum support pressure calculation including the consolidation process has been repeated for different values of additional surcharge q_o[37] and the results are displayed in Figure 56. All these cases starts from the initial minimum support pressure of 124 kPa. To conclude, for a soil layer located at tunnel face, the effect of consolidation can have a high impact on the minimum support pressure due to the consolidation-induced lateral excess pore water pressure acting on the tunnel face.

In contrast to the maximum support pressure, the minimum support pressure decreases during the consolidation process. This means that when the consolidation process not have been completed at the moment of boring, the neglection of these lateral excess pore water pressures can lead to global collapse, due to the use of a support pressure below the minimum support pressure limit.

[37] It has been assumed that these additional surcharges are placed simultaneously.

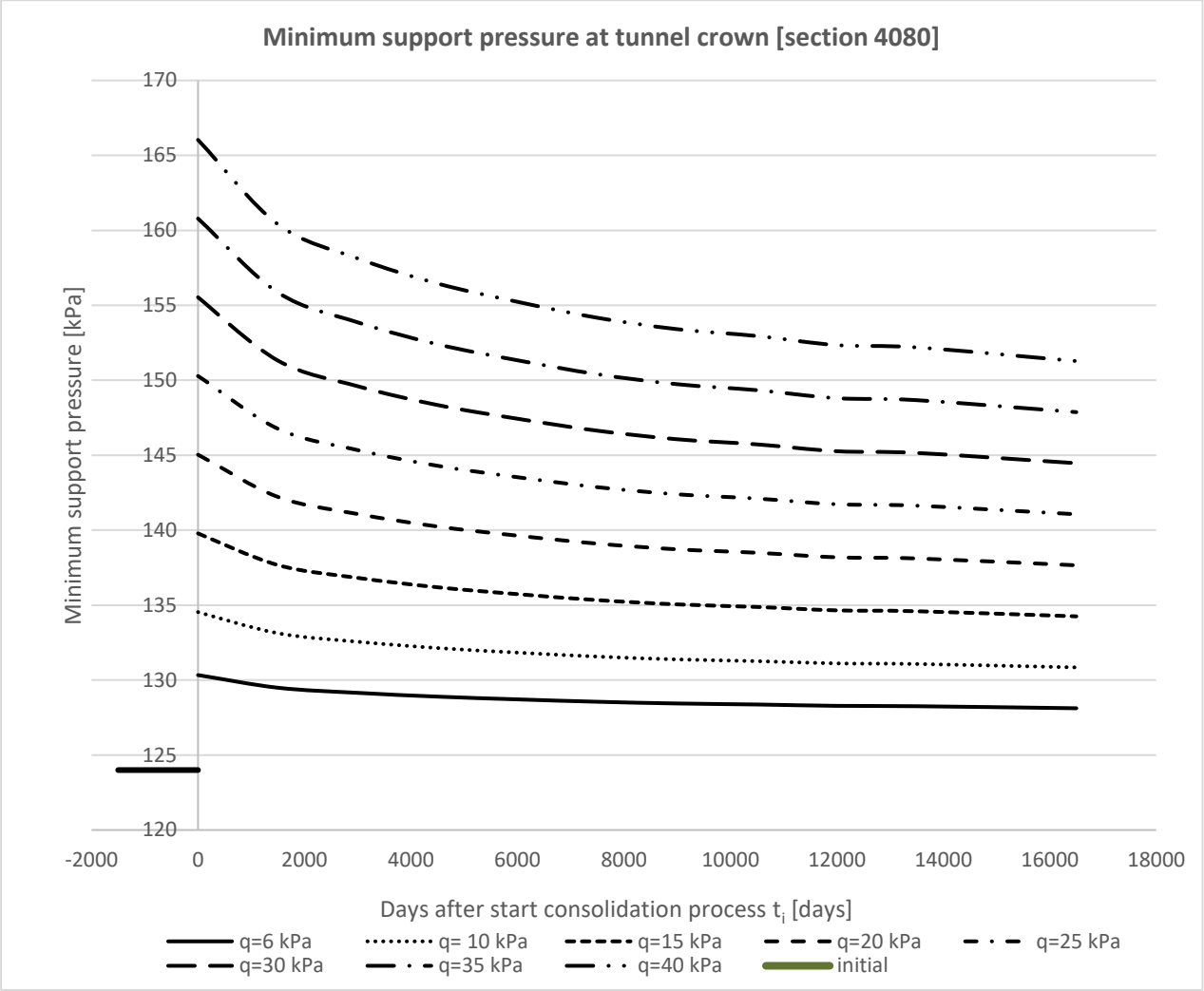

Figure 56. Decrease in the minimum support pressure for the clay layer, with time, for various values of the additional surcharge. The DIN method has been used for this analysis.

4 Transient face stability assessment

The previous chapters have analysed and compared three static face stability models in order to determine the effect of the model differences on the minimum support pressure. In this static face stability assessment, the time-dependent processes of slurry infiltration and soil excavation have been neglected.

A continuous process of slurry infiltration and excavation takes place during tunnelling; therefore, the interaction between the support fluid, advancement of the TBM and the soil needs to be taken into account. The possible influence of the inclusion of these time-dependent effects on the required minimum support pressure has consequently been investigated. In addition, a method has been proposed for the transient face stability assessment.

This research starts by examining the two processes and assuming that they are not interdependent. The time-dependent infiltration process has been investigated by neglecting the advance rate of the TBM, and this situation reflects the ring-building phase. The time-dependent excavation process has been investigated under the assumption that during boring a membrane model (negligible penetration distance) is valid. This way, the separate effect of each of those two time-dependent processes on the minimum support pressure becomes clear. The second part of this analysis is based on the combined behaviour of these two time-dependent effects. Studies by Broere (1998) and Broere & van Tol (2000, 2001) have determined that this interaction can lead to the build-up of excess pore pressures in front of the TBM. The build-up of these excess pore water pressures cannot be neglected, because these pore pressures influence the stability of the tunnel face. The last part of this chapter proposes a method for including transient face stability. As with the static face stability assessment, each analysis consists of a theoretical and practical component.

4.1 Infiltration process support medium

4.1.1 Time-dependent infiltration distance

Krause (1987) has determined the infiltration depth for the support medium, with time, for various bentonite concentrations, excess pressures Δs and soil types. The results of this study all lie within a certain bandwidth (Figure 57), which is described by a lower limit (Equation 4.1a) and an upper limit (Equation 4.1b). The curves reflect the percentage (l_e) of the final penetration depth (e_{max}), which is reached after a certain time. The maximum penetration depth e_{max} has been calculated using Equation 2.15 (Paragraph 2.5). The upper and lower limits of the infiltration process are a function of the parameter a; this value represents the time required (seconds) in order to reach half of the maximum penetration distance. The value a can be determined experimentally by performing column infiltration tests. Krause (1987) has defined this value as equal to 60 seconds for the upper bound and 180 seconds for the lower bound. The time-dependent infiltration process is therefore written in a more general form as presented Equation 4.2.

Two phases can be distinguished from the curve in Figure 57. Phase I marks the beginning of the experiment. During this phase, the suspension quickly penetrates under the excess pressure into the soil. At the same time, a filter cake/penetration zone develops at the boundary between the excavation chamber and the soil, and the penetration rate decreases. After some minutes, the filter cake/penetration zone is almost completely built up. In the second phase, the penetration rate is small and asymptotically approaches an almost constant value.

$$e_t = \frac{t}{a+t}\, e_{max} = \frac{t}{60+t}\, e_{max} = l_e\, e_{max} \quad [upper\ bound] \qquad \textbf{[Equation 4.1a]}$$

$$e_t = \frac{t}{a+t}\, e_{max} = \frac{t}{180+t} e_{max} = l_e\, e_{max} \quad [lower\ bound] \qquad \textbf{[Equation 4.1b]}$$

$$\frac{e_t}{e_{max}} = \frac{t}{a+t} \qquad \textbf{[Equation 4.2]}$$

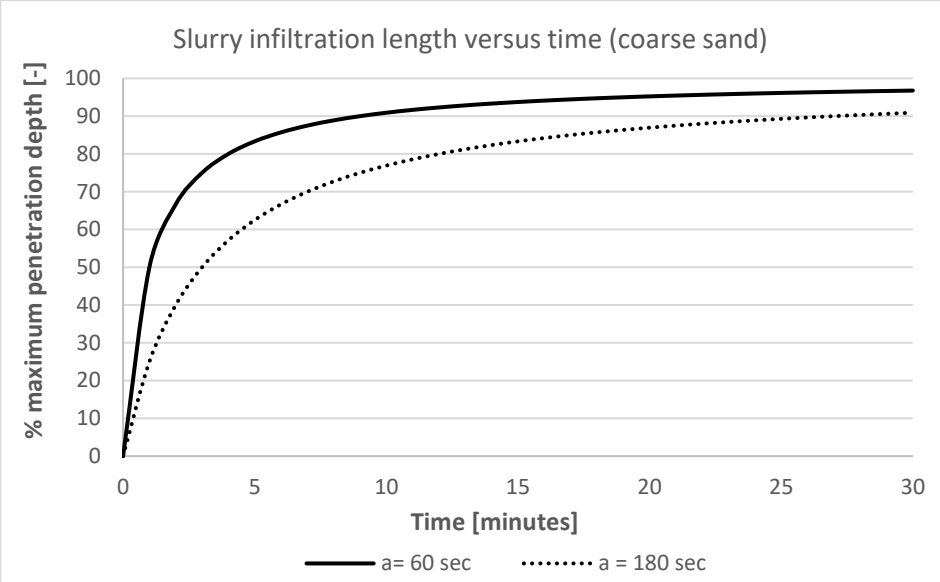

Figure 57. The upper and lower bound for the time-dependent slurry penetration process (Krause, 1987).

4.1.2 Pressure transfer mechanism

The type of pressure mechanism formed depends largely on the permeability of the soil. In fine-grained soils, it is assumed that the entire support pressure is transferred onto the soil skeleton by an infinitely thin membrane, also called filter cake. In coarse soils, the support pressure is transported onto the soil skeleton over this infiltration length by drag forces. The pressure distribution over this filter cake/penetration zone has been calculated using Equation 2.14 (Figure 16). This equation has been derived based on an equilibrium analysis between the support pressure, the water pressure and the shear stresses between the support medium and the surrounding soil. In addition, this analysis has assumed a linear pressure drop over the filter cake/penetration zone. When the maximum penetration distance e_{max} is reached, the pressure drop equals the total pressure difference (excess pressure) between the support pressure and the pore pressure at rest p_o.

The equations regarding the maximum penetration distance and the pressure drop over the filter cake/penetration zone indicate that the only parameters that can be adapted are the yield strength of the support medium and the excess pressure Δs. The effect of these two parameters on the maximum penetration distance and pressure drop over the filter cake/penetration zone has been determined using the case study project The Rijnlandroute. In addition, these results have also provided an indication of the influence of these parameters on the minimum support pressure.

4.1.3 Case-study: The Rijnlandroute

During a standstill, e.g. the ring-building phase, there is no advancement of the TBM. It can therefore be assumed that the maximum penetration distance has been reached. In the case of the two limit equilibrium models, a small penetration distance is beneficial, as less slurry penetrates outside the failure wedge and thus a high effectiveness of the support medium is obtained.

The effect of the yield strength and excess pressure on the maximum penetration distance has been investigated by determining the maximum penetration distance for different values of the yield strength and excess pressure. As obtained in test series 6, a penetration zone only develops in the sand layer, while in the other layers a membrane model is valid. This analysis has therefore concentrated on the sand layer. Its results are illustrated in Figure 58. In this analysis, a characteristic grain size diameter d_{10} equal to 0.2 mm has been used for the sand layer.

In the analysis below, no limitations have been imposed on the yield strength, while in practice this is the case. A higher yield strength contains a higher bentonite concentration and thus results in higher costs. In addition, an increase in the yield strength leads to difficulties in the separation and transport functions. An important aspect to note is that due to the thixotropic characteristics of a bentonite suspension, the dynamic yield strength and static yield strength differ.

Figure 58 illustrates that for a given excess pressure, the maximum penetration distance decreases with the increasing yield strength of the support medium. The graph reveals that the strongest reduction occurs for small yield strength values (τ <0.018 kPa), while for higher values (τ > 0.07 kPa) this reduction is much smaller. Another aspect that can be obtained from Figure 58 is the effect of the excess pressure Δs. It can be seen that for a given yield strength, the penetration distance increases as the excess pressure increases.

The percentage of reduction in the maximum penetration distance with increasing yield strengths starting from 5 Pa is indicated in Figure 59. For this analysis, the maximum penetration distance for a yield strength of 5 Pa equals 100%. This graphical representation can be translated to Equation 4.3.

$$e_{reduction} = 86{,}255\tau_F{}^{-1{,}246} \qquad \textbf{[Equation 4.3]}$$

τ_F:	slurry yield strength	[kPa]
$e_{reduction}$:	percentage of reduction in the maximum penetration distance compared to a yield strength of 5 Pa	[%]

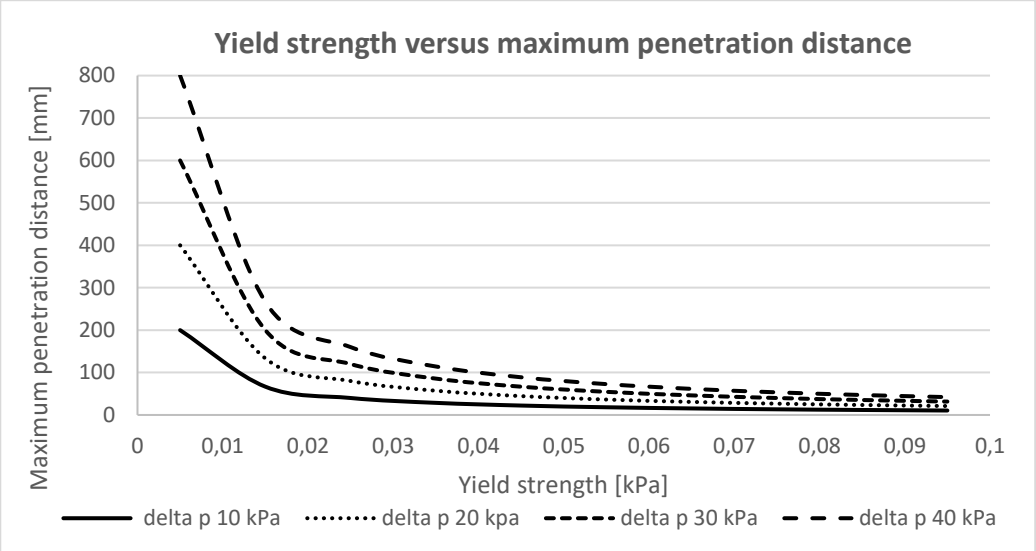

Figure 58. Effect of yield strength and excess pressure on maximum penetration distance.

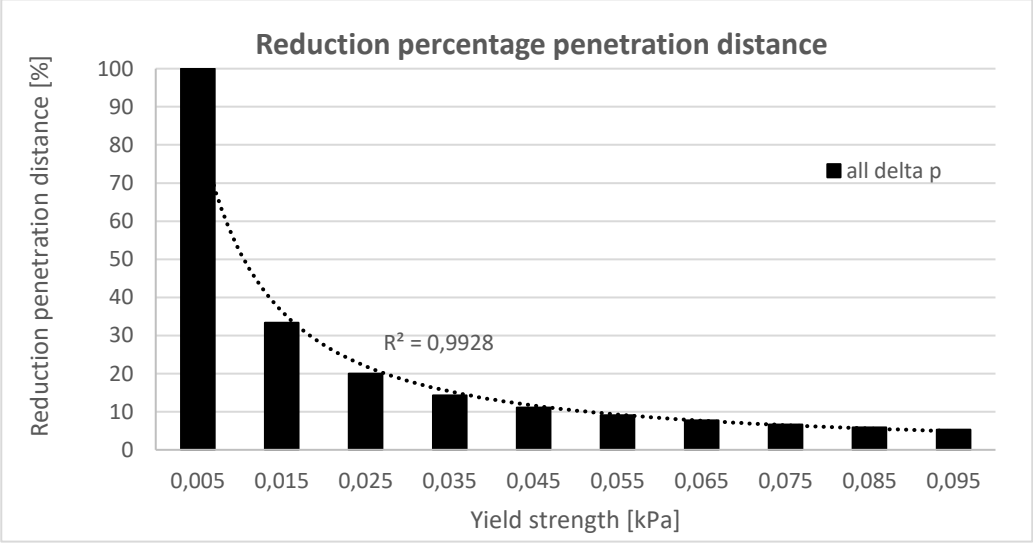

Figure 59. Percentage of reduction with an increase in the yield strength.

4.2 Advance rate of the TBM

The advance rate of the TBM is a function of the excavation depth of the cutting wheel and the capacity of the slurry treatment plant on the surface. The latter imposes a maximum advance rate for the project based on the capacity of the slurry treatment plant (STP) pumps. The excavation depth of the cutting wheel depends on the placement of the excavation tools on the cutting wheel (TBM layout) and the revolutions per minute. The cutting tools that are placed on the cutting wheel are typically:

- discs cutters: for soft to hard rock and mixed face conditions;
- scraper tools: for cohesive to non-cohesive soils and mixed face conditions;
    - buckets;
    - cutting knifes;
    - ripper tools.

In soft soil excavations, disc cutters are placed on the cutting wheel in order to excavate through the concrete wall at the start/end of the TBM drive. In the remaining part of the trajectory, the discs do not damage the filter cake/penetration zone but compacts it in an axial and tangential direction to the disc penetration direction (Figure 60a) (Köppl, Thuro, Thewes 2015). Scraper tools are placed in pairs (tandems) on one cutting wheel arm; only one tool can be active at any given time, while the second moves passively without cutting. Compared to the discs, the cutting mechanism of scraper tools cuts and displaces the soil (Figure 60b). This means that these tools damage the filter cake/penetration zone (Thewis, Schoesser and Zizka, 2016).

Thewes et al (2016) have performed a case study to investigate the penetration scale of a tool passing on the tunnel face. For each case, the cutter wheel has been divided into zones based on the amount of cutting tools (tandems) within one circular cutting track. The cutting wheel excavates the soil while the wheel simultaneously moves forward and rotates. This means that a single tool only penetrates a certain part of the total penetration depth of the cutting wheel. The penetration depth of a single tool is calculated by dividing the penetration depth of the cutting wheel per revolution by the number of cutting tools (tandems) within one track (Equation 4.4-4.5). The time span between two subsequent tool passes is the period in which the pressure transfer mechanism is formed without being disturbed or damaged (Equation 4.6).

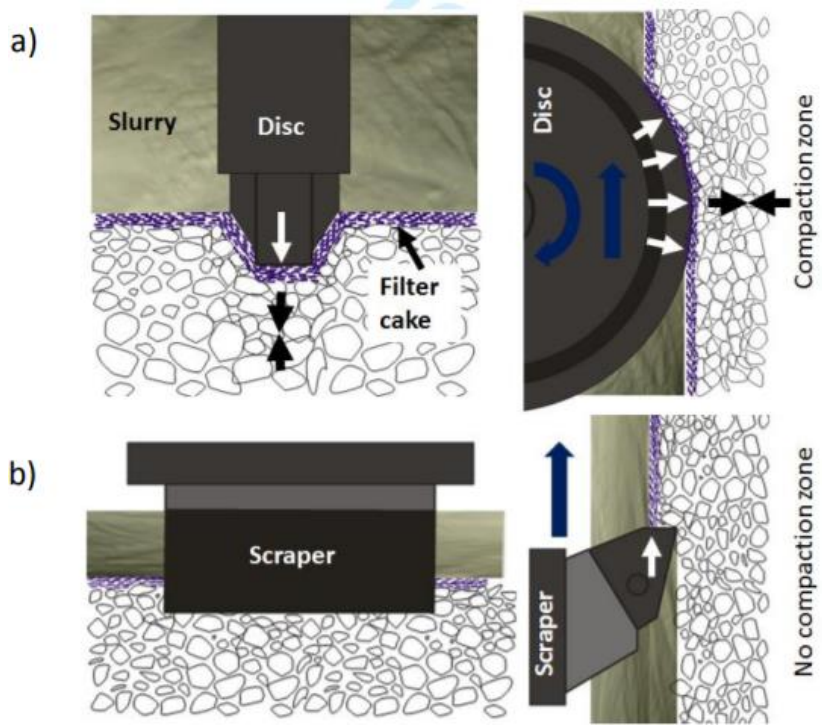

Figure 60. Cutting mechanism of (a) discs and (b) scrapers in soft non-cohesive soils (Thewes et al, 2016).

$$p_{tool} = \frac{p_{wheel}}{n}$$ **[Equation 4.4]**

$$p_{wheel} = \frac{AR}{RPM}$$ **[Equation 4.5]**

$$t_{tool} = \frac{1}{n \cdot RPM}$$ **[Equation 4.6]**

P_{wheel}:	penetration of cutting wheel per revolution	[mm/revo]
RPM:	revolutions per minute of the cutting wheel	[revolution/min]
AR:	advance rate of the TBM	[mm/min]
P_{tool}:	actual penetration of a single cutting tool per passing through a particular point	[mm/min]
n:	number of tool tandems within one track	[-]
t_{tool}:	timespan between subsequent passes of cutting tools	[min/revo]

4.2.1 Rijnlandroute case study

The placement of the cutting tools on the cutting wheel for the case study project is determined, among other things, by the geological conditions and the tunnel diameter. The TBM used for this project is illustrated in Figure 61, where two zones can be identified: Zone 1, with two cutting mechanisms within one cycle (dashed right) and Zone 2, with four cutting mechanisms within one cycle (dashed left). The maximum advance rate of the TBM based on the capacity of the STP equals 10 centimetres per minute. For the complete trajectory, an average speed of 2.5 centimetres per minute combined with 1-4 revolutions per minute (*RPM*) is applied.

For the case study project, the effect of the *RPM* and the number of cutting tools within one circular track on the penetration depth of the cutting tools has been investigated. In addition, the effect of these factors on the timespan between subsequent passes of the cutting tools has been studied. As described, this is an important parameter regarding the available time for the build-up of the filter cake/penetration zone.

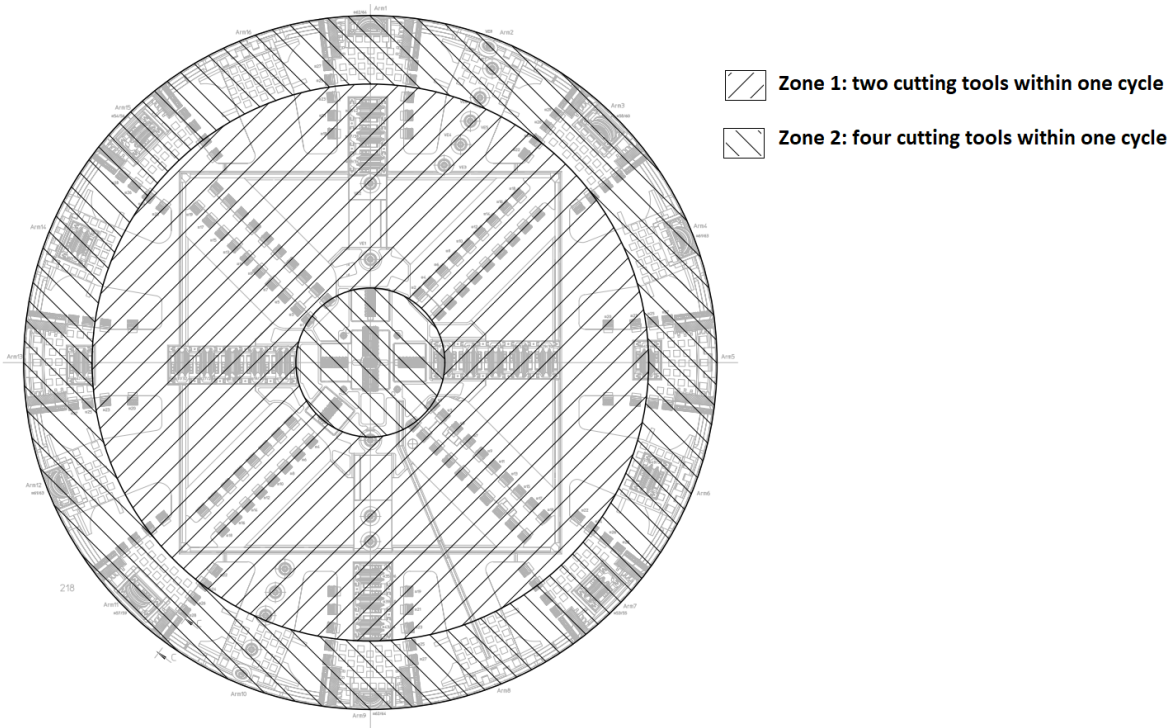

Figure 61. Layout TBM: Overview and location excavation tools cutting wheel. Zone 1 contains two cutting tools within one cycle and zone 2 contains four cutting tools within one cycle.

Table 11. Penetration depth of the cutting wheel, penetration depth of the cutting tools and the timespan between subsequent passes of the cutting tools, for a mean advance rate of 2.5 cm/minute for different RPM.

Number of tools	Revolution per minute		
1 Revolution per minute			
	P_{wheel} [mm/revo]	P_{tool} [mm/revo]	t_{tool} [sec]
Zone 1 (2 tools):	25	12,5	30
Zone 2 (4 tools):	25	6,3	15
2 Revolutions per minute			
	P_{wheel} [mm/revo]	P_{tool} [mm/revo]	t_{tool} [sec]
Zone 1 (2 tools):	12,5	6,3	15
Zone 2 (4 tools):	12,5	3,1	7,5
3 Revolutions per minute			
	P_{wheel} [mm/revo]	P_{tool} [mm/revo]	t_{tool} [sec]
Zone 1 (2 tools):	8,3	4,2	10
Zone 2 (4 tools):	8,3	2.1	5
4 Revolutions per minute			
	P_{wheel}	P_{tool} [mm/revo]	t_{tool} [sec]
Zone 1 (2 tools):	6,25	3.1	7,5
Zone 2 (4 tools):	6,25	1,55	3,75

The penetration depth of the cutting wheel/cutting tools and the time span between subsequent passes of the cutter arms for the case study project have been calculated using Equation 4.4-4.6. The results are displayed in Table 11. From this table, it can be seen that the excavation depth of the cutting wheel per revolution decreases with an increase in the *RPM*. In addition, the penetration depth of the cutting wheel is not affected by the number of cutting mechanisms within one circular track. In contrast, the excavation depth per tool and available time for the build-up of the filter cake/penetration zone decrease with an increase in the *RPM* and in the number of cutting tools within one track.

In test series 6, the shape of the filter cake/penetration zone based on the maximum penetration distance for both homogeneous and stratified soil profiles has been determined. From this analysis, it resulted that the shape of the penetration zone is a function of the excess pressure and characteristic grain size diameter. In the case of a filter cake, a constant negligible penetration distance over the height of the tunnel face can be assumed. From the results of the analysis presented in Table 11, in combination with Figure 57, it is possible to conclude that the timespan during boring is too short to reach the maximum penetration distance. Hence, during boring, a filter cake or incomplete penetration zone can develop. Due to this incomplete development, the pressure drop over the penetration zone is not equal to the excess pressure. The shape of the undeveloped penetration zone is, in addition to the two parameters described above, also influenced by the excavation depth of the cutting tools and the timespan between subsequent passes of the cutting tools. In order to determine how to cope with the shape of this undeveloped penetration zone, the combined behaviour of the slurry infiltration and excavation process is required. This topic is described in the following paragraphs.

4.3 Interaction between slurry infiltration and the excavation process

During boring, a simultaneous process of excavation and face support takes place. Each rotation of the cutting wheel consequently (partly) excavates the filter cake/penetration zone. At the same time, the slurry infiltrates the soil in order to rebuild the filter cake/penetration zone. During this process, there is a continuous inflow of filtrate water into the soil, resulting in excess pore pressures in front of the TBM. In this thesis, this interaction has been simplified by the assumption that the cutting depth of the excavation tools is so large that the entire filter cake is removed by each passage of the cutting tools. To conclude, in the interaction of slurry infiltration and excavation, the pressure drop over the penetration zone/filter cake and the build-up of the excess pore water pressure in front of the TBM needs to be analysed.

4.3.1 Pressure distribution over the wedge

Broere (1998) and Broere & van Tol (2000, 2001) have developed a model to incorporate these two aspects to a face stability assessment. Like the DIN and the Jancsecz-Steiner methods, the model is based on the limit equilibrium, as it assumes a failure wedge in front of the tunnel face.[38] Figure 62 presents the assumed pressure distribution over the wedge. The minimum support pressure S is the sum of the pore pressures at rest p_0 and the excess support pressure Δs (Equation 4.7). The latter can be further subdivided into a pressure drop over the filter cake/penetration zone Δp_f and the remaining excess pore pressure Δp_p (Equation 4.8). This first component takes the shape of the filter cake/penetration zone, due to the interaction between slurry infiltration and excavation into account. The second component Δp_p accounts for the build-up of the excess pore water pressure in front of the TBM. In order to model the build-up of excess pore pressure in front of the TBM, a groundwater flow model has been incorporated to the wedge stability model. In the subsequent paragraphs, these two components of Equation 4.8 are thoroughly described.

$$S = \Delta s + p_o \qquad \textbf{[Equation 4.7]}$$

$$\Delta s = \Delta p_f + \Delta p_p \qquad \textbf{[Equation 4.8]}$$

4.3.1.1 Pressure drop filtercake/penetration zone Δp_f

The first component of the transient face stability assessment is the pressure drop over the filter cake/penetration zone. This pressure drop has already been derived in Paragraph 2.5, based on a static face stability assessment, and is built on the assumption that there is a linear relation between the penetration distance e_t and the pressure drop over the filter cake at each moment in time, until the maximum penetration distance e_{max} is reached (Equation 2.15). This equation has been translated to the wedge model displayed in Figure 62, resulting in Equation 4.9.

$$p_f(x,t) = S - \frac{\alpha_r \, \tau_f}{d_{10}} \, x \qquad x \leq e_t \qquad \textbf{[Equation 4.9]}^{39}$$

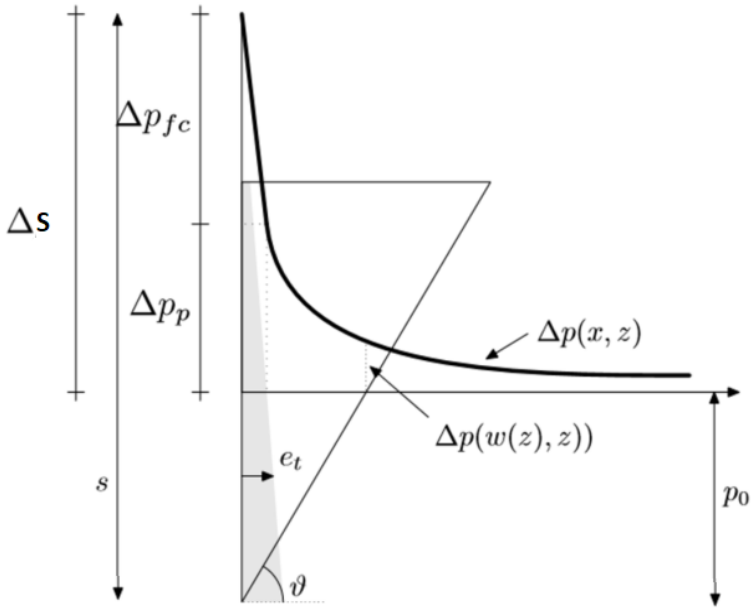

Figure 62. Pressure distribution wedge, which consists of a pressure drop over filter cake/penetration zone Δp_f and the remaining excess pore pressures Δp_p.

[38] For the theoretical background analysis of this model, the readers are referred to Broere (1998).

[39] The factor α_r describes the relation between the grain size and the effective radius of a flow channel, and normally takes values between 2 and 4, see Krause (1987) or Kilchert & Karstedt (1984). (Broere, 2000).

Equation 4.9 makes it possible to determine the support pressure at each location within the pressure transfer mechanism until the time-dependent infiltration distance e_t. The pressure drop over the filter cake/penetration zone has been derived from Equation 4.9 and results in the following equation

$$\Delta p_f(t) = e_t \frac{\alpha \cdot \tau_f}{d_{10}} \qquad \textbf{[Equation 4.10]}$$

The time-dependent infiltration distance (Equation 4.2) is a function of the available time *t* for slurry infiltration, parameter *a* and the maximum penetration distance (Equation 2.13). The available time *t* is equal to the infiltration time t_F, which is a function of the timespan between subsequent passes of the cutting tools t_t and the parameter *a*[40] (Equation 4.11). The maximum penetration distance cannot be determined analytically with Equation 2.15 due to the unknown value of the excess support pressure Δs. This excess support pressure is a function of both the pressure drop over the pressure transfer mechanism and the remaining excess pore pressure Δp_p. In the case of no development of excess pore pressures in front of the TBM, the latter component can be neglected and therefore the support pressure Δs is equal to the pressure drop over the filter cake Δp_f. It should be noted that this method is equal to the static face stability assessment. The derivation of this time-dependent infiltration has been simplified by using the previously stated assumption that the infiltration depth is equal to the excavation depth of cutting tools. In this way, the pressure drop over the filter cake/penetration zone can be determined analytically.

$$t_F = \frac{t_t}{\ln(1+\frac{t_t}{a})} - a \qquad \textbf{[Equation 4.11]}$$

4.3.1.2 Rijnlandroute case study: Time-dependent infiltration length

Despite the assumption that the infiltration depth is equal to the excavation depth of the cutting tools, the time-dependent infiltration distance e_t has been investigated in more detail. The results displayed in Table 11 have therefore been extended by the infiltration time t_f and the percentage of the maximum penetration reached during this infiltration time. Both components have been calculated for both the upper (*a* = 60 seconds) and lower (*a* = 180 seconds) bounds defined by Krause (1987). The results of this analysis are displayed in Table 12. From this table, it can be seen that these *a*-parameters have a negligible influence on the infiltration time, and the infiltration time t_f is approximately equal to half the timespan between subsequent tool passes. The time-dependent infiltration distance e_t (as a percentage of the maximum penetration distance) increases with rising infiltration times and increases in the parameter *a*.

4.3.2 Remaining excess pore pressure Δp_p

In order to take the build-up of the excess pore pressures into account, a groundwater flow model has been integrated to a wedge stability analysis. This model can be both a stationary and a transient groundwater flow model; in both cases, the remaining excess pore pressure Δp_p is used as an input value. This value is obtained by subtracting the pressure drop over the filter cake/penetration zone Δp_f from the excess support pressure Δs (Equation 4.12). The groundwater flow problem has been simplified to a single, one-dimensional, semi-confined aquifer, because the horizontal flow is dominant and only small amounts of water enter or leave the aquifer through the confining layers above and below it. The choice between a stationary and a transient groundwater flow is based on the time required to reach a stationary flow. In the case of a stationary flow model, it is assumed that the excess pore pressures reach equilibrium shortly after boring has started. For a transient flow model, the time required to reach equilibrium is greater than the average time needed to excavate the length of a single tunnel ring (Broere & van Tol, 2001).

$$\Delta p_p = \Delta s - \Delta p_{fc} \qquad \textbf{[Equation 4.12]}$$

[40] The parameter *a* represents the time required (seconds) to reach half of the maximum penetration distance. The value *a* can be experimentally determined by performing column infiltration tests.

Table 12. The available infiltration time t_F for a mean advance rate of 2.5 cm/minute and different RPMs.

Number of tools	Time tool passing t_t	Infiltration time t_f		% penetration distance of e_{max}	
1 Revolution per minute					
	t_{tool} [sec]	t_F [sec]		e_t [%]	
		a=180	a=60	a=180	a=60
Zone 1 (2 tools):	½=30	14,61	13,99	7,51	18,91
Zone 2 (4 tools):	¼ =15	7,40	7,22	3,95	10,74
2 Revolutions per minute					
	t_{tool} [sec]	t_F [sec]		e_t [%]	
		a=180	a=60	a=180	a=60
Zone 1 (2 tools):	¼ =15	7,40	7,22	3,95	10,74
Zone 2 (4 tools):	1/8 = 7,50	3,72	3,68	2,03	5,77
3 Revolutions per minute					
	t_{tool} [sec]	t_F [sec]		e_t [%]	
		a=180	a=60	a=180	a=60
Zone 1 (2 tools):	1/6 =10	4,95	4,87	2,68	7,51
Zone 2 (4 tools):	1/12= 5	2,49	2,47	1,36	3,95
4 Revolutions per minute					
	t_{tool} [sec]	t_F [sec]		e_t [%]	
		a=180	a=60	a=180	a=60
Zone 1 (2 tools):	1/8 = 7,50	3,72	3,68	2,03	5,77
Zone 2 (4 tools):	1/16= 3,75	1,87	1,86	1,03	3,00

In the case of a stationary groundwater flow model, the excess pore pressure distribution has been obtained using Equation 4.13. This equation determines the excess pore pressures at depth *z* and as a function of the distance z from the face.

$$\Delta p(x,z) = \Delta p_p(z)\, exp\left(\frac{e-x}{\lambda}\right) \qquad \textbf{[Equation 4.13]}$$

By using a transient groundwater flow model, the build-up of excess pore pressures during boring as well as the dissipation of the excess pore pressures during a standstill has been determined. Bruggeman (1999) has defined a solution for transient flow in a semi-confined aquifer with height *H*, a discharge *Q* at x=0 and a constant head φ_0 at infinity (Equation 4.14). With this equation, the build-up of the excess pore water pressures during boring have been calculated (Broere & van Tol, 2001).

$$\varphi - \varphi_0 = \frac{Q\,\lambda}{4\,KH}\left[erfc\left(\frac{xu}{2\sqrt{t}} + \frac{\sqrt{t}}{u\lambda}\right)\exp\left(\frac{x}{\lambda}\right) - erfc\left(\frac{xu}{2\sqrt{t}} - \frac{\sqrt{t}}{u\lambda}\right)\exp\left(-\frac{x}{\lambda}\right)\right] \qquad \textbf{[Equation 4.14a]}^{41}$$

$$u = \sqrt{\frac{S_s}{k}} \qquad \textbf{[Equation 4.14b]}$$

$$\lambda = \sqrt{k\,H\,\tilde{c}} \qquad \textbf{[Equation 4.14c]}$$

φ:	groundwater head	[m]
Q:	discharge	[m^3/s]
λ:	leakage length of the aquifer	[m]
erf:	complementary error function	[-]
$\tilde{c}$:	hydraulic resistance aquitard	[days]
H:	height of the aquifer	[m]
k:	permeability of the aquifer	[m/s]
S_s:	specific storage coefficient	[L^{-1}]

[41] Note that the flux q is given per unit area of the face, whereas the inflow Q is per unit width of the aquifer, so that q has to be multiplied by the (average) height of the face or layer to obtain Q

Once boring has stopped, the pressure distribution in the aquifer is initially given by the steady state hydrostatic pressure in a semi-confined aquifer (Equation 4.14). From this moment on, it can be assumed that no more water enters or leaves the working chamber. The excess pore water can therefore flow away from the face. This dissipation of the excess pore water has been calculated using Equation 4.15 (Broere & van Tol, 2001).

$$\varphi - \varphi_0 = \frac{\Delta\varphi}{2}\left[erfc\left(-\frac{xu}{2\sqrt{t}} + \frac{\sqrt{t}}{u\lambda}\right)\exp\left(-\frac{x}{\lambda}\right) + erfc\left(\frac{xu}{2\sqrt{t}} + \frac{\sqrt{t}}{u\lambda}\right)\exp\left(\frac{x}{\lambda}\right)\right] \qquad \textbf{[Equation 4.15]}$$

$\Delta\varphi$: change in head

4.3.2.1 Unconfined flow

In the case of no confining layers above the tunnel, the leakage length is adapted to unconfined conditions through a change in the leakage length (Equation 4.16).

$$\lambda = D\sqrt{C/D} \qquad \textbf{[Equation 4.16]}$$

4.3.2.2 Discharge q

The discharge component in the transient ground water flow model has been calculated by equating the amount of water displaced by the penetrating slurry for each full turn of the cutting wheel to the amount of pore water in the excavated soil (Equation 4.17).

$$q = \frac{l_{cut}}{t_{cut}} n = v_e\, n \qquad \textbf{[Equation 4.17]}$$

q:	specific discharge of the aquifer	[m/s]
l_{cut}:	cutting depth cutting wheel	[m]
t_{cut}:	time needed for a full turn of the cutting wheel	[s]
n:	porosity of the soil	[-]

4.3.2.3 Rijnlandroute case study

A parameter study (Figure 63) has been performed in order to investigate this transient groundwater flow in more detail, by considering the following four aspects:

1. ratio between the diameter of the TBM and the height of the aquifer (*D*/*H* ratio);
2. advance speed *v* of the TBM;
3. permeability of the aquifer *k*;
4. leakage length *λ*;

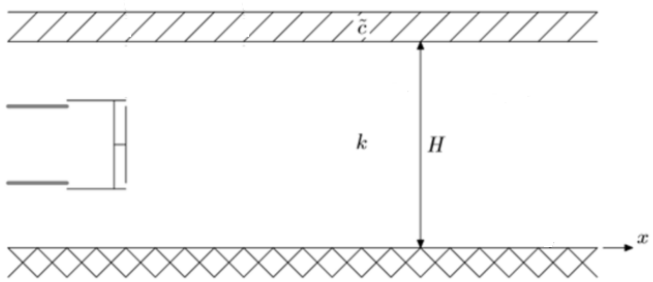

Conditions	
Leakage length λ [m]	11
Storativity soil S_s [m^{-1}]	0,0007
Permeability soil k [m/h]	0,108
Height aquifer H [m]	11
u	0,08
Porosity n [-]	0,4
Advance speed v [m/h]	1,5
Discharge q [m/h]	-0,6
Diameter tunnel [m]	11
Radius tunnel [m]	5,5
Discharge Q [m^3/h]	-6,6
Boring time [h]	5/8= 1,33
Ring building time [h]	5/6= 0,83

Figure 63. Project conditions parameter analysis [Case 1].

For this parameter analysis, the case of a TBM situated within a semi-confined aquifer with height *H* and permeability *k* has been investigated (Figure 63). For the first three aspects, the influence of the leakage length has been neglected by using a constant value for the leakage length that is equal to the diameter of the tunnel.

The excess pore pressure distribution at the tunnel face ($x = 0$) with time for Case 1 (Figure 63) is displayed in Figure 64. From this graph, two phases can be identified: The build-up of the excess pore pressures during boring and the dissipation of these excess pore pressures during ring building. An important aspect to note is that not all pore pressures have dissipated at the time of boring (remaining excess); therefore, the second boring phase starts at a different offset. As during this phase the same amount of excess pore pressures develops, the final excess pore pressure at the end of the boring phase is higher than in the previous phase.

The excess pore pressure distribution with a distance *x* from the tunnel face is displayed in Figure 65 for different time steps for one boring and one ring-building phase. It should be noted that the excess pore pressure distribution in Figure 64 represent the build-up and dissipation of the excess pore pressure at $x = 0$ in the graph of Figure 65. The excess pore pressure distribution with distance *x* at the end of the boring phase (Equation 4.14) does not coincide with the excess pore pressure distribution with distance *x* at the start of the ring-building phase (Equation 4.15). The reason for this is that the dissipation curve starts from the steady state solution and not from the excess pore pressure distribution at the end of the boring phase, as obtained by Equation 4.14. In the case of an incomplete boring process, the dissipation behaviour of this built-up excess pore water pressures does not start from the steady state excess pore water pressure.

4.3.2.3.1 Height H of the aquifer

The effect of the aquifer height on the build-up of the excess pore pressure distribution has been determined by varying the height *H* of the aquifer and keeping the other parameters constant. All calculations have been detailed in Annex 5.1 and a summary has been provided in Table 13. It can be seen that an increase in the aquifer height leads to lower excess pore pressures at the tunnel face and vice versa. The reason for this behaviour is that with an increase in the aquifer height *H*, the transmissivity *kH* (m^2/d) of the aquifer increases. It should be noted that the latter two cases (Case 5 and Case 6) do not resemble the actual behaviour, as the aquifer height is lower than the diameter of the TBM. In practice, this means that part of the confined layer is present in front of the tunnel face. At these locations, a filter cake is formed instead of a penetration zone. If for these cases the diameter of the tunnel is adapted to the aquifer height ($D/H=1$), then the same maximum excess pore pressure occurs at the tunnel face as in Case 1, with $D/H = 1$. This means that the value of the maximum excess pore pressure at the tunnel face depends on the *D*/*H* ratio. The highest excess pore pressure occurs at a D/H ratio equal to unity and decreases with a decreasing *D*/*H* ratio (increase in the height of the aquifer).

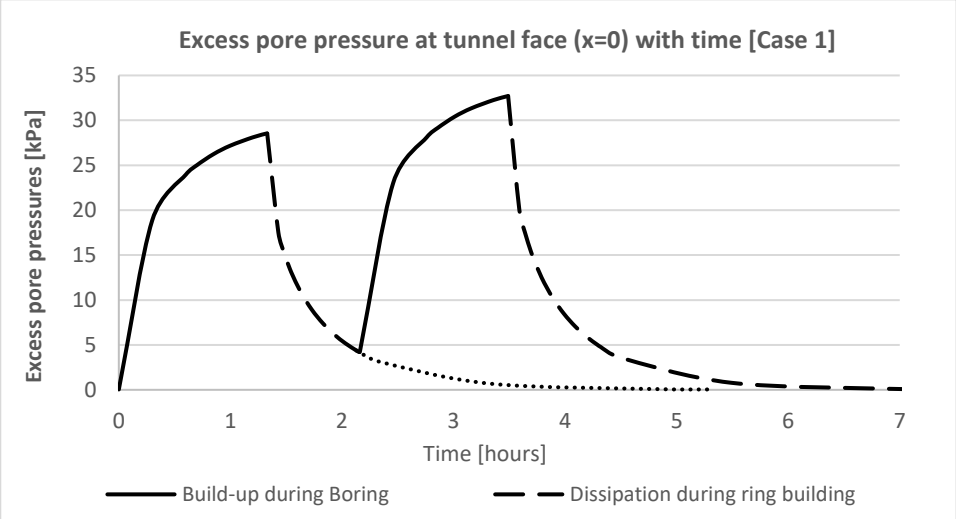

Figure 64. Excess pore pressure distribution at the tunnel face (x=0), with time, for Case 1.

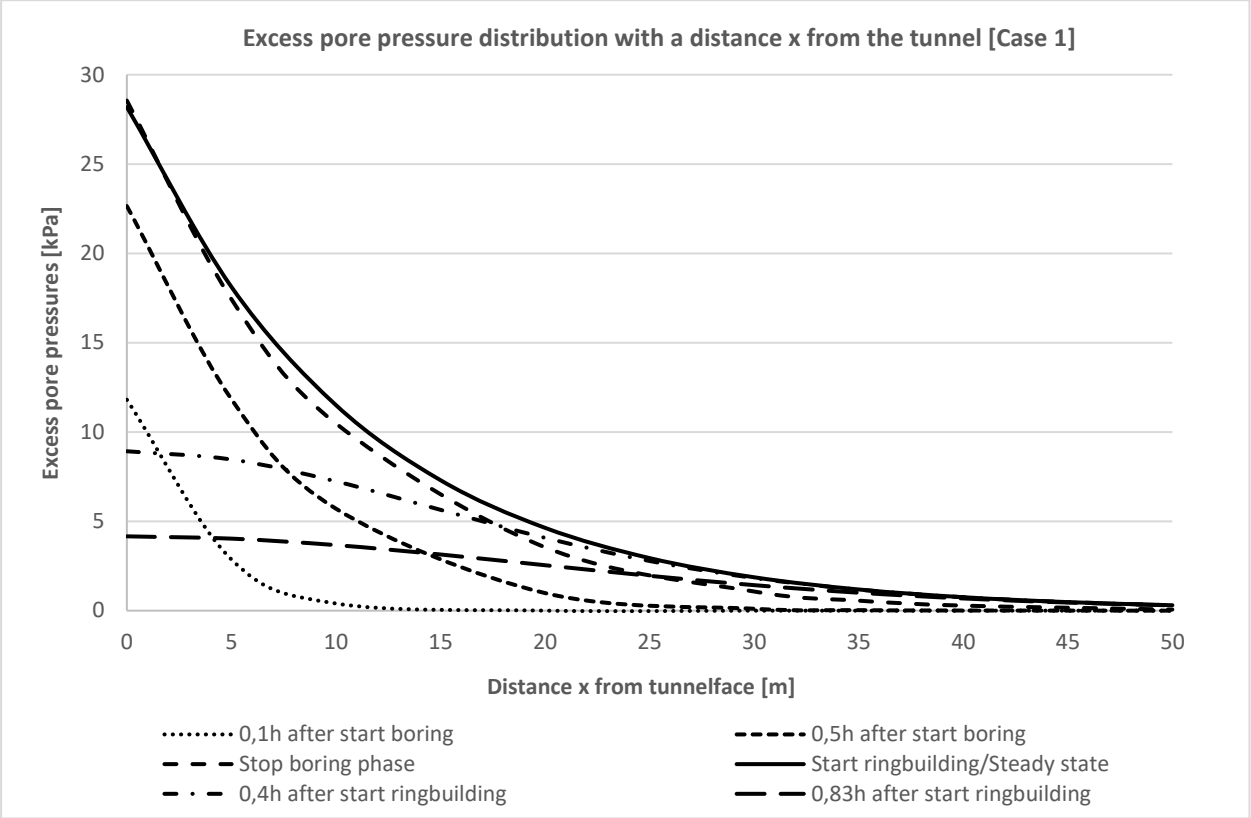

Figure 65. Excess pore pressure distribution with distance *x* from the tunnel face.

4.3.2.3.2 Advance speed v

The effect of the advance speed on the excess pore pressure distribution has been determined by varying the advance speed of the TBM. All calculations have been presented in Annex 5.1 and a summary has been provided in Table 13. It can be seen that an increase in the advance speed leads to higher values of the excess pore pressure and that the opposite effect occurs with a decrease in the advance rate. The change in the excess pore pressure at the tunnel face is proportional to the change in the advance speed. The reason for this is that the amount of discharge *q* is calculated by multiplying the soil porosity with the advance rate of the soil (Equation 4.17). As the soil porosity is constant, it can be seen that an increase in the advance speed leads to an increase in the discharge *q*.

4.3.2.3.3 Permeability K of the aquifer

The effect of the soil permeability on the excess pore pressure distribution has been determined by varying the permeability of the soil. All calculations have been presented in Annex 5.1 and a summary has been provided in Table 13. It can be seen that a decrease in the permeability (Case 1 → Case 9) leads to lower excess pore pressure values generated at the tunnel face. In the case of an increase in permeability (Case 1 → Case 10), this leads to higher excess pore pressure values. The reason for this behaviour is that, with a decrease in the permeability *k* of the aquifer, the transmissivity *kH* (m^2/h) of the aquifer increases.

4.3.2.4 Leakage length λ

The effect of the leakage length on the transient groundwater flow analysis has been investigated by determining the excess pore water pressure at the tunnel face at the end of the boring process, as a function of the leakage length. The results are displayed in Figure 66. This figure reveals that, for the given project conditions, the development of excess pore water pressures is highly influenced by the leakage length until around 50 metres. For a leakage length higher than 50 meters, the influence can be neglected. This assumption is not affected by a change in the D/H ratio, permeability or advance speed, but this results in a higher or lower offset (based on the conclusion in the previous paragraphs).

Table 13. Effect of the advance speed on the excess pore pressure distribution.

Case	Parameter	Maximum excess pore pressure at tunnel face [kPa]
Ratio tunnel diameter and height aquifer (D/H) [-]		
Case 1	D/H= 1 (H=11m)	29
Case 2	D/H=2/3 (H=16,66)	19
Case 3	D/H=0,5 (H=22m)	14
Case 4	D/H= 0,4 (H=27,5m)	11
Case 5	D/H=2 (H=5,5m)	57 (29)
Case 6	D/H=4 (H=2,75m)	114 (29)
Advance rate [m/h]		
Case 1	1,5	29
Case 2	3	57
Case 3	0,75	14,3
Permeability [m/h]		
Case 1	0,108	29
Case 9	0,216	15
Case 10	0,0108	134

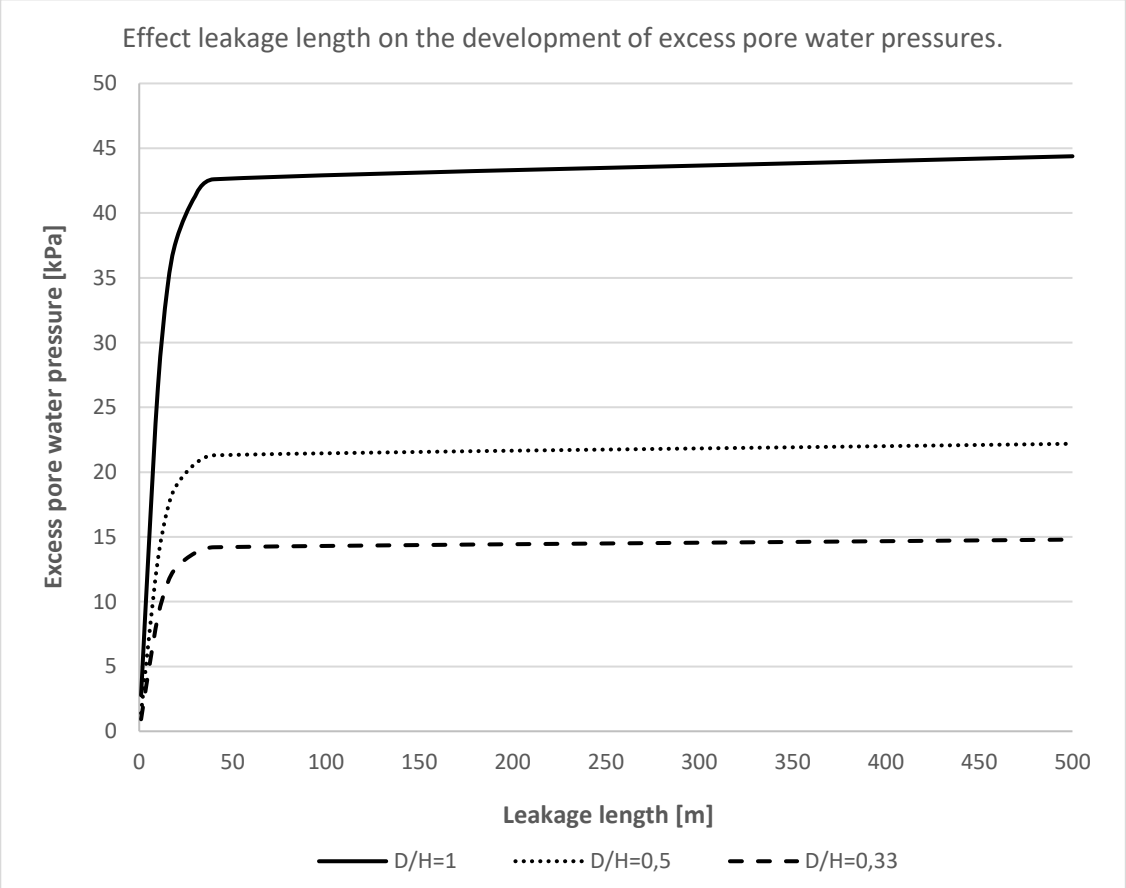

Figure 66. Effect of the leakage length on the build-up of excess pore water pressures at the tunnel face.

4.4 Implementation of the limit equilibrium models

In order to compare the static and transient face stability assessments, a groundwater flow model has been incorporated to a limit equilibrium model. Unfortunately, the time-dependent pressure distribution over the wedge is not applicable to the Ruse-Vermeer method, as it is a limit stress method. The method described in the subsequent paragraphs is therefore only applicable to the Jancsecz-Steiner and DIN models.

4.4.1 Determination minimum support pressure *S*

In the case of a transient face stability assessment, the minimum support pressure is determined by the pressure drop over the pressure transfer mechanism and the remaining excess pore pressures. These components have been thoroughly described in the previous chapters. This analysis has resulted in that an iterative solution procedure is required in order to solve this interdependence.
The iterative calculation sequence for this pressure distribution is as follows:

- *S*: support pressure;
- p_0: equilibrium pore pressure;
- Δs: excess support pressure, which is the pressure difference between S and p_0;
  - Δp_f: pressure drop over the filtercake/penetration zone;
  - Δp_p: remaining excess pore pressures;
    - $p(x,z)$: excess pore pressure distribution (Steady state or transient).

The iterative sequence starts with an estimate of the support pressure *S*. Along with the equilibrium pore pressures, the excess pressure between the support pressure and the equilibrium pore pressure has been determined. The pressure drop over the filter cake/penetration zone Δp_f has been subtracted from this excess pressure and the remaining excess pore pressure has been obtained Δp_p. Depending on the assumptions, a transient or steady state groundwater flow model has been used. Where equilibrium was lacking, a new assumption of the support pressure was made until equilibrium was achieved.

The implementation of an iterative calculation method is not preferable in the case of an analytical method, so another approach has been suggested. The analysis in the previous paragraphs resulted in that it is possible to determine the remaining excess pore pressures Δp_p without using any of the components of Figure 62 (Equation 4.7-3.12). By using a transient groundwater flow analysis in which only the TBM's characteristics and the ground parameters serve as inputs, the remaining excess pore water pressures have been determined. As the values of these pressures are known, the other two remaining factors are the pressure drop over the filter cake/penetration zone and the minimum support pressure. Equations 4.7 and 4.8 have resulted in that only one of these two parameters is required, as the other follows from equilibrium. In the foregoing, the (time-dependent) infiltration process during a standstill (Paragraph 2.5) and during boring (Paragraph 4.3) has been discussed. The maximum penetration distance is reached in the case of a standstill; this value has been calculated using Equation 2.13. In contrast, the time-dependent infiltration distance during boring depends on several factors and cannot be easily determined. Due to this difficulty, this thesis has assumed that the time-dependent infiltration distance is equal to the excavation depth of the cutting wheel. By using this transient groundwater flow model in combination with the assumption on the time-dependent infiltration distance, the minimum support pressure can be obtained. This method is based on the previously discussed calculation method, in an inversed direction. This way, from a fixed bottom boundary (equilibrium pore pressure), a support pressure is eventually obtained. In this analysis, the following sequence has been followed:

- p_0: equilibrium pore pressure;
- $p(x,z)$ excess pore pressure distribution (transient analysis);
  - Δp_p: remaining excess pore pressures;
  - e_t: depth penetration zone = excavation depth cutting tools;
  - Δp_f: pressure drop over the penetration zone;
  - Δs: pressure drop between the support pressure *S* and equilibrium pore pressures;
  - *S*: support pressure.

The second step in the implementation of transient face stability to a wedge stability analysis is to check the wedge stability. This stability has to be verified because the excess pore pressures influence it. The excess pore pressures result in an uplift force P_s that counteracts the weight of the soil overburden. This uplift force is calculated by the integral of the excess pore pressure distribution multiplied with the width of the wedge B (Equation 4.18). In addition, the excess pore pressures also affects the shear forces P_t that act on the wedge sides (Equation 4.19). The reason for this is that the shear stresses act in the opposite direction as these excess pore water pressures. The reduction of these shear stresses is calculated by the integral of the amount of excess pore water pressures which develops within the zone of the failure wedge. If the stability of the wedge is not ensured, then a higher support pressure value is required.

$$P_s = B \int_0^{tc} \Delta p(x, z. t)\, dx \qquad \textbf{[Equation 4.18]}$$

$$P_T = B \int_{z_t}^{z_b} \int_0^{w(z)} \frac{1}{\zeta_-} K_y \tan\varphi\, \Delta p(x, z. t)\, dx dz \qquad \textbf{[Equation 4.19]}$$

$$\zeta_- = \tan\varphi \cos\theta - \sin\theta \qquad \textbf{[Equation 4.19b]}$$

4.4.2 Case study Rijnlandroute

In order to make a comparison between the static and transient face stability assessment, a transient face stability assessment is performed for the eight case-studies discussed in paragraph 3.4. As obtained in test series 6, a penetration zone only develops in the sand layer, while in the other layers a membrane model is valid. This analysis, therefore, concentrates on the sand layer and thus case B and D are disregarded. In the remaining cases, it is assumed that the bottom boundary of the tunnel face is equal to the bottom boundary of the aquifer. As the most obvious difference is obtained by the determination of the excess pore pressures, this case study analysis concentrates on the built-up and dissipation of these excess pore water pressures with time during boring and during the ring building phase. In Annex 5.2 all the calculation results are displayed and a summary is shown in Figure 67.

4.4.2.1 Case A: Homogeneous sand profile (C/D= 1,0)

Case A consists of a homogeneous sand profile with a soil cover equal to the diameter of the tunnel face. In this case, no confining layer is present above the tunnel face and therefore equation 4.16 is used, for the calculation of the leakage length. The height of the aquifer is equal to the sum of the tunnel face and the soil cover and thus equal to twice the diameter of the tunnel face. By using a transient groundwater flow analysis, an excess pore water pressure equal to 14 kPa is obtained at the tunnel face (x = 0). The build-up of these excess pore pressures during boring and the dissipation during a standstill are displayed in Annex 5.2.

4.4.2.2 Case C: Homogeneous sand profile (C/D= 1,5)

Likewise case A, case C also consists of a homogeneous sand profile. The only difference is the height of the soil cover. Due to this height difference, not the same value for the leakage length applies. By using a transient groundwater flow analysis, an excess pore water pressure equal to 13 kPa is obtained at the tunnel face (x = 0). Despite the larger height of the aquifer compared to the previous case, almost the same value for the excess pore water pressure is obtained. The reason for this is the higher value of the leakage length in case C which leads to the development of a higher amount of excess pore water pressures acting at the tunnel face (Figure 66).

4.4.2.3 Case E/F/H: Heterogeneous soil profile (C/D= 1,0)

Case E/F/H consist of a heterogeneous soil profile and the three cases differ in the soil profile of the soil cover and in front of the tunnel face. Despite this fact, in all three models, the height of the aquifer is equal to half the diameter. The remaining part of the tunnel face is situated in a clay layer and it can be assumed that a filtercake develops. Therefore, the diameter of the tunnel has been reduced equal to the height of the aquifer. From Figure 66, it is obtained that leakage lengths greater than 50 meters do not have an impact on the built-up and dissipation behaviour of the excess pore water pressure. Due to this reason, the leakage length have been set equal to 50 meters within this analysis. From the

analysis displayed in Annex 5.2, an excess pore water pressure equal to 42 kPa is obtained at the tunnel face. As described, the main reason for this increase in excess pore pressure is due to a higher value of the leakage length. The effect of this leakage length on the excess pore pressure distribution at a distance *x* from the tunnel face is also indicated in Figure 67 and Table 14. It can be seen that due to the higher value of the leakage length, a higher value of the excess pore pressures is present at a value of the distance *x* from the tunnel face.

4.4.2.4 Case G: Heterogeneous soil profile (C/D= 1,0)

Likewise Case E/F/H, Case G consists of a heterogeneous soil profile with a soil cover height equal to the diameter of the tunnel. In this case, no confining layer is present above the tunnel face and therefore equation 4.16 is used, for the calculation of the leakage length. The height of the aquifer is equal to the sum of half the diameter and the height of the soil cover. The bottom half of the tunnel face is situated in a clay layer and therefore no penetration zone is developed within this zone. Therefore, the diameter of the tunnel has been reduced equal to the height of the aquifer. From the analysis displayed in Annex 5.2, an excess pore water pressure equal to 12 kPa is obtained at the tunnel face.

Table 14. The value of the excess pore water pressure at the tunnel face which are developed during the boring phase and the value of the leakage length used within this analysis.

Case	Generated excess pore water pressure at tunnel face	Leakage length
[-]	[kPa]	[m]
A	14	10,96
C	13	13,42
E/F/H	42	50
G	12	15,49

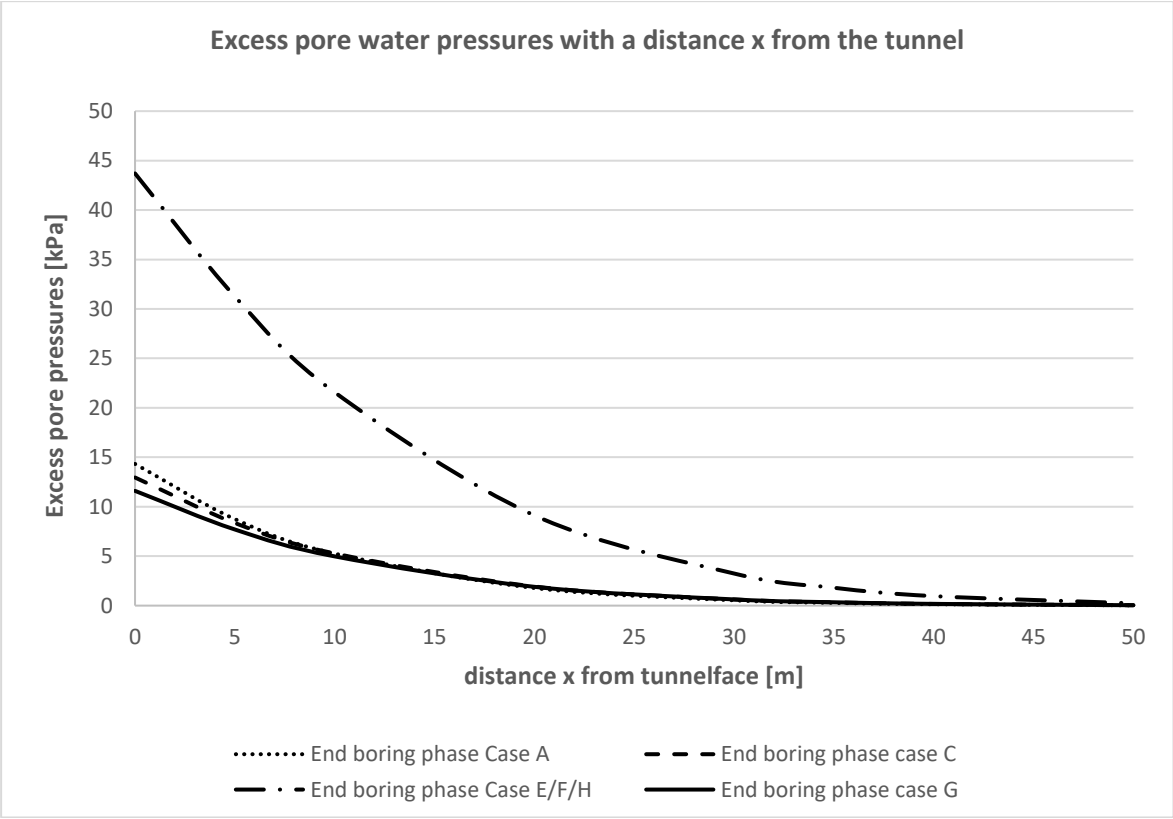

Figure 67. The build-up of the excess pore water pressure with a distance x from the tunnel face at the end of boring phase.

4.5 Conclusion transient face stability

In this chapter, the static face stability assessment is extended by taking the continuous process of slurry infiltration and excavation into account. This assessment distinguishes between two cases, the ring-building phase and the boring phase. In the ring-building phase, a lack of advancement of the TBM has been assumed; therefore, only the slurry infiltration process has been considered. On the contrary, in the boring phase, the time-dependent excavation process has been investigated under the assumption that a membrane model (negligible penetration distance) is valid. Both time-dependent components have been reviewed separately in order to determine their behaviour by varying certain parameters. Hence, a parameter study has been performed for each component. The second part of this analysis was based on the combined behaviour of these two time-dependent effects.

The time-dependent slurry infiltration process has revealed that the maximum penetration distance, yield strength, characteristic grain size d_{10} and pressure difference are strongly related. The only two factors that can be controlled are the yield strength and the excess pressure. From the parametric analysis, it turned out that an increase in the yield-strength leads to a reduction of the maximum penetration distance and the increase of the excess pressure leads to an increase in the maximum penetration distance. As described in chapter 2, the yield strength is an important parameter since it affects also other functions of the support medium. For the stabilisation function, the highest possible yield strength is required and for the transport function, the lowest possible yield strength is required. This means that the yield strength should be the optimal balance between multiple functions. The analysis of the time dependent slurry infiltration process is based on the assumption that the TBM does not advance and thus the available time-span is sufficient in order to reach the maximum penetration distance. However, during boring a continuous process of slurry infiltration and excavation takes place and the available time-span is insufficient in order to reach the maximum penetration distance. Although the penetration distance with time can be calculated as a function of the maximum penetration distance, this method is not applicable in the case of a transient face stability analysis. The reason for this is that the excess pressure is unknown.

In soft soil excavations, the type of excavation tools that are used are scraper tools and disc cutters[42]. For both type of tools, the cutting mechanism of the pressure transfer mechanism are described. As the scraper tools only affects the pressure transfer mechanism, the analysis has been focussed on this type of tool. The time-dependent excavation process has revealed that the number of cutting wheels per track and the RPMs strongly determine the advancement of the TBM and the penetration depth of the tools and wheels. In practice, this excavation speed is limited due to the capacity of the slurry treatment process. Within this analysis, the effect of the advancement of the TBM on the available time-span for the development of the pressure transfer mechanism has been investigated. It turned out, that a high advancement of the TBM is negative for the available timespan in order to built-up the filtercake/penetration zone, but positive for the timespan of the project.

The continuous process between excavation and slurry infiltration leads to the build-up of excess pore pressures in front of the tunnel face. These excess pore pressures result in an increase of the support pressure. Broere (1998) and Broere & van Tol (2000, 2001) have developed a model to incorporate these two aspects to a face stability assessment. Within this model, the minimum support pressure S is the sum of the pore pressures at rest p_0 and the excess support pressure Δs. The latter can be further subdivided into a pressure drop over the filter cake/penetration zone Δp_f and the remaining excess pore pressure Δp_p. In order to take the build-up of the excess pore pressures into account, a groundwater flow model has been integrated to a wedge stability analysis. By using a transient groundwater flow model, the built-up of excess pore pressures during boring and the dissipation of these excess pore pressure during the ring building have been investigated. A parametric analysis have been performed in order to determine the effect of the parameters within this analysis. It turned out that it is important for project design processes to review this aspect, as excess pore pressures can reach high values.

[42] In soft soil excavations, disc cutters are placed on the cutting wheel in order to excavate through the concrete wall at the start/end of the TBM drive. In the remaining part of the trajectory, the discs do not have a specific function.

5 The role of slurry the TBM parameters on ground deformation

At the face of the TBM, called the bore front, a pressurised slurry has been used as a face support. In order to ensure stable working conditions, the support pressure applied lies between two limits that correspond to certain failure mechanisms, e.g. ultimate limit states. A support pressure below the lower limit results in a deformation of the soil toward the face, causing a large settlement at the ground surface. A support pressure above the upper limit results in an upward deformation of the soil or in a blow out, with the subsequent loss of the support medium. In practice, the value of the support pressure used is determined by the serviceability limit state. The serviceability limit state focusses on keeping the ground deformations below a pre-determined limit and determines the support pressure based on the required ground deformation limit.

Previous chapters have discussed the concept of ultimate limit states in the static face stability assessment and both of the support medium's limits have been determined. In this analysis, the effect of the support medium's properties on the minimum and maximum support pressure has been determined. Nevertheless, the effect of these support medium properties and other TBM parameters on ground deformations has not been considered.

This chapter begins with a short introduction on the different volume components that induce settlement during tunnelling and the corresponding empirical assessment of these settlements. The second part focusses on the volume components that are affected by the face support and support medium properties. By using the eight case studies presented in Paragraph 3.4, a connection has tried to be established between the support medium/TBM properties and ground deformations.

5.1 Volume loss in tunnelling

The loss of volume is an important parameter for estimating ground movements in the design stage; this value is often determined by experience. Mair and Taylor (1997) have summarised the following primary ground movement components associated to closed shield tunnelling (Figure 68):

- volume loss at the tunnelling face $V_{L,f}$;
- volume loss along the shield $V_{L,s}$;
- volume loss at the tail $V_{L,t}$;
- volume loss due to deformation of the lining (minor importance)
- radial ground movement toward the lining due consolidation $V_{L,c}$;

The total volume loss V_L during the tunnelling progress can therefore be estimated as:

$$V_L = V_{L,f} + V_{L,s} + V_{L,t} + V_{L,c} \qquad \textbf{[Equation 7.1]}$$

5.1.1 Volume loss at the tunnel face

During the boring process, the soil at the tunnel face tends to move into the cavity created by the TBM. The volume of soil that moves toward the face depends on the support pressure applied, the soil conditions and the hydraulic conditions. The settlement can be controlled by assuming neutral ground conditions (Paragraph 2.3). When an adequate face support exists, this first ground deformation component is relatively small.

5.1.2 Volume loss along the shield

The radial ground loss around the tunnel shield can occur due to one of the following possibilities:

- overcutting, due to a larger diameter of the cutting wheel in front of the TBM than the diameter of the shield;
- a gap, called annulus, between the shield skin and the surrounding soil, due the tapered shape of the TBM;
- additional gapping when the TBM moves in curves (Festa, 2015).

5.1.3 Volume loss behind the TBM

The volume loss at the tail is due to radial ground movements into the tail void (gap between the lining and soil formation). This component is usually the major cause of settlement and can be minimised by grouting. The volume loss depends on the grout pressure applied: A high grout pressure leads to local heaves, while a low grout pressure results in settlement. In addition, if the grout along the tunnel lining consolidates and forms a grout cake, this leads to long-term consolidation settlements in the soil volume above the tunnel. *As this topic falls outside the scope of this thesis, this topic has not been considered further.*

5.1.4 Empirical assessment of settlements

5.1.4.1 Transverse surface settlement of the settlement trough

Regardless of the tunnelling method used, the ground becomes loaded or unloaded and deformations inevitably take place, leading to the typical Gaussian settlement through described in Figure 69 (Möller, 2006). The transverse settlement shape of the ground surface (Equation 7.2) is based on the value of the maximum settlement $S_{v,max}$ at the surface directly above the tunnel axis, and the trough width parameter i (Schmidt,1969)(Peck,1969)(Figure 70). The volume of this settlement trough V_s depends on the ground loss component V_t, which is the volume of ground that has deformed into the tunnel after the tunnel has been constructed. When tunnelling in undrained ground, the settlement volume is more or less equal to the ground loss component, but when tunnelling in drained ground the settlement volume is somewhat smaller ($V_s \approx V_t$). As the ground loss component V_t is a function of the excavated area of the tunnel face, this component can also be expressed as the ratio between the ground loss component and the excavated area A_t (Equation 7.3)(Figure 70). The volume of the settlement trough (per unit length of tunnel) is obtained by integrating Equation 7.2, which leads to Equation 7.4 (Möller, 2006).

$$S_v(y) = S_{v,max} \cdot e^{\left(\frac{-y^2}{2i^2}\right)} \qquad \textbf{[Equation 7.2]}$$

$$GLR = \frac{V_t}{A_t} \approx \frac{V_s}{A_t} \qquad \textbf{[Equation 7.3]}$$

$$V_s = \int S_v \, dx = \sqrt{2\pi} \; i \, S_{v,max} \cong 2{,}5 \, i \, S_{v,max} \qquad \textbf{[Equation 7.4]}$$

$$S_{v,max} \approx \frac{A_t}{i \cdot \sqrt{2\pi}} \, GLR \approx \frac{0{,}31 \, V \, D^2}{i} \qquad \textbf{[Equation 7.5]}$$

$$S_v(y) = \frac{A_t}{i \cdot \sqrt{2\pi}} GLR \; e^{\left(\frac{-y^2}{2i^2}\right)} \qquad \textbf{[Equation 7.6]}$$

S_v:	settlement at a given location	[mm]
$S_{v,max}$:	maximum settlement at the tunnel axis location	[mm]
y:	horizontal distance between the observed location and the tunnel axis	[mm]
i:	horizontal distance from the tunnel centre line to the point of inflection of the settlement trough	[mm]
V_s:	volume of the settlement trough (per unit length of tunnel)	[mm³]

5.1.4.2 Width of the settlement trough

The width of the settlement trough has been described using a Gaussian distribution. In the setup of this distribution, the parameter *i* reflects the horizontal distance from the tunnel centre to the point of inflection. At the point of inflection, the depth of the settlement trough equals 60% of the maximum settlement depth. In the case of homogeneous soil conditions, the parameter *i* can be calculated as the multiplication of a trough width parameter K[43] and the depth of the tunnel z_o (Equation 7.7).

$$i = K\, z_o \qquad \textbf{[Equation 7.7]}$$

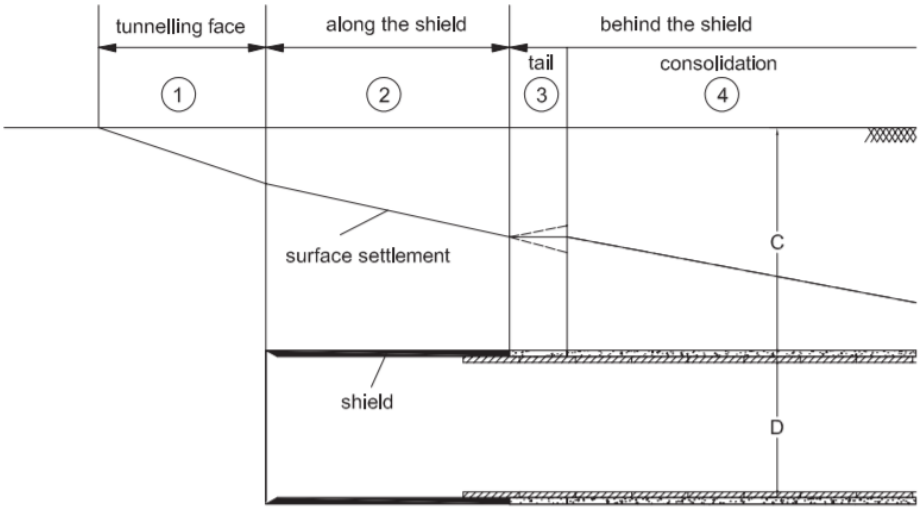

Figure 68. Volume loss components (Vu Minh, 2016).

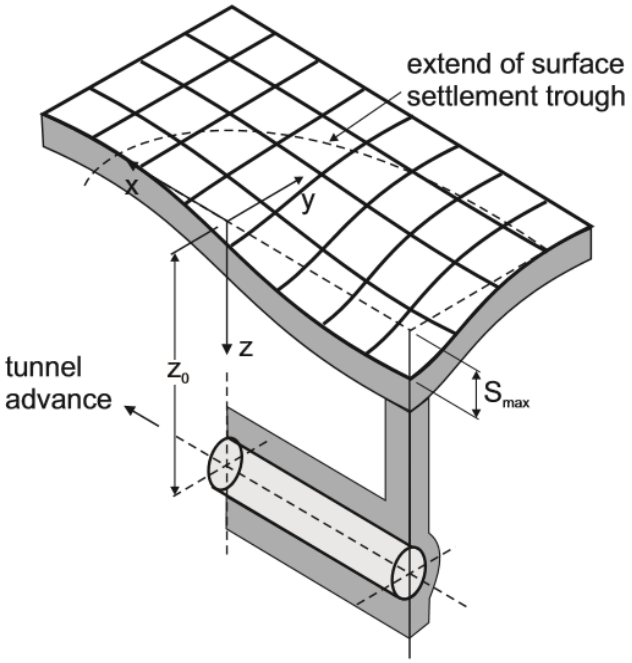

Figure 69. Tunnel-induced settlement trough (Möller, 2006, after Attewell et al, 1986).

[43] The trough width parameter equals $K \approx 0.5$ for clayey ground and $K \approx 0.25$ for sandy ground (Möller, 2006).

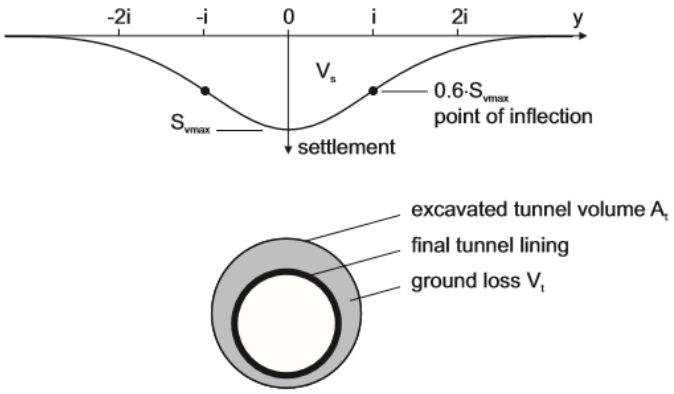

Figure 70. Gaussian curve for transverse settlement trough and ground loss *Vt* (Möller, 2006).

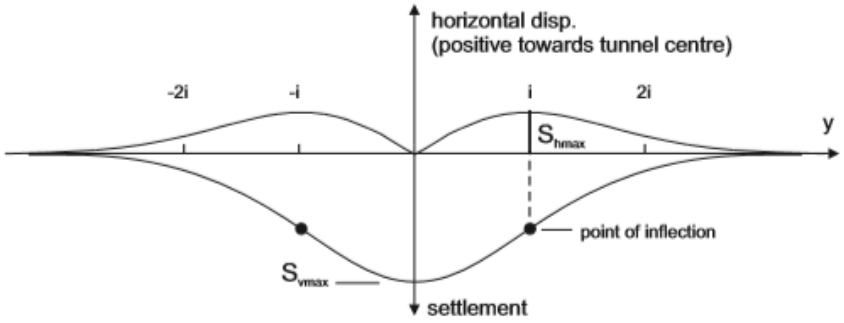

Figure 71. Horizontal surface displacements and transverse settlement trough (Möller, 2006).

For tunnels in layered ground, Equation 7.7 has been rewritten to take the effect of the different ground layers into account. The point of inflection *i* can be calculated as the sum of the trough width parameter K_i and thickness of the soil layer z_i for each soil layer.

$$i = \sum K_i \, z_i \qquad \textbf{[Equation 7.8]}$$

5.1.4.3 Horizontal displacement of the settlement trough

Like vertical displacement, horizontal displacement is important to consider, as it can lead to building damage. O'Reilly and New (1982) have proposed a relation between the vertical and horizontal displacement of the settlement trough (Equation 7.9)(Figure 71). By combining Equation 7.9 with Equation 7.6., the horizontal displacement can be immediately calculated from the parameters of the Gaussian distribution. In Figure 71, the horizontal surface settlement has been plotted together with the transverse settlement trough. This figure reveals that the theoretical maximum horizontal displacement S_{hmax} occurs at the point of inflection.[44]

$$S_h(y) = \frac{y}{z_o} \, S_v \qquad \textbf{[Equation 7.9]}$$

$$S_h(y) = \frac{y}{z_o} \, \frac{A_t}{i\sqrt{2\pi}} \, GLR \, e^{\left(\frac{-y^2}{2i^2}\right)} \qquad \textbf{[Equation 7.10]}$$

$$S_h(y) = \frac{y}{z_o} \, 0{,}6 \, S_{vmax} \qquad \textbf{[Equation 7.11]}$$

[44] At this location, $S_v(y) = 0.6 \cdot S_{max}$, as indicated in Figure 70.

5.2 Processes around a TBM

The total volume loss during closed shield tunnelling is controlled by the volume loss at the face, along the shield and behind the TBM. The volume loss at the face can be directly affected by adequate support. In contrast, the volume loss along the shield is highly influenced by processes around the TBM and is indirectly affected by the other two components. These processes around the TBM are the consequence of the gap between the shield skin and the surrounding soil, the face support method and the grouting of the tail void.

5.2.1 Processes in front of the TBM

A support pressure is required at the face of the TBM in order to counter the horizontal effective stress and pore water pressure acting on the tunnel face (Figure 72). As the pressure of the support medium is greater than the pore water pressure, the slurry infiltrates the soil to a certain extent. The value of the support pressure used is a function of the two limit state approaches and lies between the two limits of the support medium.

Due to overcutting (when the excavated diameter is larger than the shield diameter) and the tapered shape of the TBM, a joint is present between the shield skin and the soil formation. It has been assumed that the shield has been 'positioned' concentrically within the excavated diameter so that the shield is hydraulically connected to the tunnel face. This means that the annulus is pressurised with bentonite slurry originating from the face (Bezuijen, 2007) (Mooney et al, 2016). Due to the uniform pressure of the support medium, the slurry radial shield pressure at the annulus is equal to the slurry pressure at the tunnel face (Figure 72). Along the depth of the annulus, the slurry pressure is constant. The support medium in the TBM excavation chamber varies between the tunnel crown and the invert due to the unit weight of the slurry used.

5.2.2 Behind the TBM

The gap between the lining and the soil formation is called the tail void. In order to prevent the surrounding soil from moving into the gap, the void is filled by a grout injection. Due to the very short gel time of grout compared to the time required for a ring cycle, it is reasonable to assume that only one ring's annulus is subjected to pressure from the grout during a ring advance. In addition, the grout present in all trailing rings solidifies and primarily contains elastic properties (Mooney et al, 2016).

Ground deformations may occur if the grout pressure is less than the total vertical stress or if grout voids occur (Li et al, 2015). As the grout pressure during grout injections is higher than the soil pressure, the soil is pushed away from the TBM and grout flows from the tail over the shield (Bezuijen and Talmon, 2008). In this thesis, the grout pressure at the tail void is likewise the face support pressure limited to a pressure of around 90% of the total vertical stress of the soil cover. This flow has therefore not been taken into account.

5.2.3 Flow around the TBM

This analysis has assumed that the annulus between the shield skin and the soil formation is pressurised with the bentonite slurry that flows from the tunnel face. The flow of grout from the tail void is restricted by a maximum support pressure limit.

5.3 Relation of the TBM parameters and ground deformations

The face support pressure applied counteracts the horizontal effective stress and the pore water pressure acting on the tunnel face. As the support medium's flow has been taken into account, this means that the support medium also pressurises the annulus along the shield. In order to obtain zero surface deformations, the support pressure must match the exact geostatic stress conditions at the location of the tunnel axis, the tunnel crown and invert, the annulus and the tail void. If this is not the case, then ground deformations inevitably occur. The problem in this analysis is that it is impossible to match the exact geostatic stress at all locations, due to the properties of the support medium and the difference in the horizontal and vertical effective stress.

Mooney et al (2016) have performed a data-driven modelling study to characterise the relation between ground deformations and the TBM slurry parameters. For this analysis, a coupled soil-fluid finite difference model has been used. In this model, the top model boundary (z = 0) was set to be free, whereas the vertical movement at the bottom boundary was fixed. In order to model the soil conditions, a homogeneous, highly permeable granular soil has been used (Table 15). The diameter of the TBM equals 6,9 metres with a soil cover of 19 meters (*C*/*D*=2,8). The unit weight of the support medium equals 12 kN/m^3 and the unit weight of the grout equals 21 kN/m^3. The influence of coupling the slurry pressure with the face and the annulus has been determined by using three types of pressure distributions (Figure 73). The green pressure distribution was obtained when the support pressure distribution equals the geostatic stress at tunnel invert, the red distribution equals the geostatic stress at the tunnel axis and the black pressure distribution equals the geostatic stress at the tunnel crown. In addition, the blue pressure distribution represents the geostatic stress conditions at each location.

In order to determine the limitations of the support medium properties and the TBM parameters, in first instance, the hydraulic connection between the face and the annulus is neglected, e.g. case B (Figure 73). The horizontal stress acting at the top of the tunnel crown equals 227 kPa and 326 kPa at the tunnel invert. Figure 73 reveals that the pressure gradient of the support medium is insufficient to match the geostatic stress at each location of the tunnel face. For the given situation, a support pressure gradient of around 14 kPa is required.

Figure 73 indicates that due to the hydraulic connection between the tunnel face and the annulus, the same stress is present, whereas the geostatic stress at these two locations is different. At the tunnel crown annulus (Case A), the geostatic stress is equal to the total vertical stress of the soil profile above the TBM, while the geostatic stress at the tunnel crown (Case B) is equal to the horizontal stress acting on the tunnel crown. The pore water pressure at both locations is equal, as the pore water pressure is equal in all directions. This means that, due to the ratio between the vertical and the horizontal effective stress, the geostatic stress cannot be matched at both locations.

Mooney et al (2016) have determined the vertical displacement of the ground surface corresponding to the four stress distributions[45]. As expected, when the geostatic stress is not exactly matched at each location, the surface settles. In this analysis, all three pressure distributions have led to approximately the same vertical displacement. The reason for this is a combination of the dense, stiff, till material and the high face support pressures. The latter results from the use of an earth pressure coefficient equal to neutral ground conditions.

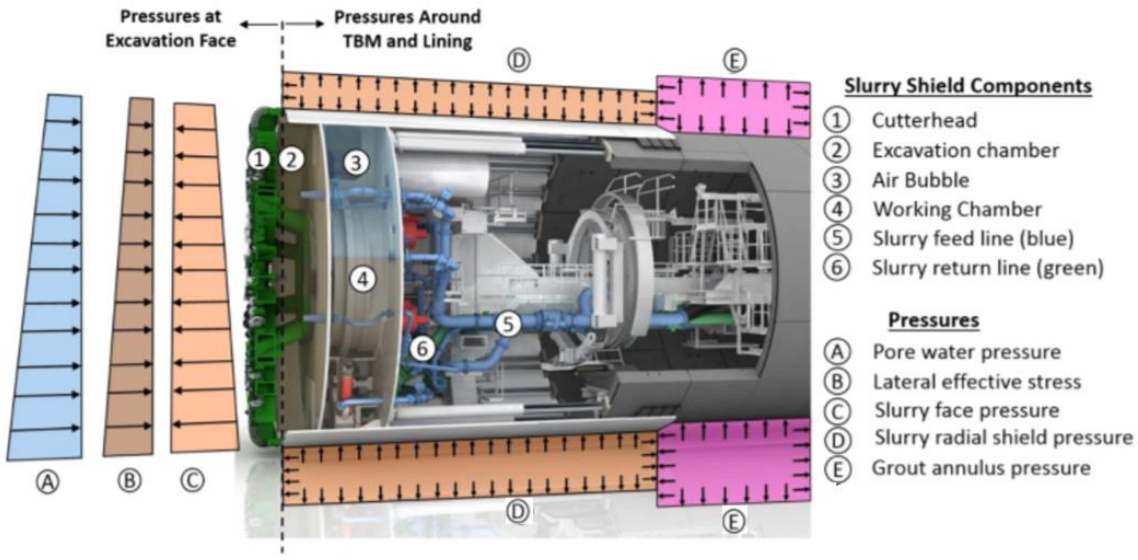

Figure 72. Schematic overview of the TBM slurry shield and pressure components (Mooney et al, 2016).

[45] The blue pressure distribution is a fictional pressure distribution that cannot be reached in practice.

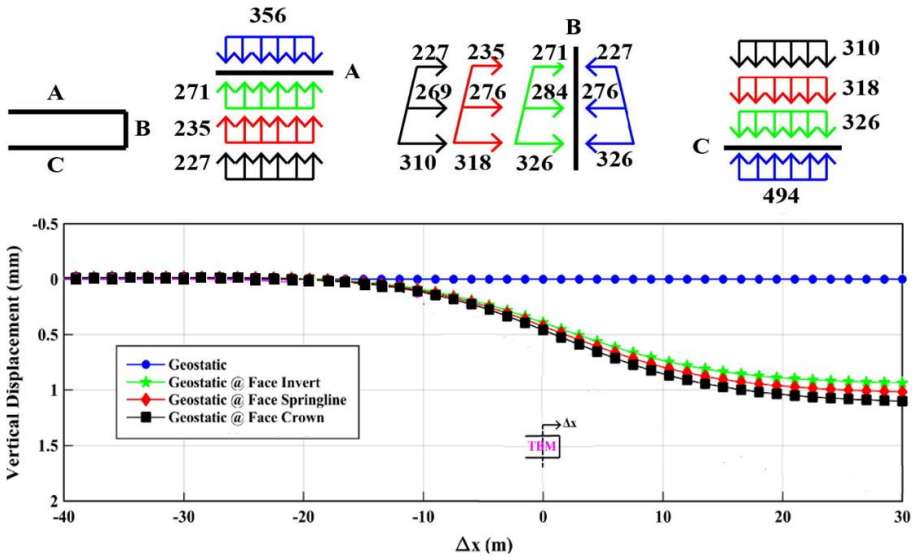

Figure 73. Three possible stress distributions for the support medium have been obtained in order to determine the relation between the TBM slurry parameters and ground deformations.

Table 15. Assumed homogeneous soil, slurry and grout properties.

Property	Value
Dry unit weight soil [kN/m^3]	16
Saturated unit weight soil [kN/m^3]	20
Young's modulus [MPa]	200
Poisson's ratio [-]	0,3
Friction angle [°]	40
Dilatation angle [°]	10
Coefficient of lateral earth pressure at rest [-]	0,5
Slurry pressure gradient [kN/m^3]	12
Grout pressure gradient [kN/m^3]	21

5.3.1 Rijnlandroute case study

The total vertical and horizontal stress distribution in front of the tunnel face has been determined for the eight case studies discussed in Paragraph 3.4 (Annex 6). The total vertical stress distribution has been used to determine the geostatic stress along the shield. As it has been assumed that the shield is positioned concentrically within the excavated diameter, this means that an annulus is present along the entire circumference of the TBM. The annulus pressure must therefore match the exact geostatic stress along the entire height of the tunnel face and not only at the location of tunnel crown and invert. The total horizontal stress acting at the tunnel face has to be counteracted by the support medium. In the calculation of the horizontal effective stress it is assumed that the soil has zero lateral strain; therefore, a neutral earth pressure coefficient has been used. The pressure distribution of the excavation chamber has been determined using a support pressure gradient equal to 12 kN/m^3.
Due to the hydraulic connection between the tunnel face and the annulus, the same stress is present, whereas the geostatic stress at these two locations is different. At each location within the annulus the stress difference between the geostatic stress and the support is determined. Figure 74 indicates the calculation results for a homogeneous sand profile. Due to the constant unit weight of the soil, all pressure distributions increase linearly with depth. As the pressure gradient of the support medium is lower than the gradient of the soil, an offset is present between the horizontal stress and the support pressure. Figure 75 indicates the calculation results for a heterogeneous soil profile (Case G). In contrast to the homogeneous soil profile, these pressure distributions do not increase linearly with depth, but a jump is present at the boundary between the two layers. Due to this discontinuous pressure distribution, a large offset is present at the upper layer between the horizontal stress and the support medium. This much larger support pressure than required does not benefit the construction costs or time, but on the other hand, it results in smaller ground deformations.

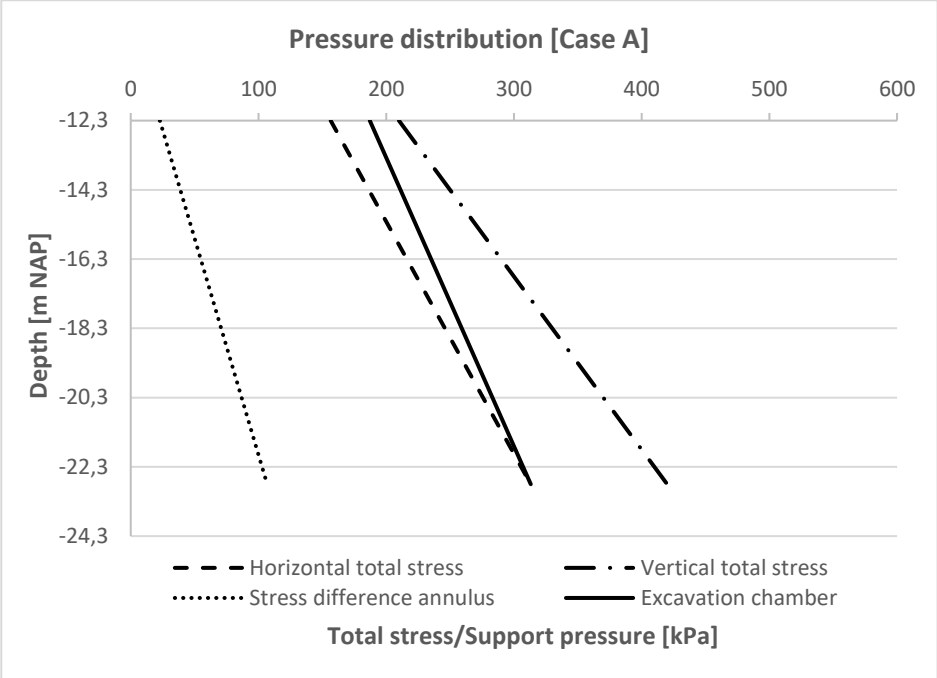

Figure 74. Pressure distribution at the tunnel face, annulus and excavation chamber for a homogeneous sand profile (Case A).

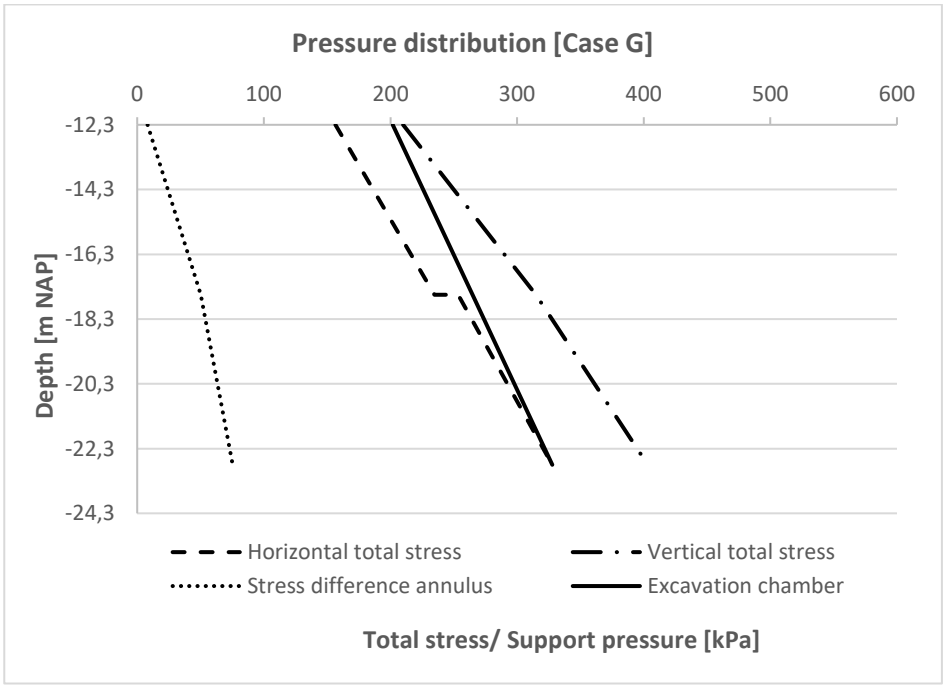

Figure 75. Pressure distribution at the tunnel face, annulus and excavation chamber for a heterogeneous soil profile (Case G).

6 Conclusions

The goal of this thesis was to find an answer to the question:

What is the difference between static and transient face stability? Case study: The Rijnlandroute.

To be able to answer this question, sub-questions were stated. The answers to the sub-questions are as follows:

1. **What is the required minimum support pressure based on a static face stability assessment for the eastern entrance zone (chainage 3900-4300)?**
    a) What are the differences between the three original face support models, and what is the effect of these differences on the value of the minimum support pressure?

This research consists of a comparative study between the Ruse-Vermeer model (2002), the Jancsecz-Steiner model (1994) and the DIN4126+4085-model (2007,2013). The latter two models are both based on limit equilibrium, which assumes a failure mechanism in front of the tunnel face. The Jancsecz-Steiner model is based on a three-dimensional wedge model that consists of a sliding wedge loaded by a soil silo. The DIN model originates from the stability of diaphragm walls and therefore assumes a two-dimensional sliding wedge extending from the tunnel invert to ground surface. In contrast to the limit equilibrium models, the RV model is a limit stress method that assumes a possible stress distribution at the tunnel face and from that determines the support pressure at collapse. The parameters in this model can be considered as safety factors (called stability numbers) obtained by performing multiple numerical calculations.

Regardless of the choice of model, all three face stability models can be written as a summation of the horizontal effective stress σ'_h multiplied by a safety factor γ_h and the pore water pressure u_1 multiplied by a safety factor γ_{u1}. For all three models, the input values for the pore water pressure are the same, whereas the input values for the horizontal effective stress differ.

The Jancsecz-Steiner model[46] calculates the horizontal effective stress acting at the tunnel face by a multiplication of the vertical effective stress in front of the tunnel face with a three-dimensional earth pressure coefficient $K_{A3D.}$ The value of this coefficient for friction angles (> 20°) is approximately equal to the active earth pressure coefficient. This model does not take the influence of cohesion into account. Vertical soil arching can be implement in the soil profile above the TBM and this leads to a reduction in the vertical effective stress distribution. In contrast, the horizontal soil arching component is implemented within the K_{A3D} coefficient. A disadvantage of this model occurs when both soil arching components are implemented simultaneously. The reason for this is that the horizontal soil arching component is based on the vertical effective stress distribution next to the wedge and the vertical soil arching component is based on the vertical effective stress distribution in front of the tunnel face. In cases where vertical soil arching has been implemented, the vertical effective stress in front of the tunnel face reduces but this is not the case for the vertical effective stress distribution next to the wedge.

In the DIN-model, the horizontal effective stress acting at the tunnel face is calculated by a multiplication of the vertical effective stress in front of the tunnel face with an active earth pressure coefficient. In case of a non-zero cohesion component, this horizontal effective stress is reduced by the effect of cohesion. As this model originates from the stability of diaphragm walls, no soil cover above the TBM is present and therefore, vertical soil arching is not considered. In contrast, horizontal soil arching is taken into account by shape coefficients. These shape coefficients reduces the horizontal stress based on the depth/length ratio of the tunnel face. An important aspect to note is that within this thesis there are some uncertainties about this horizontal soil arching component.

[46] Only the K_{A3D} model is described.

In the Ruse-Vermeer model, the horizontal effective stress distribution at the tunnel face is calculated with one single equation. This horizontal effective stress is assumed to be constant and equal to the horizontal effective stress at tunnel invert. The equation consists of stability numbers in order to account for an additional surcharge on ground surface, reduction due to a cohesion component and the unit weight of the soil. One of the most important assumptions in the Ruse Vermeer model is that for friction angles larger than 20° and C/D >1, the stress arch carries the ground cover (and additional surcharge) regardless of the magnitude of its thickness. In the equation of the model, this effect is translated to a vertical effective stress equal to zero at tunnel crown. The disadvantage of this model is that the above assumption is based on the soil profile in front of the tunnel face instead of the soil profile above tunnel crown. Therefore, this model needs to be used with great caution.

In order to determine the effect of these models' differences on the minimum support pressure, eight case studies have been set up. The first test-series is based on the original models and the outcomes of this test series showed that for each case the Ruse-Vermeer model results in the lowest minimum support pressure. The Jancsecz-Steiner model (without vertical soil arching) and the DIN-model result in the highest minimum support pressure. The Jancsecz-Steiner model including vertical soil arching lies between those two limits.

b) Is it possible to improve the three face stability models by using aspects of other models?

Yes, in this research the DIN-model is extended in order to take vertical soil arching into account by the same method as used in the Jancsecz-Steiner model. From the background analysis of the DIN-model, it resulted that this model is based on the stability of diaphragm walls. This method is translated to a tunnel face stability assessment, by replacing the diaphragm wall through a TBM. However, the failure wedge is still based on the presence of a diaphragm wall. Compared to a retaining wall, the tunnel face does not extend to ground surface but extends from tunnel invert to tunnel crown. This 'reduced wedge' is taken into account, by assuming that an active state is only valid at the location of the TBM. Due to this modification, we can assume that the soil profile above the TBM acts as a surcharge. This situation is equal to the Jancsecz-Steiner model and therefore we use the same method in order to incorporate vertical soil arching within this model.

In test series 4 of the case study analysis, the effect of this incorporation in the DIN model, on the minimum support pressure is determined. As expected, the inclusion of this vertical soil arching component leads to a lower minimum support pressure. The obtained support pressure can even be lower than the Jancsecz-Steiner model including soil arching due to the cohesion reduction effect and horizontal soil arching component of the DIN-model. As described, there are some uncertainties about the horizontal soil arching component of the DIN-model.

The DIN-model takes vertical horizontal soil arching into account by using shape-coefficients. These shape coefficients determine a reduced value of horizontal effective stress which acts on the tunnel face. The amount of reduction depends on the depth z below ground surface and length of the tunnel face. As described, the failure wedge of a diaphragm wall extends from wall toe to ground surface with no ground cover on top, while in the case of a tunnel face stability assessment, it is assumed that an active state is only valid at the location of the tunnel face. This means that horizontal soil arching only occurs at the location of the tunnel face. Due to this, the depth z below ground surface has to be modified for the depth z below the tunnel crown (z*). This modification is supported by the Jancsecz-Steiner wedge model. In this wedge model, horizontal soil arching is taken into account by shear stresses which acts on the sides of the wedge. The corresponding shear forces are determined by the multiplication of these shear stresses with the areas of the triangular sides of the wedge. As the height of this wedge is equal to the diameter of the tunnel, this means that the height of the soil overburden does not influence the area of this triangular failure plane.

c) How do the support medium properties influence static face stability?

The support medium fulfils several roles during tunnelling, and for each role, different parameters are important. Therefore, not for each function, the most optimal parameters can be used. For the transport function as low as possible yield strength is required and for the stabilisation function as high as possible yield strength is required. The support medium properties that influence static face stability are part of the stabilisation function of the support medium.

At the face of the TBM, called bore front, a pressurised slurry is used as face support. Due to the pressure difference between the support pressure and the (equilibrium) pore water pressure, the bentonite suspension infiltrates the soil. In the case of fine-grained soil, this infiltration length is practically zero and a small impermeable layer develops, also called filter cake. In case of an filtercake, the excess pressure is transferred onto the soil skeleton by an infinitely thin membrane. In the case of coarse-grained soil layers, the slurry penetrates a certain distance into the soil, also called penetration zone. In this case, the support pressure is transported onto the soil skeleton over the infiltration length by drag forces. The excess pressure is fully transferred when the maximum penetration distance is reached.

In case of static face stability assessment, the time-dependent infiltration process is neglected, and therefore we assume that in each case the maximum penetration distance is reached. This maximum penetration distance of the support medium is a function of the excess pressure Δs, the characteristic grain size diameter d_{10} and the yield strength of the support medium. *The effect of these parameters on the minimum support pressure are equal for both a static and transient face stability and therefore the results are discussed at research question 2a.*

d) How can the effect of slurry infiltration be modelled in the case of static face stability?

From a study by Xanthakos (1979), it resulted that the stabilizing force of the support medium depends essentially on the penetration distance of the support medium into the ground. In case of a limit equilibrium model which assumes a pre-defined failure mechanism, the amount of slurry that penetrates outside this failure mechanism exerts its thrust on a soil zone that is not involved in this mechanism. Therefore, the amount of forces outside the failure mechanism reduces the effectiveness of the support force. As the infiltration process of the support medium is time-dependent, this process cannot be integrated within a static face stability process. Nevertheless, the effect of slurry infiltration can be incorporated by using the two limit cases; the membrane model (negligible penetration distance) and the penetration zone model (maximum penetration distance). By using these limits, the effectiveness of the support medium can be determined as the ratio between the penetrated zone within the wedge A_s with the total penetrated zone of the support medium A_t.

In test series 6, the effectiveness of the support medium is investigated for both a homogeneous and heterogeneous soil profile. In case of a homogeneous soil profile, the slip angle of the wedge is constant and therefore the shape of the wedge is easily determined. In addition, the shape of the penetration zone as a function of the maximum penetration distance increases with depth. The reason for this is that the excess pressure Δs increases with depth, due to the difference in unit weight between water and the support medium. In case of a heterogeneous soil profile, the slip angle and the characteristic grain size diameter d_{10} are not constant over the face. Despite these facts, a method has been developed to determine the effectiveness of the support medium in case of a stratified soil profile. In this method, each soil layer is seen as a separate wedge analysis, and for each layer, the amount of support medium which infiltrates outside the failure wedge is determined. The main reason which supports this calculation method is the fact that the penetration distance of each layer is independent of the soil properties of the other layers.

The results of test series 6 indicate that a soil layer with a high permeability (d_{10} value) has the greatest effect on the effectiveness of the support medium when this layer is situated at the bottom of the wedge due to the smallest dimensions of the wedge as this location. In addition, the total area of the suspension saturated zone is not the main parameter, but the total area of the suspension saturated zone outside the failure wedge.

2. **What is the minimum required support pressure for the eastern entrance zone (chainage 3900-4300) based on a transient face stability assessment?**

a) How can the time-dependent infiltration process be modelled?

In order to model the time-dependent infiltration process, it is assumed that the infiltration process is not interdependent with the time-dependent excavation process. Therefore, this process has been investigated by neglecting the advance rate of the TBM, and this situation can be reflected by the ring-building phase.

The infiltration depth of the support medium with time is determined by using the equation obtained by Krause (1987). This equation reflects the amount of percentage I_e of the final penetration depth (e_{max}) which is reached after a certain time. The percentage I_e is a function of the parameter a; this value represents the time required in order to reach half of the maximum penetration distance. The value a can be determined experimentally by performing column infiltration tests.

In this research, the parameters which affects this penetration distance are investigated. From this research, it turned out that the only two factors which can be controlled are the excess pressure and yield strength of the support medium. It can be concluded that for the same soil profile, an increase in the yield strength parameter leads to a smaller penetration depth of the support medium. In contrast, an increase in the excess pressure leads to an increase of the penetration depth.

For a transient face stability assessment, an as small as possible penetration distance is beneficial. The reason for this is that in case of a penetration zone model, the excess pressure will only be fully transferred when the maximum penetration distance is reached. In addition, during boring the available time-span for the built-up of the filter cake is limited. Therefore, the most optimal yield strength of the support medium is highly influenced by the time dependent excavation process.

b) How can the time-dependent behaviour of the excavation process be modelled?

In order to model the time-dependent excavation process, it is assumed that the excavation process is not interdependent with the time-dependent infiltration process. Therefore, this time-dependent excavation process has been investigated under the assumption that during boring a membrane model is valid. The advance rate (mm/min) of the TBM is a function of the lay-out of the cutting wheel, revolutions per minute and the capacity of the slurry treatment plant (STP) on the surface. The latter imposes a maximum advance rate for the project based on the capacity of the STP pumps.

For a transient face stability assessment, two parameters are important which are the penetration depth of the cutting wheel/tools and the time span between subsequent passing of the cutting tools. The time span between two subsequent tool passes is the period in which the pressure transfer mechanism is formed without being disturbed or damaged. From this thesis, it can be concluded that for the same advance rate (mm/min), an increase in the revolutions per minute (*RPM*), results in a lower value of the excavation depth per tool passing in combination with smaller time span between tool passing. The most optimal combination between the advance rate and revolutions per minute depends highly on the properties of the support medium.

c) How can the built-up of excess pore pressures be modelled?

During boring, a simultaneous process of excavation and face support takes place. Each rotation of the cutting wheel consequently (partly) excavates the filter cake/penetration zone. At the same time, the slurry infiltrates the soil in order to rebuild the filter cake/penetration zone. During this process, there is a continuous inflow of filtrate water into the soil, resulting in excess pore pressures in front of the TBM. In this thesis, this interaction has been simplified by the assumption that the cutting depth of the excavation tools is so large that the entire filter cake is removed by each passage of the cutting tools.

The development of the excess pore pressures during boring can be modelled by using the method developed by Broere (1998) and Broere & van Tol (2000, 2001). In his model, the built-up of the excess pore water pressure in front of the TBM are determined by the inclusion of a groundwater flow model in a wedge stability model. By using a transient groundwater flow model, the built-up of excess pore pressures during boring as well as the dissipation of the excess pore pressures during a

standstill has been determined. A parameter study has been performed in order to investigate this transient groundwater flow in more detail, by considering the following four aspects: advance speed of the TBM, permeability aquifer *k*, leakage length λ and the ratio *D*/*H*. From this analysis, it resulted that an increase in the height and permeability of the aquifer, the excess pore water pressures decreases. The reason for this behaviour is that the transmissivity *kH* of the aquifer increases. As the advance rate of the TBM is increased, more excess pore water pressures will be generated at the tunnel face due to the fact that the discharge of the TBM has increased. The leakage length has, till a certain value, a high impact on the amount of excess pore water pressures which develops. From the parametric analysis, it turned out, that a leakage length larger than 50 metres have a negligible influence on the excess pore pressure distribution.

The only factor from the parametric study which we can control is the advance speed of the TBM. In certain cases, it is highly required to reduce the built-up of the excess pore water pressures due to the fact that a groundwater flow is induced. For example, in case of a contaminated zone within the soil, this groundwater flow will spread this contaminant further. At such locations, the ground water flow can be limited by reducing the advance rate of the TBM.

d) How do the support medium properties influence transient face stability?

The answer to this research question is described at research question 2a.

e) What is the effect of the additional surcharge on the minimum required support pressure?

The placement of the additional surcharge on ground surface leads to a total stress increment equal to the load q_o of the surcharge. With time, this total stress increment is transferred to the effective stress component. In case of a not fully consolidated soil layer above or in front of the tunnel face, at the moment of boring, this consolidation process affects both the maximum and minimum support pressure limits. In this thesis, two methods have been proposed in order to incorporate the effect of consolidation process within a face stability assessment. These two methods are described in paragraph 3.5.3.

3. What is the influence of the (slurry) TBM parameters on ground deformations?

a) What are the components that determine the amount of ground deformations?

The amount of ground deformation that occur due to tunnelling is a function of the volume loss components which occur at the face of the TBM, along the shield, at the tail and due to the deformation of the lining. Despite the fact that this thesis is based on tunnel face stability assessment, both the volume components at the face and along the shield are important. The reason for this is that due to overcutting (when the excavated diameter is larger than the shield diameter) and the tapered shape of the TBM, a joint (annulus) is present between the shield skin and the soil formation. It has been assumed that the shield has been 'positioned' concentrically within the excavated diameter so that the shield is hydraulically connected to the tunnel face. This means that the annulus is pressurised with bentonite slurry originating from the face (Bezuijen, 2007) (Mooney et al, 2016). Due to the uniform pressure of the support medium, the slurry radial shield pressure at the annulus is equal to the slurry pressure at the tunnel face. In order to obtain zero surface deformations, the support pressure must match the exact geostatic stress conditions at the location of the tunnel axis, the tunnel crown and invert, the annulus and the tail void.

b) How can these ground deformations be assessed analytically?

This calculation method is described in paragraph 5.2

c) How do the support medium properties influence the support pressure distribution over the tunnel face?

The total vertical and horizontal stress distribution in front of the tunnel face has been determined for the eight case studies. The horizontal stress is calculated by assuming neutral ground conditions. The pressure distribution of the excavation chamber has been determined using a support pressure gradient equal to 12 kN/m^3. From this research, it turned out that it is not possible to match the exact geostatic stress at each required location due to the support pressure gradient and the hydraulic connection between the face and annulus. In contrast to the homogeneous soil profile, these pressure distributions in case of a heterogenous soil profile do not increase linearly with depth, but a jump is present at the boundary between the two layers. Due to this discontinuous pressure distribution, a large offset is present at the upper layer between the horizontal stress and the support medium. This much larger support pressure than required does not benefit the construction costs or time, but on the other hand, it results in smaller ground deformations.

Bibliography

[1]. G. Anagnostou and K. Kovári. The face stability of slurry-shield-driven tunnels. *Tunnelling and Underground Space Technology*, 9(2):165–174, 1994.

[2]. G. Anagnostou and K. Kovári. Face stability conditions earth-pressure-balanced shields. *Tunnelling and Underground Space Technology*, 11(2):165–173, 1996.

[3]. Arthe Civil & Structure. Face stability calculations. Internal memo. 2016.

[4]. J.H. Atkinson, and R.J. Mair. Soil mechanics aspects of soft ground tunnelling. In *Ground Engineering* 14, No. 5, pp. 20-38, 1981.

[5]. P.B. Attewel., J. Yeates, and A.R. Selby. *Soil Movements Induced by Tunnelling and their Effects on Pipelines and Structures*. Blackie, Glasgow, 1986.

[6]. M. Backus. Tunnel face stability in Dutch soil. Master's thesis, Delft University of Technology, 1998.

[7]. A. Bezuijen and M. Huisman. Afpleistering en mudspurt tijdens boren. Technical Report 27, Boren Tunnels en Leidingen, 1997.

[8]. A.Bezuijen and A.M. Talmon. Processes around a TBM. *Vakblad Geotechniek*, 2008,

[9]. W. Broere. *Tunnel Face Stability & New CPT Applications.* PhD thesis, Delft University of Technology, Delft, 2001.

[10]. W. Broere, and A.F .van Tol. Influence of infiltration and groundwater flow on tunnel face stability. In *Kusakabe, O., K. Fujita & Y. Miyazaki (eds), Geotechnical Aspects of Underground Construction in Soft Ground*, pp. 339– 344. 2000. Balkema.

[11]. W. Broere and A.F .van Tol. Time-dependent infiltration and groundwater flow in a face stability analysis. In Modern Tunneling Science and Technology, Kyoto, Japan, 2001, pp. 629–634.

[12]. G.A. Bruggeman. *Analytical Solutions in Geohydrological Problems.* Elsevier, 1999.

[13]. P. Chambon and J.F. Corté. Shallow tunnels in cohesionless soil: Stability of tunnel face. *ASCE Journal of Geotechnical Engineering,* 120:1148–1165, 1994.

[14]. COMOL5. DBM-overeenkomst RijnlandRoute Contractnummer: DOS-2015-0004005 Aanbieding: COMOL5. 2017.

[15]. R.N. Craig and A.M. Muir Wood. A review of tunnel lining practice in the united kingdom. Supplem. 335, Transport and Road Research Laboratory,1978.

[16]. CUR B&!. Handboek diepwanden. Ontwerp en uitvoering. CUR231, 2010.

[17]. Deutscher Ausschuss für unterirdisches Bauen e. V. (DAUB). Recommendations for Face Support Pressure Calculations for Shield Tunneling in Soft Ground. 2016.

[18]. DIN 4085:2007-10: Baugrund – Berechnung des Erddruckes (Subsoil – calculation of earthpressure), 2007.

[19]. DIN 4126, Nachweis der Standsicherheit von Schlitzwänden (Stability analysis of diaphragm walls), Deutsche Institut für Normung, 2013.

[20]. D. Festa. *On the interaction between a Tunnel Boring Machine and the Surrounding Soil.*. PhD thesis, Delft University of Technology, Delft, 2015.

[21]. Herrenknecht AG. Herrenknecht Seperation plants- keep it flowing. Product brochure, 2009.

[22]. S. Jancsecz and W. Steiner. Face support for a large mix-shield in heterogeneous ground conditions. In *Tunneling '94*, London, 1994. Institution of Mining and Metallurgy.

[23]. M.A. Janssen. Versuche über Getreidedruck in Silozellen. Zeitschrift des Vereins deutscher Ingenieure, Band XXXIX, No. 35,pp. 1045-1049,1894.

[24]. M. Kilchert and J. Karstedt. *Schlitzwände als Trag- und Dichtungwände, Band 2, Standsicherheitberechnung von Schlitzwänden*, pages 28–34. DIN, Berlin, 1984.

[25]. A. Kirsch and D. Kolymbas. Theoretische Untersuchung zur Ortsbruststabilität. Bautechnik 82(7): pp. 449–456,2005.
[26]. F. Köppl, K. Thuro and M. Thewes. Factors with an influence on the wear to excavation tools in hydroshield tunnelling in soft ground. *In Geomechanics and Tunnelling*, pages 248 -257,2015.
[27]. T. Krause. *Schildvortrieb mit flüssigkeits- und erdgestützter Ortsbrust.* PhD thesis, Technischen Universität Carolo-Wilhelmina, Braunschweig, 1987.
[28]. P. Longchamp. AFTES recommendations concerning slurry for use in slurry shield TBM, Tunnels et ouvrages souterrains, No. 1 2005, S. 164-183
[29]. R.J. Mair and R.N. Taylor. Bored tunnelling in the urban environment. In *14th international Conference on Soil Mechanics and Foundation Engineering*, pages 2353-2385, Hamburg, 1997. Balkema: Rotterdam.
[30]. P. Mélix. Modellversuche und Berechnungen zur Standsicherheit oberflächennaher Tunnel. Veröff. des Inst. für Boden- und Felsmechanik der Univ. Fridericiana in Karlsruhe, 103 ,1987.
[31]. S. Möller. *Tunnel induced settlements and structural forces in linings*. PhD thesis, Universität Stuttgart, 2006.
[32]. M.A. Mooney, J.Grasmick, B.Kenneally,Y.Fang. The role of slurry TBM parameters on ground deformation: Field results and computational modelling. *Tunnelling and Underground Space Technology*, 2016.
[33]. MS. Slurry treatment plant. Rijnlandroute project. 2017. [internal document]
[34]. H. Müller-Kirchenbauer. Stability of slurry trenches in inhomogeneous subsoil. In N.N., editor, *9th International Conference on Soil Mechanics and Foundation Engineering*, pages 125–132, 1977.
[35]. B.M. New and M.P. O'Reilly. Tunnelling induced ground movements predicting their magnitude and effects. In *4th International Conference on Ground Movements and Structures*, volume 1, pages 671-697, Cardiff, 1991. Pentech Press.
[36]. M.P. O'Reilly and B.M. New. Settlements above tunnels in the united kingdom- their magnitude and prediction. *Tunneling 82*, pages 173-181,1982.
[37]. R.B. Peck. Deep excavations and tunnelling in soft ground. In *7th int. Conference on Soil Mechanics and Foundation Engineering*, pages 225-290. Sociedad Mexican de Mecanica de Suelos, A.C., 1969.
[38]. A. Piaskowki and A. Kowalewski Z. Application of thixotropic clay suspensions for stability of vertical sides of deep trenches without strutting, Proc. Of 6th Int. Conf. on Soil Mech. And Found. Eng. Montreal, Vol. 111,1965.
[39]. M. Plantinga. Boorfrontstabiliteit bij Vloeistofschilden: Inventarisatie van modellen en analytische beschouwing voor gelaagde grond. Msc Thesis. Delft University of Technology, 1998.
[40]. S. Praetorius and B.Schoesser. *Bentonite handbook. Lubrication for Pipe Jacking*, Stuttgart, 2017.
[41]. B.F. Schmidt. *Settlements and ground movements associated with tunnelling in soils*. Phd thesis, University of Illinois, Urbana, 1969.
[42]. P.A. Vermeer, N. Ruse and T. Marcher. Tunnel Heading Stability in Drained Ground. In FELSBAU 20, volume 6. pages 8-18, 2002.
[43]. P.A. Vermeer and N. Ruse. Die Stabilität der Tunnelortsbrust in homogenem Baugrund. *In geotechnik24,* volume 3, pages 186-193, 2001.
[44]. N. Vu Minh. *Reducing the cover-to-diameter ratio for shallow tunnels in soft soils*. PhD thesis, Delft University of Technology, Delft, 2016.

[45]. K. Terzaghi. Stress Distribution in Dry and in Saturated Sand Above a Yielding Trap-Door, Proceedings. In *First International Conference on Soil Mechanics and Foundation Engineering*, Cambridge, Massachusetts, pp. 307-311, 1936.
[46]. K. Terzaghi. Theoretical Soil Mechanics, John Wiley and Sons, New York, pp. 66-76,1943.
[47]. K. Terzaghi and R. Jelinek. Theoretische Bodenmechanik, Springer-Verlag, Berlin,1954.
[48]. M. Thewes, B. Schoesser and Z. Zizka. Transient face support in slurry shield tunnelling due to different time scales for excavation sequence of cutting tools and penetration time of support fluid. *Proceedings of the ITA World Tunnel Congress*, San Francisco, 2016.
[49]. B. Walz, J. Gerlach, and M. Pulsfort. Schlitzwandbauweise, Konstruktion, Berechnung und Ausführung. Technical report, Bergische Universität Gesamthochschule Wuppertal, 1983.
[50]. W.Burger. Slurry,Hybrid and Large TBMs. Tunnelling Short Course, 2016.
[51]. P. Xanthakos. *Slurry Walls*. New York a.o.: McGraw-Hill.
[52]. Zusätzliche Technische Vertragsbedingungen und Richtlinien für Ingenieurbauten (ZTV-ING) – Teil 5 Tunnelbau, Bundesanstalt für Strassenwesen. 2012.

Annex 1: Tunnel alignment

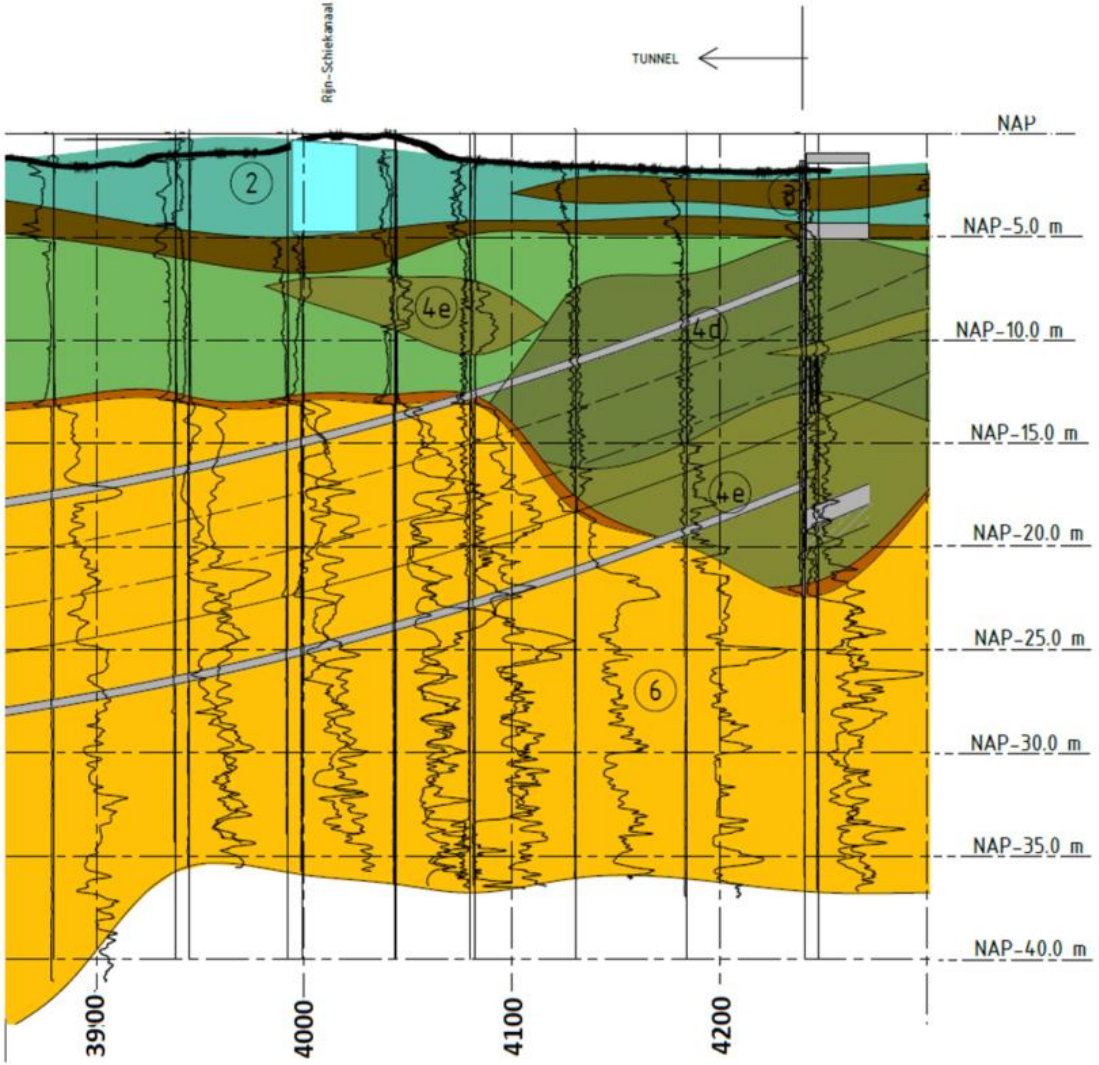

LEGENDA

- Layer 0: Anthropogenic layers
  - 0A: Clay
  - 0B: Sand
- Layer 1: Naaldwijk Formation
  - 1: Fine sand
- Layer 2: Naaldwijk Formation
  - 2A: Clay, strong humeus
  - 2B: Clay, moderate humeus
  - 2C: Clay, moderate silty
- Layer 3: Nieuwkoop Formation
  - 3: Peat
- Layer 4: Naaldwijk Formation
  - 4A: Clay, strong humeus
  - 4B: Clay, moderate humeus
  - 4C: Clay, moderate silty
  - 4D: Sand, strong clayey
  - 4E: Sand, medium fine
- Layer 5: Nieuwkoop Formation
  - 5: Peat
- Layer 6: Pleistocene
  - 6A: Sand, loose
  - 6B: Sand. medium dense
  - 6C: Sand, dense

Annex 2: Wedge -model

Equilibrium in the horizontal direction:

$\sum H = 0 \rightarrow \quad E + 2T\ \cos\theta + (K + R)\cos\theta - N\sin\theta = 0$ **[Equation A]**

Equilibrium in the vertical direction:

$\sum V = 0 \rightarrow \quad G_s + G_w - 2T\ \sin\theta - (K + R)\sin\theta - N\cos\theta\ = 0$ **[Equation B]**

Substitute equation C in equation A and B, this results in equation D:

$R = N\tan\varphi$ **[Equation C**

$G_s + G_w + 2T\frac{1}{\zeta_-} + K\frac{1}{\zeta_-} + E\frac{\zeta_+}{\zeta_-} = 0$ **[Equation D]**

$\zeta_- = \tan\varphi\cos\theta - \sin\theta$ **[Equation D-1]**

$\zeta_+ = \tan\varphi\sin\theta + \cos\theta$ **[Equation D-2]**

Solve equation D for E:

$E = -\frac{\zeta-(G_s+G_w)+(K+2T)}{\zeta+}$ **[Equation E]**

$G_s = B\ D\cot\theta\ \ \sigma'_v(zt)$ **[Equation F]**

$G_w = \frac{B\ D^2\cot\theta}{2}\gamma'$ **[Equation G]**

$K = \frac{B\ D}{\sin\theta}c$ **[Equation H]**

$T = \frac{D^2\cot\theta}{2}(c + K_y\,\overline{\sigma'_v}\tan\varphi)$ **[Equation I]**

$\overline{\sigma'_v} = \ \sigma'_v(z_t) + \frac{1}{3}D\ \gamma'$ **[Equation J]**

Annex 3: Calculation minimum support pressure

Case study (Series 1)

I.1.1 Case study A: Homogenous sand profile C/D=1,0

Calculation results minimum support pressure

Soil parameters								DIN					JS						JS*		RV			
	γ_{sat}	c	φ	σ_v	u_1	σ'_v	$\sigma'_{v;3D}$	K_a	K_{ac}	$D^{(r)}$	$\sigma'^{(r)}_{h;d}$[1]	$P_{min;d}$	β	α	K	K_{a3D}	$\sigma'_{h;d}$[1]	$P_{min;d}$	$\sigma'_{h;d}$[1]	$P_{min;d}$	N_γ	N_c	$\sigma'_{h;d}$[1]	$P_{min;d}$
[m NAP]	[kPa]	[kPa]	[°]	[kPa]	[kPa]	[kPa]	[kPa]	[-]	[-]	[m]	[kPa]	[kPa]	[-]	[-]	[-]	[-]	[kPa]	[kPa]	[kPa]	[kPa]	[-]	[-]	[kPa]	[kPa]
-12,30	20	0	30,60	210	105	105	59	0,33	1,14	8,80	43	153	66	1,33	0,41	0,22	34	144	19	129	0,23	1,13	24	129
-17,55	20	0	30,60	315	158	158	111	0,33	1,14	8,00	58	224	66	1,33	0,41	0,22	51	216	36	201	0,23	1,13	24	182
-17,55	20	0	30,60	315	158	158	111	0,33	1,14	8,00	58	224	66	1,33	0,41	0,22	51	216	36	201	0,23	1,13	24	182
-22,80	20	0	30,60	420	210	210	164	0,33	1,14	7,20	70	291	66	1,33	0,41	0,22	68	288	53	273	0,23	1,13	24	234

[1]: Design value of the horizontal effective stress
σ'_{v3D}: Vertical effective stress distribution including three dimensional soil arching within the soil overburden

Case study parameters

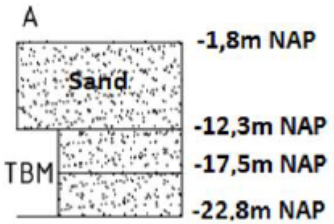

Design value minimum support pressure distribution at tunnel face

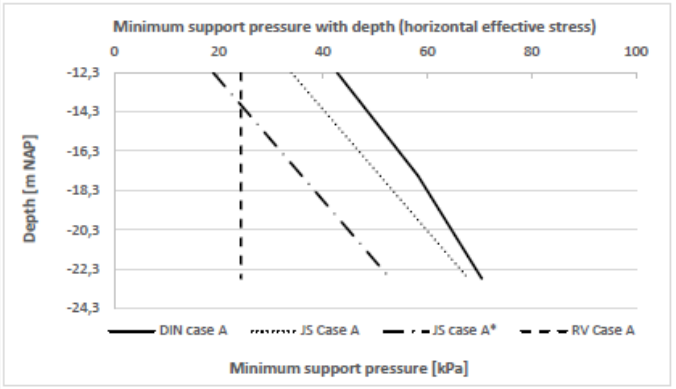

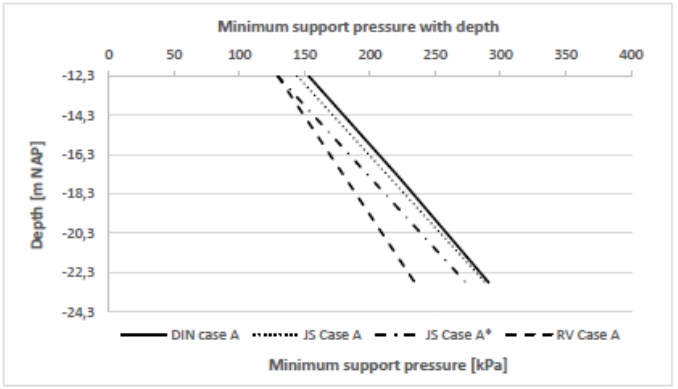

Case A assumes a homogenous soil profile consisting of sand with a soil cover ratio of C/D=1,0 in combination with a hydrostatic pore water pressure distribution (Groundwater level= -1,8m NAP):

- Due to the homogeneous soil conditions, the soil parameters are constant over the tunnel face. As a result, the vertical (effective) stress increases linearly with depth.
- The RV model results in the lowest minimum support pressure required. This method uses a constant vertical effective stress within the analysis, which is equal to the effective soil weight at tunnel invert. The constant vertical effective stress distribution is multiplied with a constant stability number N_γ which results in a horizontal effective stress acting at the tunnel face. The other two stability numbers are equal to zero as there is no additional load present on ground surface and the soil profile does not contains cohesion. The RV model includes both vertical and horizontal soil arching and due to the fact that the friction angle of the sand profile larger than 20 degrees, the soil weight of the overburden may be neglected. This means that the vertical effective stress at tunnel crown is equal to zero.
- The JS* model (with vertical soil arching) calculates the horizontal effective stress acting at tunnel face by multiplying the constant coefficient K_{A3D} with the vertical effective stress $\sigma'_{v;3D}$. This vertical effective stress distribution takes the effect of vertical soil arching within the overburden into account and therefore the stress at tunnel crown is lower than σ'_v. From the tunnel crown, the vertical (effective) stress increases linearly with depth due to the combination of a constant unit weight and hydrostatic pore water pressure distribution.
- The JS model (without vertical soil arching) calculates the horizontal effective stress acting at tunnel face by multiplying the constant coefficient K_{A3D} with the vertical effective stress σ'_v. The multiplication of both components results in a linearly increasing horizontal effective stress with depth.
- The DIN-model results in the highest minimum support pressure required. This method calculates the horizontal effective stress at tunnel face by multiplying the linearly increasing vertical effective stress with an active earth pressure coefficient. Due to zero cohesion, this horizontal effective stress is not reduced. In order to account for the spatial stress-state in the soil, shape factors are used. These factors are a function of both the friction angle of the soil and the depth z below ground surface. Due to the set-up of these shape coefficients, the minimum support pressure results in an nonlinear minimum support pressure.

1.1.2 Case study B: Homogenous clay profile C/D=1,0

Calculation results minimum support pressure

Soil parameters								DIN					JS						JS*		RV			
	γ_{sat}	c	φ	σ_v	u_1	σ'_v	$\sigma'_{v;3D}$	K_a	K_{ac}	$D^{(r)}$	$\sigma'^{(r)}_{h;d}$[1]	$P_{min;d}$	β	α	K	K_{a3D}	$\sigma'^{1}_{h;d}$	$P_{min;d}$	$\sigma'^{1}_{h;d}$	$P_{min;d}$	N_γ	N_c	$\sigma'^{1}_{h;d}$	$P_{min;d}$
[m NAP]	[kPa]	[kPa]	[°]	[kPa]	[kPa]	[kPa]	[kPa]	[-]	[-]	[m]	[kPa]	[kPa]	[-]	[-]	[-]	[-]	[kPa]	[kPa]	[kPa]	[kPa]	[-]	[-]	[kPa]	[kPa]
-12,3	16,80	4,50	23	177	105	71	31	0,44	1,32	9,2	32	142	63	1,33	0,52	0,31	33	143	14	124	0,34	1,57	20	125
-17,55	16,80	4,50	23	265	158	107	67	0,44	1,32	8,5	48	214	63	1,33	0,52	0,31	49	215	31	196	0,34	1,57	20	177
-17,55	16,80	4,50	23	265	158	107	67	0,44	1,32	8,5	48	214	63	1,33	0,52	0,31	49	215	31	196	0,34	1,57	20	177
-22,80	16,80	4,50	23	353	210	143	102	0,44	1,32	7,9	62	283	63	1,33	0,52	0,31	66	286	47	268	0,34	1,57	20	230

[1]: design value of the horizontal effective stress
$\sigma'_{v;3D}$: Vertical effective stress distribution including three dimensional soil arching within the soil overburden

Case study parameters

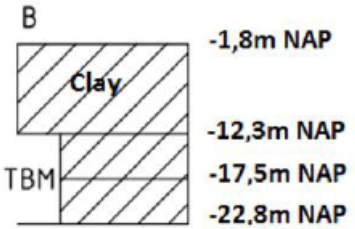

Design value minimum support pressure distribution at tunnel face

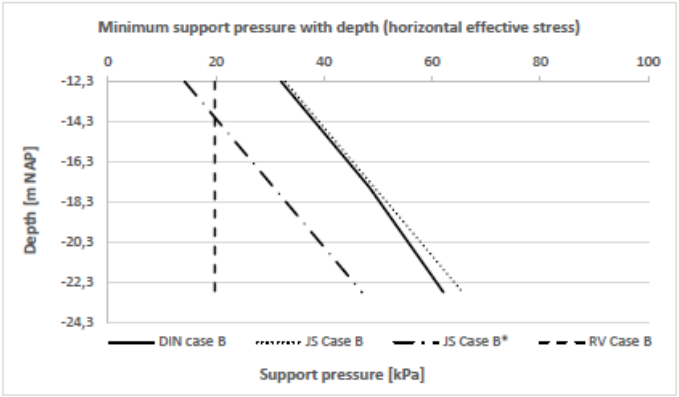

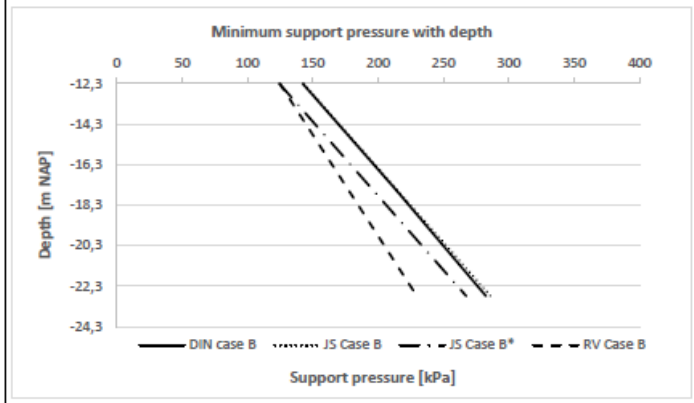

Case B assumes a homogenous soil profile consisting of clay with a soil cover ratio of C/D=1,0 in combination with a hydrostatic pore water pressure distribution (Groundwater level= -1,8m NAP):

- Due to the homogeneous soil conditions, the soil parameters are constant over the tunnel face. As a result, the vertical (effective) stress increases linearly with depth.
- The RV model results in the lowest minimum support pressure required. This method uses a constant vertical effective stress within the analysis, which is equal to the effective soil weight at tunnel invert. The constant vertical effective stress distribution is multiplied with a constant stability number N_γ which results in a horizontal effective stress acting at the tunnel face. Due to a non-zero cohesion component, this stress is reduced. The RV model includes both vertical and horizontal soil arching and due to the fact that the friction angle of the sand profile larger than 20 degrees, the soil weight of the overburden may be neglected. This means that the vertical effective stress at tunnel crown is equal to zero.
- The JS* model (with vertical soil arching) calculates the horizontal effective stress acting at tunnel face by multiplying the constant coefficient K_{A3D} with the vertical effective stress $\sigma'_{v;3D}$. This vertical effective stress distribution takes the effect of vertical soil arching within the overburden into account and therefore the stress at tunnel crown is lower than σ'_v. From the tunnel crown, the vertical (effective) stress increases linearly with depth due to the combination of a constant unit weight and hydrostatic pore water pressure distribution.
- The JS model (without vertical soil arching) calculates the horizontal effective stress acting at tunnel face by multiplying the constant coefficient K_{A3D} with the vertical effective stress σ'_v. The multiplication of both components results in a linearly increasing horizontal effective stress with depth.
- The DIN-model results in the highest minimum support pressure required. This method calculates the horizontal effective stress at tunnel face by multiplying the linearly increasing vertical effective stress with an active earth pressure coefficient. Due to a non-zero cohesion component, this stress is reduced. In order to account for the spatial stress-state in the soil, shape factors are used. These factors are a function of both the friction angle of the soil and the depth z below ground surface. Due to the set-up of these shape coefficients, the minimum support pressure results in an nonlinear minimum support pressure.

1.1.3 Case study C: Homogenous sand profile C/D=1,5

Calculation results minimum support pressure

Soil parameters								DIN					JS						JS*		RV			
	γ_{sat}	c	φ	σ_v	u_1	σ'_v	$\sigma'_{v;3D}$	K_a	K_{ac}	$D^{(r)}$	$\sigma'^{(r)}_{h;d}$[1]	$P_{min;d}$	β	α	K	K_{a3D}	$\sigma'^{1}_{h;d}$	$P_{min;d}$	$\sigma'^{1}_{h;d}$	$P_{min;d}$	N_γ	N_c	$\sigma'^{1}_{h;d}$	$P_{min;d}$
[m NAP]	[kPa]	[kPa]	[°]	[kPa]	[kPa]	[kPa]	[kPa]	[-]	[-]	[m]	[kPa]	[kPa]	[-]	[-]	[-]	[-]	[kPa]	[kPa]	[kPa]	[kPa]	[-]	[-]	[kPa]	[kPa]
-17,55	20	0	30,60	315	158	158	67	0,33	1,14	8,00	58	224	67	1,38	0,41	0,21	50	216	22	187	0,23	1,13	24	182
-22,80	20	0	30,60	420	210	210	120	0,33	1,14	7,20	70	291	67	1,38	0,41	0,21	67	287	38	259	0,23	1,13	24	234
-22,80	20	0	30,60	420	210	210	120	0,33	1,14	7,20	70	291	67	1,38	0,41	0,21	67	287	38	259	0,23	1,13	24	234
-28,05	20	0	30,60	535	263	263	172	0,33	1,14	6,60	80	356	67	1,38	0,41	0,21	84	359	55	331	0,23	1,13	24	287

[1]: design value of the horizontal effective stress
$\sigma'_{v;3D}$: Vertical effective stress distribution including three dimensional soil arching within the soil overburden

Case study parameters

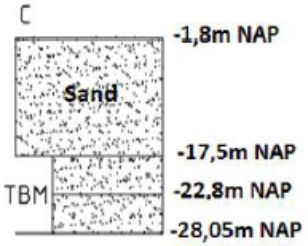

Design value minimum support pressure distribution at tunnel face

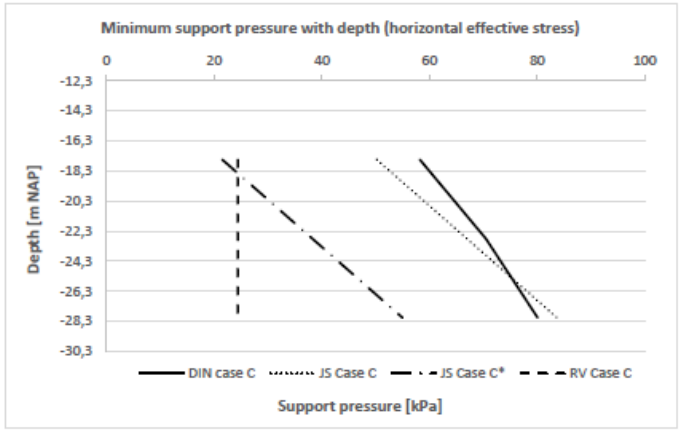

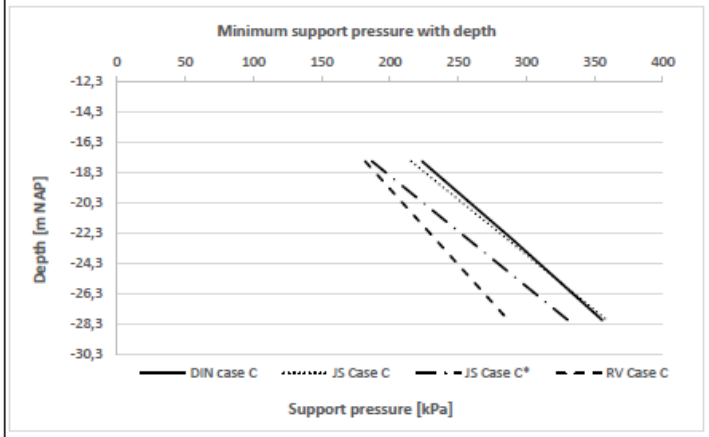

Case C assumes a homogenous soil profile consisting of sand with a soil cover ratio of C/D=1,5 in combination with a hydrostatic pore water pressure distribution (Groundwater level= -1,8m NAP):

- The soil profile of Case C is equal to the soil profile of Case A. The only difference between these two cases is that the height of the overburden in case C is 5,25 meters higher (=0,5 Diameter tunnel).
- In case of the RV model, the change in height of the soil cover does not affect the minimum support pressure distribution and therefore the same horizontal effective stress is calculated as in case A. The reason for this is that this model neglects the soil weight of the overburden by assuming that the vertical effective stress at tunnel crown is equal to zero.
- In case of both JS models, the change in height of the soil cover only affects the vertical effective stress distribution used within the calculation. Due to this increase, the vertical effective stress increases and therefore a higher minimum support pressure is required. As the soil profile in front of the tunnel face remains equal, the model coefficients are not affected.
- In case of the DIN-model, the change in height of the soil cover affects the vertical effective stress distribution and the value of the shape factors. Due to this height increase, the vertical effective stress increases and the shape coefficients reduces. Due to these reduced shape coefficients, the reduction of the horizontal effective stress acting at tunnel face is higher. This means that the increase in minimum support pressure is partly counteracted by the shape coefficients. In test-series 4, the applicability of this wall-length reduction component is discussed.

1.1.4 Case study D: Homogenous clay profile C/D=1.5

Calculation results minimum support pressure

Soil parameters								DIN					JS							JS*		RV			
	γ_{sat}	c	φ	σ_v	u_1	σ'_v	σ'_v	K_a	K_{ac}	$D^{(r)}$	$\sigma'^{(r)}_{h;d}{}^{1}$	$P_{min;d}$	β	α	K	K_{a3D}	$\sigma'^{1}_{h;d}$	$P_{min;d}$	$\sigma'^{1}_{h;d}$	$P_{min;d}$	N_γ	N_c	$\sigma'^{1}_{h;d}$	$P_{min;d}$
[m NAP]	[kPa]	[kPa]	[°]	[kPa]	[kPa]	[kPa]	[kPa]	[-]	[-]	[m]	[kPa]	[kPa]	[-]	[-]	[-]	[-]	[kPa]	[kPa]	[kPa]	[kPa]	[-]	[-]	[kPa]	[kPa]
-17,55	16,80	4,50	23	265	158	107	38	0,44	1,32	8,50	48	214	63	1,38	0,52	0,30	49	214	17	183	0,34	1,57	20	177
-22,8	16,80	4,50	23	353	210	143	74	0,44	1,32	7,90	62	283	63	1,38	0,52	0,30	65	285	34	254	0,34	1,57	20	230
-22,8	16,80	4,50	23	353	210	143	74	0,44	1,32	7,90	62	283	63	1,38	0,52	0,30	65	285	34	254	0,34	1,57	20	230
-28,05	16,80	4,50	23	441	263	179	109	0,44	1,32	7,40	74	349	63	1,38	0,52	0,30	81	337	50	325	0,34	1,57	20	282

[1]: design value of the horizontal effective stress
$\sigma'_{v;3D}$: Vertical effective stress distribution including three dimensional soil arching within the soil overburden

Case study parameters

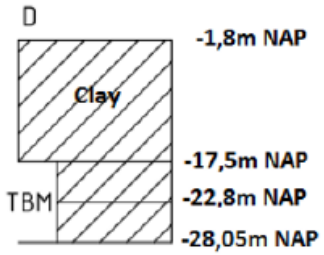

Design value minimum support pressure distribution at tunnel face

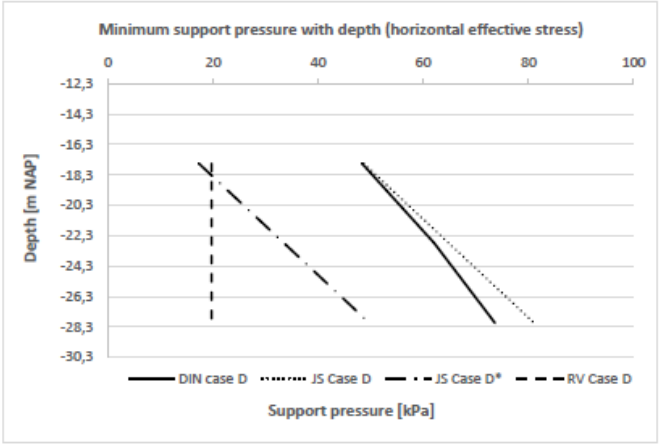

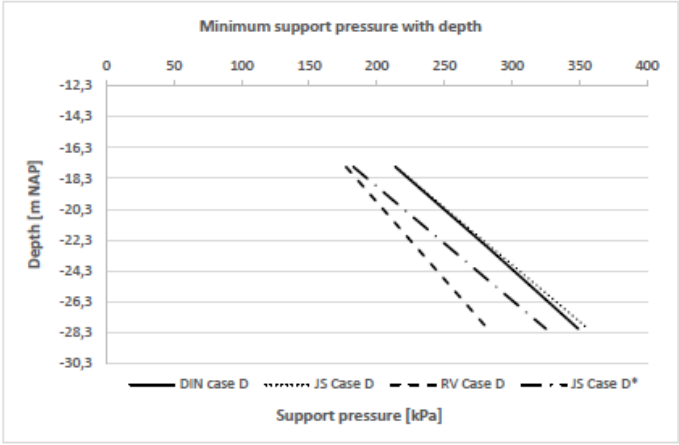

Case D assumes a homogenous soil profile consisting of clay with a soil cover ratio of C/D=1,5 in combination with a hydrostatic pore water pressure distribution (Groundwater level= -1,8m NAP):

- The soil profile of Case D is equal to the soil profile of Case B. The only difference between these two cases is that the height of the overburden in case C is 5,25 meters higher (=0,5 Diameter tunnel).
- In case of the RV model, the change in height of the soil cover does not affect the minimum support pressure distribution and therefore the same horizontal effective stress is calculated as in case B. The reason for this is that this model neglects the soil weight of the overburden by assuming that the vertical effective stress at tunnel crown is equal to zero.
- In case of both JS models, the change in height of the soil cover only affects the vertical effective stress distribution used within the calculation. Due to this increase, the vertical effective stress increases and therefore a higher minimum support pressure is required. As the soil profile in front of the tunnel face remains equal, the model coefficients are not affected.
- In case of the DIN-model, the change in height of the soil cover affects the vertical effective stress distribution and the value of the shape factors. Due to this height increase, the vertical effective stress increases and the shape coefficients reduces. Due to these reduced shape coefficients, the reduction of the horizontal effective stress acting at tunnel face is higher. This means that the increase in minimum support pressure is partly counteracted by the shape coefficients. In test-series 4, the applicability of this wall-length reduction component is discussed.

- Case E: heterogenous soil profile C/D=1

Calculation results minimum support pressure

Soil parameters								DIN					JS						JS*		RV			
	γ_{sat}	c	φ	σ_v	u_1	σ'_v	$\sigma'_{v;3D}$	K_a	K_{ac}	$D^{(r)}$	$\sigma'^{(r)}_{h;d}$[1]	$P_{min;d}$	β	α	K	K_{a3D}	$\sigma'^{1}_{h;d}$	$P_{min;d}$	$\sigma'^{1}_{h;d}$	$P_{min;d}$	N_γ	N_c	$\sigma'^{1}_{h;d}$	$P_{min;d}$
[m NAP]	[kPa]	[kPa]	[°]	[kPa]	[kPa]	[kPa]	[kPa]	[-]	[-]	[m]	[kPa]	[kPa]	[-]	[-]	[-]	[-]	[kPa]	[kPa]	[kPa]	[kPa]	[-]	[-]	[kPa]	[kPa]
-12,30	16,80	4,50	23	210	105	105	59	0,44	1,32	9,20	51	162	63	1,33	0,52	0,31	48	159	27	137	0,34	1,57	8	113
-17,55	16,80	4,50	23	298	158	141	94	0,44	1,32	8,50	66	232	63	1,33	0,52	0,31	65	230	43	209	0,34	1,57	8	165
-17,55	20	0	30,60	298	158	141	94	0,33	1,14	8,00	52	217	66	1,33	0,41	0,22	46	211	31	196	0,23	1,13	20	178
-22,80	20	0	30,60	403	210	193	147	0,33	1,14	7,20	65	285	66	1,33	0,41	0,22	62	283	47	268	0,23	1,13	20	230

[1]: design value of the horizontal effective stress
$\sigma'_{v;3D}$: Vertical effective stress distribution including three dimensional soil arching within the soil overburden

Case study parameters

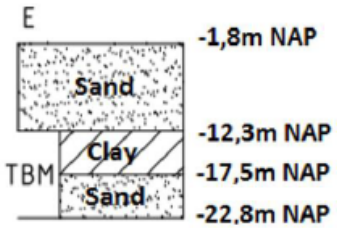

Design value minimum support pressure distribution at tunnel face

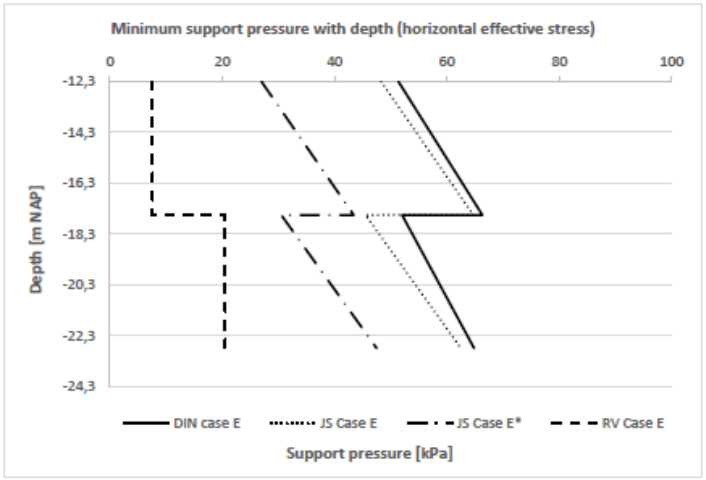

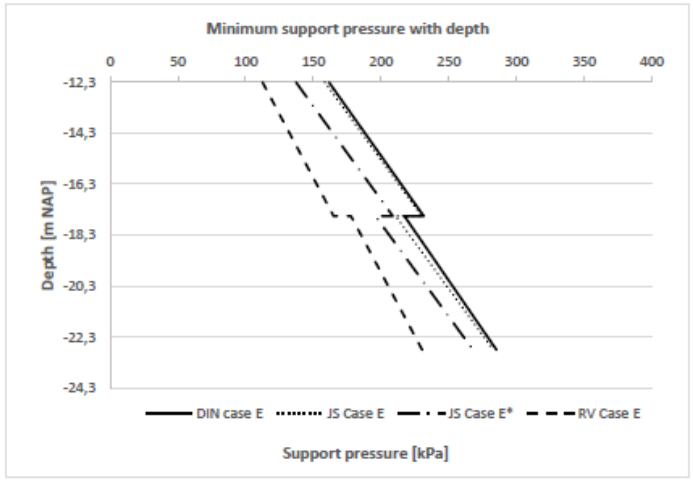

Case E assumes a heterogeneous soil profile. The soil profile in front of the TBM consists of an upper layer of clay and a bottom layer of sand. The soil cover consists of a sand layer (C/D=1,0):

- The soil profile of the soil overburden of Case E is equal to the soil profile of the overburden in case A. This means that the vertical effective stress acting at tunnel crown is equal. In addition, this also applies to the vertical effective stress distribution including arching. Due to this heterogenous soil profile, the horizontal effective stress required can lead to sharp transitions at the layer boundaries.
- The RV model results in the lowest minimum support pressure required. This method assumes a vertical (effective) stress equal to the bottom of each soil layer to be valid for each separate soil layer. The shape of the minimum support pressure profile is due to a combination of the vertical effective stress distribution, stability number N_γ and the cohesion reduction component. The vertical effective stress is higher for the sand-layer than for the clay-layer. The stability number N_γ is higher for the clay-layer than for the sand layer. The minimum support pressure for the upper soil layer is reduced due to a non-zero cohesion component.
- In the JS-models, the effect of a heterogenous soil profile in front of the tunnel face affects both the vertical effective stress distribution and the model coefficient K_{A3D}. For the clay layer a lower vertical effective stress in combination with a higher K_{A3D} value applies and for the sand layer, a higher vertical effective stress in combination with a lower K_{A3D} value applies. Despite the lower vertical stress, the upper clay part results in a higher support pressure.
- The DIN model results in the highest support force required. The shape of the minimum support pressure profile is due to a combination of the vertical effective stress distribution, active earth pressure coefficient, the cohesion reduction component, and the shape coefficients. The vertical effective stress is higher for the sand-layer than for the clay-layer. The earth pressure coefficient K_a is higher for the clay-layer than for the sand layer. The minimum support pressure for the upper soil layer is reduced due to a non-zero cohesion component.

1.1.5 Case F: heterogenous soil profile C/D=1

Calculation results minimum support pressure

Soil parameters								DIN					JS						JS*		RV			
	γ_{sat}	c	φ	σ_v	u_1	σ'_v	$\sigma'_{v;3D}$	K_a	K_{ac}	$D^{(r)}$	$\sigma'^{(r)}_{h;d}{}^{1}$	$P_{min;d}$	β	α	K	K_{a3D}	$\sigma'^{1}_{h;d}$	$P_{min;d}$	$\sigma'^{1}_{h;d}$	$P_{min;d}$	N_γ	N_c	$\sigma'^{1}_{h;d}$	$P_{min;d}$
[m NAP]	[kPa]	[kPa]	[°]	[kPa]	[kPa]	[kPa]	[kPa]	[-]	[-]	[m]	[kPa]	[kPa]	[-]	[-]	[-]	[-]	[kPa]	[kPa]	[kPa]	[kPa]	[-]	[-]	[kPa]	[kPa]
-12,30	16,80	4,50	23	177	105	71	31	0,44	1,32	9,20	32	142	63	1,33	0,52	0,31	33	143	14	124	0,34	1,57	8	114
-17,55	16,80	4,50	23	265	158	107	67	0,44	1,32	8,50	48	214	63	1,33	0,52	0,31	49	215	31	196	0,34	1,57	8	165
-17,55	20	0	30,60	265	158	107	67	0,33	1,14	8,00	40	205	66	1,33	0,41	0,22	35	200	22	187	0,23	1,13	20	178
-22,80	20	0	30,60	370	210	160	119	0,33	1,14	7,20	54	274	66	1,33	0,41	0,22	52	272	39	259	0,23	1,13	20	230

[1]: design value of the horizontal effective stress
$\sigma'_{v;3D}$: Vertical effective stress distribution including three dimensional soil arching within the soil overburden

Case study parameters

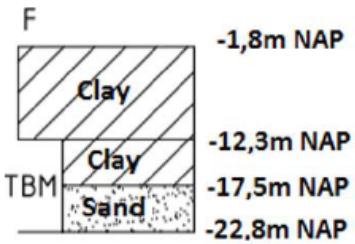

Design value minimum support pressure distribution at tunnel face

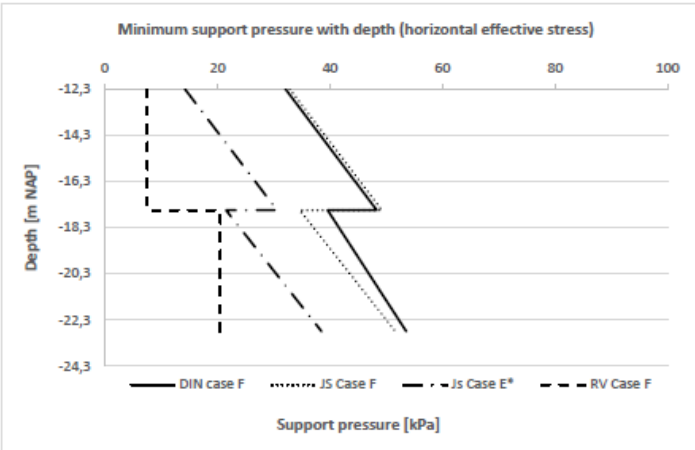

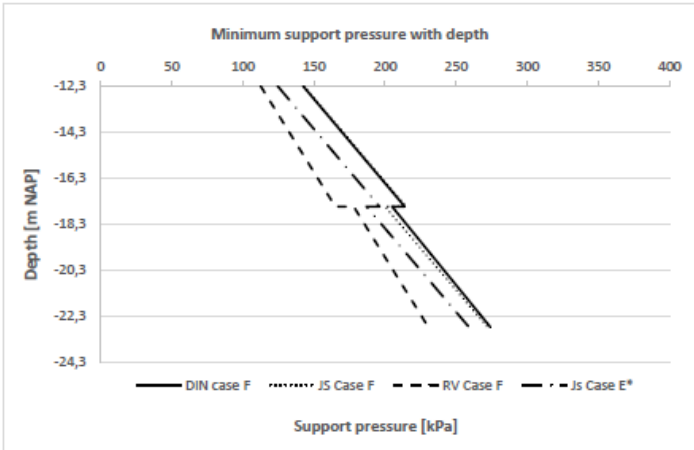

Case F assumes a heterogeneous soil profile. The soil profile in front of the TBM consists of an upper layer of clay and a bottom layer of sand. The soil cover consists of a clay layer (C/D=1,0):

- The soil profile of the soil overburden of Case F is equal to the soil profile of the overburden in case B. This means that the vertical effective stress acting at tunnel crown is equal. In addition, this also applies to the vertical effective stress distribution including arching. Due to this heterogenous soil profile, the horizontal effective stress required can lead to sharp transitions at the layer boundaries. The soil profile in front of the tunnel face is equal to the soil profile in case E. This means that the difference between case E and F is a change in the vertical effective stress distribution. As the clay-layer has a lower value of the unit weight compared to the sand-layer, the minimum support pressure required is lower in case F than case E.
- The conclusions described in Case E are also valid for case F.

1.1.6 Case G: heterogenous soil profile C/D=1

Calculation results minimum support pressure

Soil parameters								DIN					JS						JS*		RV			
	γ_{sat}	c	φ	σ_v	u_1	σ'_v	$\sigma'_{v;3D}$	K_a	K_{ac}	$D^{(r)}$	$\sigma'^{(r)}_{h;d}{}^{1}$	$P_{min;d}$	β	α	K	K_{a3D}	$\sigma'^{1}_{h;d}$	$P_{min;d}$	$\sigma'^{1}_{h;d}$	$P_{min;d}$	N_γ	N_c	$\sigma'^{1}_{h;d}$	$P_{min;d}$
[m]	[kPa]	[kPa]	[°]	[kPa]	[kPa]	[kPa]	[kPa]	[-]	[-]	[m]	[kPa]	[kPa]	[-]	[-]	[-]	[-]	[kPa]	[kPa]	[kPa]	[kPa]	[-]	[-]	[kPa]	[kPa]
-12,30	20	0	23	210	105	105	59	0,33	1,14	8,80	43	153	66	1,33	0,41	0,22	34	144	19	129	0,23	1,13	12	117
-17,55	20	0	23	315	158	158	111	0,33	1,14	8,00	58	224	66	1,33	0,41	0,22	51	216	36	201	0,23	1,13	12	170
-17,55	16,80	4,50	30,60	315	158	158	111	0,44	1,32	8,50	75	241	63	1,33	0,52	0,31	72	238	51	216	0,34	1,57	26	183
-22,80	16,80	4,50	30,60	403	210	193	147	0,44	1,32	7,90	87	308	63	1,33	0,52	0,31	89	309	68	288	0,34	1,57	26	236

[1]: design value of the horizontal effective stress
$\sigma'_{v;3D}$: Vertical effective stress distribution including three dimensional soil arching within the soil overburden

Case study parameters

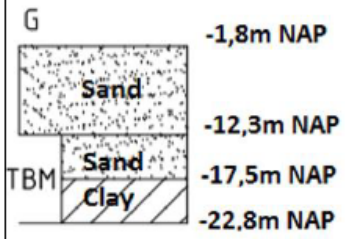

Design value minimum support pressure distribution at tunnel face

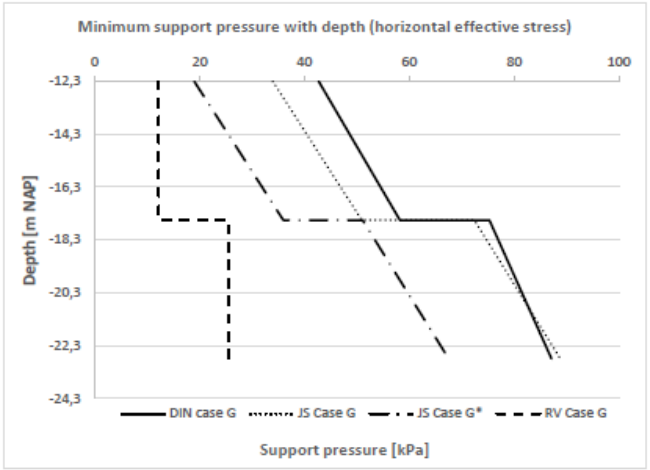

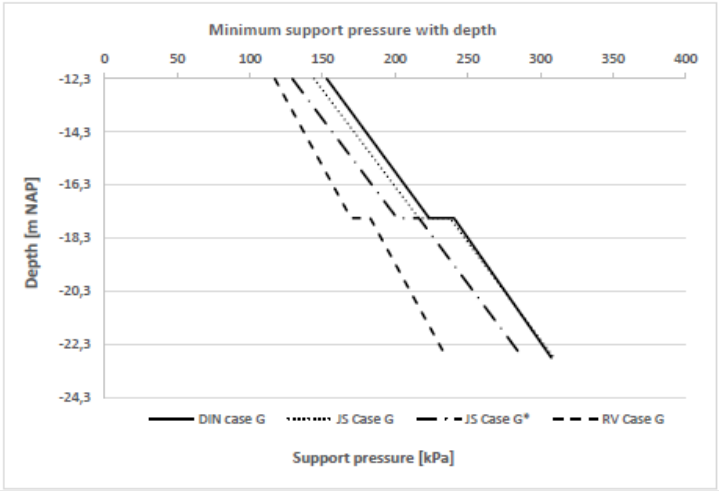

Case G assumes a heterogeneous soil profile. The soil profile in front of the TBM consists of an upper layer of sand and a bottom layer of clay. The soil cover consists of a sand layer (C/D=1,0):

- The soil profile of the soil overburden of Case G is equal to the soil profile of the overburden in case A and case E. This means that the vertical effective stress acting at tunnel crown is equal. In addition, this also applies to the vertical effective stress distribution including arching. Due to this heterogenous soil profile, the horizontal effective stress required can lead to sharp transitions at the layer boundaries.
- The RV model results in the lowest minimum support pressure required. This method assumes a vertical (effective) stress equal to the bottom of each soil layer to be valid for each separate soil layer. The shape of the minimum support pressure profile is due to a combination of the vertical effective stress distribution, stability number N_γ and the cohesion reduction component. The stability number N_γ is higher for the clay layer than for the sand layer. The minimum support pressure for the bottom soil layer is reduced due to a non-zero cohesion component. The vertical effective stress is higher for the clay layer than for the sand layer. Due to this higher vertical effective stress and higher stability number than the upper sand-layer, the minimum support pressure required for the clay layer is higher than for the sand layer.
- In the JS-models, the effect of a heterogenous soil profile in front of the tunnel face affects both the vertical effective stress distribution and the model coefficient K_{A3D}. For the sand layer a lower vertical effective stress in combination with a lower K_{A3D} value applies and for the clay layer, a higher vertical effective stress in combination with a higher K_{A3D} value applies. Likewise, the RV model the minimum support pressure required for the clay layer is higher than for the sand layer.
- The DIN model results in the highest support force required. The shape of the minimum support pressure profile is due to a combination of the vertical effective stress distribution, active earth pressure coefficient, the cohesion reduction component, and the shape coefficients. The vertical effective stress is higher for the clay layer than for the sand layer. The earth pressure coefficient K_a is higher for the clay-layer than for the sand layer. The minimum support pressure for the upper soil layer is reduced due to a non-zero cohesion component. Likewise, the RV model the minimum support pressure required for the clay layer is higher than for the sand layer.

1.1.7 Case H: heterogenous soil profile C/D=1

Calculation results minimum support pressure

Soil parameters								DIN					JS						JS*		RV			
	γ_{sat}	c	φ	σ_v	u_1	σ'_v	$\sigma'_{v;3D}$	K_a	K_{ac}	$D^{(r)}$	$\sigma'^{(r)}_{h;d}$[1]	$P_{min;d}$	β	α	K	K_{a3D}	$\sigma'_{h;d}$[1]	$P_{min;d}$	$\sigma'_{h;d}$[1]	$P_{min;d}$	N_γ	N_c	$\sigma'_{h;d}$[1]	$P_{min;d}$
[m]	[kPa]	[kPa]	[°]	[kPa]	[kPa]	[kPa]	[kPa]	[-]	[-]	[m]	[kPa]	[kPa]	[-]	[-]	[-]	[-]	[kPa]	[kPa]	[kPa]	[kPa]	[-]	[-]	[kPa]	[kPa]
-12,30	20	0	30,60	176	105	71	31	0,33	1,14	8,8	29	139	66	1,33	0,41	0,22	23	133	10	120	0,23	1,13	12	117
-17,55	20	0	30,60	265	158	107	83	0,33	1,14	8,0	46	211	66	1,33	0,41	0,22	40	205	27	192	0,23	1,13	12	170
-17,55	16,80	4,50	23	265	158	107	83	0,44	1,32	8,5	57	223	63	1,33	0,52	0,31	57	222	38	204	0,34	1,57	26	183
-22,80	16,80	4,50	23	370	210	160	119	0,44	1,32	7,9	70	291	63	1,33	0,52	0,31	73	294	55	275	0,34	1,57	26	236

[1]: design value of the horizontal effective stress
σ'_{v3D}: Vertical effective stress distribution including three dimensional soil arching within the soil overburden

Case study parameters

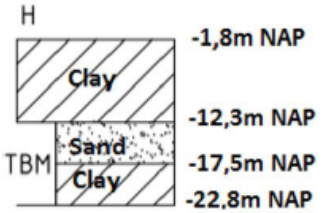

Design value minimum support pressure distribution at tunnel face

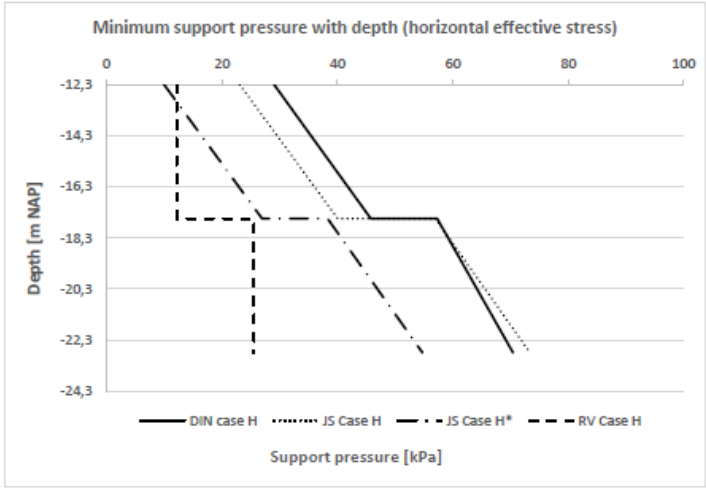

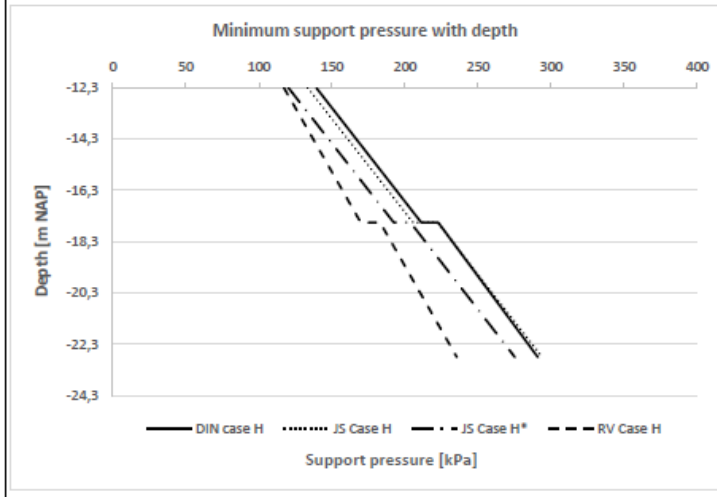

Case H assumes a heterogeneous soil profile. The soil profile in front of the TBM consists of an upper layer of sand and a bottom layer of clay. The soil cover consists of a clay layer (C/D=1,0):

- The soil profile of the soil overburden of Case H is equal to the soil profile of the overburden in case B and case F. This means that the vertical effective stress acting at tunnel crown is equal. In addition, this also applies to the vertical effective stress distribution including arching. Due to this heterogenous soil profile, the horizontal effective stress required can lead to sharp transitions at the layer boundaries. The soil profile in front of the tunnel face is equal to the soil profile in case G. This means that the difference between case G and H is a change in the vertical effective stress distribution. As the clay-layer has a lower value of the unit weight compared to the sand-layer, the minimum support pressure required is lower in case H than case G.
- The conclusions described in Case G are also valid for case H.

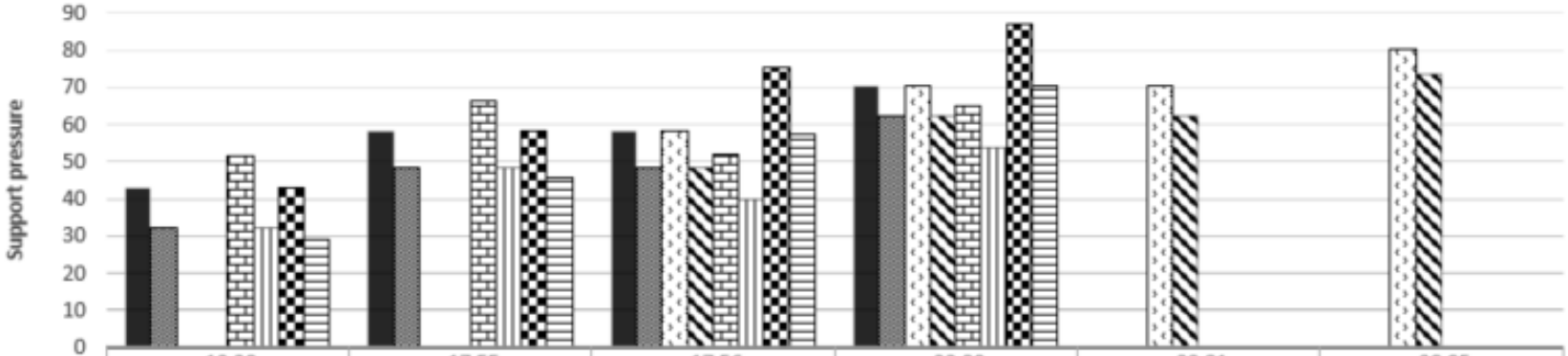

	-12,30	-17,55	-17,56	-22,80	-22,81	-28,05
Case A	43	58	58	70		
Case B	32	48	48	62		
Case C			58	70	70	80
Case D			48	62	62	74
Case E	51	66	52	65		
Case F	32	48	40	54		
Case G	43	58	75	87		
Case H	29	46	57	70		

DIN-model (Serie 1- All cases):

- Comparing **Case A** (homogeneous sand) with **Case B** (homogeneous clay) show that a higher support pressure is required for the sand layer. The friction angle is higher for the sand layer than for the clay layer and therefore the earth pressure coefficient is lower for the sand-layer. Despite this lower friction angle, the unit weight of the sand-layer results in a much higher vertical (effective) stress than the clay-layer. These two factors combined lead to a higher support pressure for the sand-layer.
- Comparing **Case A** (homogeneous sand C/D=1,0) with **Case C** (homogeneous sand C/D=1,5) show that these two cases result in the same support force at a depth of -17,6m NAP and -22,8 m NAP. This means that the support pressure increases linearly with depth, due to the homogeneous soil profile. In addition, the wall length reduction is also the same for these two cases at these two locations due to the same depth and friction angle. This also applies for the comparison of **Case B** (homogeneous clay C/D=1,0) with **Case D** (homogeneous clay C/D=1,5).
- Comparing **Case E** (sand above; upper part clay and lower part sand) with **Case F** (clay above; upper part clay and lower part sand) show that the change in soil profile above the TBM results in a strong reduction of the support force. The reason for this is that the vertical effective stress distribution in front of the tunnel face is lower due to the lower unit weight of clay than sand. The soil profile in front of the TBM is the same and therefore also the earth pressure coefficient are constant. This also applies for the comparison of **Case G** (sand above; upper part sand and lower part clay) with **Case H** (clay above; upper part sand and lower part clay).
- Comparing **Case E** (sand above; upper part clay and lower part sand) with Comparing **Case G** (sand above; upper part sand and lower part clay) show the effect of the variation of the soil profile in front of the TBM. For both cases a high vertical (effective) stress distribution is present due to the sand cover. The friction angle is lower for the clay layer than for the sand layer and therefore the earth pressure coefficient is higher for the clay-layer. As this layer situated on top, this high coefficient is multiplied with the weight of the soil cover and clay layer. When this layer is located at the bottom, this high coefficient is multiplied with of the soil cover of sand, upper layer of sand and clay layer. Therefore, the presence of a soft soil layer has the greatest effect on the support pressure when this layer is located at the tunnel invert. This also applies for the comparison of **Case F** (clay above; upper part clay and lower part sand) with **Case H** (clay above; upper part sand and lower part clay). Jancsecz-Steiner All cases

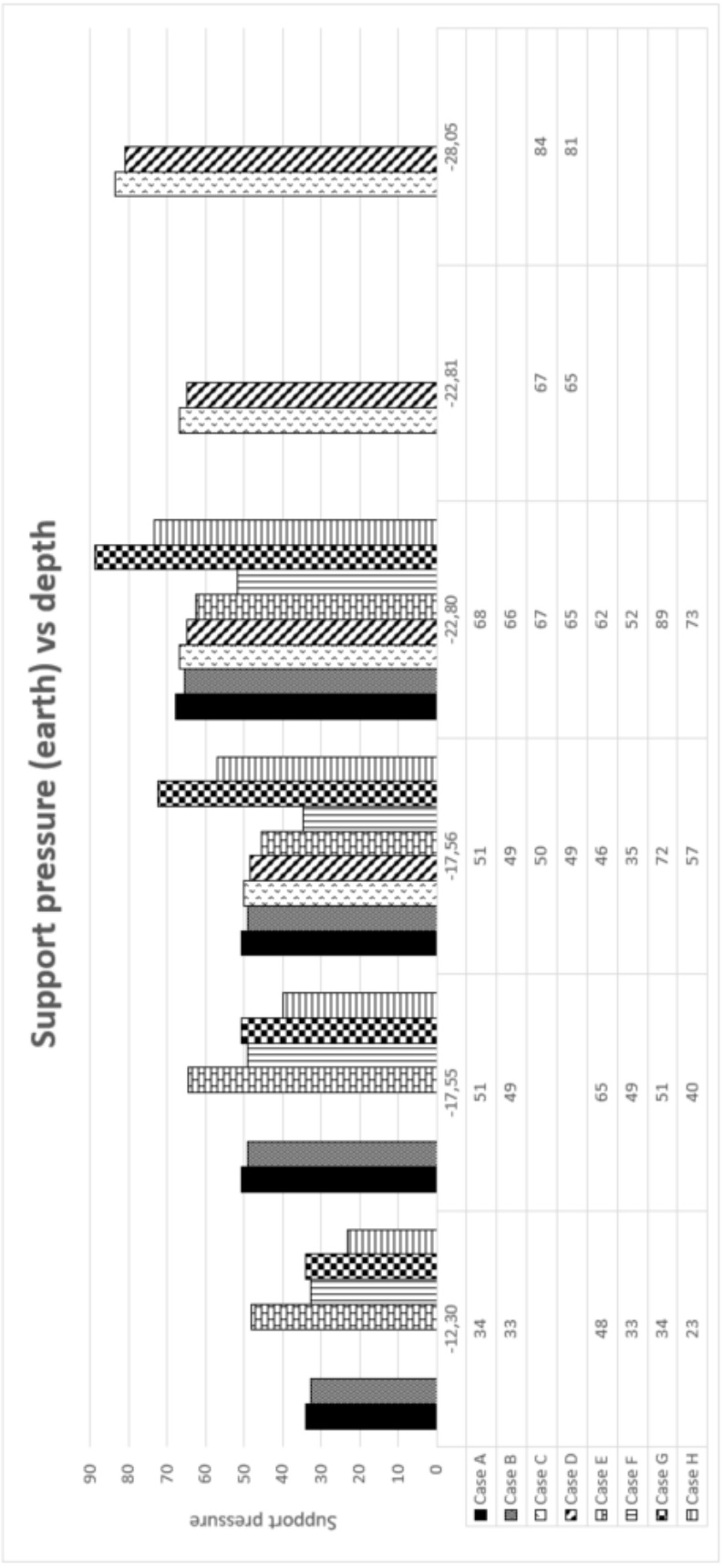
Support pressure (earth) vs depth
Support pressure
0
10
20
30
40
50
60
70
80
90
-12,30
-17,55
-17,56
-22,80
-22,81
-28,05
Case A 34 51 49 50 49 46 35 72 57
Case B 33 49 66 67 65 62 52 89 73
Case C 67 65
Case D 84 81
Case E 48 65
Case F 33 49
Case G 34 51
Case H 23 40

Jancsecz-Steiner model (Serie 1- All cases):

- Comparing **Case A** (homogeneous sand) with **Case B** (homogeneous clay) show that a higher support pressure is required for the sand layer. The friction angle is higher for the sand layer than for the clay layer and therefore the earth pressure coefficient is lower for the sand-layer. Despite this lower friction angle, the unit weight of the sand-layer results in a much higher vertical (effective) stress than the clay-layer. These two factors combined lead to a higher support pressure for the sand-layer.
- Comparing **Case A** (homogeneous sand C/D=1,0) with **Case C** (homogeneous sand C/D=1,5) show that these two cases result in the same support force at a depth of -17,6m NAP and -22,8 m NAP. This means that the support pressure increases linearly with depth, due to the homogeneous soil profile. This also applies for the comparison of **Case B** (homogeneous clay C/D=1,0) with **Case D** (homogeneous clay C/D=1,5).
- Comparing **Case E** (sand above; upper part clay and lower part sand) with **Case F** (clay above; upper part clay and lower part sand) show that the change in soil profile above the TBM results in a strong reduction of the support force. The reason for this is that the vertical effective stress distribution in front of the tunnel face is lower due to the lower unit weight of clay than sand. The soil profile in front of the TBM is the same and therefore also the earth pressure coefficient are constant. This also applies for the comparison of **Case G** (sand above; upper part sand and lower part clay) with **Case H** (clay above; upper part sand and lower part clay).
- Comparing **Case E** (sand above; upper part clay and lower part sand) with Comparing **Case G** (sand above; upper part sand and lower part clay) show the effect of the variation of the soil profile in front of the TBM. For both cases a high vertical (effective) stress distribution is present due to the sand cover. The friction angle is lower for the clay layer than for the sand layer and therefore the earth pressure coefficient is higher for the clay-layer. As this layer situated on top, this high coefficient is multiplied with the weight of the soil cover and clay layer. When this layer is located at the bottom, this high coefficient is multiplied with of the soil cover of sand, upper layer of sand and clay layer. Therefore, the presence of a soft soil layer has the greatest effect on the support pressure when this layer is located at the tunnel invert. This also applies for the comparison of **Case F** (clay above; upper part clay and lower part sand) with **Case H** (clay above; upper part sand and lower part clay).
- Comparing **Case A&B** (JS model) with **Case A&B** (DIN model) show that the difference between a homogeneous cohesionless layer and a homogeneous cohesive is higher in the DIN-model. The reason for this is that in case of the DIN-model the earth pressure component is reduced with a cohesion component.

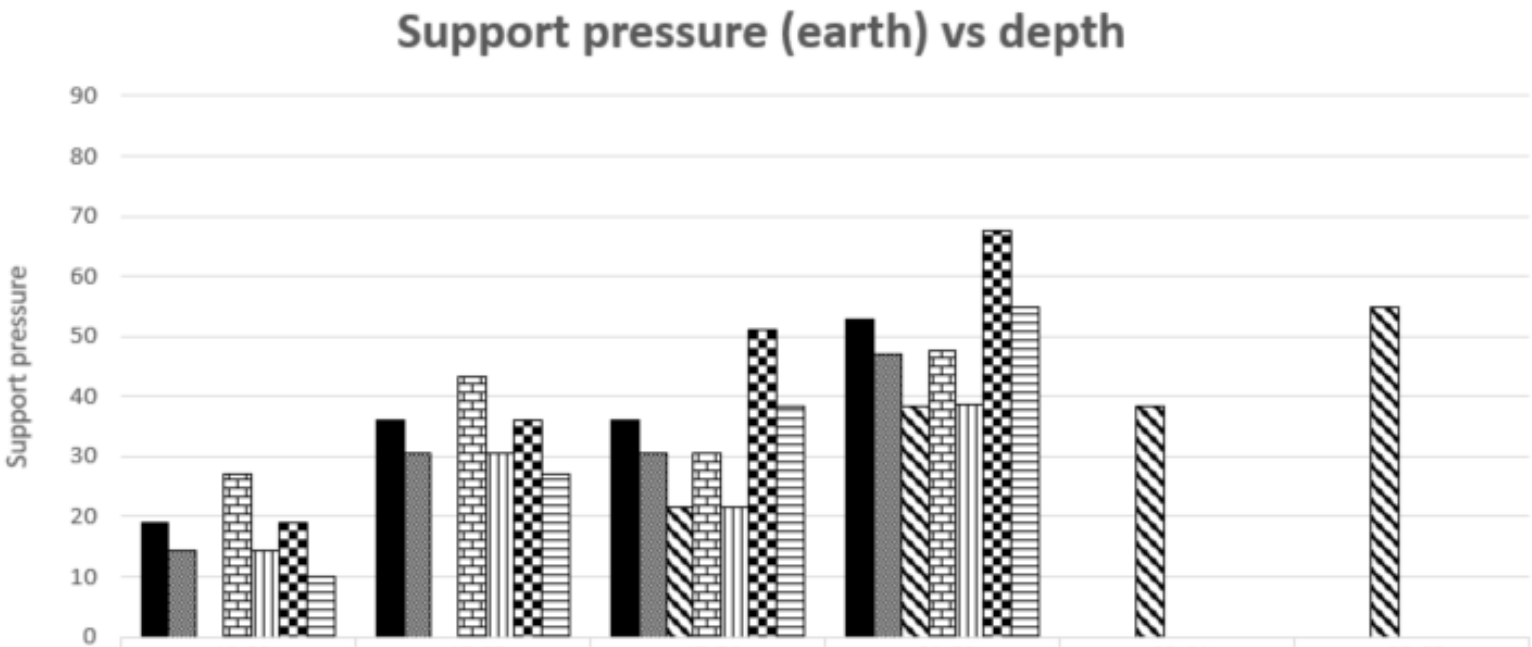

	-12,30	-17,55	-17,56	-22,80	-22,81	-28,05
Case A	19	36	36	53		
Case B	14	31	31	47		
Case C			22	38	38	55
Case E	27	43	31	47		
Case F	14	31	22	39		
Case G	19	36	51	68		
Case H	10	27	38	55		

Jancsecz-Steiner model* (Serie 1- All cases):

- Comparing **Case A** (homogeneous sand) with **Case B** (homogeneous clay) show that a higher support pressure is required for the sand layer. The friction angle is higher for the sand layer than for the clay layer and therefore the earth pressure coefficient is lower for the sand-layer. Despite this lower friction angle, the unit weight of the sand-layer results in a much higher vertical (effective) stress than the clay-layer. These two factors combined lead to a higher support pressure for the sand-layer.
- Comparing **Case A** (homogeneous sand C/D=1,0) with **Case C** (homogeneous sand C/D=1,5) show that these two cases result in the same support force at a depth of -17,6m NAP and -22,8 m NAP. This means that the support pressure increases linearly with depth, due to the homogeneous soil profile. This also applies for the comparison of **Case B** (homogeneous clay C/D=1,0) with **Case D** (homogeneous clay C/D=1,5).
- Comparing **Case E** (sand above; upper part clay and lower part sand) with **Case F** (clay above; upper part clay and lower part sand) show that the change in soil profile above the TBM results in a strong reduction of the support force. The reason for this is that the vertical effective stress distribution in front of the tunnel face is lower due to the lower unit weight of clay than sand. The soil profile in front of the TBM is the same and therefore also the earth pressure coefficient are constant. This also applies for the comparison of **Case G** (sand above; upper part sand and lower part clay) with **Case H** (clay above; upper part sand and lower part clay).
- Comparing **Case E** (sand above; upper part clay and lower part sand) with Comparing **Case G** (sand above; upper part sand and lower part clay) show the effect of the variation of the soil profile in front of the TBM. For both cases a high vertical (effective) stress distribution is present due to the sand cover. The friction angle is lower for the clay layer than for the sand layer and therefore the earth pressure coefficient is higher for the clay-layer. As this layer situated on top, this high coefficient is multiplied with the weight of the soil cover and clay layer. When this layer is located at the bottom, this high coefficient is multiplied with of the soil cover of sand, upper layer of sand and clay layer. Therefore, the presence of a soft soil layer has the greatest effect on the support pressure when this layer is located at the tunnel invert. This also applies for the comparison of **Case F** (clay above; upper part clay and lower part sand) with **Case H** (clay above; upper part sand and lower part clay).
- Comparing **Case A-H** (JS model without arching) with **Case A-H** (JS model with arching) show that the minimum support pressures are lower due to the effect of vertical soil arching.

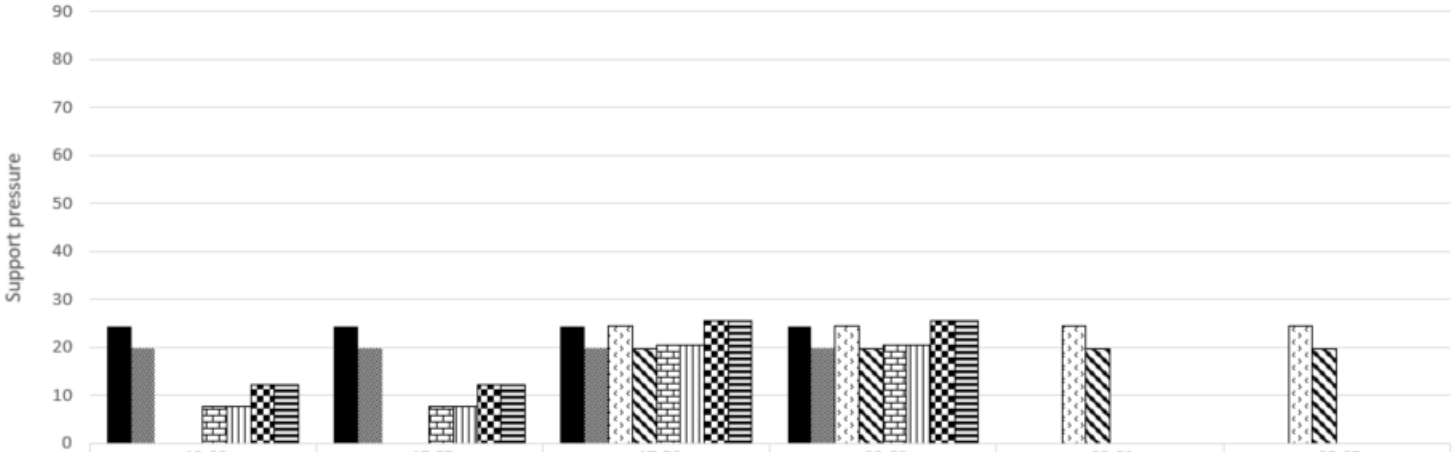

	-12,30	-17,55	-17,56	-22,80	-22,81	-28,05
Case A	24	24	24	24	0	
Case B	20	20	20	20	0	
Case C			24	24	24	24
Case D			20	20	20	20
Case E	8	8	20	20		
Case F	8	8	20	20		
Case G	12	12	26	26		
Case H	12	12	26	26		

Ruse-Vermeer model (Serie 1- All cases):

- Comparing **Case A** (homogeneous sand C/D=1,0) with **Case C** (homogeneous sand C/D=1,5) at a depth of -17,6m NAP and -22,8 m NAP show that the value for the support pressure is constant over the complete tunnel face. The reason for this is that the soil cover is neglected due to a friction angle greater than 20°. This also applies for the comparison of **Case B** (homogeneous clay C/D=1,0) with **Case D** (homogeneous clay C/D=1,5).
- Comparing **Case E** (sand above; upper part clay and lower part sand) with **Case F** (clay above; upper part clay and lower part sand) show that the due to the neglection of the overburden, the same support force applies while the soil profile above the TBM varies. This also applies for the comparison of **Case G** (sand above; upper part clay and lower part sand) with **Case H** (clay above; upper part clay and lower part sand).
- Comparing **Case E** (sand above; upper part clay and lower part sand) with Comparing **Case G** (sand above; upper part sand and lower part clay) show that a soil type with a low friction angle at the bottom results in a higher support force at this part as the vertical stress is multiplied with an higher earth pressure coefficient. This also applies for the comparison of **Case F** (clay above; upper part clay and lower part sand) with **Case H** (clay above; upper part sand and lower part clay).

Case-study (Series 2)

- **Case E:** Minimum support pressure (horizontal effective stress) with depth. Soil profile in front of the TBM consists of an upper layer of clay and a bottom layer of sand. The soil cover consists of a sand layer.

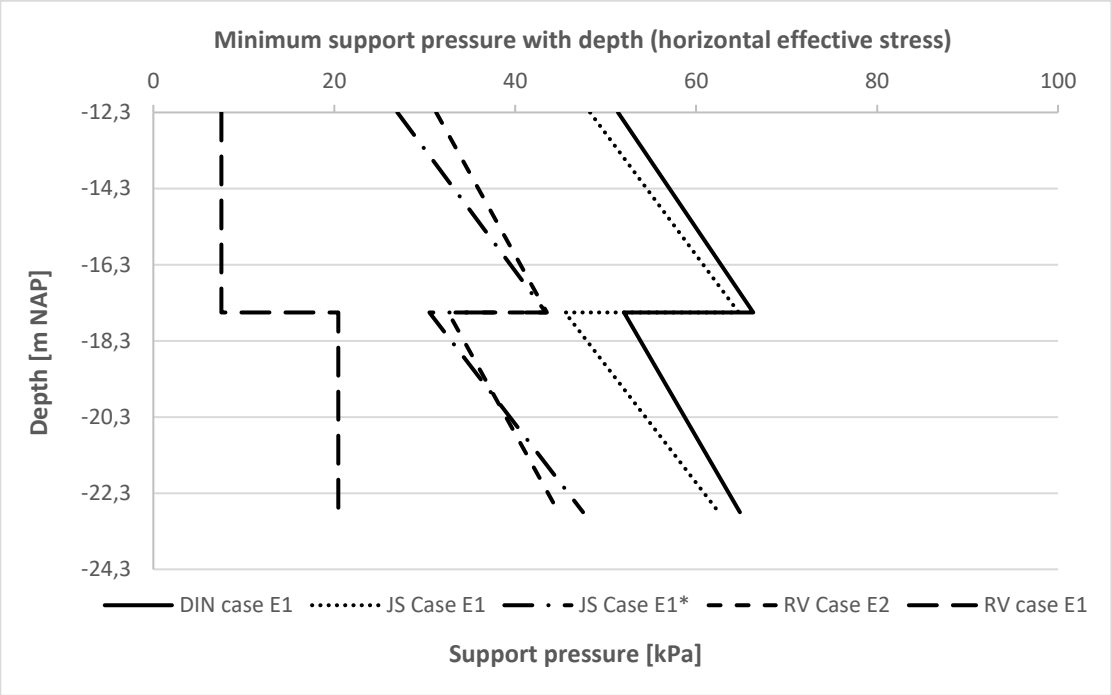

- **Case F:** Minimum support pressure (horizontal effective stress) with depth. Soil profile in front of the TBM consists of an upper layer of clay and a bottom layer of sand. The soil cover consists of a clay layer.

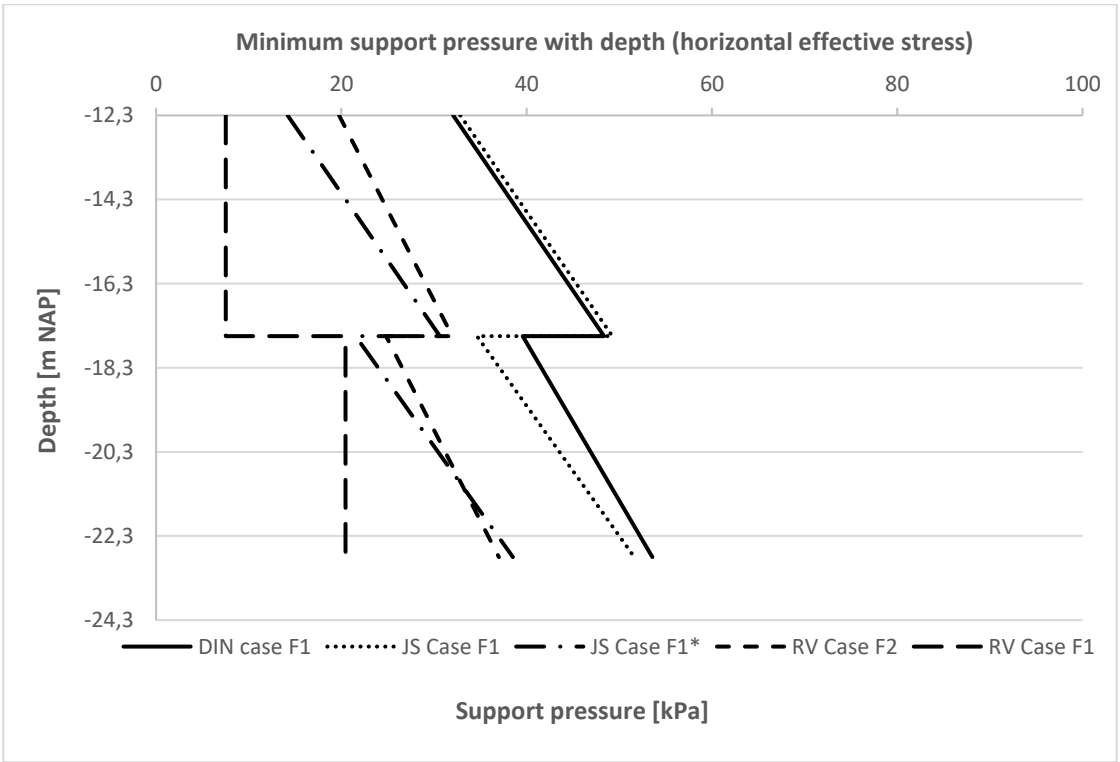

- **Case G:** Minimum support pressure (horizontal effective stress) with depth. Soil profile in front of the TBM consists of an upper layer of sand and a bottom layer of clay. The soil cover consists of a sand layer.

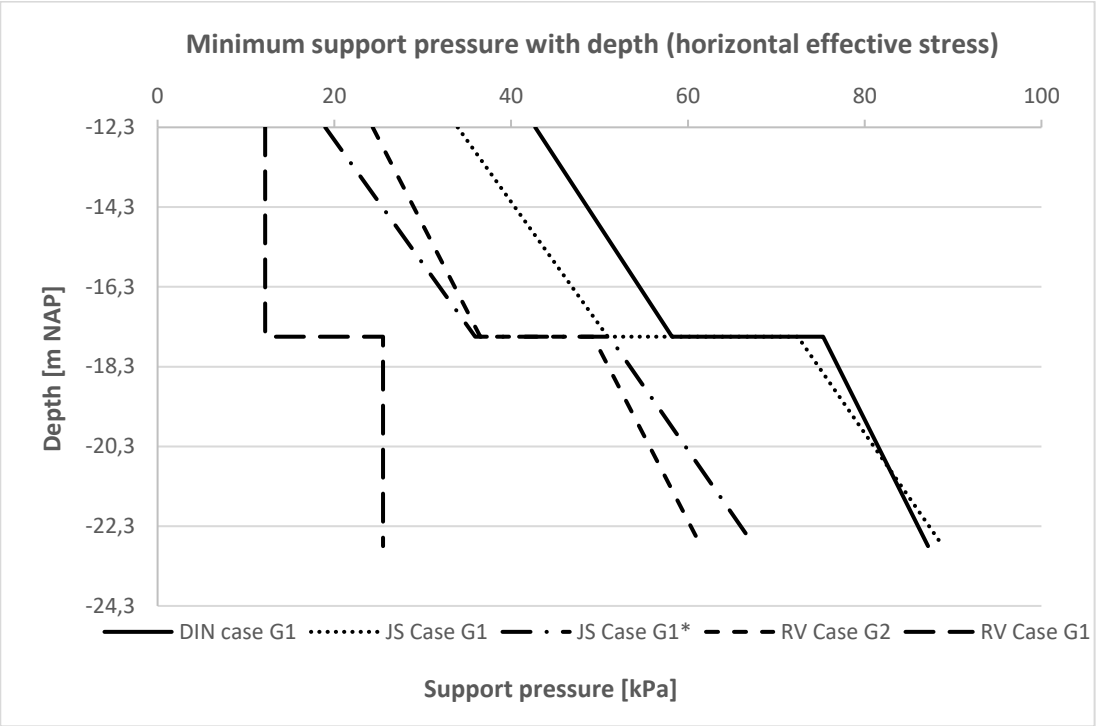

- **Case H:** Minimum support pressure (horizontal effective stress) with depth. Soil profile in front of the TBM consists of an upper layer of sand and a bottom layer of clay. The soil cover consists of a clay layer.

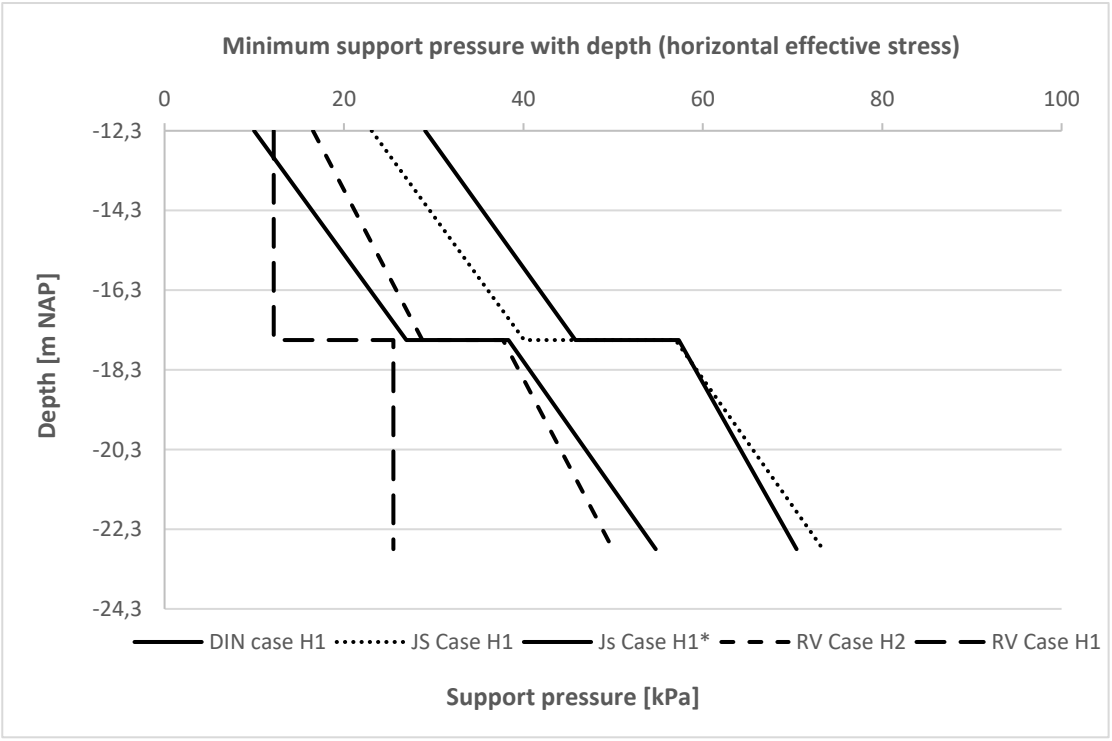

Case study (Series 3)

- **Case E:** Minimum support pressure (horizontal effective stress) with depth. Soil profile in front of the TBM consists of an upper layer of clay and a bottom layer of sand. The soil cover consists of a sand layer.

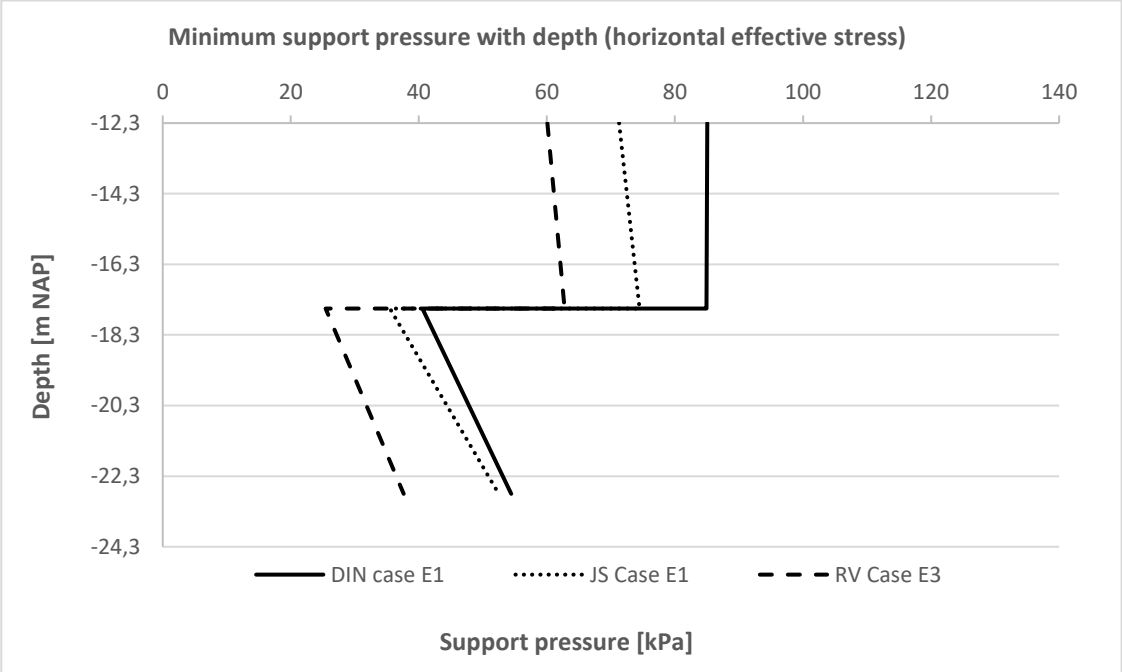

- **Case F:** Minimum support pressure (horizontal effective stress) with depth. Soil profile in front of the TBM consists of an upper layer of clay and a bottom layer of sand. The soil cover consists of a clay layer.

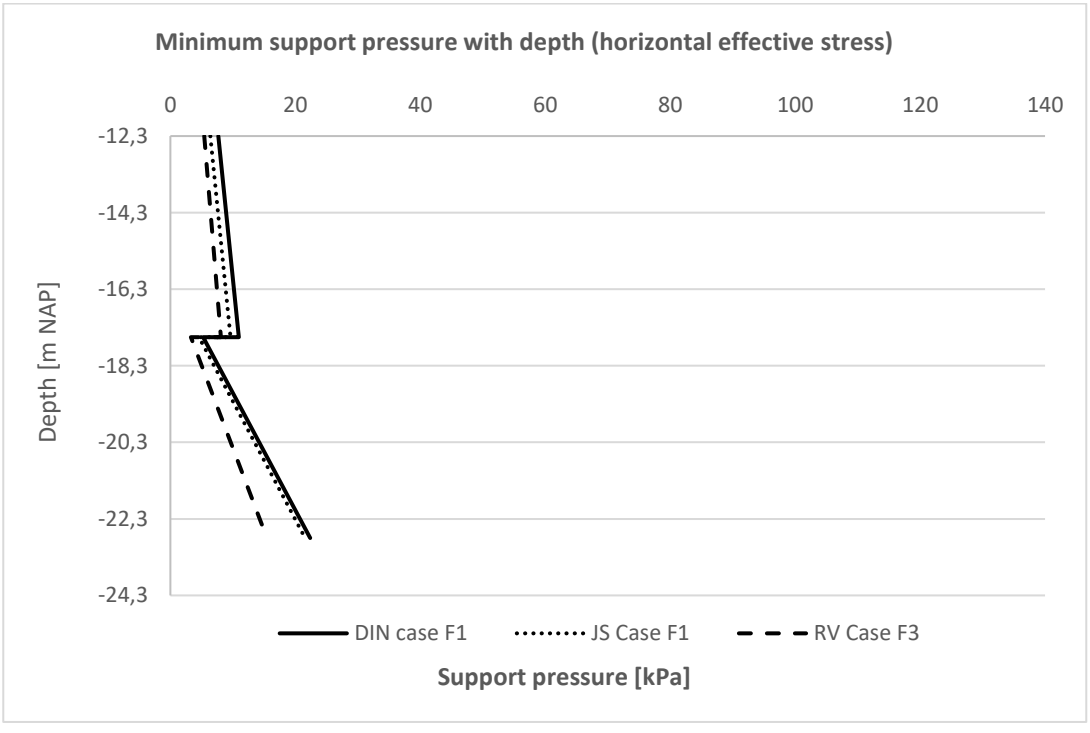

- **Case G:** Minimum support pressure (horizontal effective stress) with depth. Soil profile in front of the TBM consists of an upper layer of sand and a bottom layer of clay. The soil cover consists of a sand layer.

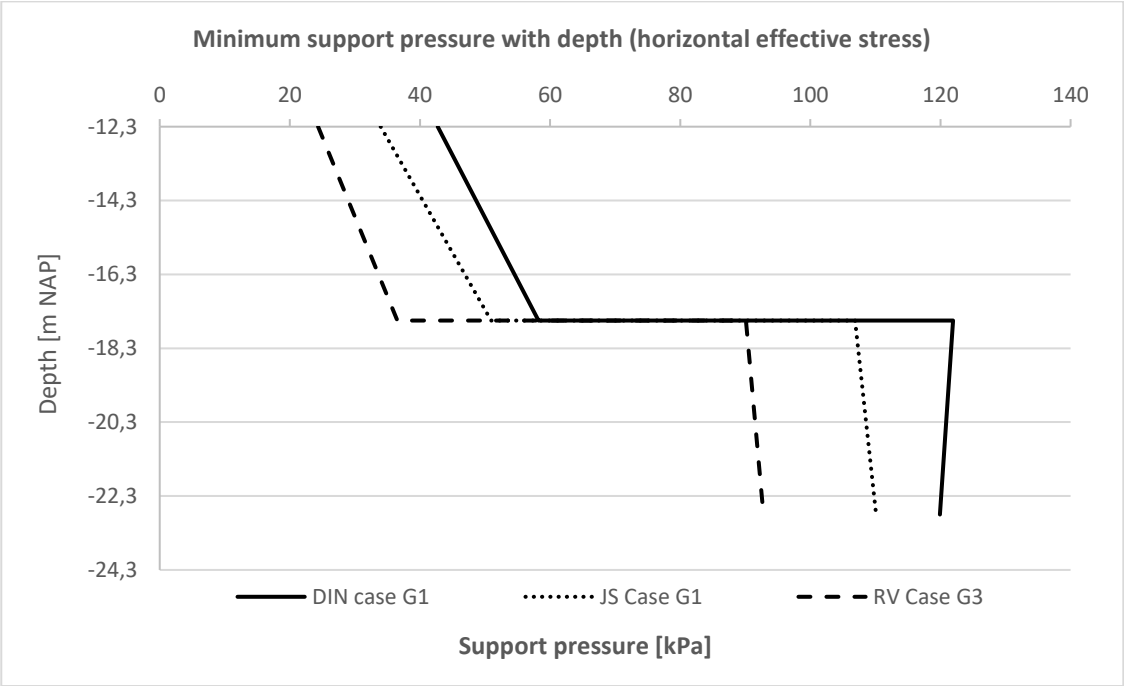

- **Case H:** Minimum support pressure (horizontal effective stress) with depth. Soil profile in front of the TBM consists of an upper layer of sand and a bottom layer of clay. The soil cover consists of a clay layer.

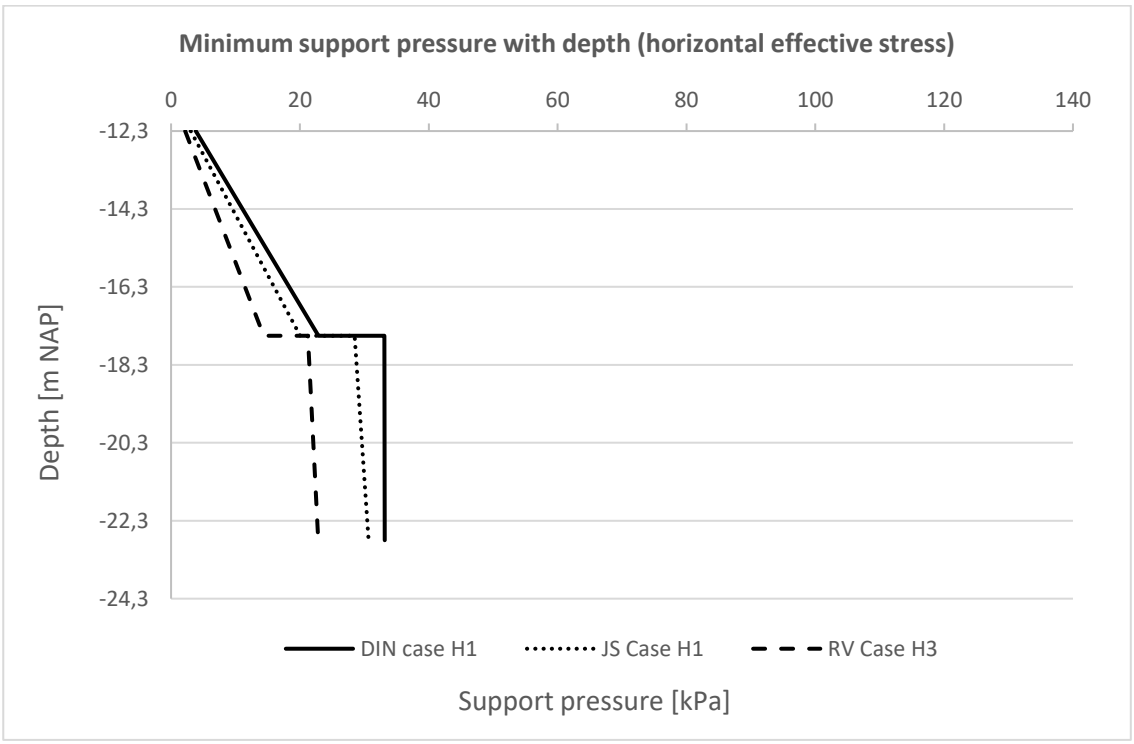

Case study (Series 4)

- **Case A:** Minimum support pressure (horizontal effective stress) with depth for a homogeneous sand profile (C/D=1,0).

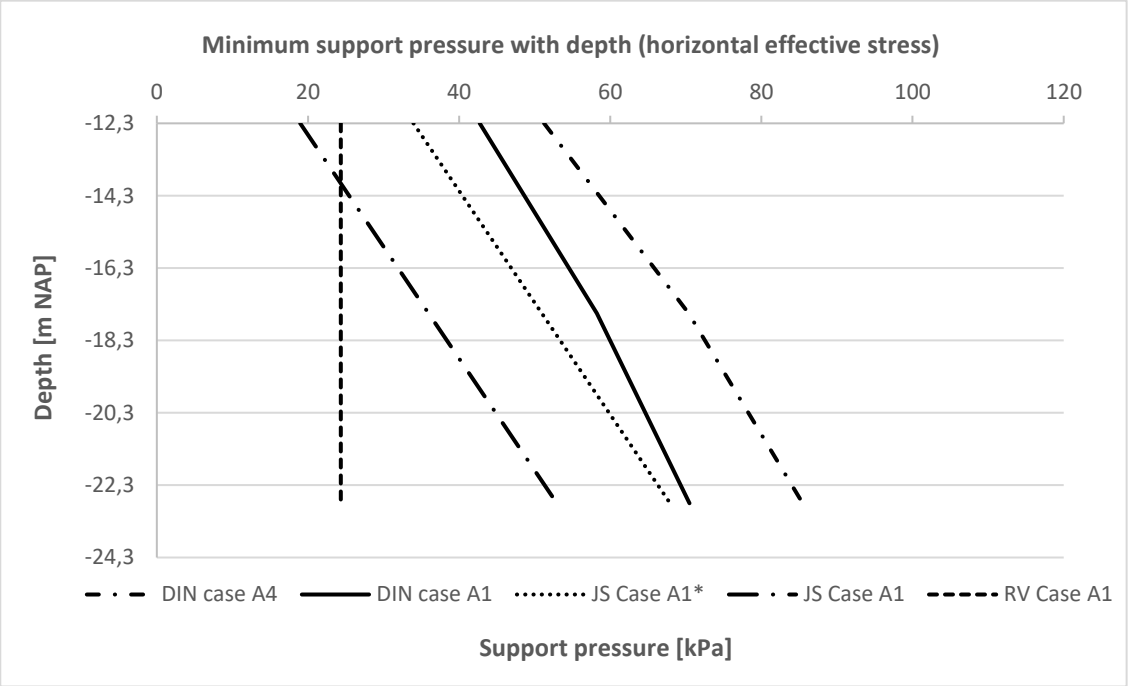

- **Case C:** Minimum support pressure (horizontal effective stress) with depth for a homogeneous sand profile (C/D=1,5).

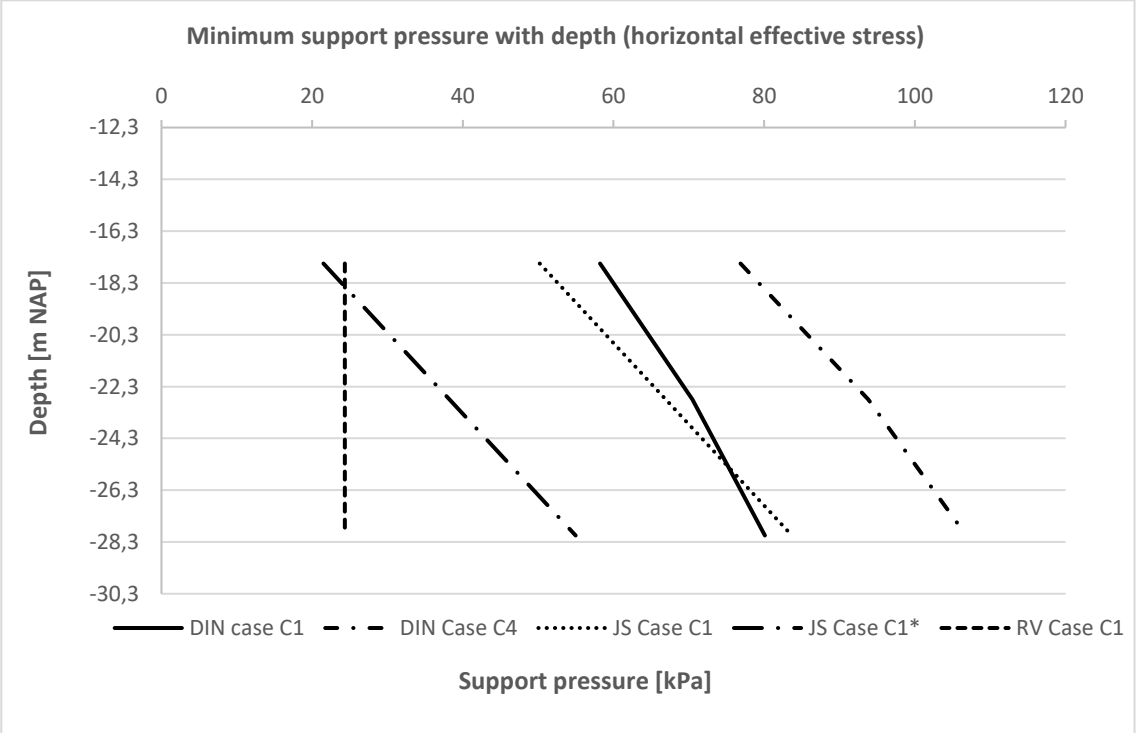

- **Case B:** Minimum support pressure (horizontal effective stress) with depth for a homogeneous clay profile (C/D=1,0).

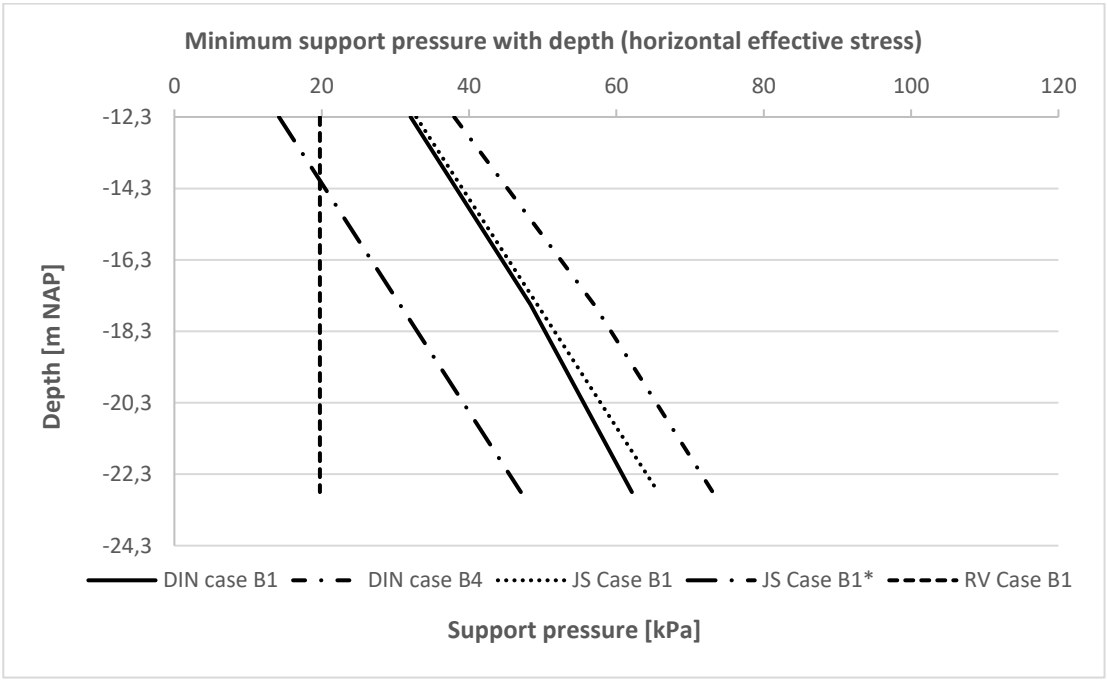

- **Case D:** Minimum support pressure (horizontal effective stress) with depth for a homogeneous clay profile (C/D=1,5).

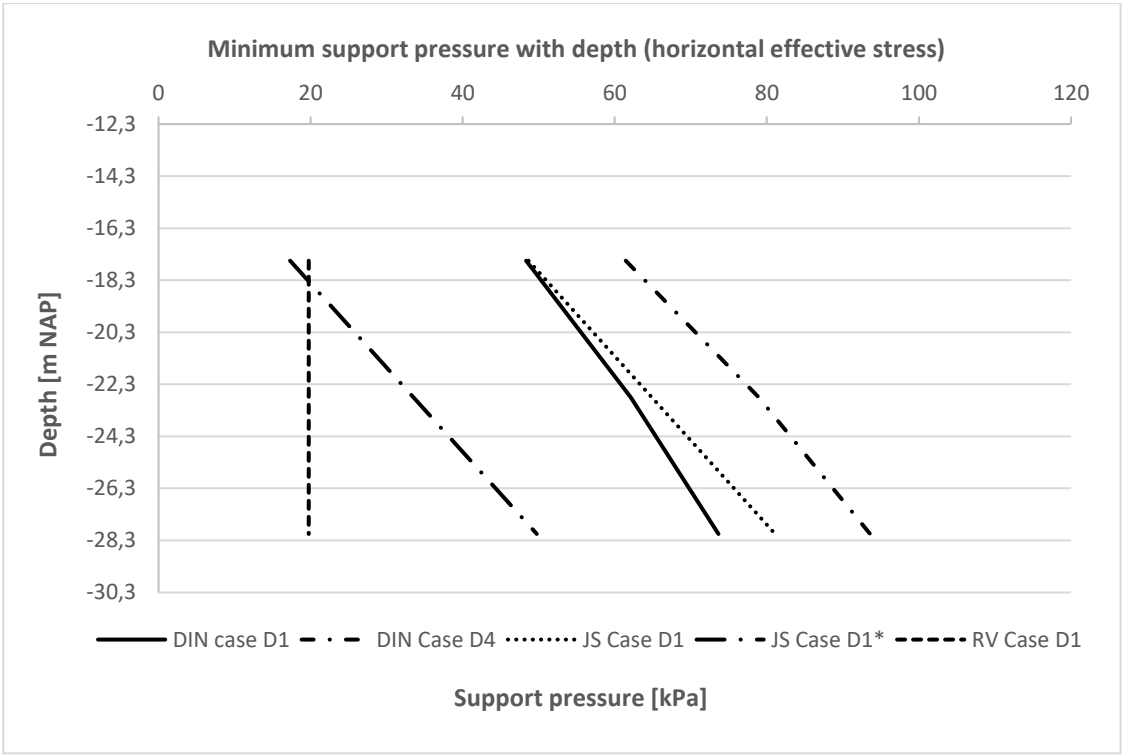

Case-study (Series 5)

- **Case A:** Minimum support pressure (horizontal effective stress) with depth for a homogeneous sand profile (C/D=1,0).

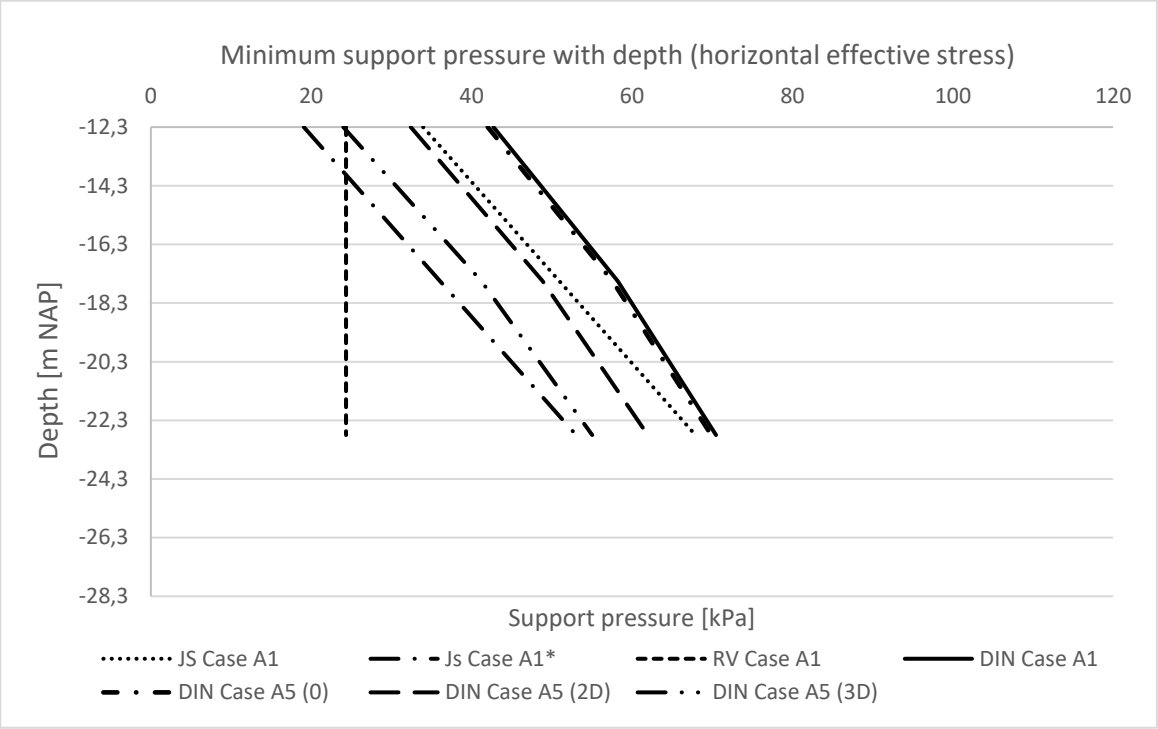

- **Case C:** Minimum support pressure (horizontal effective stress) with depth for a homogeneous sand profile (C/D=1,5).

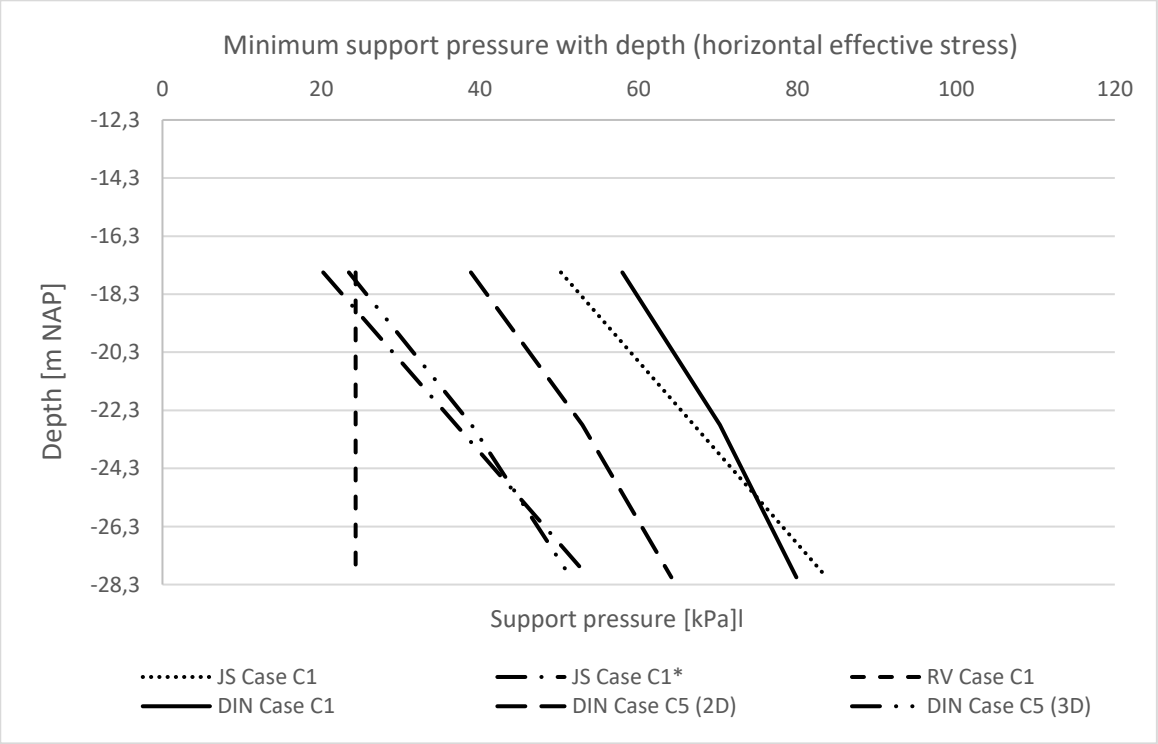

- **Case I:** Minimum support pressure (horizontal effective stress) with depth for a homogeneous sand profile (C/D=2,0).

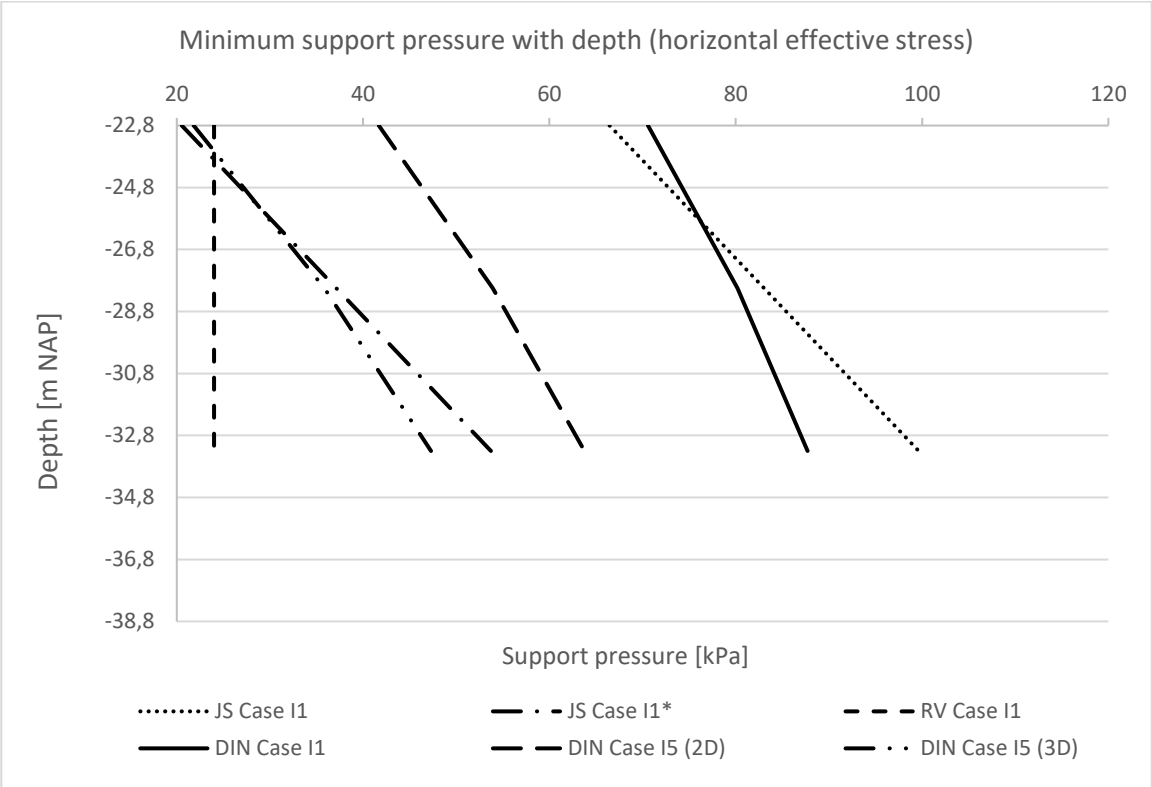

- **Case J:** Minimum support pressure (horizontal effective stress) with depth for a homogeneous sand profile (C/D=2,5).

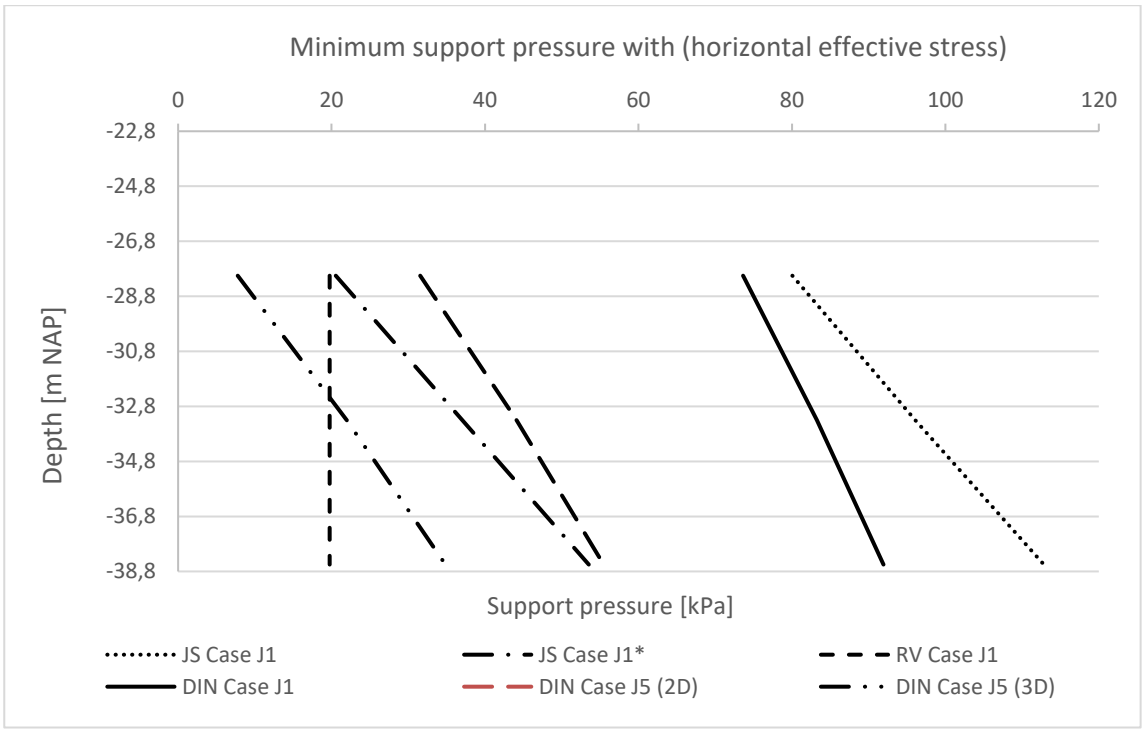

- **Case B:** Minimum support pressure (horizontal effective stress) with depth for a homogeneous clay profile (C/D=1,0).

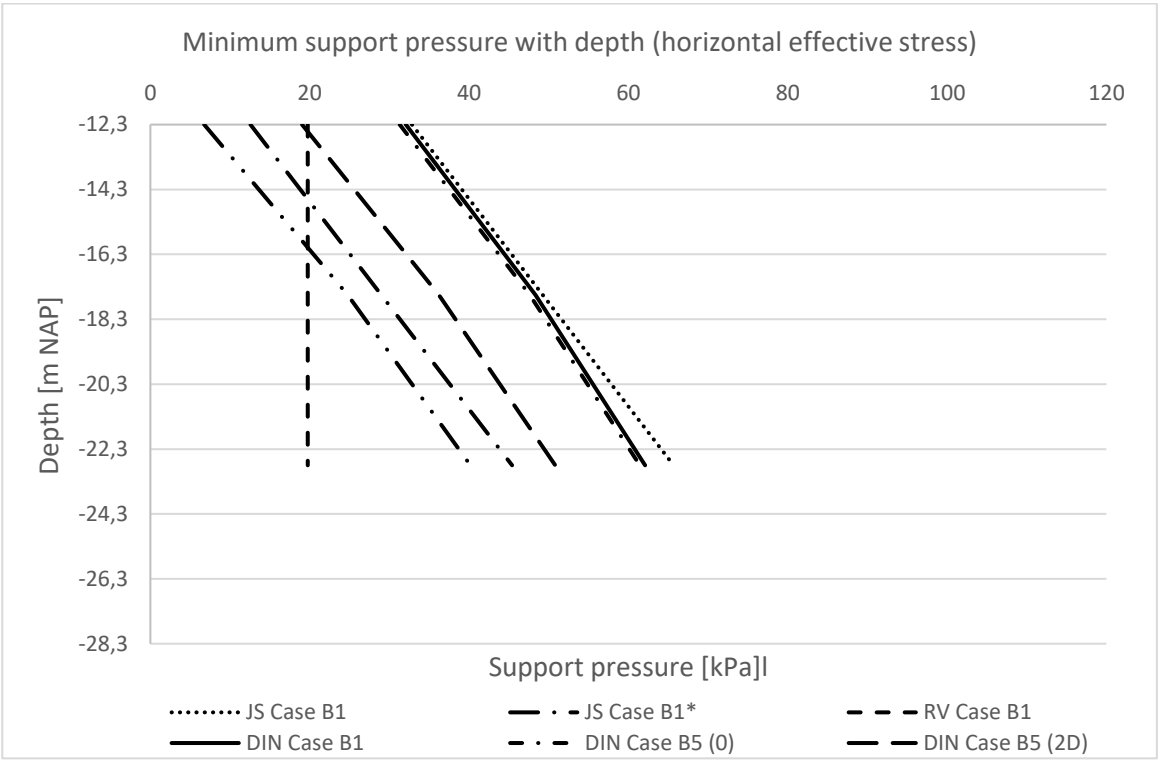

- **Case D:** Minimum support pressure (horizontal effective stress) with depth for a homogeneous clay profile (C/D=1,5).

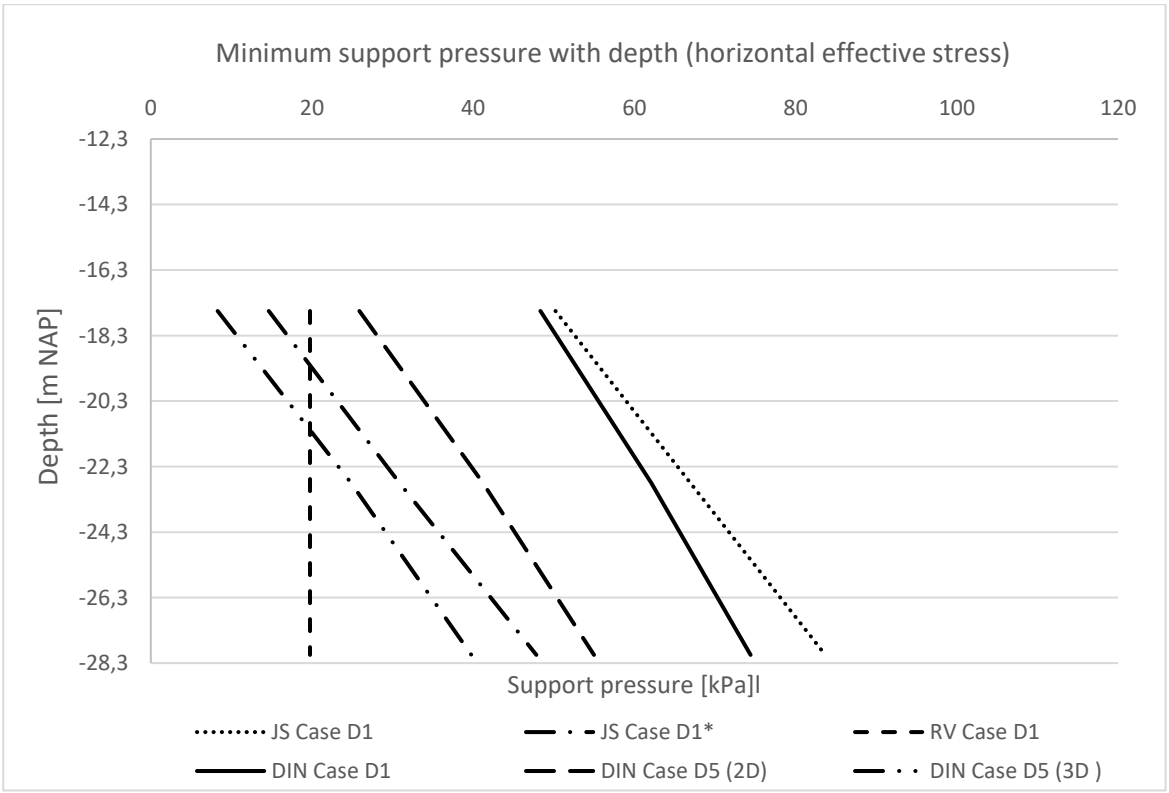

- **Case K:** Minimum support pressure (horizontal effective stress) with depth for a homogeneous clay profile (C/D=2,0).

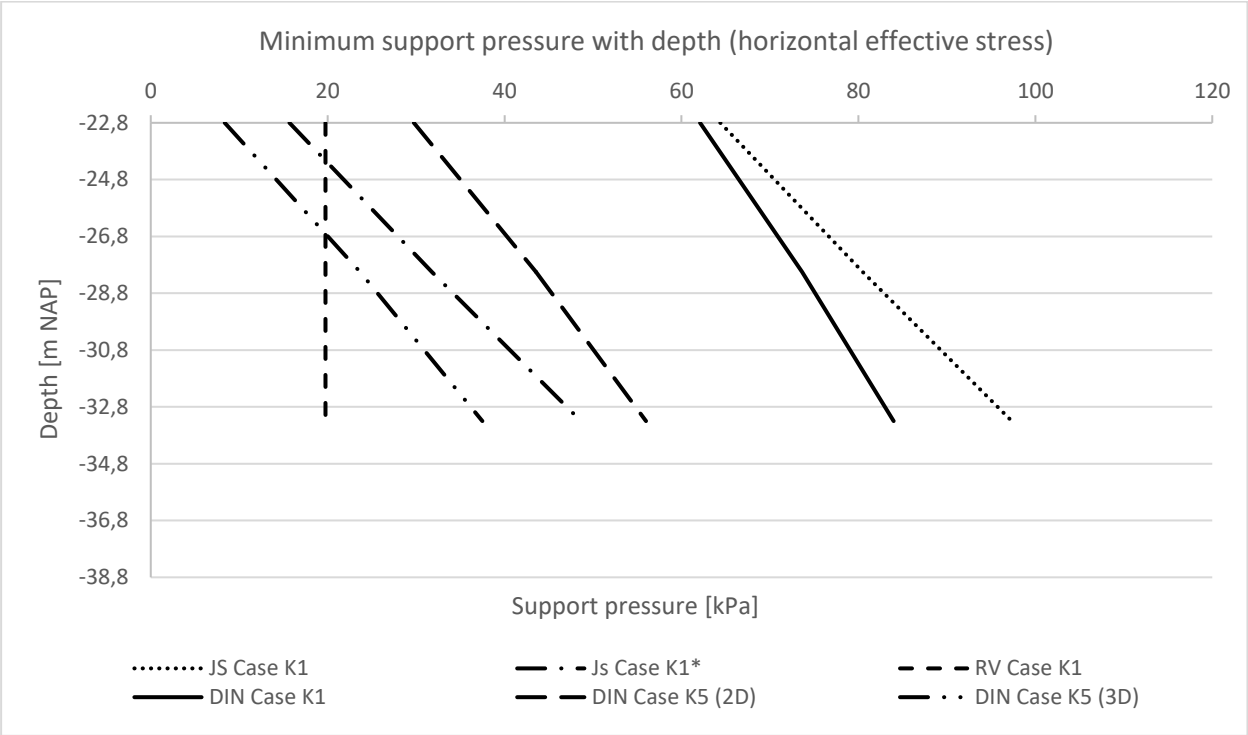

- **Case L:** Minimum support pressure (horizontal effective stress) with depth for a homogeneous clay profile (C/D=2,5).

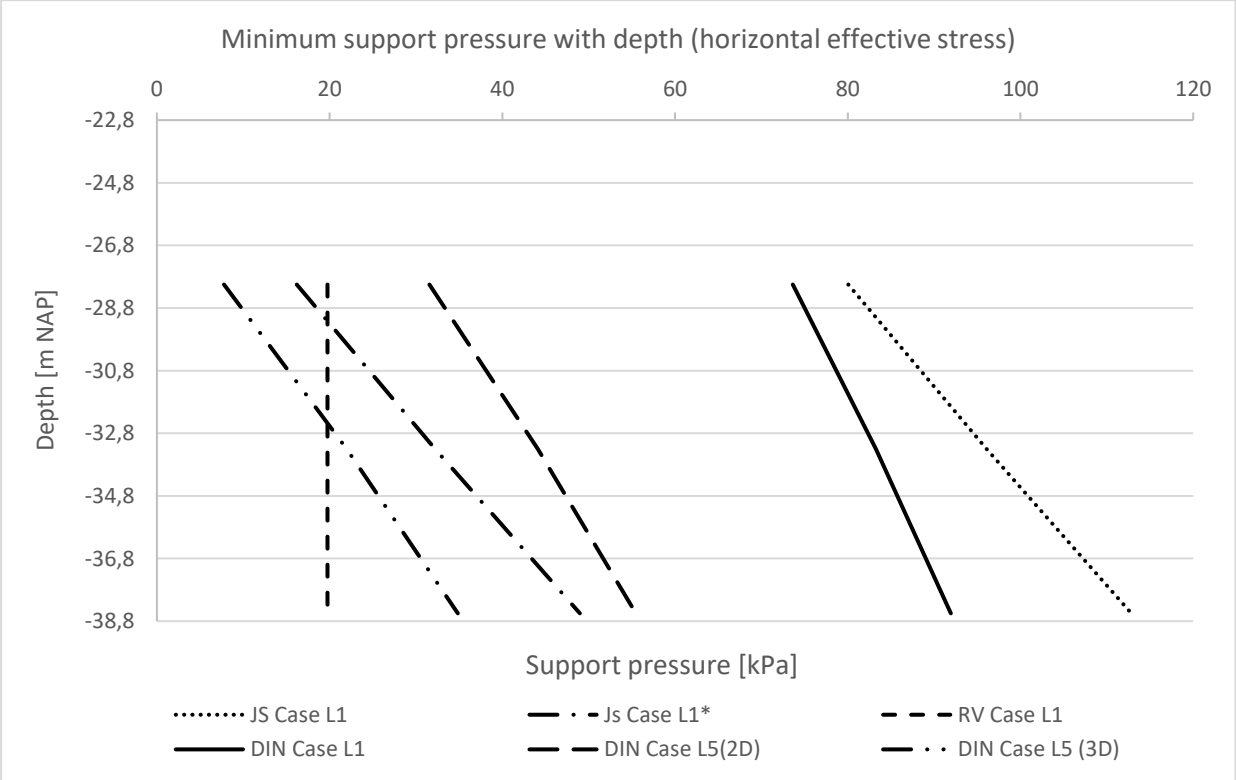

Case study (Series 6)

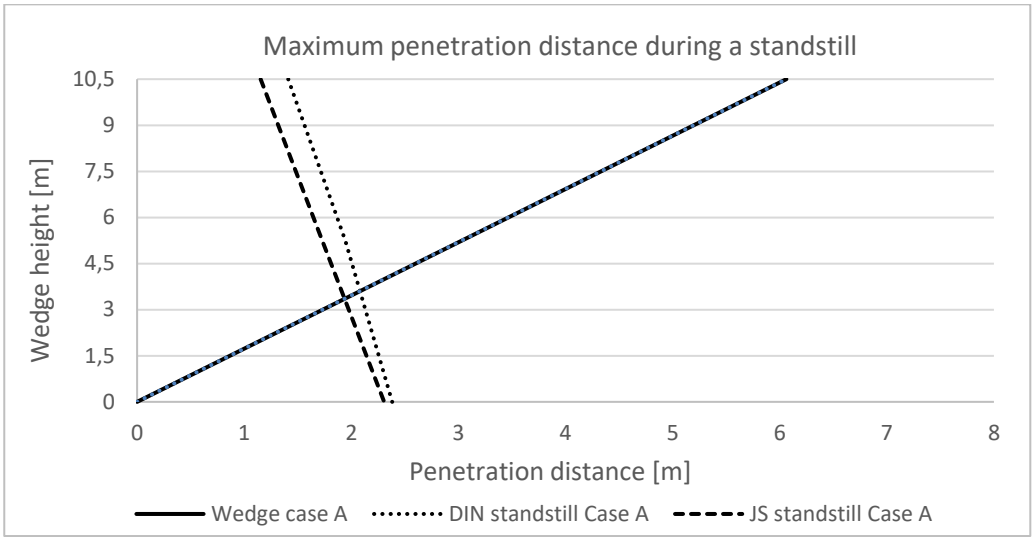

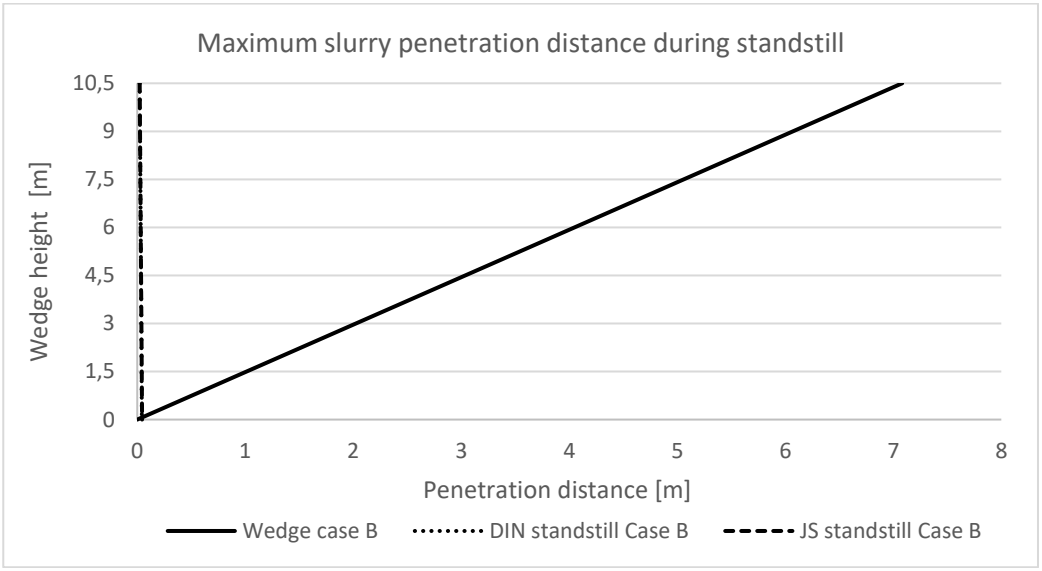

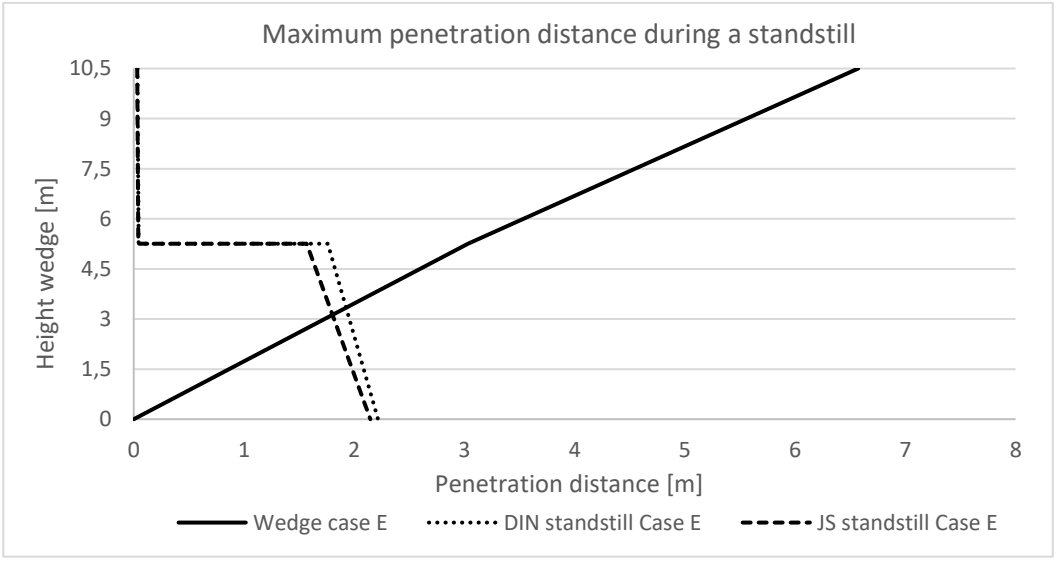

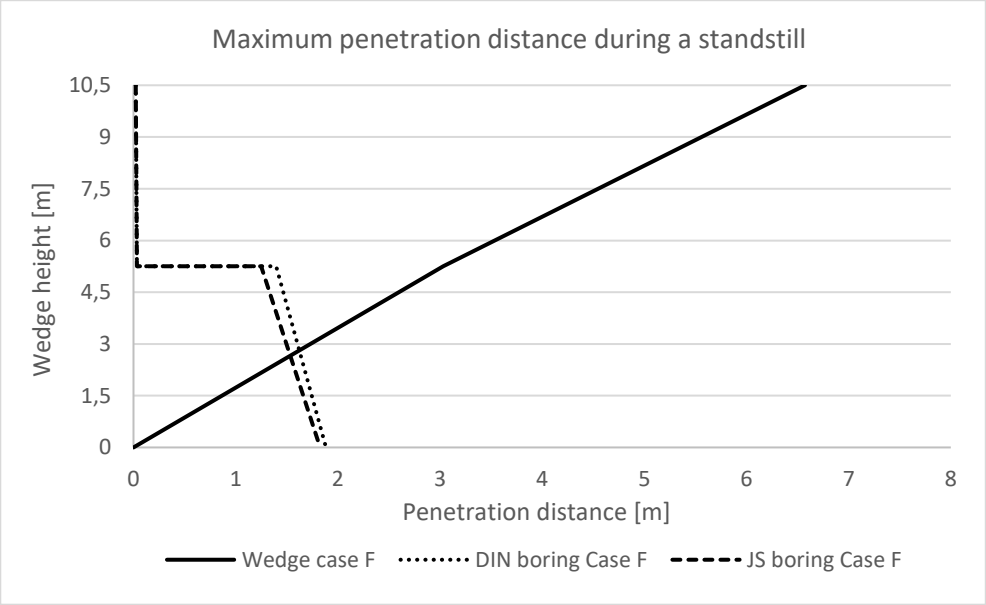
Maximum penetration distance during a standstill
Wedge height [m]
10,5
9
7,5
6
4,5
3
1,5
0
0 1 2 3 4 5 6 7 8
Penetration distance [m]
Wedge case F
DIN boring Case F
JS boring Case F

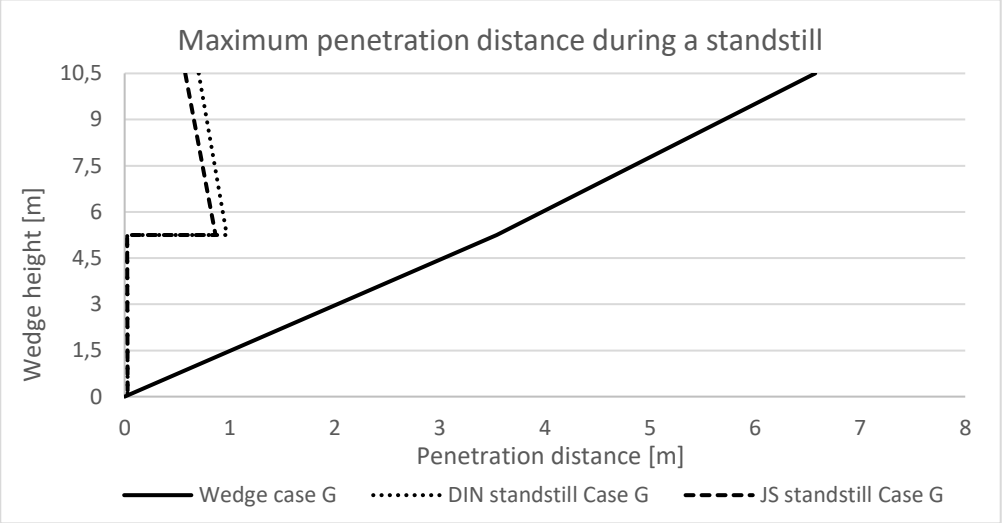
Maximum penetration distance during a standstill
Wedge height [m]
10,5
9
7,5
6
4,5
3
1,5
0
0 1 2 3 4 5 6 7 8
Penetration distance [m]
Wedge case G
DIN standstill Case G
JS standstill Case G

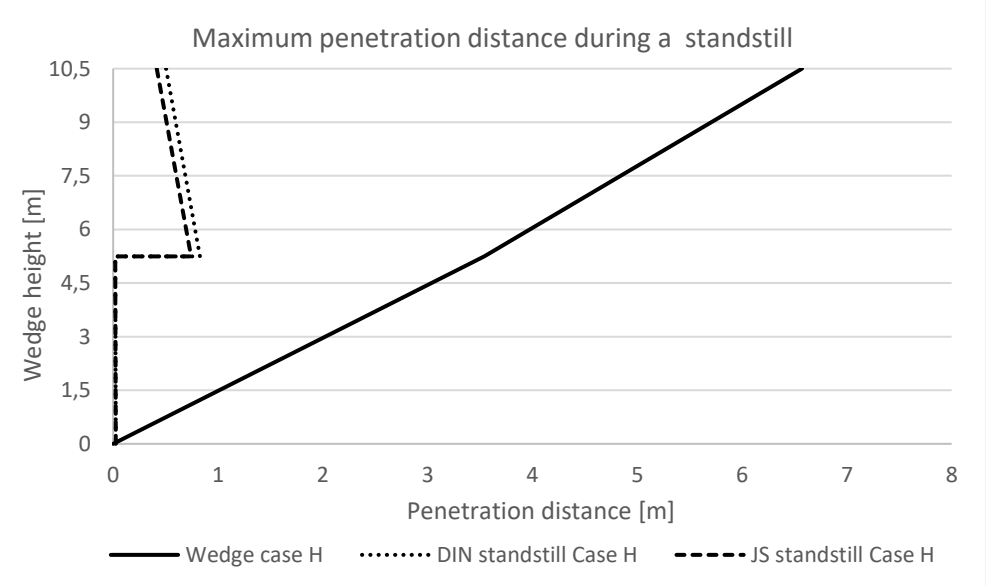
Maximum penetration distance during a standstill
Wedge height [m]
10,5
9
7,5
6
4,5
3
1,5
0
0 1 2 3 4 5 6 7 8
Penetration distance [m]
Wedge case H
DIN standstill Case H
JS standstill Case H

Annex 4: Consolidation calculations

Chainage 4080

Location 4080: Consolidation calculation

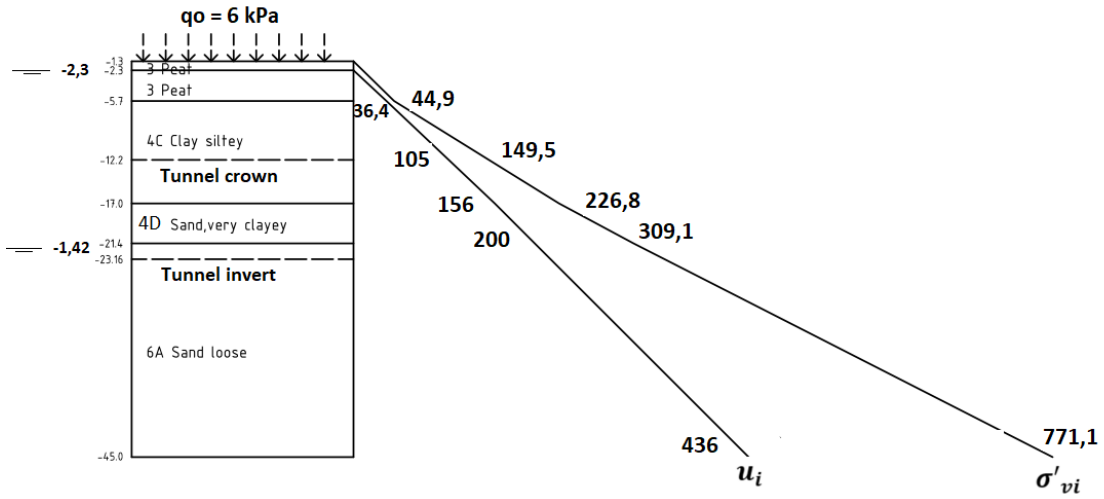

Parameters

Layer	Thickness layer	Consolidation coefficient c_v	Drainage length d	Consolidation time
[-]	[m]	[m²/s]	[m]	[days]
3 Peat	4,4	$3 \cdot 10^{-8}$	4,4	7496
4C Clay	11,3	$1 \cdot 10^{-7}$	11,3	14779
Combined	15,7	$6 \cdot 10^{-8}$	7,85	11887

$t = \frac{T_v \cdot d^2}{c_v}$ $(consolidation\ 95\%\ complete\ \approx\ T_v = 1{,}0)$ $c_{v:combined} = \frac{\sum H_i}{\sum \frac{H_i}{c_{vi}}}$

Face support calculations

Placement additional surcharge 2 years (63 113 852 seconds) before construction

- Half-closed peat layer → maximum u_e bottom peat layer (assume no interaction)

$$T_v = \frac{c_v t}{d^2} = \frac{3 \cdot 10^{-8} \cdot 63\,113\,852}{4{,}4^2} \approx 0{,}01 \qquad \frac{u_e}{\Delta q} = 0{,}98 \;\; so\ u_e = \Delta q = 5{,}88\ kPa$$

- Half-closed clay layer → maximum u_e top clay layer (assume no interaction)

$$T_v = \frac{c_v t}{d^2} = \frac{1 \cdot 10^{-7} \cdot 63\,113\,852}{11{,}3^2} \approx 0{,}05 \qquad \frac{u_e}{\Delta q} = 0{,}96 \;\; so\ u_e = \Delta q = 5{,}76\ kPa$$

Pore waterpressure distribution

$$k_{eq} = \frac{\sum H_i}{\sum \frac{H_i}{k_i}} = \frac{\sum(3{,}4+11{,}3+3{,}4)}{\sum(\frac{3{,}4}{4E09}+\frac{11{,}3}{5E09}+\frac{3{,}4}{6E06})} = 5 \cdot 10^{-9}\ m/s \qquad q_i = k^{eq} \cdot i^{eq} = k^{eq} \cdot \frac{\Delta h}{H_i} \rightarrow \;\; \Delta h_i = \frac{q_i}{k_i} \cdot H_i$$

$\Delta h_1 = 0{,}24\ m$
$\Delta h_2 = 0{,}64\ m$
$\Delta h_3 \approx 0\ m$
$\Delta h \approx 0{,}88\ m$

Chainage 4100

Location 4100: Consolidation calculation

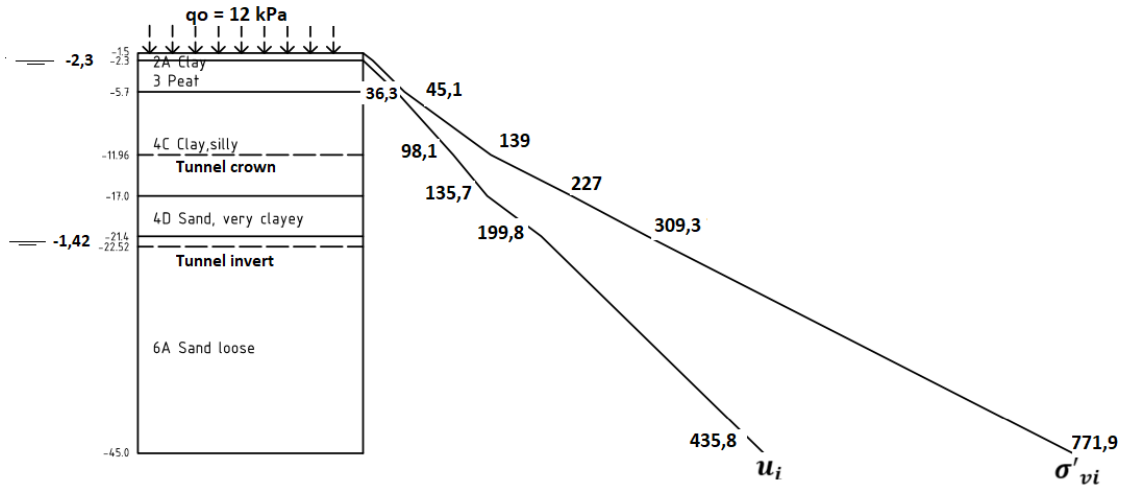

Parameters analysis

Layer	Thickness layer	Consolidation coefficient c_v	Drainage length d	Consolidation time
[-]	[m]	[m²/s]	[m]	[days]
2A clay	0,8	$4 \cdot 10^{-8}$	0,8	185
3 Peat	3,4	$3 \cdot 10^{-8}$	x (3,4)	x (4460)
4C Clay	11,3	$1 \cdot 10^{-7}$	11,3	14779
Combined	15,5	$6{,}3 \cdot 10^{-8}$	7,75	11034

$$t = \frac{T_v \cdot d^2}{c_v} \quad (consolidation\ 95\%\ complete\ \approx\ T_v = 1{,}0) \qquad c_{v:combined} = \frac{\sum H_i}{\sum \frac{H_i}{c_{vi}}}$$

Face support calculations

Placement additional surcharge 2 years (63 113 852 seconds) before construction

- Open layer → maximum u_e middle (-8,5 m NAP)

$$T_v = \frac{c_v t}{d^2} = \frac{6{,}3 \cdot 10^{-8} \cdot 63113852}{7{,}75^2} \approx 0{,}06 \qquad \frac{u_e}{\Delta q} = 0{,}96 \ \ so\ \ u_e = 0{,}96 \Delta q = 11{,}52\ kPa$$

Pore waterpressure distribution

$$k_{eq} = \frac{\sum H_i}{\sum \frac{H_i}{k_i}} = \frac{\sum(3{,}4+11{,}3+3{,}4)}{\sum(\frac{3{,}4}{4E09}+\frac{11{,}3}{5E09}+\frac{3{,}4}{6E06})} = 5 \cdot 10^{-9}\ m/s \qquad q_i = k^{eq} \cdot i^{eq} = k^{eq} \cdot \frac{\Delta h}{H_i} \rightarrow\ \ \Delta h_i = \frac{q_i}{k_i} \cdot H_i$$

$\Delta h_1 = 0{,}23\ m$
$\Delta h_2 = 0{,}64\ m$
$\Delta h_3 \approx 0\ m$
$\Delta h \approx 0{,}87\ m$

Chainage 4120-4140

Location 4120/4140: Consolidation calculation

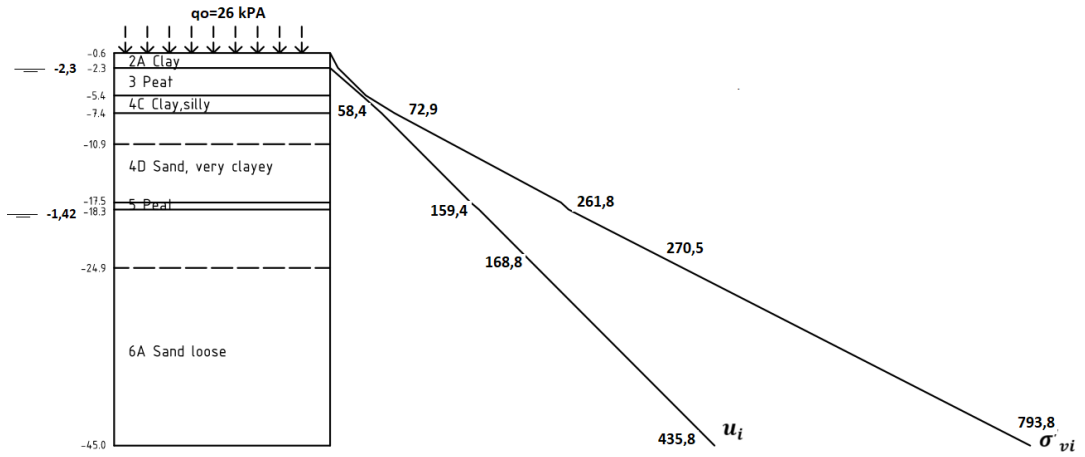

Parameters analysis

Layer	Thickness layer	Consolidation coefficient c_v	Drainage length d	Consolidation time
[-]	[m]	[m²/s]	[m]	[days]
2A clay	0,7	$4 \cdot 10^{-8}$	0,7	142
3 Peat	3,1	$3 \cdot 10^{-8}$	X (3,1)	X (3708)
4C Clay	2	$1 \cdot 10^{-7}$	2	462
Combined	5,8	$4{,}14 \cdot 10^{-8}$	2,9	2351
5 Peat	0,8	$7 \cdot 10^{-8}$	0,4	106

$t = \frac{T_v \cdot d^2}{c_v}$ $(consolidation\ 95\%\ complete\ \approx\ T_v = 1{,}0)$ $c_{v:combined} = \frac{\sum H_i}{\sum \frac{H_i}{c_{vi}}}$

Face support calculations

Placement additional surcharge 2 years (63 113 852 seconds) before construction

- Open layer → maximum u_e middle (-4,5 m NAP)

$T_v = \frac{c_v t}{d^2} = \frac{4{,}14 \cdot 10^{-8} \cdot 63113852}{2{,}9^2} \approx 0{,}31$ $\frac{u_e}{\Delta q} = 0{,}6 \quad so\ u_e = 0{,}6\ \Delta q$

$=$ $15{,}6\ kPa\ (4120)\ \ or\ 19{,}8\ (4140)$

$T_v = \frac{c_v t}{d^2} = \frac{7 \cdot 10^{-8} \cdot 63113852}{2{,}9^2} \approx 0{,}52$ $\frac{u_e}{\Delta q} = 0{,}37 \quad so\ u_e = 0{,}37\ \Delta q$

$=$ $9{,}62\ kPa\ (4120)\ \ or\ 12{,}21\ (4140)$

Pore waterpressure distribution

$k_{eq} = \frac{\sum H_i}{\sum \frac{H_i}{k_i}} = \frac{\sum(3{,}4+11{,}3+3{,}4)}{\sum(\frac{3{,}4}{4E09}+\frac{11{,}3}{5E09}+\frac{3{,}4}{6E06})} = 1{,}23 \cdot 10^{-8}\ m/s$ $q_i = k^{eq} \cdot i^{eq} = k^{eq} \cdot \frac{\Delta h}{H_i} \rightarrow\ \Delta h_i = \frac{q_i}{k_i} \cdot H_i$

$\Delta h_1 = 0{,}49\ m$
$\Delta h_2 = 0{,}25\ m$
$\Delta h_3 \approx 0\ m$
$\Delta h_4 = 0{,}12\ m$
$\Delta h \approx 0{,}88\ m$

Annex 5: Transient face stability

Parameter study

Case-study 1
Conditions

Conditions case 1	
Leakage length λ [m]	11
Storativity soil S_s [m^{-1}]	0,0007
Permeability soil k [m/h]	0,108
Height aquifer H [m]	11
u	0,08
Porosity n [-]	0,4
Advance speed v [m/h]	1,5
Discharge q [m/h]	-0,6
Diameter tunnel [m]	11
Radius tunnel [m]	5,5
Discharge Q [m^3/h]	-6,6
Boring time [h]	5/8= 1,33
Ring building time [h]	5/6= 0,83

Build-up and dissipation excess pore pressures with time

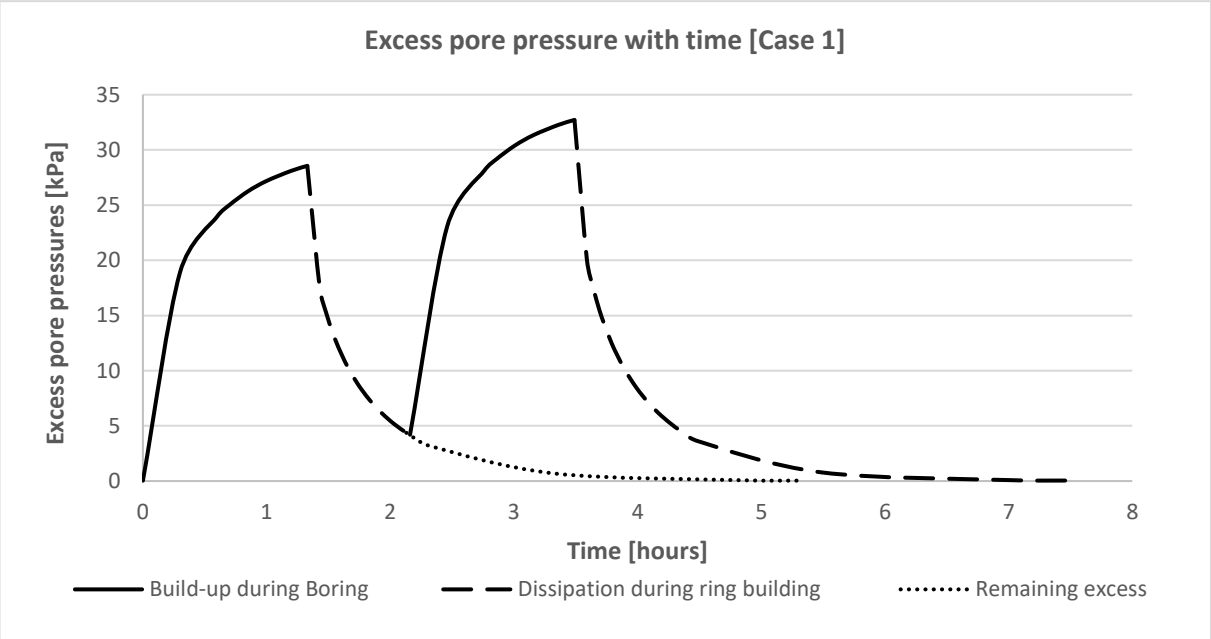

Case-study 2

Conditions

Conditions case 2	
Leakage length λ [m]	11
Storativity soil S_s [m^{-1}]	0,0007
Permeability soil k [m/h]	0,108
Height aquifer H [m]	16,66
u	0,081
Porosity n [-]	0,4
Advance speed v [m/h]	1,5
Discharge q [m/h]	-0,6
Diameter tunnel [m]	11
Radius tunnel [m]	5,5
Discharge Q [m^3/h]	-6,6
Boring time [h]	5/8= 1,33
Ring building time [h]	5/6= 0,83

Build-up and dissipation excess pore pressures with time

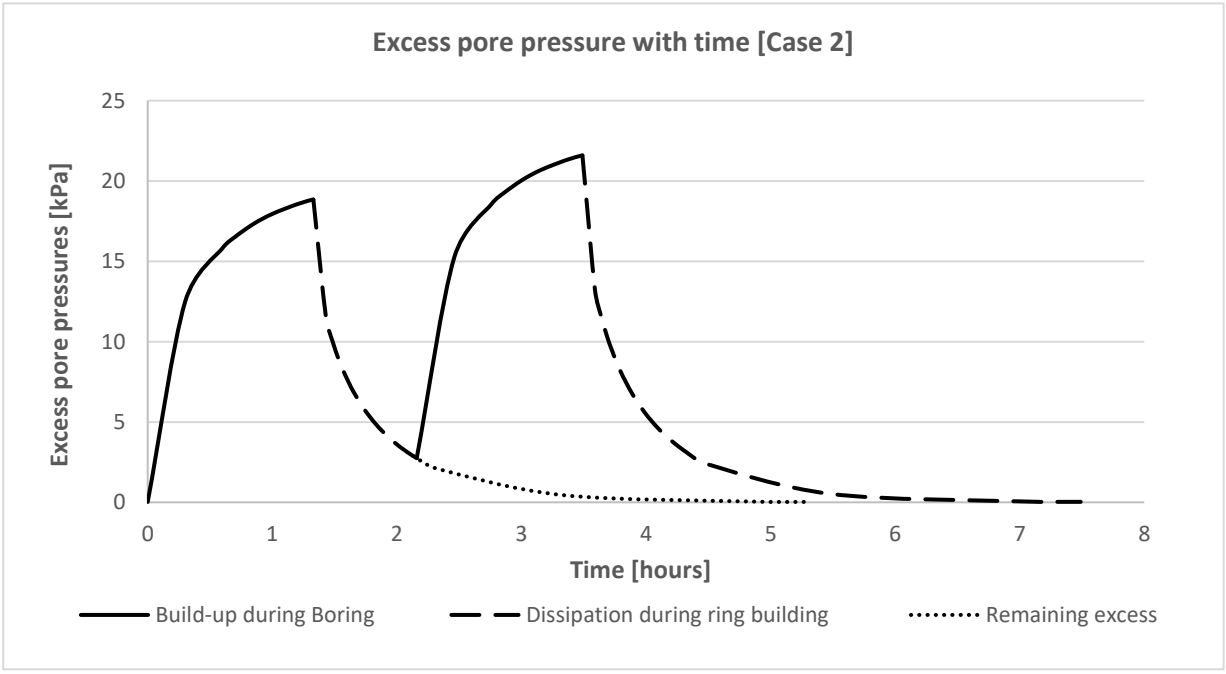

Case-study 3

Conditions

Conditions case 3	
Leakage length λ [m]	11
Storativity soil S_s [m^{-1}]	0,0007
Permeability soil k [m/h]	0,108
Height aquifer H [m]	22
u	0,081
Porosity n [-]	0,4
Advance speed v [m/h]	1,5
Discharge q [m/h]	-0,6
Diameter tunnel [m]	11
Radius tunnel [m]	5,5
Discharge Q [m^3/h]	-6,6
Boring time [h]	5/8= 1,33
Ring building time [h]	5/6= 0,83

Build-up and dissipation excess pore pressures with time

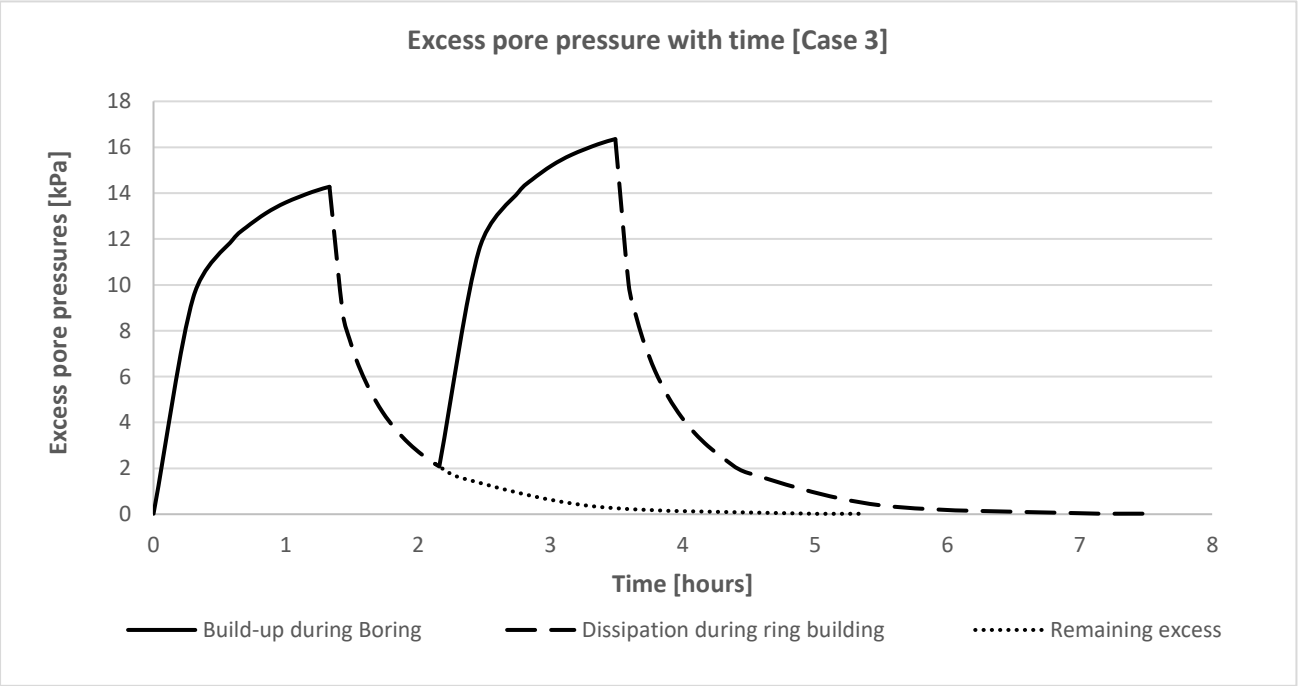

Case-study 4

Conditions

Conditions case 4	
Leakage length λ [m]	11
Storativity soil S_s [m^{-1}]	0,0007
Permeability soil k [m/h]	0,108
Height aquifer H [m]	27,5
u	0,081
Porosity n [-]	0,4
Advance speed v [m/h]	1,5
Discharge q [m/h]	-0,6
Diameter tunnel [m]	11
Radius tunnel [m]	5,5
Discharge Q [m^3/h]	-6,6
Boring time [h]	5/8= 1,33
Ring building time [h]	5/6= 0,83

Build-up and dissipation excess pore pressures with time

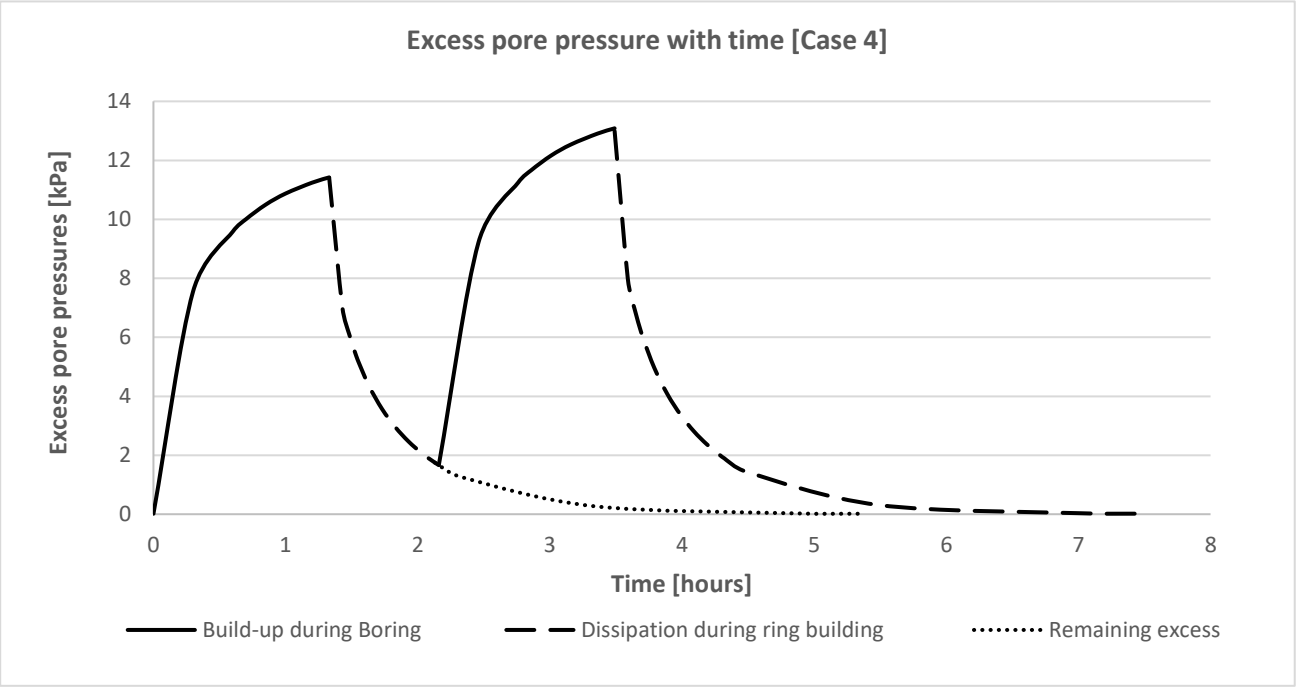

Case-study 5

Conditions

Conditions case 5	
Leakage length λ [m]	11
Storativity soil S_s [m^{-1}]	0,0007
Permeability soil k [m/h]	0,108
Height aquifer H [m]	5,5
u	0,081
Porosity n [-]	0,4
Advance speed v [m/h]	1,5
Discharge q [m/h]	-0,6
Diameter tunnel [m]	11
Radius tunnel [m]	5,5
Discharge Q [m^3/h]	-6,6
Boring time [h]	5/8= 1,33
Ring building time [h]	5/6= 0,83

Build-up and dissipation excess pore pressures with time

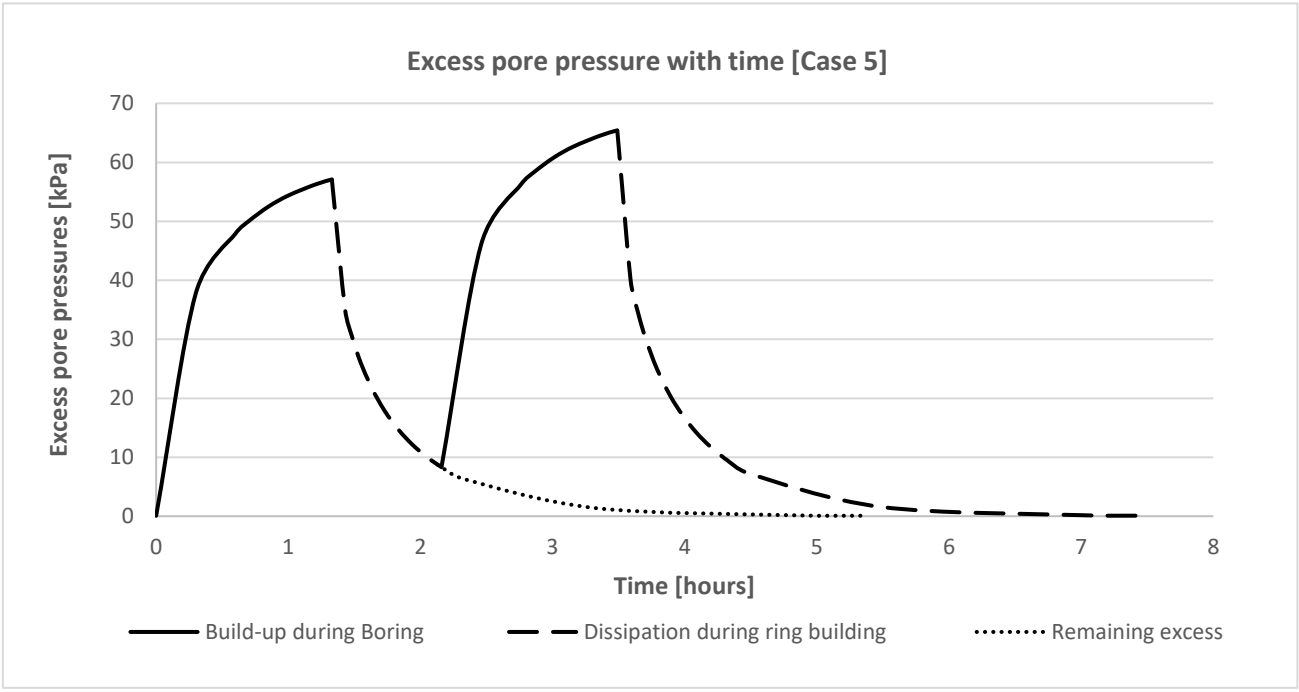

Case-study 6

Conditions

Conditions case 6	
Leakage length λ [m]	11
Storativity soil S_s [m^{-1}]	0,0007
Permeability soil k [m/h]	0,108
Height aquifer H [m]	2,75
u	0,081
Porosity n [-]	0,4
Advance speed v [m/h]	1,5
Discharge q [m/h]	-0,6
Diameter tunnel [m]	11
Radius tunnel [m]	5,5
Discharge Q [m^3/h]	-6,6
Boring time [h]	5/8= 1,33
Ring building time [h]	5/6= 0,83

Build-up and dissipation excess pore pressures with time

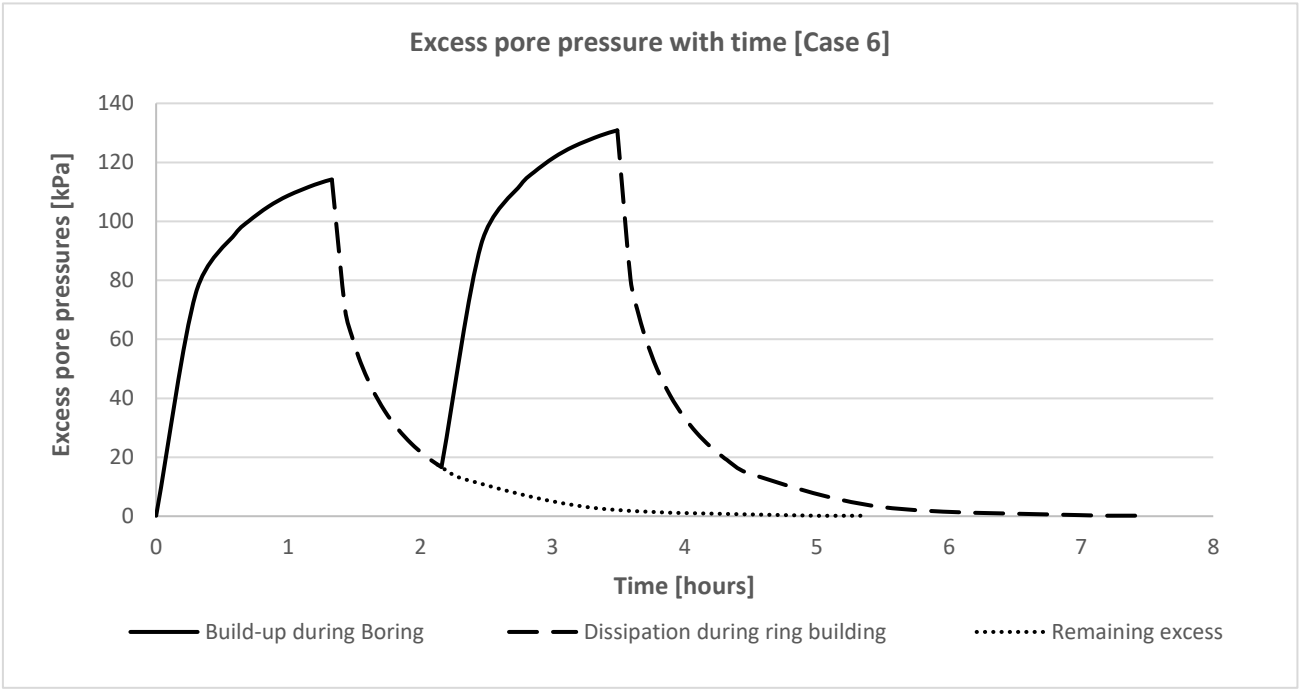

Case-study 7

Conditions

Conditions case 7	
Leakage length λ [m]	11
Storativity soil S_s [m^{-1}]	0,0007
Permeability soil k [m/h]	0,108
Height aquifer H [m]	11
u	0,081
Porosity n [-]	0,4
Advance speed v [m/h]	3
Discharge q [m/h]	-1,2
Diameter tunnel [m]	11
Radius tunnel [m]	5,5
Discharge Q [m^3/h]	-13,2
Boring time [h]	5/8= 1,33
Ring building time [h]	5/6= 0,83

Build-up and dissipation excess pore pressures with time

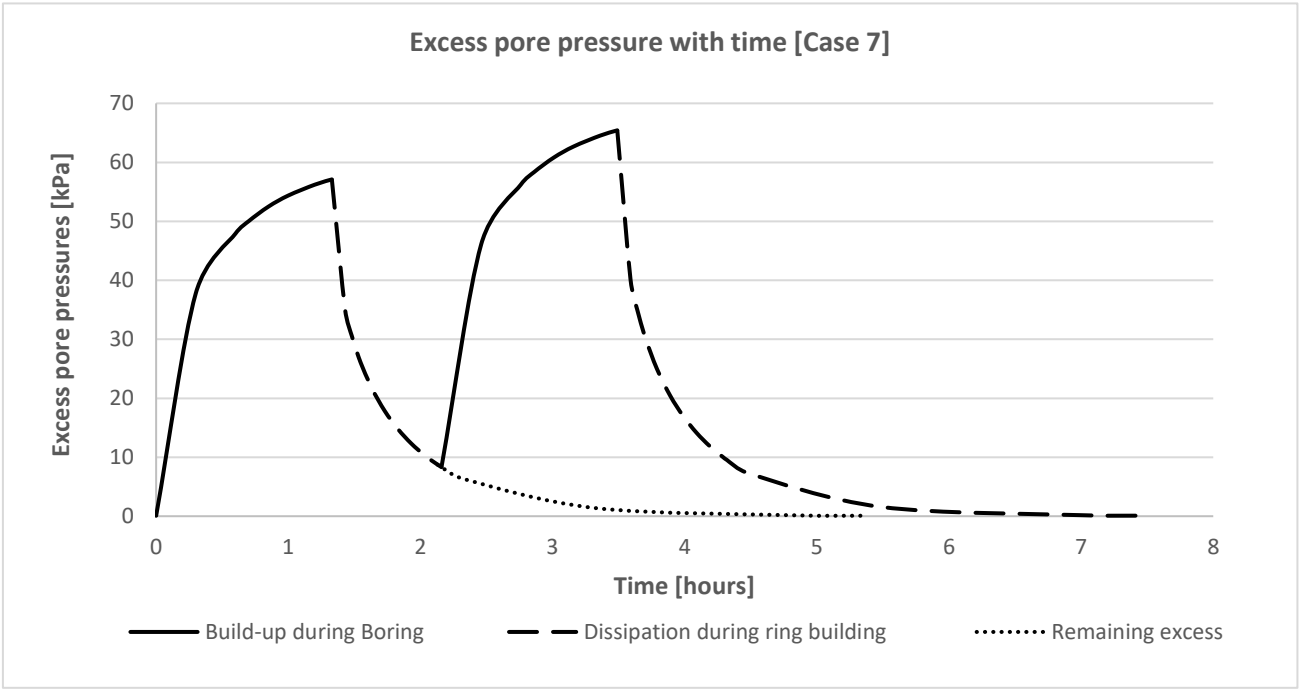

Case-study 8

Conditions

Conditions case 8	
Leakage length λ [m]	11
Storativity soil S_s [m^{-1}]	0,0007
Permeability soil k [m/h]	0,108
Height aquifer H [m]	11
u	0,081
Porosity n [-]	0,4
Advance speed v [m/h]	0,75
Discharge q [m/h]	-0,3
Diameter tunnel [m]	11
Radius tunnel [m]	5,5
Discharge Q [m^3/h]	-3,3
Boring time [h]	5/8= 1,33
Ring building time [h]	5/6= 0,83

Build-up and dissipation excess pore pressures with time

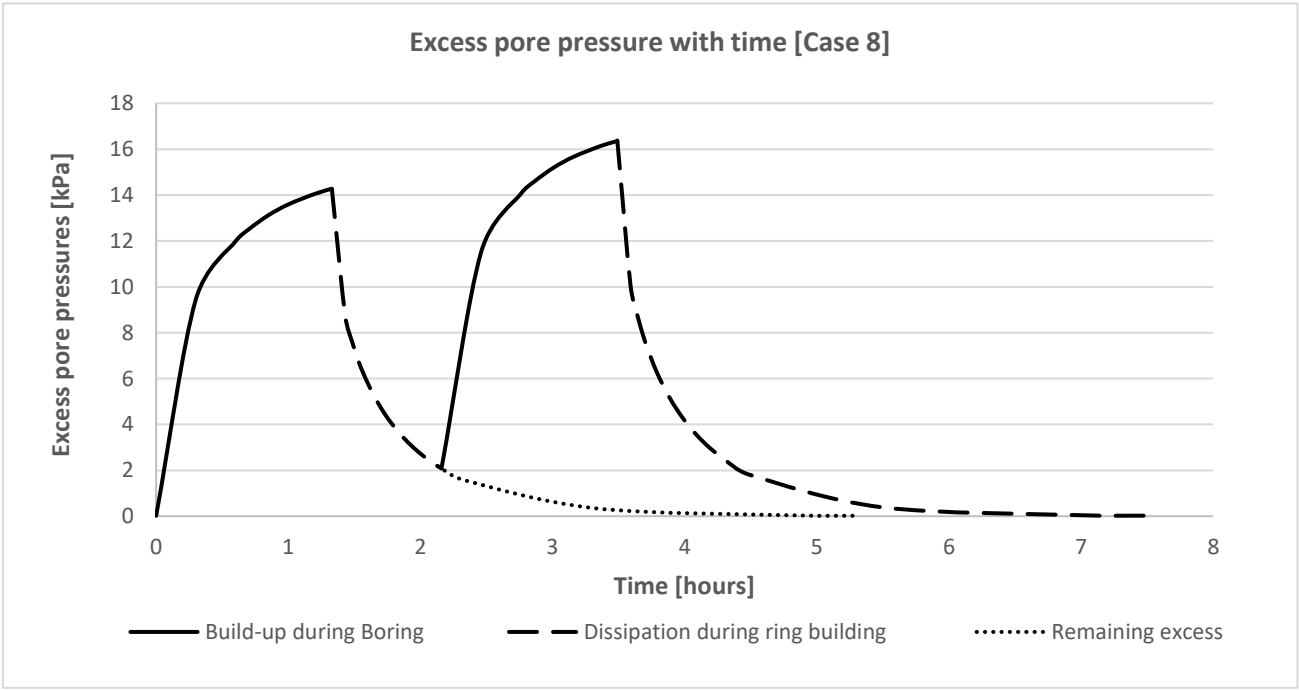

Case-study 9

Conditions

Conditions case 9	
Leakage length λ [m]	11
Storativity soil S_s [m^{-1}]	0,0007
Permeability soil k [m/h]	0,216
Height aquifer H [m]	11
u	0,06
Porosity n [-]	0,4
Advance speed v [m/h]	1,5
Discharge q [m/h]	-0,6
Diameter tunnel [m]	11
Radius tunnel [m]	5,5
Discharge Q [m^3/h]	-6,6
Boring time [h]	5/8= 1,33
Ring building time [h]	5/6= 0,83

Build-up and dissipation excess pore pressures with time

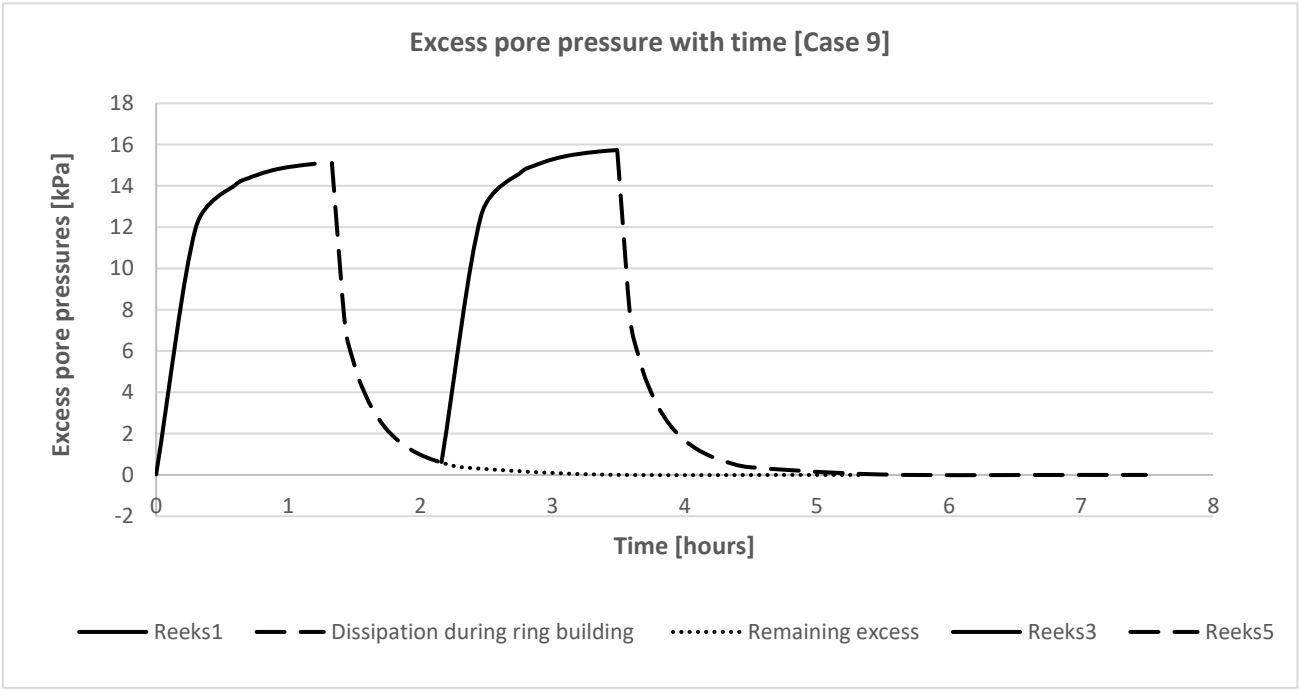

Case-study 10

Conditions

Conditions case 10	
Leakage length λ [m]	11
Storativity soil S_s [m^{-1}]	0,0007
Permeability soil k [m/h]	0,0108
Height aquifer H [m]	11
u	0,25
Porosity n [-]	0,4
Advance speed v [m/h]	1,5
Discharge q [m/h]	-0,6
Diameter tunnel [m]	11
Radius tunnel [m]	5,5
Discharge Q [m^3/h]	-6,6
Boring time [h]	5/8= 1,33
Ring building time [h]	5/6= 0,83

Build-up and dissipation excess pore pressures with time

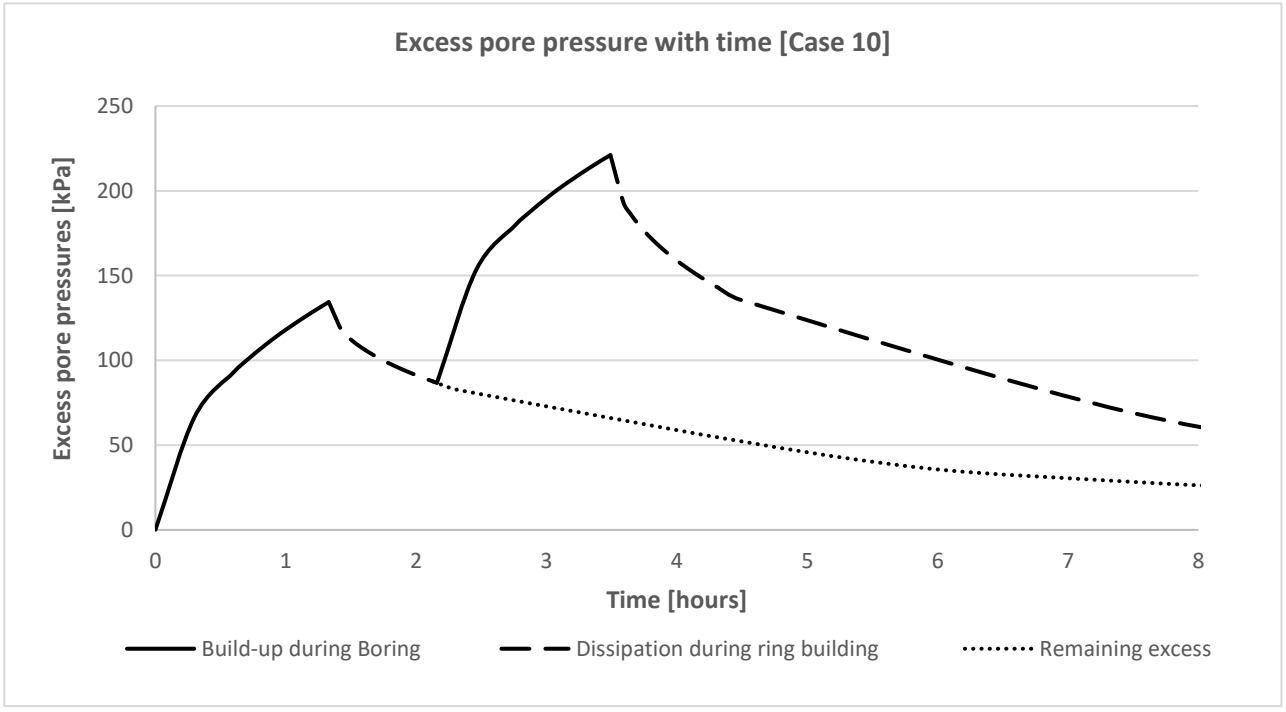

Case study Rijnlandroute

Case-study A

Conditions

Conditions case A	
Leakage length λ [m]	10,96
Storativity soil S_s [m^{-1}]	0,0007
Permeability soil k [m/h]	0,108
Height aquifer H [m]	21,92
u	0,08
Porosity n [-]	0,4
Advance speed v [m/h]	1,5
Discharge q [m/h]	-0,6
Diameter tunnel [m]	10,96
Radius tunnel [m]	5,48
Discharge Q [m^3/h]	-6,6
Boring time [h]	5/8= 1,33
Ring building time [h]	5/6= 0,83

Build-up and dissipation of the excess pore pressures with distance x from tunnel face

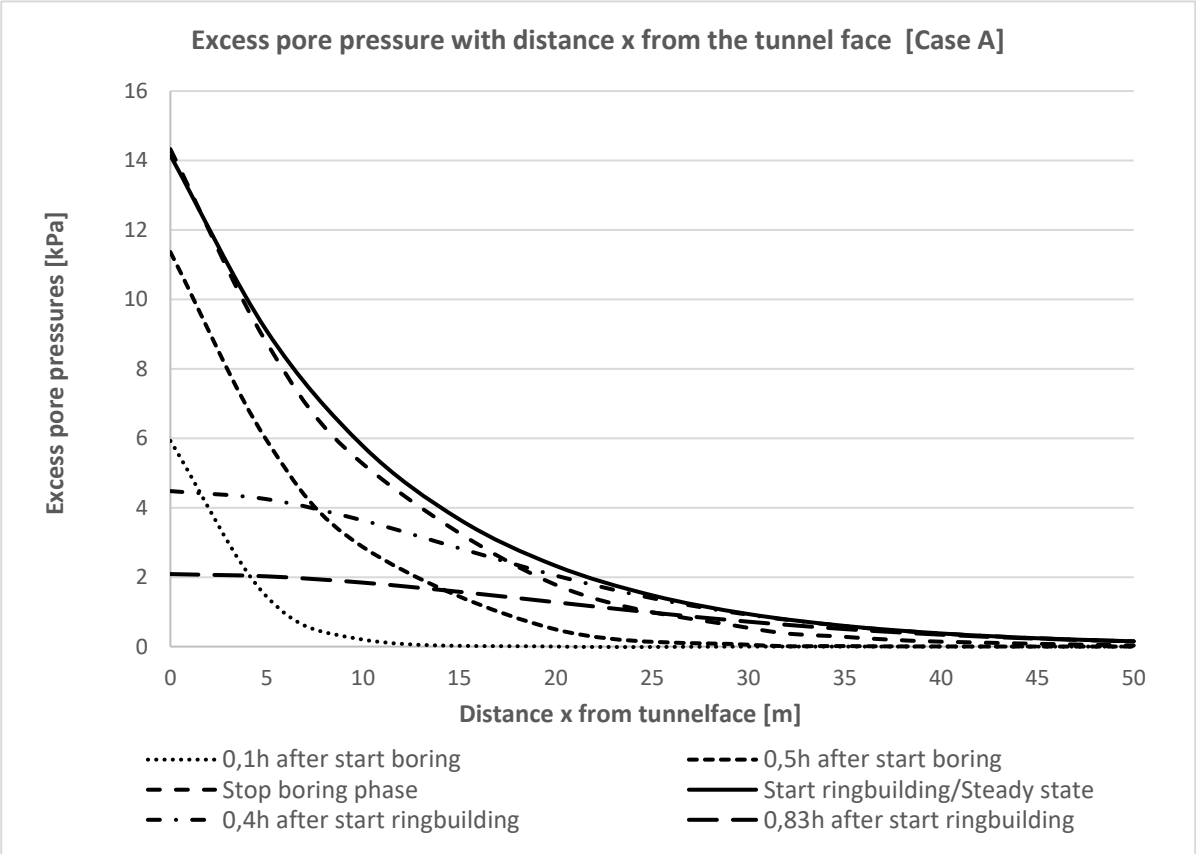

Case-study C

Conditions

Conditions case C	
Leakage length λ [m]	13,42
Storativity soil S_s [m^{-1}]	0,0007
Permeability soil k [m/h]	0,108
Height aquifer H [m]	27,4
u	0,08
Porosity n [-]	0,40
Advance speed v [m/h]	1,50
Discharge q [m/h]	-0,6
Diameter tunnel [m]	10,96
Radius tunnel [m]	5,48
Discharge Q [m^3/h]	-6,57
Boring time [h]	5/8= 1,33
Ring building time [h]	5/6= 0,83

Build-up and dissipation of the excess pore pressures with distance x from tunnel face

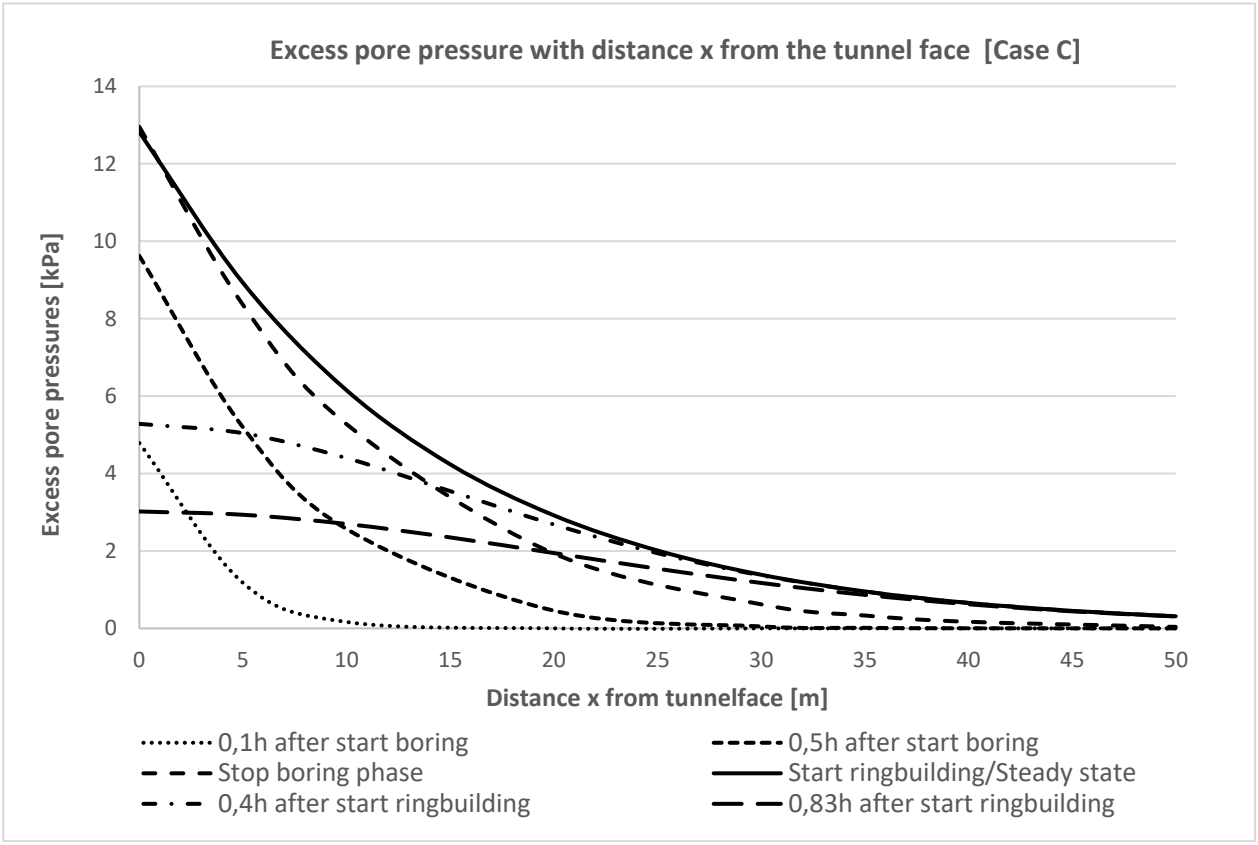

Case-study E/F/H

Conditions

Conditions case E/F/H	
Leakage length λ [m]	50
Storativity soil S_s [m^{-1}]	0,0007
Permeability soil k [m/h]	0,108
Height aquifer H [m]	5,48
u	0,08
Porosity n [-]	0,40
Advance speed v [m/h]	1,50
Discharge q [m/h]	-0,6
Diameter tunnel [m]	5,48
Radius tunnel [m]	2,74
Discharge Q [m^3/h]	-3,28
Boring time [h]	5/8= 1,33
Ring building time [h]	5/6= 0,83

Build-up and dissipation of the excess pore pressures with distance x from tunnel face

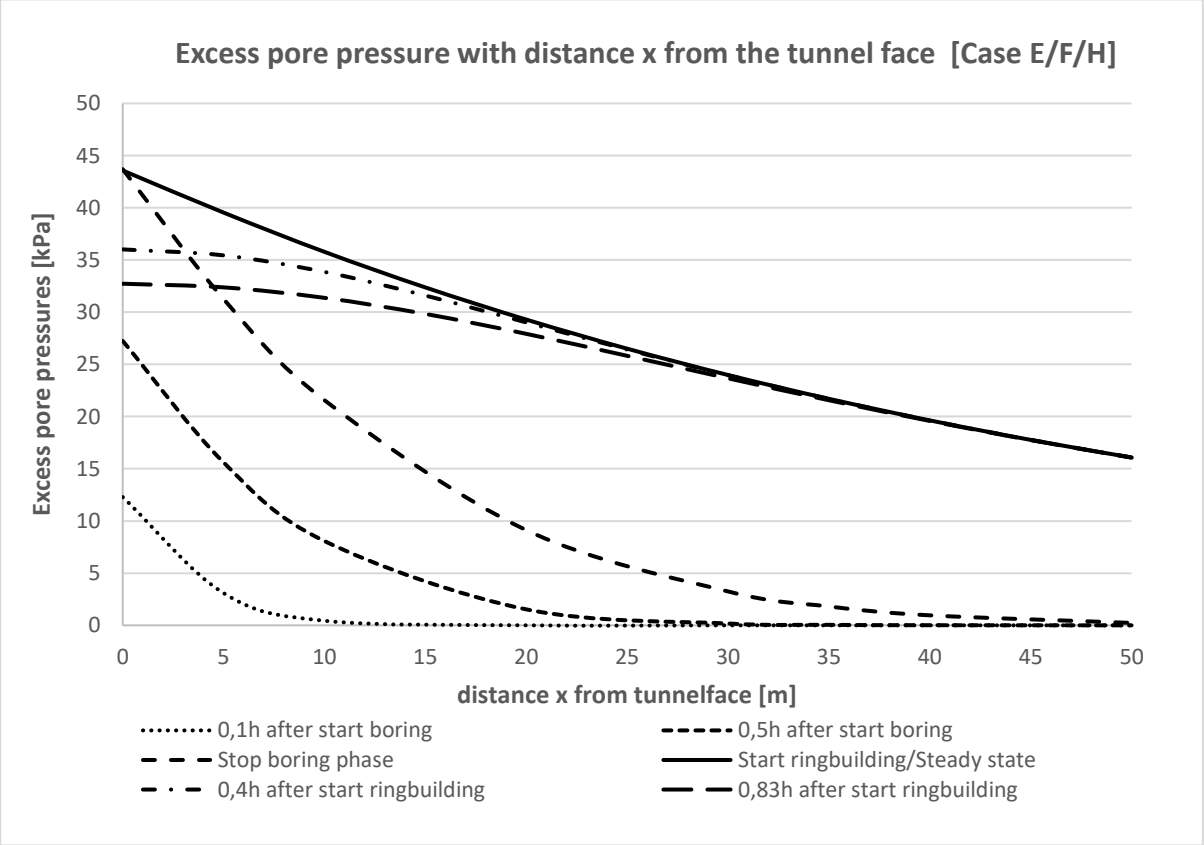

Case-study G

Conditions

Conditions case G	
Leakage length λ [m]	15,49
Storativity soil S_s [m^{-1}]	0,0007
Permeability soil k [m/h]	0,108
Height aquifer H [m]	16,44
u	0,08
Porosity n [-]	0,40
Advance speed v [m/h]	1,50
Discharge q [m/h]	-0,6
Diameter tunnel [m]	5,48
Radius tunnel [m]	2,74
Discharge Q [m^3/h]	-3,28
Boring time [h]	5/8= 1,33
Ring building time [h]	5/6= 0,83

Build-up and dissipation of the excess pore pressures with distance x from tunnel face

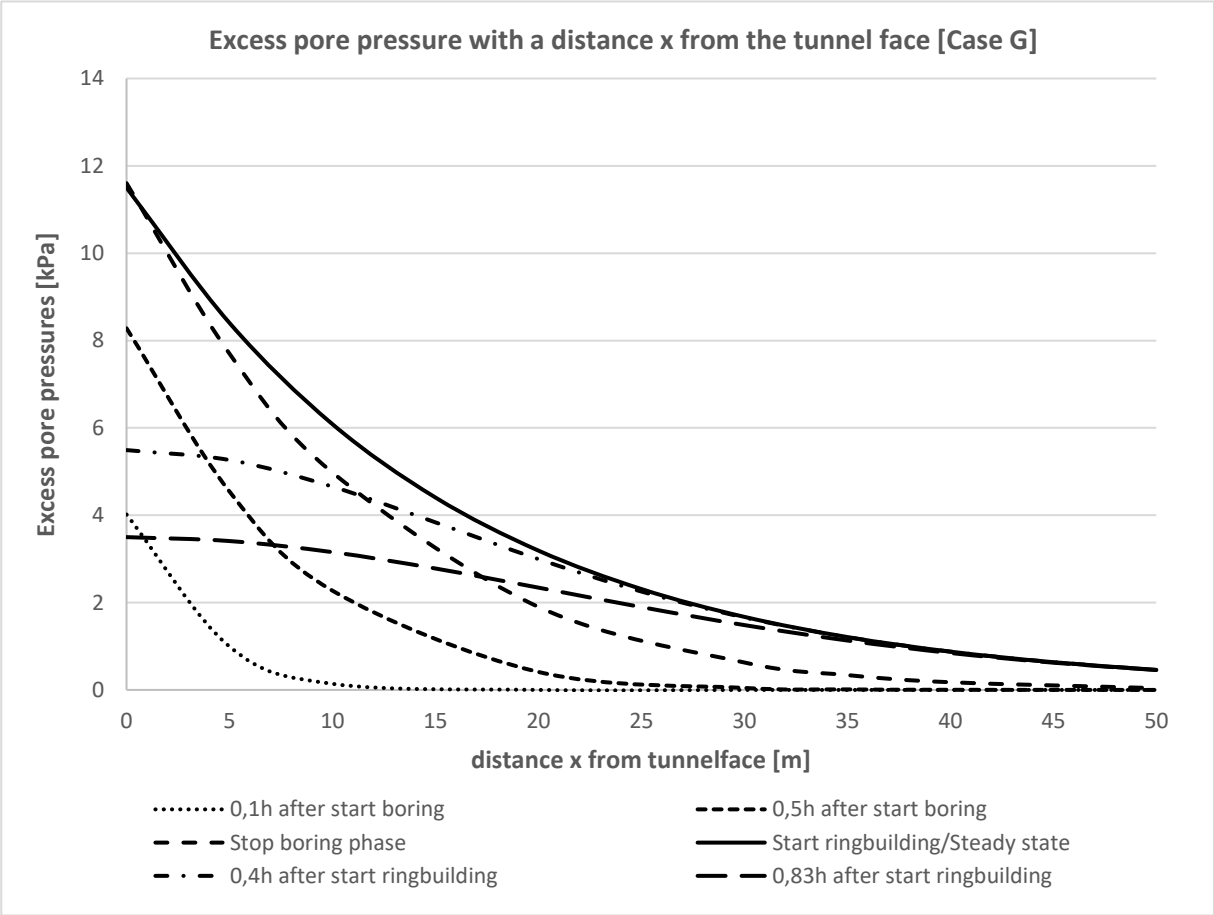

Annex 6: Pressure distributions cases

- **Case A:** Minimum support pressure (horizontal effective stress) with depth for a homogeneous sand profile (C/D=1,0).

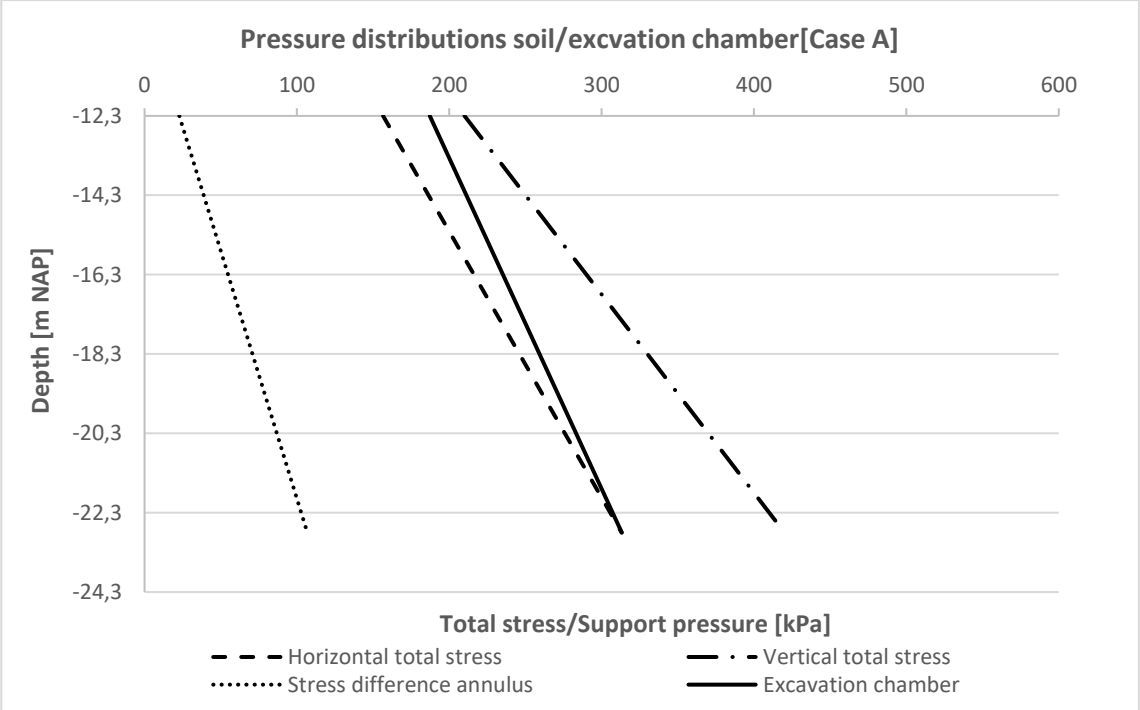

- **Case B:** Minimum support pressure (horizontal effective stress) with depth for a homogeneous clay profile (C/D=1,0).

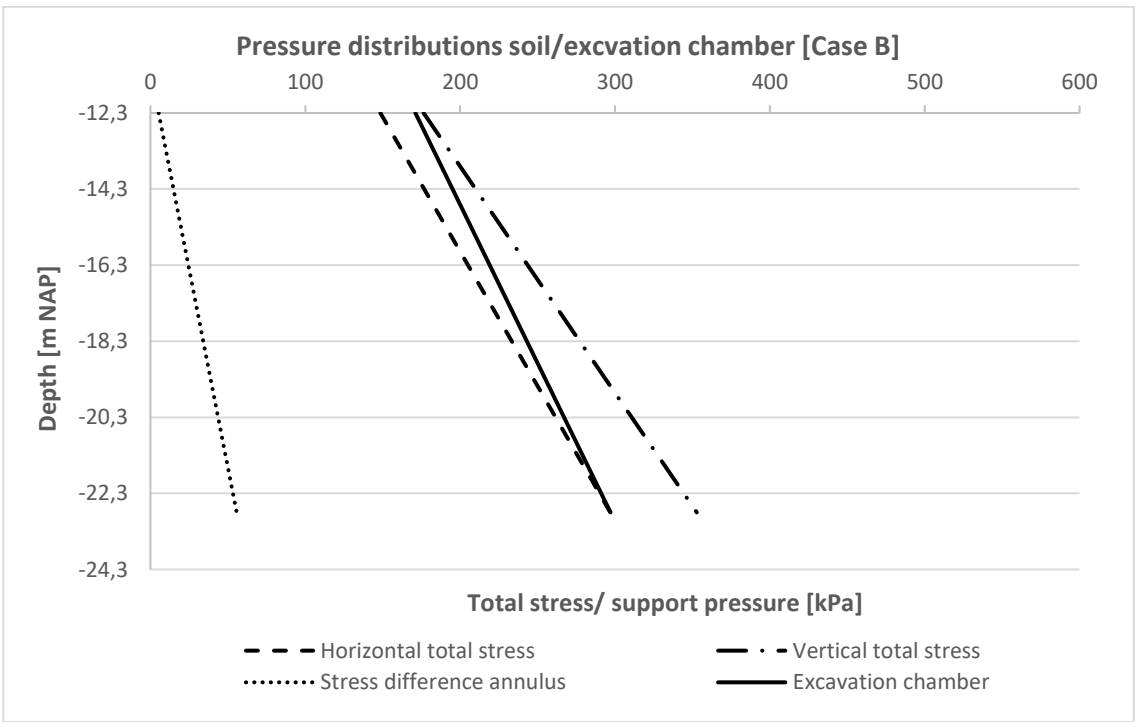

- **Case C:** Minimum support pressure (horizontal effective stress) with depth for a homogeneous sand profile (C/D=1,5).

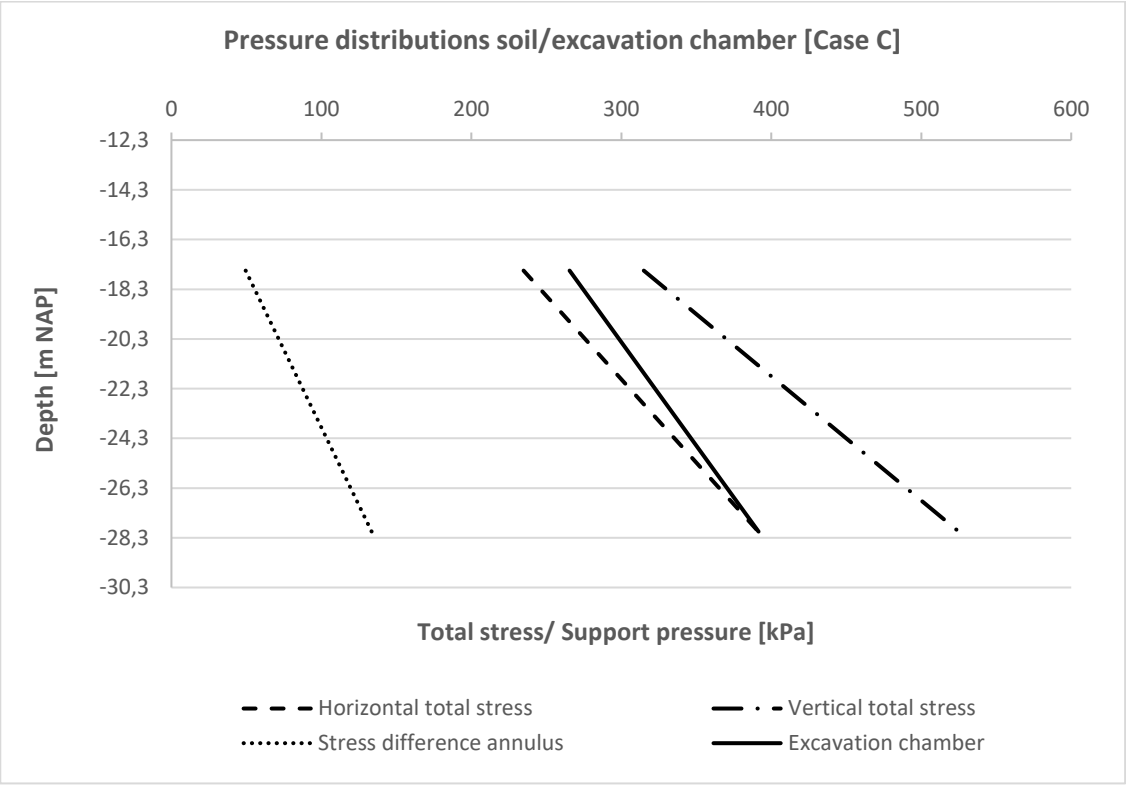

- **Case D:** Minimum support pressure (horizontal effective stress) with depth for a homogeneous clay profile (C/D=1,5).

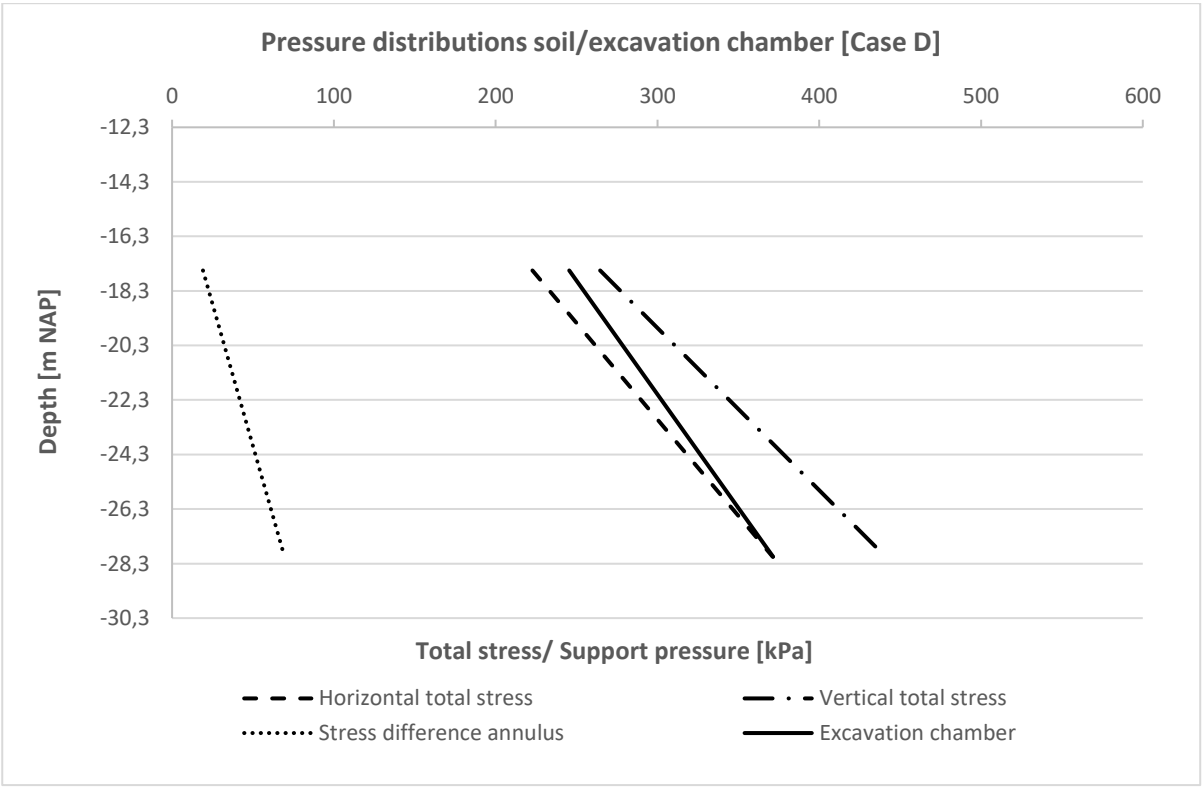

- **Case E:** Minimum support pressure (horizontal effective stress) with depth. Soil profile in front of the TBM consists of an upper layer of clay and a bottom layer of sand. The soil cover consists of a sand layer.

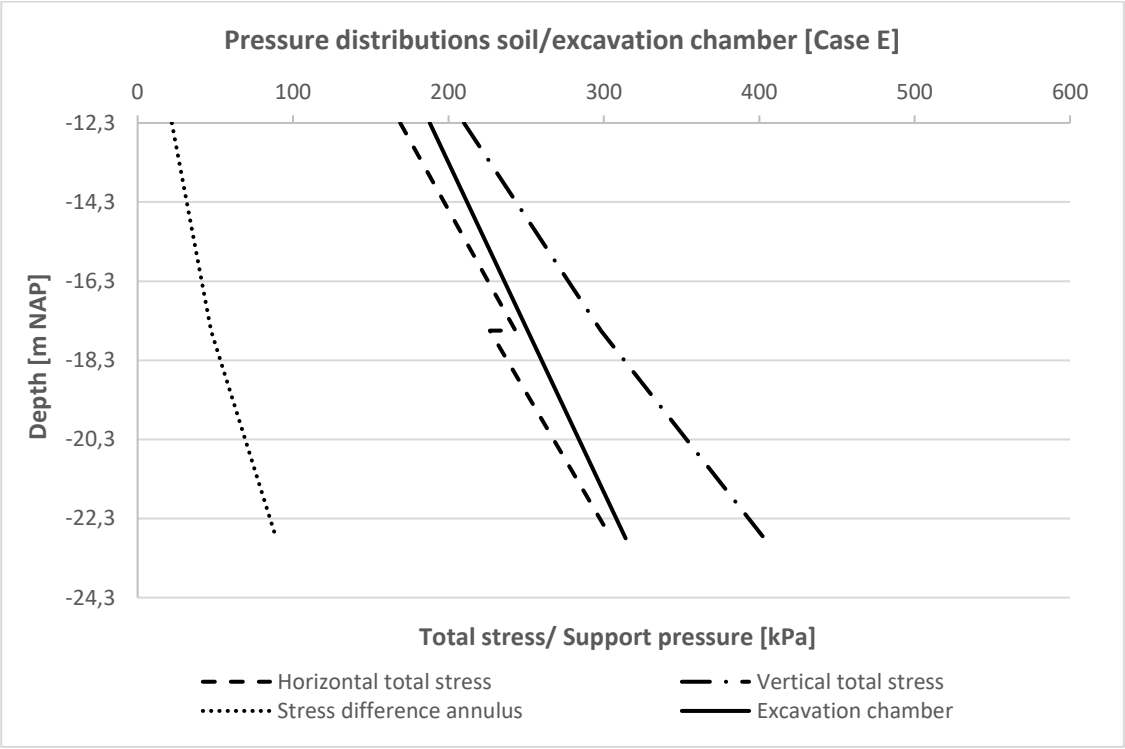

- **Case F:** Minimum support pressure (horizontal effective stress) with depth. Soil profile in front of the TBM consists of an upper layer of clay and a bottom layer of sand. The soil cover consists of a clay layer.

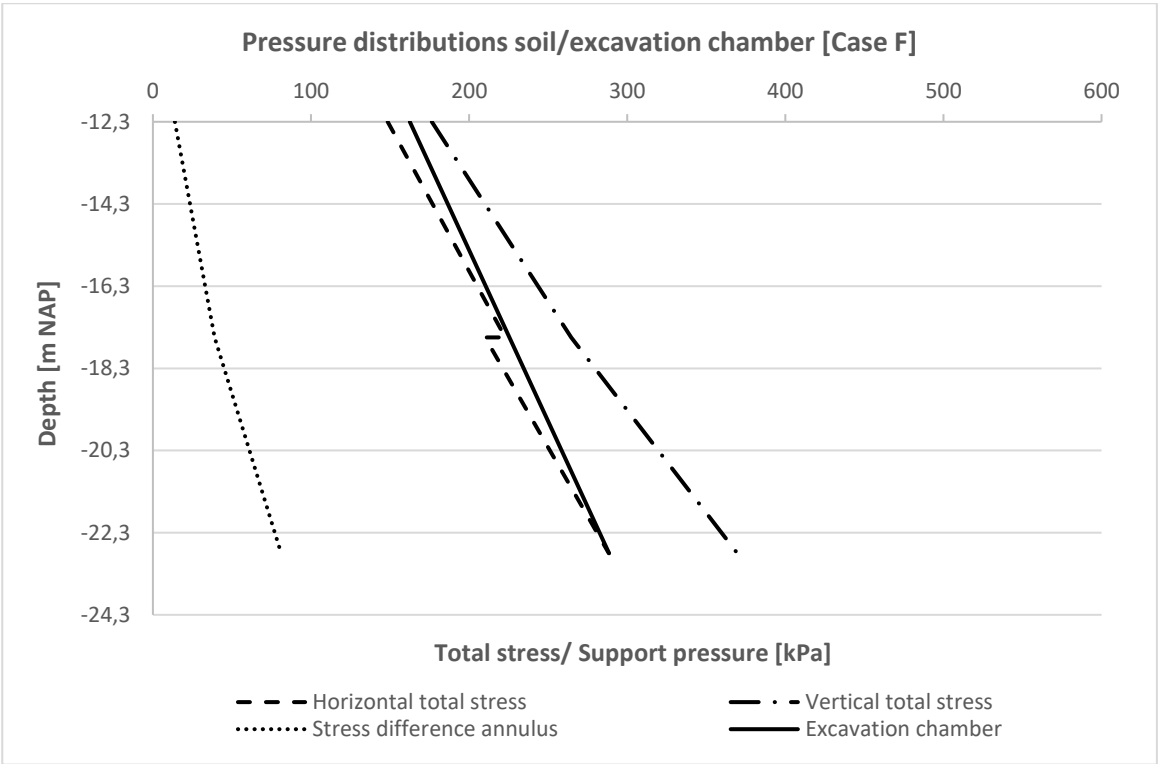

- **Case G:** Minimum support pressure (horizontal effective stress) with depth. Soil profile in front of the TBM consists of an upper layer of sand and a bottom layer of clay. The soil cover consists of a sand layer.

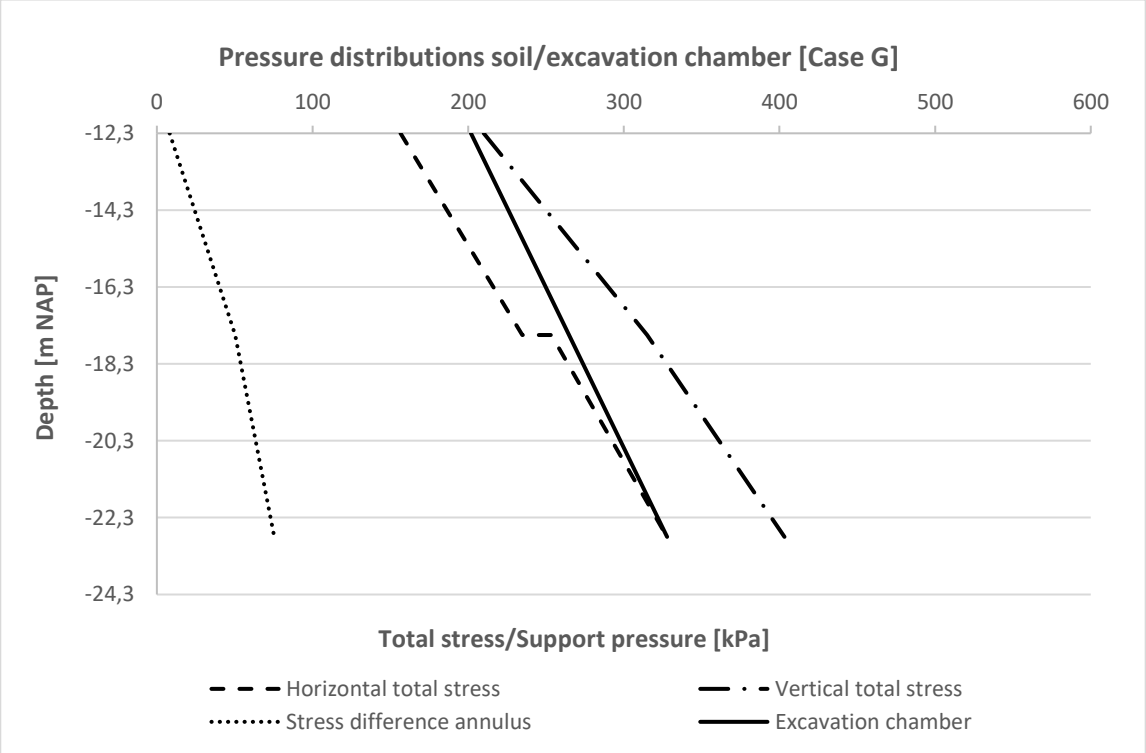

- **Case H:** Minimum support pressure (horizontal effective stress) with depth. Soil profile in front of the TBM consists of an upper layer of sand and a bottom layer of clay. The soil cover consists of a clay layer.